

TOYOTA

Technical Review

2021 / **3**
236



技術
進化

Special
Feature

Contrasts in Value and Manufacturing

-The Second-Generation Mirai and New GR Yaris-

Vol. 66

Cover design:

This issue of the Toyota Technical Review features in-depth descriptions of the second-generation Mirai FCV and the new GR Yaris. The cover pairs the Japanese character “超” (pronounced “cho” or “koeru”), which means “to exceed” or “to go beyond the normal,” with “躍” (pronounced “yaku”), which means “to leap up” or “to move vigorously.” This combination was selected to express how these models have exceeded and powerfully reinvented the ordinary conventions of car making as a step toward the creation of new values under Toyota’s philosophy of building ever-better cars. The color design symbolically places the concept colors of the cars side-by-side.

TOYOTA Technical Review

236

Vol. 66 Mar. 2021

Contents

Preface

- Mass Production to Create Happiness
Masahiko Maeda, Operating Officer 4

▷ Special Feature: Contrasts in Value and Manufacturing –The Second-Generation Mirai and New GR Yaris–

- Development of the Second-Generation Mirai –A Wholly New Type of Environmentally Friendly Vehicle–
Yoshikazu Tanaka/Ryotaro Shimizu/Hitoshi Nomasa/Makoto Inoue 6
- Outline of the New Fuel Cell System in the Second-Generation Mirai –Development of a Fuel Cell Suitable for Mass Production–
Tsuyoshi Takahashi/Yoshihiro Ikogi/Hiroyuki Imanishi/Yuji Kakeno 12
- Development of the Fuel Cell System for the Second-Generation Mirai
Osamu Yumita/Hiroyasu Kato/Shuya Kawahara/Takahiro Ito/Ryoichi Namba/Tsutomu Shirakawa 16
- Development of the Fuel Cell Stack for the Second-Generation Mirai
Seiji Mizuno/Tomokazu Hayashi/Hideki Kubo/Masao Okumura/Takuya Kurihara/Kazuhiro Mori 22
- Development of the High-Pressure Hydrogen Storage System for the Second-Generation Mirai
Akira Yamashita/Kotaro Nakamichi/Takashi Ino/Koji Kida/Hiroki Yahashi/Sogo Goto 28
- Production Engineering Technology for the Fuel Cell Stack of the Second-Generation Mirai
Takeshi Nagasawa/Atsushi Nogi/Teppey Ikeda/Shimpei Yano/Shinya Takeshita/Takuya Itakura 34
- Production Engineering Technology for the High-Pressure Hydrogen Tanks of the Second-Generation Mirai
Yoichiro Baba/Masato Ueda/Hideaki Kondo 40
- The Platform and Body Structure of the Second-Generation Mirai
Yasuyuki Kumazawa/Daisuke Teramoto/Noboru Ogura/Hiroshi Bando/Yoshiki Ishikawa 45
- The New Character of the Second-Generation Mirai
Akira Kubota 50
- Development of the Noise and Vibration Performance of the Second-Generation Mirai
Tepei Ishikawa/Yusaku Hamuro/Tomohisa Kato/Chie Fukuhara/Kazuhiro Kamei 55
- Development of the Dynamic Vehicle Performance of the Second-Generation Mirai
Wataru Ashikawa/Shugo Okamatsu/Makoto Inoue 60
- Development of the Aerodynamic Performance of the Second-Generation Mirai
Hideaki Takeda/Akihito Hosoi/Hiroshi Kuroda/Aoi Kodama 65
- Development of the Passive Safety Performance of the Second-Generation Mirai
Toshihiro Fujiwara/Hiromasa Tanaka/Shuji Hirakata 68
- Vehicle Production Engineering Technology to Enhance the Mass-Production Capabilities and Product Appeal of the Second-Generation Mirai
Masaru Yokoyama/Rin Masuhara/Yukinori Nasu/Hiroto Kozuki/Toshimitsu Saijo/Masanori Kokume/Jun Matsuoka/Yoji Hamamoto 70
- Development of Air Cleaner Realizing Minus Emissions
Tetsuya Ichikawa/Kuniho Kasugai/Koichi Masuda/Hiroto Maruyama/Jun Goto/Kimiko Yoshida 75
- Development of Toyota Safety Sense
Yuto Shimbo/Yusuke Tanaka/Hiroto Katsuda/Chenyu Wang/Masami Ishihara/Keiji Yamashita 78

· Development of the Toyota Teammate Advanced Park Function Yasutaka Matsunaga/Yuki Minase/Yu Hiei	82
· Development of Sudden Acceleration Suppression System Using Big Data Takuya Kaminade/Yuhi Kishimoto/Takashi Unigame/Masashi Takagi/Hiroaki Daba/Masashi Oishi	88
· Connected Vehicle Services Satoru Sakuma/Tetsu Yajima/Kano Asai/Masaya Hizaki	92
· Development of Low-CO ₂ Recycled Aluminum Alloy Naoki Nishikawa/Yuya Masuda/Kazumi Otake/Ryo Kuramoto/Yuki Yamazaki/Takeshi Nagai	94
· Born from the World Rally Championship –Introduction to the GR Yaris– Naohiko Saito/Takashi Doi	98
· Designed for Driving Performance –Styling that Emphasizes the Performance of the GR Yaris– Yoshiharu Nakajima/Tatsuhide Hoshi/Kosuke Taniguchi/Kiyotaka Yoshida/Satoshi Nishikatsu	105
· Development of a High-Performance Engine for the GR Yaris –The New 1.6-Liter Turbocharged Engine– Kenji Yamanari/Kazunori Yamaji/Takeshi Hagiwara/Atsunori Kumagai/Hiroyasu Koyama	111
· GR-Four –The 4WD System of the GR Yaris– Masayuki Arai/Naoaki Maeda/Shinichiro Ishikawa	117
· Realization of Superlative Driving Performance –Development of the Chassis and Dynamic Performance of the GR Yaris– Takaaki Nagata/Keita Oba/Masahiro Ogane/Yosuke Iwata/Masanori Horie/Kohei Kozono	123
· Weight Reduction for Exhilarating Performance –Weight Reduction Technology for the Body of the GR Yaris– Tomohisa Kanamori/Haruki Nakamura/Kazuhiro Morita/Kyohei Yamaji	130
· Expressing Driving Performance through Sound –Development of the Sound of the GR Yaris– Hisashi Tajima/Chie Fukuhara/Hideyuki Kasamatsu	134
· Cooling to Support Driving Performance –The Cooling Performance of the GR Yaris– Keisuke Ishita/Masaru Matsuda/Atsushi Murakawa/Yoshifumi Nishio/Shinichiro Hattori	140
· The Dedicated Sports Car Production Line –The GR Factory– Motoyasu Machino/Hiroyuki Kitagawa/Yuya Arai/Hidetsugu Kitaori	146

▷ Technical Papers/Technical Articles

· Development of Teammate Advance Drive –An Advanced Driving Assistance System Using Automated Driving Technology– Masaki Matsunaga/Osamu Ozaki/Koichiro Kimura/Koichi Hara/Shinya Okawa/Takeshi Sasuga	152
· Research into Generation of Atmospheric Secondary Organic Aerosols from Gasoline Vehicle Emissions Using Photochemical Reaction Experiments Simulating Solar Radiation Daisuke Hayashi/Tetsuya Yamashita	157
· Optimization of Motion Controls of Highly Realistic Dynamic Driving Simulator in Urban Driving Scenarios Quy Hung Nguyen Van/Shogo Konishi/Shoji Ito	163

▷ Technical Award News

170

Mass Production to Create Happiness

Masahiko Maeda

Masahiko Maeda,
Operating Officer



We are in the middle of an unprecedented situation, with the novel coronavirus pandemic causing massive disruption to our lives and social systems, and forcing us to face up to the necessity of making even more profound changes to our business. It is well known that tough times also bring opportunity. Toyota has to grasp this opportunity and fully transform itself into a mobility company to ensure steady growth rooted in the new reality.

In addition, in 2015, we announced the Toyota Environmental Challenge 2050. Through this initiative, we are working actively to lessen the environmental impact of vehicles to as close to zero as possible, while taking action to contribute positively to the Earth and its communities with the aim of achieving a sustainable society. We are promoting this initiative alongside the Sustainable Development Goals (SDGs) established by the United Nations General Assembly. We have set targets for six challenges, including lowering CO₂ emissions, and incorporated them into our vehicle development principles.

In the midst of this situation, how might the automotive market change in the future?

On top of the impact of the novel coronavirus and measures for the environment, another major driver of transformation in the automotive industry is a change in customers' values. According to various observers, we are witnessing a shift to people valuing experiences over possessions, entering the era of the digital native, or even seeing the advent of a non-contact society. Although these are useful expressions to describe how customers' values are changing, we need to be most strongly aware of the fact that people are finding happiness in dramatically diversifying ways. Conventional mass-marketing approaches are no longer enough to communicate to customers.

In other words, it is becoming increasingly important to communicate the type of product and the values it represents clearly and in an even more understandable manner, and the methods of achieving this are becoming more and more varied.

We are seeing a switch from purchases based on a desire *for* something to purchases based on a desire to *do* something. At the same time, the individualistic preferences of customers are becoming more pronounced through an emphasis on the personalized customization of the cars that they care for.

With the advent of a non-contact society, working to achieve greater logistical efficiency is likely to become even more valuable. For Toyota, ensuring mobility for people without easy access to transportation will also be an important value to offer as we aim to become a mobility company that provides freedom of movement to all.

In 2016, Toyota introduced its in-house company system with the aim of building cars that satisfy these diversifying values. This edition of the *Toyota Technical Review* describes two cars that, in some sense, stand at the extremes of this diversification. Both were developed taking advantage of the strengths of the in-house company system, neither are for the mass-market, and both were developed with completely different approaches.

The first is the second-generation Mirai. The second-generation Mirai was developed primarily for customers that strongly value state-of-the-art technologies. While remaining true to its core mission of helping to further lower the environmental impact of vehicles through advancements in fuel cell technology, it also features various innovations aimed purely at creating a fun-to-drive experience, as well as the latest active safety and advanced driving assist systems to help achieve zero traffic accident casualties. New components were also developed with greater applicability to commercial vehicles.

The second is the GR Yaris. Kiichiro Toyoda, the founder of Toyota, stated that, “...manufacturers must participate in auto-racing to test their vehicles’ durability and performance, and display their utmost performance. With competition comes progress, as well as excitement among motoring fans.” This belief is central to the development philosophy of President Toyoda under his pseudonym “Morizo.” With the aim of building an unprecedentedly different vehicle, Toyota decided to completely reverse its normal development approach by starting out with a racing car and then planning the development, testing, and production steps for building a model for the market. As a result of these efforts, the GR Yaris won the ST-2 class of the 2020 Pirelli Super Taikyu Series.

We hope that these cars bring happiness to our customers. The in-house company system has made it easier for us to build cars to satisfy the increasing diversification of customer values, and I think that the benefits of this system are now becoming clearly visible. As the title suggests, creating even greater happiness through mass production is a continued aim of Toyota, and one that we want to achieve by building cars that satisfy the values of the widest possible range of people.

Development of the Second-Generation Mirai* –A Wholly New Type of Environmentally Friendly Vehicle–

Yoshikazu Tanaka*¹
Ryotaro Shimizu*¹
Hitoshi Nomasa*¹
Makoto Inoue*²

1. Introduction

As well as providing freedom of mobility, cars have contributed greatly to economic, social, and cultural development. However, cars are also impacting the global environment in various ways. Climate change caused partially by CO₂ and other greenhouse gases is having an even greater effect on the world than previously anticipated.

Toyota regards addressing environmental issues as one of its highest priorities, and has adopted a wide range of initiatives to this end. The Toyota Environmental Challenge 2050, which was announced in 2015, consists of six separate challenges to help realize sustainable development together with society (Fig. 1).

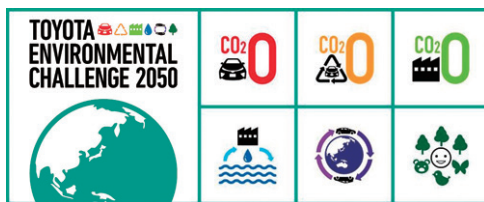


Fig. 1 Toyota Environmental Challenge 2050

One of these challenges aims to lower tailpipe CO₂ emissions from new cars by 90% from 2010 levels. Accordingly, Toyota has announced an annual sales target of 5.5 million electrified vehicles, including at least 1 million electric vehicles (EVs) and fuel cell vehicles (FCVs), by 2030 as an important milestone toward achieving this difficult target (Fig. 2).

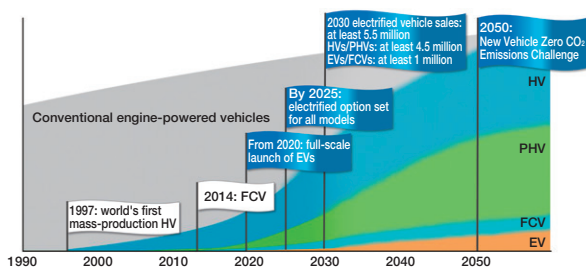


Fig. 2 2030 Vehicle Electrification Milestone

In other words, Toyota would like to help reduce CO₂ emissions and contribute to environmental preservation by popularizing and spreading electrified vehicles on a global scale.

2. Significance of Hydrogen as an Energy Source

The adoption of hydrogen as an energy source is an effective way of reducing CO₂ emissions. Hydrogen is also an important weapon in the fight to address energy issues. Hydrogen in the form of water is one of the most abundant elements on Earth. In addition to its ready availability, hydrogen is more energy-dense than electricity and can be transported and stored more easily. Since hydrogen can be produced by the electrolysis of water using electricity generated from wind, wave, or solar power, and then stored and transported, it can offset the unpredictable nature of renewable energy sources and can also be used to correct regional energy imbalances.

For these reasons, great expectations have been placed on hydrogen as an energy source for a sustainable society, as summarized by the policy of the Japanese government to help realize a hydrogen energy based society (the Strategic Road Map for Hydrogen and Fuel Cells).

Hydrogen-fueled FCVs have several advantages, including a high energy efficiency, short refueling time, long cruising range, and zero tailpipe emissions other than water. FCVs are therefore seen as the ultimate environmentally friendly vehicle for helping to realize sustainable mobility and the popularization of FCVs is regarded as a key prerequisite of a hydrogen energy based society.

3. The Second-Generation Mirai: Major Progress toward the True Popularization of FCVs

As an ultimate environmentally friendly vehicle, the Mirai will play an emblematic role in the popularization of FCVs and the subsequent progress toward realizing a hydrogen energy based society.

The first-generation Mirai was launched in 2014 as the world's first mass-production FCV. It was developed as the forerunner of the next century of vehicle development focusing on hydrogen energy. Since its launch, the first-generation Mirai

* The officially registered name of the vehicle in Japan is MIRAI (all capital letters). This edition of the *Toyota Technical Review* uses "Mirai" in accordance with previous usage and regular English conventions.

*¹ MS Product Planning Div., Mid-size Vehicle Company

*² MS Vehicle Evaluation & Engineering Div., Mid-size Vehicle Company

sold over 10,000 units and helped to open up the market for FCVs.

As well as further developing some of the aspects of the first generation, the second-generation Mirai (**Fig. 3**) was designed to achieve a significant evolution in fundamental vehicle appeal. Toyota aimed to develop a car that customers would select simply because it is an attractive car, not because of its status as an FCV. Therefore, in addition to environmental performance, a bold plan was formulated from the beginning to expand and deepen the appeal of every aspect of the vehicle, including its design, styling, packaging, dynamic performance, handling, safety and so on.



Fig. 3 The Second-Generation Mirai

By rising to this challenge, Toyota has created an FCV with brand new appeal, widened the possibilities of FCVs, and brought this new appeal to an even wider audience of potential customers. The development of the second-generation Mirai was motivated by the desire to make a strong contribution to the further popularization of FCVs. To realize this objective, the Mirai features a revised platform as well as a totally redesigned fuel cell (FC) system. Toyota has held nothing back and taken a full swing at developing a car that customers will genuinely want to own.

3.1 The newly developed second-generation Toyota Fuel Cell System (TFCS)

The development team of the second-generation Mirai faced a wide range of difficult challenges, one of the most important being the FC system at the heart of the vehicle. The component layout of the TFCS developed in 2014 was substantially revised (**Fig. 4**), realizing a clear evolution in weight reduction, compactness, and packaging, as well as substantial enhancements in various performance aspects (**Fig. 5**).



Fig. 4 Layout of the Second-Generation TFCS

Item	Performance
FC system output	134 kW
Cruising range (WLTC)	Approximately 850 km*
Refueling time	Approximately 3 minutes

* Value calculated in the Worldwide Harmonized Light Vehicles Test Cycle (WLTC) with the effective onboard hydrogen fuel amount for FCVs specified by Japanese Electric Vehicle Association Standard (JEVS) Z902-2018.

Fig. 5 Main Performance Aspects of the Second-Generation TFCS

Furthermore, production innovations to enable full-scale mass-production were adopted. These innovations helped to dramatically boost mass-production capabilities and build a production system with an annual capacity of up to around 30,000 units as a step toward the popularization of FCVs.

3.2 Selection of vehicle packaging and platform

The vehicle packaging is an extremely important element in determining all aspects of the vehicle, including comfort, usability, styling, and performance. For an FCV, the packaging plays a particularly important role in determining the layout of components such as the FC stack and hydrogen tanks. Therefore, the planning of the packaging for the second-generation Mirai placed a major focus on the following two points.

- (1) Ensuring sufficient hydrogen storage capacity to increase cruising range.
- (2) Enhancing comfort and styling, which were two aspects of the first-generation Mirai that needed to be addressed.

First, the optimum platform to achieve these two objectives was studied. This process encompassed all types of platforms and went on around the clock to identify which one would be capable of realizing the targeted packaging and performance. In particular, the development team wanted to increase both the efficiency of the FC stack and the physical hydrogen storage capacity of the vehicle to realize a sufficient cruising range to enable customers to drive the Mirai with confidence. In addition, from the standpoint of enhancing comfort and styling, the size of the FC stack was reduced, enabling it to be moved from below the front seats of the first-generation Mirai to a new position under the hood of the second-generation.

Eventually, after repeated studies, the GA-L platform was selected. Measures such as mounting the FC stack at the front of the vehicle, revising the component layout, and the like enabled three high-pressure hydrogen tanks to be installed in a “T” configuration. This helped to increase the hydrogen storage capacity of the vehicle from 4.6 to 5.6 kg and also helped to greatly expand the legroom of rear seat occupants (**Fig. 6**).

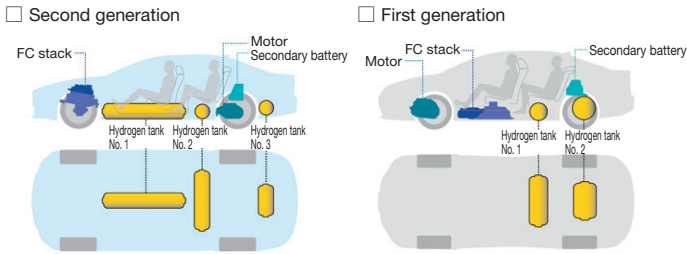


Fig. 6 Comparison of Component Layout in First- and Second-Generation Mirai

The platform allowed the vehicle height to be lowered, thereby maximizing the potential to create a well-proportioned and stylish vehicle. The platform also made a major contribution to enhancing dynamic performance by mounting heavy components low down at the center of the vehicle to lower the center of gravity and optimizing the front/rear weight distribution (**Fig. 7**).

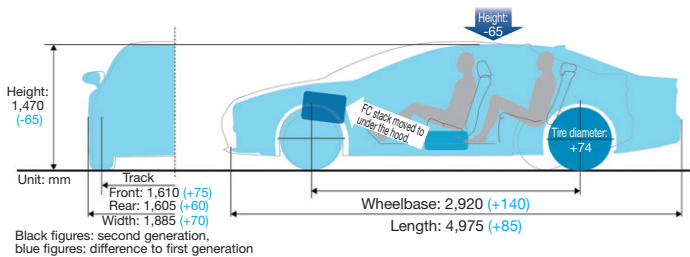


Fig. 7 Outline of Packaging of Second-Generation Mirai

3.3 Emotional styling with direct appeal

One of the most important missions of the second-generation Mirai was to achieve a significant evolution in fundamental vehicle appeal. The styling is one of the most important elements of this. The development team was motivated from the beginning by the desire to transcend the image of the Mirai as an environmentally friendly vehicle and achieve a truly stylish design. The development theme for the styling was called Silent Dynamism. The aim was to inspire customers to select the Mirai because of its emotional styling, not simply because of its status as an FCV or as an environmentally friendly vehicle. The styling development focused on creating speedy and sleek proportions overflowing with dynamism, and a minimalistic yet bold design without relying on drastic surface changes or character lines (**Figs. 8.1 to 8.3**).



Fig. 8.1 Powerful Wide-Bodied and Firmly Planted Styling with a Low Center of Gravity



Fig. 8.2 Impressive Side View with a Flowing and Speedy Form and a Swept-Back Center of Gravity



Fig. 8.3 Distinct Rear View with a Low Center of Gravity and Wide Stance

The interior of the second-generation Mirai was designed to create a new kind of personal space that represents the emotional value of the vehicle by expressing an ideal balance between driving enjoyment and relaxation while realizing a feeling of leading-edge technology. This was achieved through a new way of coordinating a minimalistic functional expression with material textures that cocoon the occupants, resulting in an uplifting interior styling that simultaneously expresses the joy of driving and relaxes the occupants (**Fig. 9**).



Fig. 9 Interior Styling

3.4 Refined and fun-to-drive vehicle performance

The second-generation Mirai was developed to be a fun-to-drive vehicle with comfortable acceleration that combines refinement with a vibration and noise-free driving experience from the moment that the vehicle moves off.

3.4.1 Dynamic performance (acceleration feeling, handling, and ride comfort)

An FCV combines the low vibration and noise of an electric traction motor with torque-full and highly linear acceleration performance that responds instantly when the driver depresses the accelerator. Additionally, the driving force of the vehicle was designed with acceleration and deceleration characteristics that help the driver to control the vehicle speed and load shifts in accordance with the driving scenario.

The main focus of the development was to realize a confident, natural, and enjoyable driving experience during acceleration and at high vehicle speeds through ride comfort with low vibration, solid handling, and direct and responsive cornering performance with high limits.

This was realized by laying out the powertrain parts to achieve a 50:50 front/rear weight distribution, and focusing strongly on the torsional rigidity of the rear body to give the vehicle a greater sense of stiffness while driving (**Fig. 10**).



Fig. 10 Annular (Ring-Shaped) Structure to Enhance Rear Rigidity

For the finishing touches, further confident and natural dynamic performance was realized by ensuring a sense of uniformity between the sensations experienced by the driver when accelerating, braking, and steering.

3.4.2 Noise and vibration (NV) performance

The NV performance development aimed to achieve a refined driving sensation from the moment that the vehicle moves off.

The lack of NV generated from an engine means that an FCV operates very quietly. However, this low level of noise causes other sounds that are virtually inaudible in a conventional vehicle to stand out. Therefore, in addition to wind noise and road noise, the development addressed operation noise from FC system components and motor noise to realize a refined NV

performance by decreasing noise at the source, reducing noise transmission intensity through innovative mounting structures, and incorporating sound insulation and the like into the body (**Fig. 11**).

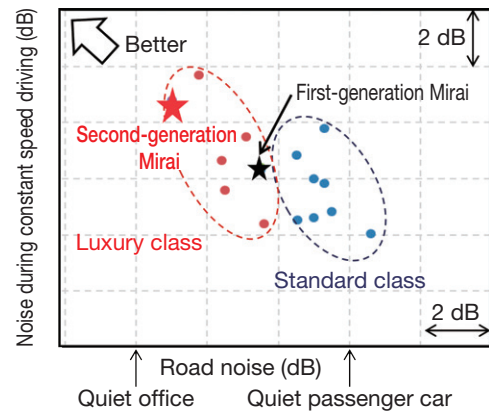


Fig. 11 Reduction of Noise while Driving

A torque-full acceleration feeling with virtually no noise or vibration is something that only a car powered by a motor can realize. However, although silent acceleration is a distinguishing feature of motor-powered cars, a particular acceleration sound was developed to create an even more uplifting fun-to-drive experience.

This sound was realized by creating and controlling a tonal balance that matches the emotional styling of the vehicle in accordance with the vehicle speed and acceleration, as well as the air intake and power generation status of the FC system. The result is an acceleration sound that enables communication between the vehicle and driver, and demands to be experienced at first hand.

3.4.3 Extending the cruising range

Being able to drive without concern for the cruising range of the vehicle is an important part of a fun-to-drive experience. The key measures to extend the cruising range were to increase the hydrogen storage capacity and reduce the running resistance (i.e., the drag and tire rolling resistance). Therefore, the aerodynamic packaging was designed to enable three hydrogen tanks to be mounted under the vehicle floor while still lowering the height of the vehicle, and a full underbody cover was adopted to smooth the airflow passing below the vehicle. In addition, close collaboration was carried out between the front styling and component development teams to ensure sufficient air intake for power generation and cooling and to realize efficient airflows, without sacrificing vehicle styling (**Fig. 12**).

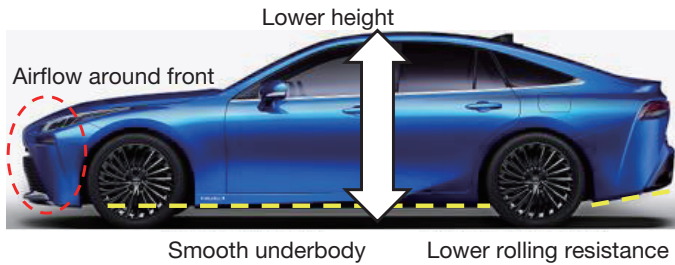


Fig. 12 Measures to Reduce Running Resistance

The tire development also aimed to reduce rolling resistance while achieving the optimum balance between the braking distance, road noise, handling, and ride comfort.

Furthermore, unlike an EV that has no heat source and consumes large amounts of energy for heating, which has a large adverse impact on cruising range, an FCV can use the heat from power generation effectively in the heating system. The second-generation Mirai is fully equipped with comfort functions that heat or cool the occupants directly (such as a steering wheel heater as well as heated and ventilated seats). The Mirai is also provided with an “ALL AUTO” function that automatically integrates the controls of these items to realize a comfortable interior while restricting the impact on the cruising range.

3.4.4 Crashworthiness

With the FC system layout of the second-generation Mirai being completely different from the first generation and with a high-voltage motor and three high-pressure hydrogen tanks mounted under the floor, the importance of crashworthiness was understood from the start of development. In addition to achieving obvious targets such as class-leading results in preventative safety performance assessments around the world, the second-generation Mirai provides occupants with the highest possible protection against high voltages while also incorporating excellent hydrogen-leakage prevention performance.

3.5 Cutting-edge systems for confident, natural, and safe performance

3.5.1 Mounting of the latest advanced safety functions

The development aimed to ensure confident, natural, and safe driving performance. This is one of the fundamental objectives for all vehicles developed by Toyota. The second-generation Mirai is equipped with the latest version of the next-generation Toyota Safety Sense safety packages, and adopts a wide range of state-of-the-art active safety technologies. Toyota has worked to further develop its active safety technologies to help address accidents caused by accelerator pedal misapplication, a phenomenon that is increasingly being regarded as a serious social issue. As a result, the Mirai is also equipped with a system that suppresses vehicle acceleration if the accelerator is

mistakenly depressed even when an object is not present in front of the vehicle.

3.5.2 The Toyota Teammate advanced driving assistance system

The second-generation Mirai is equipped with Toyota Teammate, the latest advanced driving assistance system that operates in concert with driver perceptions. Toyota Teammate was developed based on a unique approach that aims to create a mutually beneficial relationship between the vehicle and driver, treats the driver and vehicle as partners, and aims to enhance the understanding between them, rather than simply taking over control and replacing the role of the driver.

By mutual interaction, confirmation, and assistance between the driver and vehicle, this system aims to realize even safer and more comfortable driving performance.

4. Environmental Performance and Social Contribution

4.1 Air purification system using the characteristics of an FCV

It is widely appreciated that water is the only by-product emitted by the reaction between hydrogen and oxygen in an FCV. For this reason, FCVs are recognized as an inherently environmentally friendly vehicle with zero tailpipe CO₂ emissions. An FCV obtains the oxygen to generate electricity by taking in air while driving. Using this central characteristic of FCVs, a new type of added value was created by the development of a system that cleans up and then discharges this air. It was realized that the atmosphere around the vehicle could be cleaned by passing this air through a high-performance air cleaner. This air cleaner was developed by applying electret processing to the dust filter to enhance the fine particulate matter (PM2.5) filtration efficiency, and by adding a filter that targets various chemical substances.

In addition, the intake air volume is displayed on the navigation system screen via an air purification meter that resembles a tachometer. This function helps to stimulate the driver’s imagination and mindset in various ways.

4.2 Use of recycled aluminum alloy for body components

In addition to zero tailpipe CO₂ emissions, the Mirai was developed with a universal approach to reducing CO₂ in the manufacturing process from the standpoint of the lifecycle assessment (LCA) of the vehicle. The hood uses aluminum recycled from process scrap (including clad sheets) obtained from aluminum manufacturers. This is the first application of such technology to automotive body stampings and demonstrates a close understanding and application of a new

technology capable of enhancing the LCA of the vehicle to the *monozukuri* process.

4.3 Emergency external power supply function

FCVs are a type of electrified vehicle that generates electricity during driving. Taking advantage of this characteristic, the Mirai can also be operated as a mobile generator.

To address the growing possibility of large-scale power cuts caused by natural disasters in Japan and around the world, the effectiveness of this function has been demonstrated in the real world by evacuation centers and households (**Fig .13**).

The extended cruising range of the second-generation Mirai also enables an enhanced and even more versatile power supply function. It can directly power household electronic appliances up to 1,500 W from two on-board AC 100 V outlets, as well as supply high-capacity power up to a maximum of 9 kW using an AC converter (sold separately).

The Mirai is equipped with this function as standard, which allows it contribute to society as a high-capacity mobile generator in an emergency.

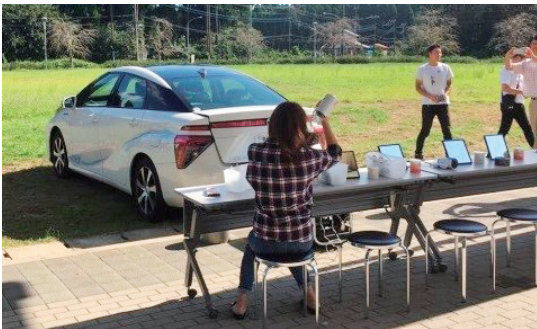


Fig. 13 Supplying Power to Hair Driers

5. Conclusion

The first-generation Mirai was launched in 2014 and has sold over 10,000 units around the world. A large number of customers are aware and positively inclined toward FCVs, a fact demonstrated by the excited reaction of children after spotting a Mirai.

Society as a whole is making steady progress toward the adoption of hydrogen energy, with the availability of hydrogen refueling stations and other infrastructure expanding. At the same time, the social situation is changing and environmentally friendly automotive technologies are making great progress. As various forms of electrified vehicles become more advanced, it is necessary to further popularize FCVs to help realize a hydrogen energy based society. To encourage this process, development and production teams across Toyota have worked together as hard as possible with the objective of creating a desirable vehicle with a universal appeal.

The result is the all-new second-generation Mirai. Its outstanding environmental performance goes without saying.

The Mirai provides an elegant, refined, and quiet passage through the bustle of urban life, and is just as at home if the driver wants a change in scenery and heads to the winding roads outside the city. The sharp acceleration feeling typical of an electrified vehicle, and the comfortable handling in tune with the driver's intentions will bring a smile to the face of the driver. Any doubts about the acceptability of pushing the accelerator pedal to the floor will be dispelled by the air purification meter on the center display that shows how the Mirai goes beyond the conventional concept of zero emissions and realizes "negative" emissions that are cleaner than the surrounding air. The vehicle reaches out and tells the driver that it is fine to depress the accelerator as much as possible. After all, it's for the sake of the Earth.

Toyota believes very strongly that supporting the second-generation Mirai is the best way to demonstrate the new possibilities of FCVs and to take the next steps toward the realization of a hydrogen energy based society.

Authors



Y. TANAKA



R. SHIMIZU



H. NOMASA



M. INOUE

Outline of the New Fuel Cell System in the Second-Generation Mirai –Development of a Fuel Cell Suitable for Mass Production–

Tsuyoshi Takahashi*¹
 Yoshihiro Ikogi*¹
 Hiroyuki Imanishi*¹
 Yuji Kakeno*¹

Abstract

Fuel cell vehicles (FCVs) are being developed as a potential solution for environmental and energy-related issues. In 2014, the Toyota Fuel Cell System (TFCS) was developed and installed in the first-generation Mirai to help promote the use of hydrogen and encourage the wider adoption of FCVs. This article describes the challenges that were faced, and the productivity innovations and practicality improvements that were adopted in the second evolution of the TFCS to help further popularize FCVs.

Keywords: fuel cell (FC) system, FC stack, high-pressure hydrogen tank, cost reduction, cruising range, productivity

1. Introduction

Toyota is currently developing a wide range of environmentally friendly technologies to help facilitate the harmonious coexistence of vehicles with the global environment. As the electrification of vehicles accelerates, there are increasing expectations for the use of both electricity and hydrogen. Toyota began fuel cell (FC) development in 1992 and was the first automaker in the world to start sales of a fuel cell hybrid vehicle (FCHV) on a limited lease basis in December 2002. Subsequently, after making progress toward the resolution of the main technical issues of cruising range and cold start performance, Toyota launched the FCHV-adv in 2008. Then, in 2014, Toyota launched the first-generation Mirai equipped with the Toyota Fuel Cell System (TFCS), the world's first fuel cell vehicle (FCV) that can be truly regarded as a commercial mass-production vehicle.⁽¹⁾⁻⁽⁵⁾ This article describes the development of the second-generation TFCS (**Fig. 1**), which was designed to facilitate the mass market penetration of the redesigned Mirai. In addition to further performance gains in weight reduction and packaging, the development of the second-generation TFCS took on a wide range of challenges to achieve substantially lower costs, higher power, and a longer cruising range, as well as quieter performance and the adoption of innovative production technologies (**Fig. 2**). An outline of these challenges is presented below. In addition, the following articles describe the development of the FC system, FC stack, high-pressure hydrogen storage system, as well as the production engineering (PE) technologies for the FC stack and high-pressure hydrogen tanks for the second-generation TFCS in more detail.



Fig. 1 Layout of the Second-Generation TFCS

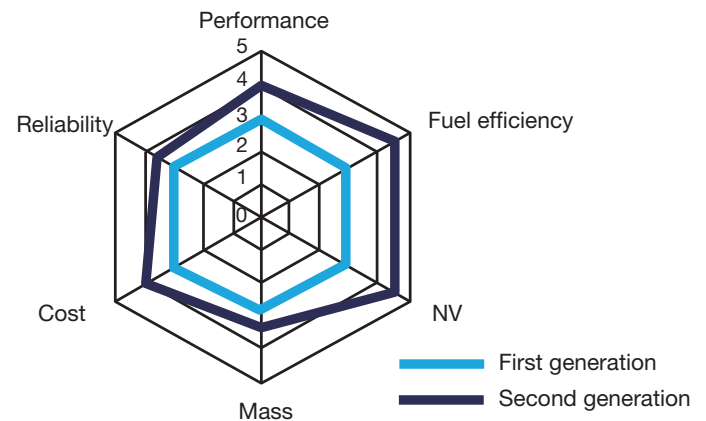


Fig. 2 Comparison of First- and Second-Generation TFCS Performance

2. Cost Reduction for the Second-Generation TFCS

Fig. 3 compares the costs of the first- and second-generation TFCS. The overall cost of the second-generation system is approximately 70% lower than the first generation.

*¹ Fuel Cell Products Development Div., Toyota ZEV Factory

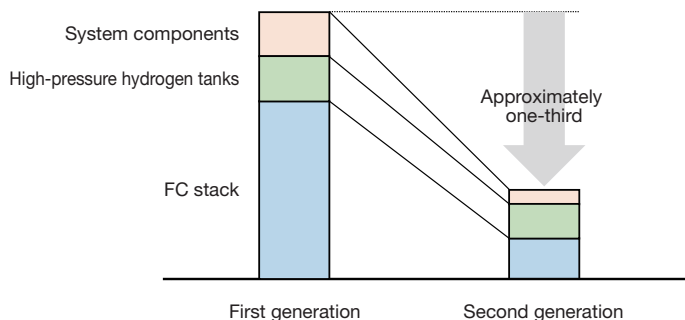


Fig. 3 Comparison of Costs of First- and Second-Generation TFCS

In addition to the economies of scale achieved through mass production, the cost reduction strategy involved reducing the amount of expensive materials used, reducing the size of components, and integrating separate elements of the system.

In the FC stack, refining the electrodes enabled the amount of expensive Pt catalytic materials to be reduced by approximately half. In addition, enhancing the performance of the cells in the stack allowed the number of cells to be reduced from 370 to 330, which requires a substantially smaller amount of materials.

The air compressor (ACP) was changed from a compression-type Roots model to a turbo model, thereby helping to reduce size and cost.

The carbon fiber material used by the high-pressure hydrogen tanks was strengthened, allowing the carbon fiber content per unit volume to be reduced by 7%.

Furthermore, productivity was boosted by the adoption of innovative PE technologies involving the simultaneous development of materials, product structures, and production processes. These technologies also contributed to lowering the manufacturing costs of the FC stack and high-pressure hydrogen tanks.

3. Development of Longer Cruising Range

Fig. 4 shows the FC stack assembly for the second-generation Mirai. One of the merits of an FCV is as an electric vehicle (EV) with a longer cruising range. By revising the layout, three hydrogen tanks could be mounted in the second-generation Mirai, increasing the hydrogen storage capacity of the vehicle from 4.6 to 5.6 kg, without sacrificing occupant space. System efficiency was increased by Toyota's first adoption of silicon carbide (SiC) devices in the FC boost converter (FCPC). As a result, the system achieves one of the highest fuel efficiency ratings in the world, up from 67 MPGe in the first-generation Mirai to 74 MPGe. This efficiency enables a substantially longer cruising range, up from 312 miles in the first-generation Mirai to 402 miles, as measured in a test cycle.

4. Enhancement of FC System Performance

The power rating of the FC stack was raised from 114 kW in the first-generation TFCS, to 128 kW in the second generation. This was accomplished by enhancing the performance of the electrodes to boost the per-unit area amount of power generation by 15%. At the same time, the size of the stack was reduced from 33 to 24 liters (excluding end plates) through measures such as enhancing the cell layout, adopting thinner cells, and so on. As a result, the volumetric power density of the system was raised from 3.5 to 5.4 kW/L (excluding end plates), while lowering the mass of the stack by approximately 40%.

Additionally, model-based development (MBD) was applied to the system controls. The entire FC system was modeled according to physical laws and the controllers were designed and implemented by this MBD approach. As an example, highly responsive compressor control was realized that also avoids surging in areas of the turbo compressor that are susceptible to this phenomenon. The developed controls help to realize stable water management in the FC stack even without a humidifier, resulting in greater power stability.

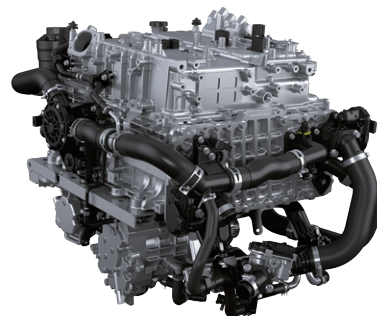


Fig. 4 FC Stack Assembly for the Second-Generation Mirai

5. Enhancement of Practicality

With the first-generation TFCS, the FC stack and FCPC were mounted below the floor. With the second generation, these two components were integrated and mounted under the hood. This helped to enhance the vehicle packaging and comfort, while expanding the occupant capacity of the vehicle from four to five people. As the system contains few moving parts, the development focused closely on its operating principles to substantially reduce system noise and achieve a much quieter ride than the first-generation Mirai. Fuel efficiency was also enhanced by taking advantage of the connected technology of the Mirai. The system control looks-ahead to the route programmed in the navigation system and optimizes the power of the FC stack and high-voltage battery in accordance with the route.

The remote start function also helps to enhance practicality when starting the vehicle in cold temperatures.

6. Productivity Innovations for the Second-Generation TFCS

The productivity of the second-generation TFCS was substantially enhanced to help the Mirai achieve mass-market penetration. As the FC stack consists of 330 fuel cells arranged in layers, it is extremely important to minimize the time required to assemble each cell. A web handling (roll-to-roll) process was adopted for the electrodes and the cycle time for cell assembly was reduced to several seconds per cell. Since the conventional rubber vulcanization process requires time to complete (tens of minutes per cell), this represents a major improvement in productivity (**Photo 1**). In addition, highly reliable stacking was achieved by automating the layering process.

The high-pressure hydrogen tanks are produced entirely in-house, starting from the liner molding process. The conventional laser welding technique used to join the liner together was replaced by an innovative infrared (IR) welding technique that greatly reduced the processing time and the number of defects. In the carbon fiber filament winding (FW) process, the weight of the moving parts of the winding equipment was thoroughly reduced and automatic winding quality measurement technology was introduced. These measures helped to increase productivity while ensuring high quality (**Photo 2**).



Photo 1 FC Stack Cell Creation Process



Photo 2 High-Pressure Hydrogen Tank Manufacturing Plant

7. Summary

In addition to further performance gains based on the first-generation TFCS, the development of the second-generation TFCS took on a wide range of challenges to achieve substantially lower costs, a longer cruising range, and greater performance, as well as to adopt innovative production technologies. Developing and mounting this system in the second-generation Mirai has helped to significantly boost the product appeal of FCVs.

In addition, Toyota also intends to utilize the developed FC system model and MBD technique to apply the TFCS to stationary power generators and commercial vehicle systems.

8. Conclusion

The development of the second-generation TFCS was accomplished thanks to the invaluable cooperation of a wide range of Toyota's partner companies. The authors would like to take this opportunity to express their sincere gratitude. With the introduction of a new generation, there is a tangible sense that progress has been achieved. However, it is important to continue taking on the challenges that remain to promote the wider acceptance of FCVs in society. Environmental and energy-related issues have to be addressed for the sake of future generations, not just the present. The popularization of FCVs also depends on the establishment of hydrogen and other social infrastructure, as well as the application of FCs in a wider range of fields outside the sphere of mobility. Toyota intends to continue its development initiatives to help realize the hydrogen energy based society of the future.

References

- (1) M. Kizaki, Asai, Yumiya. "Advancing into the Future with the Mirai Fuel Cell System." *Toyota Technical Review* Vol. 61 (2015) pp. 11-14.
- (2) T. Hasegawa, Imanishi, Nada, Ikogi. "Development of the Fuel Cell System in the Mirai FCV." *SAE 2016 World Congress and Exhibition* (2016).
- (3) T. Maruo, Toida, Ogawa, Ishikawa, Imanishi, Nada, Ikogi. "Development of Fuel Cell System Control for Sub-Zero Ambient Conditions." *WCX™ 17: SAE World Congress Experience* (2017).
- (4) N. Konno, Mizuno, Nakaji, Ishikawa. "Development of Compact and High-Performance Fuel Cell Stack." *SAE 2015 World Congress & Exhibition* (2015).
- (5) A. Yamashita, Kondo, Goto, Ogami. "Development of High-Pressure Hydrogen Storage System for the Toyota Mirai." *SAE 2015 World Congress & Exhibition* (2015).

Authors



T. TAKAHASHI



Y. IKOGI



H. IMANISHI



Y. KAKENO

Development of the Fuel Cell System for the Second-Generation Mirai

Osamu Yumita*¹
 Hiroyasu Kato*¹
 Shuya Kawahara*¹
 Takahiro Ito*²
 Ryoichi Namba*¹
 Tsutomu Shirakawa*¹

Abstract

The development of the fuel cell (FC) system for the second-generation Mirai succeeded in expanding production capabilities through further cost reductions and productivity improvements, while maintaining the humidifier-free design and cold start capability of the system adopted in the first-generation Mirai. At the same time, the performance (output and efficiency) of the FC system was enhanced while reducing size. This article focuses on the configuration of the FC system, the initiatives carried out to increase cruising range, and the approaches adopted to reduce noise.

Keywords: fuel cell (FC) system, cruising range, low noise, silicon carbide (SiC), FC stack

1. Introduction

Toyota launched the Mirai, the world’s first mass-produced fuel cell vehicle (FCV), in November 2014.

The fuel cell (FC) system in the first-generation Mirai was designed to realize excellent cold start performance, durability, and reliability. Building on these accomplishments, further enhancing the productivity and cost of the FC system was regarded as a critical goal to achieve wider popularization of fuel cell vehicles (FCVs) and to help realize a hydrogen energy based society in which cars, a central element of peoples’ lives, are powered by hydrogen (H₂).

Therefore, the FC system for the second-generation Mirai was designed to achieve even greater product appeal and user-friendliness through mass-production, lower costs, and an even longer cruising range.

This article describes the development of the FC system for the second-generation Mirai.

2. Second-Generation Mirai System Configuration

2.1 Hybrid system configuration

The basic electrical circuit of the system installed in the second-generation Mirai retains the same configuration as the system in the first-generation Mirai (**Fig. 1**).

It was also decided to achieve thorough cost reductions by using the same motor, power control unit (PCU), battery, and other component as those adopted in hybrid vehicles (HVs).

In addition, to increase cruising range by improving system

efficiency, a lithium-ion (Li-ion) secondary battery was adopted and silicon carbide (SiC) used in the FC boost converter (FCDC) (see Section 4.1.1).

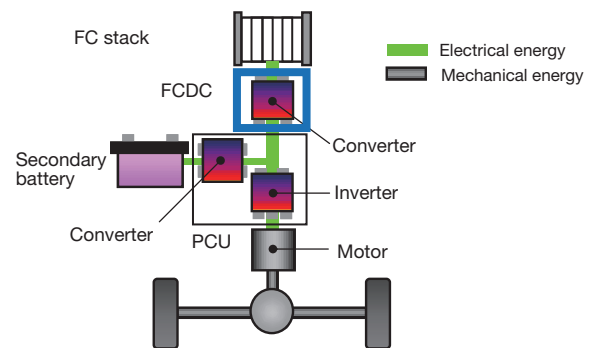


Fig. 1 HV System

2.2 FC system configuration

Similarly, the basic FC system circuit configuration containing flow paths for air, hydrogen, and coolant was also retained from the first-generation Mirai (**Fig. 2**). The development of the system for the second-generation Mirai focused on enhancing the performance of each of these components. For example, the air compressor (ACP) was changed from a compression-type Roots model to a turbo model, helping to reduce the size of the system by increasing the rotational speed.

In the same way as in the first-generation Mirai, the new system also ensures cold start performance and a humidifier-free design. In addition, the power rating of the FC was increased by approximately 20% to boost the dynamic performance of the vehicle.

*¹ Fuel Cell System Products Development Div., Toyota ZEV Factory

*² Denso Corporation

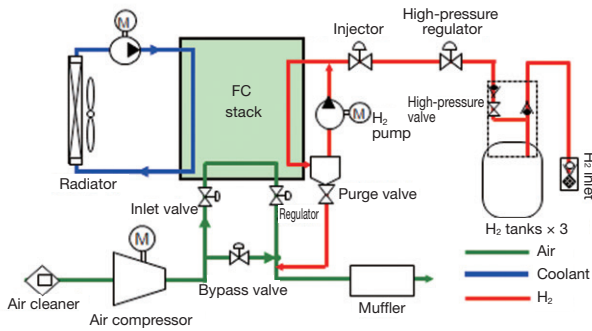


Fig. 2 FC System

3. FC System Integration and Size Reduction

The FC system in the second-generation Mirai is mounted under the hood. This was accomplished by integrating different elements of the system and reducing the size of individual components. The following sections describe some typical examples of these measures.

3.1 FC system integration

The following measures were taken to further enhance the product appeal of the second-generation Mirai: (1) reduce the size of the FC stack by using fewer cells, (2) develop a new fuel cell power control unit (FCPC) that integrates the high-voltage components that were mounted in different locations in the first-generation Mirai, and (3) adopt a turbo air compressor (ACP). The size of the FC system was substantially reduced by integrating these items, allowing the system to be mounted under the hood and achieving a consolidated component layout (Fig. 3).

These measures also allow the Mirai to be assembled on the same line as conventional vehicles, further enhancing the mass-production capability of the vehicle.

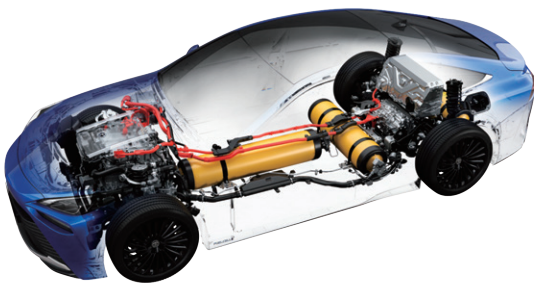


Fig. 3 Layout of FC System

3.2 Adoption of compact ACP

Common issues with turbo ACPs include low flow rates and surging that occurs in high-pressure ratio regions. In a system consisting of a compressor and pipes, surge is a phenomenon

that causes vibration in the direction of gas flow. Significant surging can cause gas to flow back from the compressor outlet toward the inlet. Flow division control was adopted to help avoid operating points in this region. Under this control, the ACP supplies a higher airflow rate than that required by the FC stack and diverts the excess flow rate to an air line bypassing the FC stack.

To realize this control, the pressure loss of the whole air supply system including the FC stack had to be identified. This was accomplished by creating a physical model of the system (i.e., model-based development). The model was divided into functional blocks representing each component from intake to exhaust (Fig. 4). The changes in the flow rate, pressure, temperature, and composition of each block were calculated in real time to estimate the pressure loss without using sensors. As a result, this control protects the ACP from surging while facilitating water management inside the FC stack, thereby further enhancing the power stability of the FC stack.

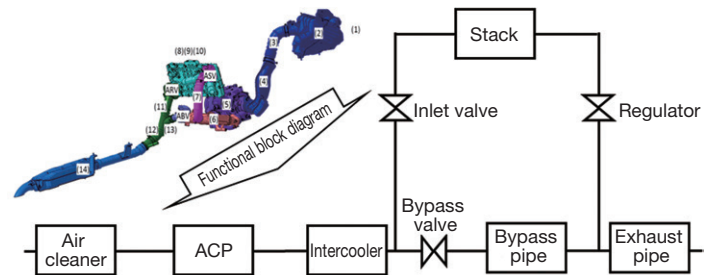


Fig. 4 Functional Blocks of Air System

4. Development to Maximize Fuel Efficiency (Enhancement of Cruising Range)

With hydrogen infrastructure still in the process of being established, extending the cruising range is an important challenge for FCVs.

For the second-generation Mirai, this was accomplished by enhancing fuel efficiency (i.e., the distance that can be driven using 1 kg of hydrogen) by approximately 10% and increasing the hydrogen storage capacity by approximately 20%, realizing a cruising range roughly 30% longer than the first-generation Mirai.

Higher fuel efficiency was achieved by enhancing the performance of the FC system components, such as by using SiC for the FCDC (Section 4.1.1) and adopting a Li-ion battery, and by enhancing controls such as the refresh control (Section 4.2).

4.1 Enhancement of FCDC efficiency

The role of the FCDC is to transmit power from the FC to the motor as efficiently as possible. The FCDC was originally adopted in the first-generation Mirai (Fig. 1). The following section describes the measures applied to enhance efficiency of the FCDC adopted in the second-generation Mirai.

4.1.1 SiC power semiconductors

New SiC power semiconductors (metal-oxide-semiconductor field-effect transistors (MOSFETs) and Schottky barrier diodes (SBDs)) were developed as low-loss FCDC switching devices. **Fig. 5** shows an outline of the intelligent power module (IPM) that comprises the FCDC and the configuration of the IPM circuit. **Fig. 6** shows the external appearance of a power card and the power semiconductors. The FCDC is a 4-phase boost converter and includes eight MOSFETs and eight SBDs (**Fig. 5**). To satisfy the requirements for an on-board device, temperature and current sensors are incorporated into the MOSFETs.

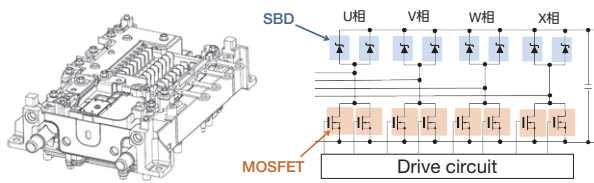


Fig. 5 Outline and Circuit Configuration of IPM

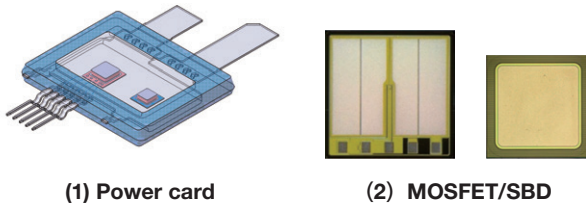


Fig. 6 External Appearance of Power Card and SiC Power Semiconductors

Fig. 7 compares the current/voltage characteristics and **Fig. 8** compares the switching waveforms of silicon (Si) IGBTs and SiC MOSFETs. Using the inherent characteristics of SiC, the developed MOSFETs reduced both conduction and switching losses.

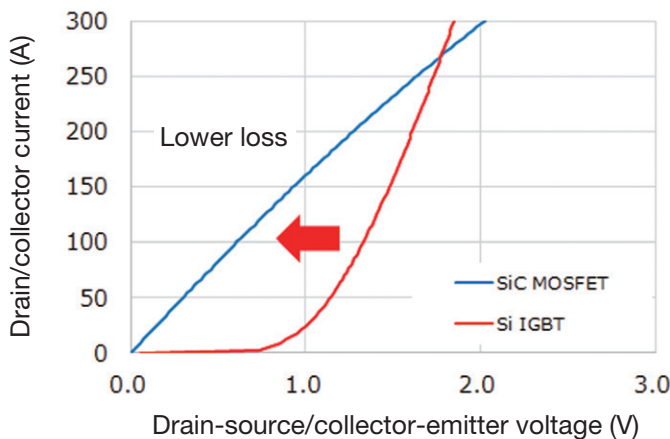


Fig. 7 Comparison of Current/Voltage Characteristics

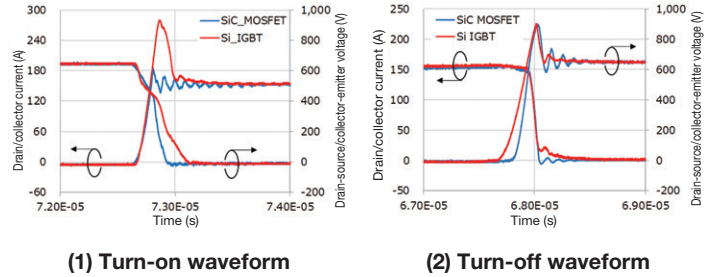


Fig. 8 Comparison of Switching Waveforms

Fig. 9 illustrates the total loss of the IPM. The total loss of the newly developed IPM is approximately 80% lower than the loss of the Si power semiconductor-based IPM in the first-generation Mirai. This reduction in loss helps to enhance the fuel efficiency of the vehicle.

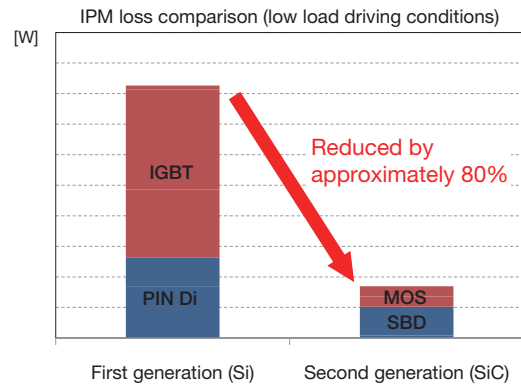


Fig. 9 Comparison of IPM Loss

4.2 Higher fuel efficiency through refresh control

Increasing the FC power generation efficiency is an important way of enhancing fuel efficiency.

In current load regions that impact fuel efficiency, the predominant form of energy loss is the energy required for the electron exchange process that occurs during electrochemical reactions in the electrodes. This energy loss in electrode reactions changes depending on the surface state of the platinum (Pt) catalyst. If the surface is in an oxidative state, catalytic activity falls. If the surface is in a reductive state, catalytic activity increases. Therefore, the FC power generation efficiency can be heightened by maintaining the surface of the Pt catalyst in a constant reductive state.

To realize this state, if power generation under low load continues for a predetermined time, the operating voltage of the FC is periodically and momentarily lowered to reduce the surface of the Pt catalyst. This is called “refresh control” (**Fig. 10**). This control facilitates efficient power generation, thereby helping to further enhance the fuel efficiency of the FC.

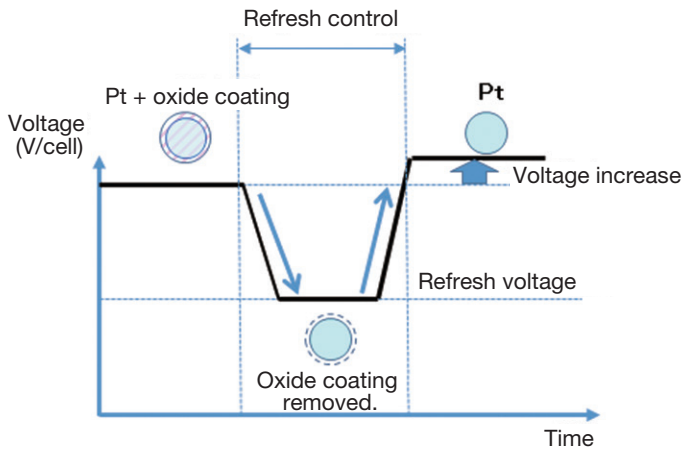


Fig. 10 Refresh Control

5. Noise Reduction

FCVs are expected to be extremely quiet due to the absence of an internal combustion engine. However, since hydrogen and oxygen must be supplied to the FC stack to generate power, the FC system contains various sources of vibration and noise. These include the ACP that supplies large volumes of air (Section 3.2), the injector that supplies the hydrogen, the hydrogen circulation pump, the high-pressure valve that shuts off the high-pressure gas, and so on. The development of the second-generation Mirai aimed to thoroughly reduce any noise not directly connected with driver operation to achieve an even greater level of comfort.

Some typical examples of these noise reduction efforts are described below.

(1) Operation noise of high-pressure valve

The high-pressure valve is a solenoid valve for the high-pressure hydrogen tanks. It functions to open and shut-off the supply of hydrogen to the tanks. In the Mirai, the valve opens and closes with a 700-bar pressure difference between the tank and the valve. The valve is particularly designed to shut off (close) the flow of hydrogen in an emergency, such as when a collision is detected. Vibration caused by operation of this solenoid valve is transmitted to the vehicle body via the tank frame. This vibration can be heard as noise inside the occupant compartment. To reduce this noise, the structural reliability and durability of the solenoid valve was ensured and an innovative method of applying current to the valve was adopted (Fig. 11). Specifically, when the valve is opened (or closed), the stepped current input was replaced by a control that increases (or decreases) the current gradually over a time curve, thereby reducing the operation noise of the valve and ensuring reliability without increasing costs (Fig. 12).

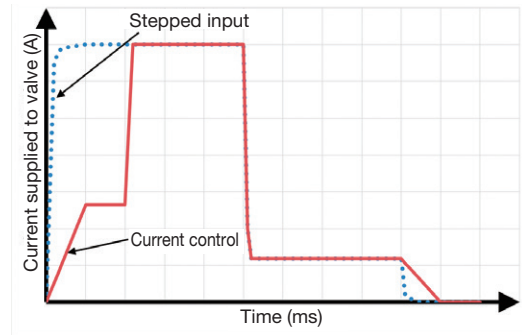


Fig. 11 Current Supply Time Chart

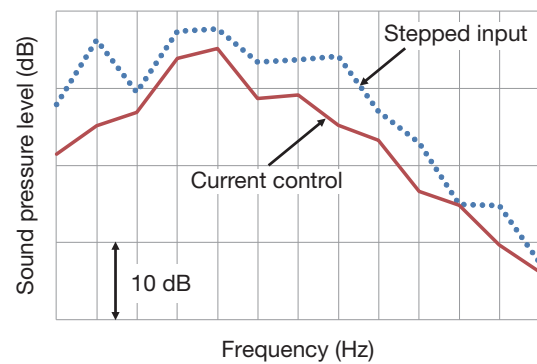


Fig. 12 Operation Noise Reduction by Gradual Current Change

(2) Bypass airflow noise

The air introduced from the ACP passes through the FC stack and the bypass pipe (Fig. 2). During wide-open throttle acceleration and the like, there is little airflow noise since the air is supplied to the high-capacity FC stack. In contrast, during regenerative braking and other occasions that requires the ACP to rotate at high speeds, the air must pass through the bypass pipe. This pipe is a source of airflow noise.

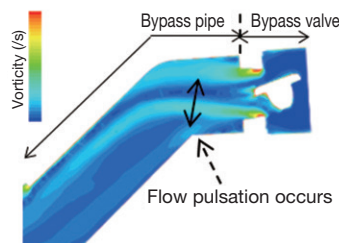


Fig. 13 Flow Field (before Countermeasure Applied)

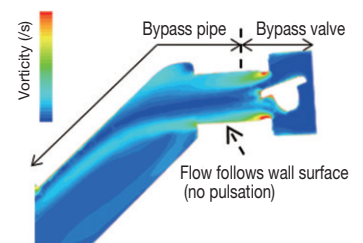


Fig. 14 Flow Field (after Countermeasure Applied)

As shown in Fig. 13, the difference in diameter between the bypass valve in the bypass pipe and the joint creates a sudden change in cross-section. As a result, flow separation occurs immediately after the bypass valve, which causes pulsation. A countermeasure was applied to the flow source by extending the flat part of the pipe, which allows the flow to follow the wall and reduces the pulsation (Fig. 14). This measure reduced the sound pressure by over 10 dB (Fig. 15).

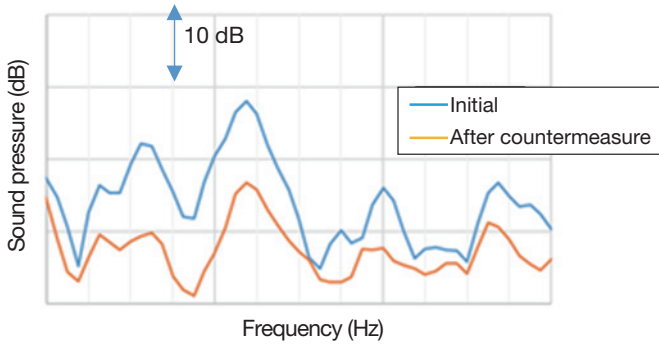


Fig. 15 Sound Pressure Reduction Effect

6. System Control in Freezing Environments

The development of the FC system for the second-generation Mirai aimed to further enhance the cold start performance realized in the first generation, boost the power response immediately after a cold start, and improve the controllability of the FC stack operating point.

6.1 Higher power immediately after cold start

The FC system in the second-generation Mirai utilizes the rapid warm-up control developed for the first generation (Fig. 16). Then, to boost the power response immediately after a cold start, the operating point of the FC system is set to a higher current than the system in the first-generation Mirai (Fig. 17) to raise the rate of temperature increase by drawing more heat from the stack. As a result, at least 50 kW is available from the FC system immediately after a start at -30°C , which is roughly 2.5 times higher than the available power of the first-generation Mirai (approximately 20 kW).

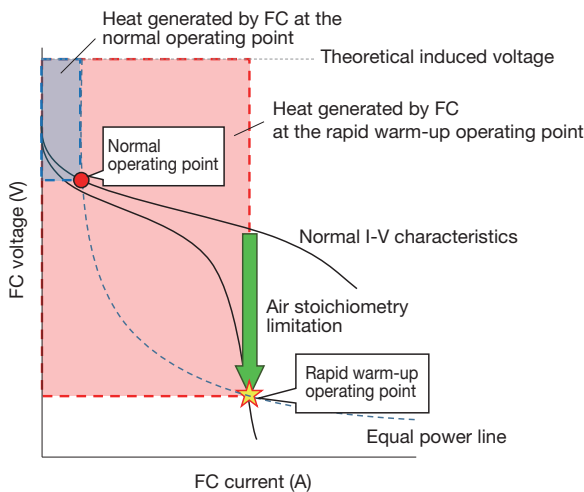


Fig. 16 Illustration of Rapid Warm-Up Control

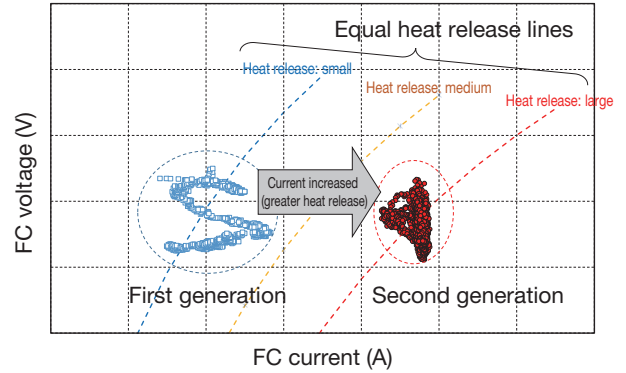


Fig. 17 Comparison of Rapid Warm-Up Operating Points

6.2 Improved controllability of FC stack operating point

To realize the operating points shown in Fig. 17, the appropriate airflow commands must be issued in accordance with the state of the FC stack, which changes during the warm-up process.

During the development of the FC system control for the second-generation Mirai, the state of the FC stack was precisely modelled so that the airflow can be calculated and controlled factoring in the power and overvoltage characteristics during the warm-up process. This approach improved the controllability of the FC stack operating point, thereby helping to ensure cold start performance (Fig. 18).

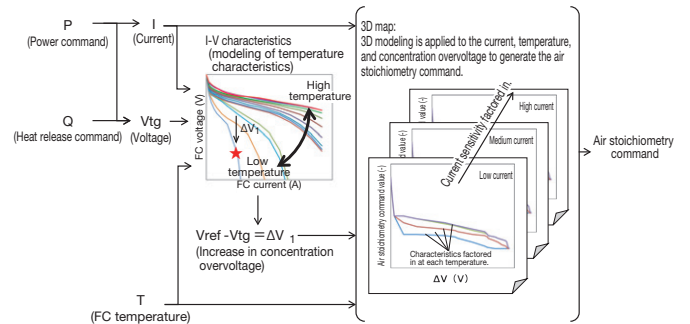


Fig. 18 Determination of Airflow Commands by Rapid Warm-Up Control

7. Summary

The development of the FC system for the second-generation Mirai succeeded in enhancing the dynamic performance and cruising range of the vehicle, while maintaining the humidifier-free design and cold start performance of the system adopted in the first-generation Mirai. Reducing the size of the FC system components and achieving greater system integration enabled the FC system to be mounted under the hood. The development also helped to emphasize the inherent merits of an FCV by achieving a quieter and more comfortable ride.

8. Conclusion

This development is the result of extensive cooperation between Toyota, the people who chose to purchase and drive the first-generation Mirai, dealers, partner companies, suppliers, hydrogen infrastructure companies, the relevant government ministries, and local authorities. The authors would like to express their gratitude to everyone involved.

To help establish a hydrogen energy based society as a viable option for future generations, Toyota intends to utilize the knowledge it gained during this development to further lower the price and enhance the performance of the FC system.

References

- (1) Y. Nonobe et al. "Development of the Fuel Cell System in the Mirai FCV." *Toyota Technical Review* Vol. 61 (2015) pp. 15-20.
- (2) M. Kondo et al. "The High-Pressure Hydrogen Storage System for the Mirai FCV." *Toyota Technical Review* Vol. 61 (2015) pp. 27-32.
- (3) S. Mizuno et al. "Development of High Performance and Low Cost Fuel Cell Stack." *Toyota Technical Review* Vol. 61 (2015) pp. 21-26.

Authors



O. YUMITA



H. KATO



S. KAWAHARA



T. ITO



R. NAMBA



T. SHIRAKAWA

Development of the Fuel Cell Stack for the Second-Generation Mirai

Seiji Mizuno*¹
 Tomokazu Hayashi*¹
 Hideki Kubo*¹
 Masao Okumura*¹
 Takuya Kurihara*¹
 Kazuhiro Mori*¹

Abstract

The first-generation Mirai was launched in November 2014 as the world's first commercial fuel cell vehicle (FCV). Compared to the fuel cell (FC) stack used in the first-generation Mirai, the FC stack in the second-generation Mirai achieved one of the highest power densities in the world (5.4 kW/L, excluding end plates) by adopting innovative material technologies for the cell flow field structure and electrodes to boost performance and reduce size. In addition to installing the FC stack under the hood of the vehicle, a new external filling constraint structure was adopted to help prevent cell deviation. These measures enhanced the gravitational acceleration (G)-resistant characteristics of the FC stack by 1.6 times, thereby helping to ensure impact performance. Furthermore, measures to help reduce costs and facilitate mass production included halving the amount of platinum (Pt) used in the electrocatalyst, adopting a continuous roll-to-roll production process for the titanium bipolar plate nano composite (NC) surface treatment, and achieving a high-speed adhesion process by redesigning the cell sealing structure. These measures helped to reduce the cost of the FC stack by three-quarters, leading to dramatic improvements in productivity.

Keywords: fuel cell (FC) stack, cell, power density, flow field structure, surface treatment, electrode, catalyst, gravitational acceleration (G) resistance, low cost, mass production

1. Introduction

The pioneering first-generation Mirai was launched in November 2014 as the world's first commercial fuel cell vehicle (FCV).⁽¹⁾ Based on the fuel cell (FC) stack used in the first-generation Mirai, the mass production FC stack in the second-generation Mirai was developed to facilitate the further popularization of FCVs by realizing greater performance and lower costs.

This newly developed FC stack achieves one of the highest power densities in the world (5.4 kW/L, excluding end plates) by adopting an innovative cell flow field structure and electrodes to boost performance and reduce size. In addition, by integrating the FC stack with the FC system (including components such as the FC boost converter (FCPC) and pumps), it was possible to mount the whole system under the hood of the vehicle (**Fig. 1**).

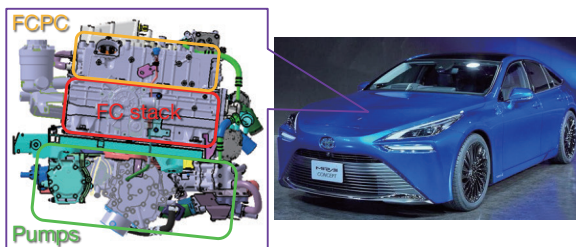


Fig. 1 Under-Hood Layout of FC Stack in the Second-Generation Mirai

In addition, measures to help reduce costs and facilitate mass production included reducing the amount of high-cost special FC materials and precious metal platinum (Pt) used in the electrocatalysts, adopting a continuous roll-to-roll production process for the bipolar plate nano composite (NC) surface treatment, and achieving a high-speed adhesion process by redesigning the cell structure. These measures helped to reduce the cost of the FC stack by three-quarters.

This article describes the innovative cell flow field structure and electrodes, which are the key technologies for enhancing the performance and reducing the size of the FC stack. It also details the technologies for enhancing the reliability of the FC stack against impacts in its new location under the hood, as well as technologies for reducing cost and enabling mass production.

2. Enhancing FC Stack Performance

Raising current density (i.e., increasing the available sweep current per unit area of the electrodes) is an important way to realize a higher performance and more compact FC stack. This was accomplished by adopting innovative cell flow field structure and electrode materials, by enhancing the capability of the FC stack to remove the large volumes of water generated in high-current regions, and by promoting oxygen diffusion to the electrocatalyst layer. As a result, the power of the FC stack was increased by 15% per unit area of the electrodes.

*¹ Fuel Cell Products Development Div., Toyota ZEV Factory

2.1 Innovative cell flow field structure

With a cell flow field structure consisting of conventional straight channels, the generated water tends to accumulate inside the flow field and electrodes. This water inhibits oxygen diffusion and affects the stability of power generation (Fig. 2).⁽²⁾

For this reason, an innovative three-dimensional (3D) fine-mesh air flow field consisting of a fine 3D lattice was developed for the FC stack in the first-generation Mirai. This approach used the hydrophilic properties of the flow field structure to rapidly draw up generated water discharged from the electrode surfaces, thereby helping to restrict the inhibition of oxygen diffusion and boost performance (Fig. 3).

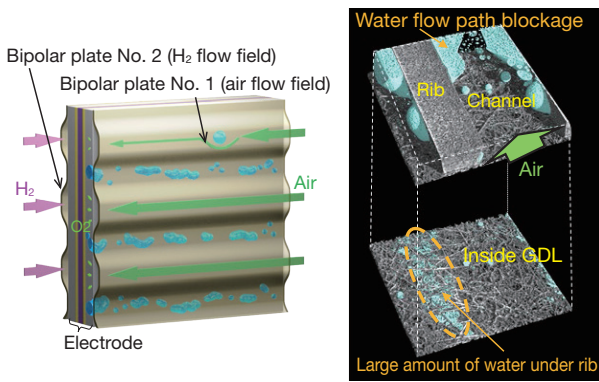


Fig. 2 State of Residual Water in Straight Channel Structure

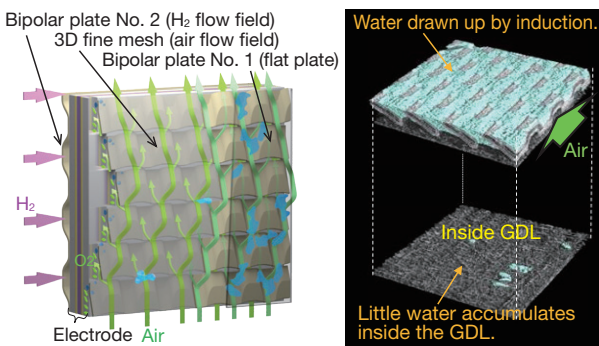


Fig. 3 State of Residual Water in 3D Fine-Mesh Flow Field (X-Ray Computerized Tomography (CT))

In contrast, for the FC stack in the second-generation Mirai, a new partially narrow straight flow field was developed to reduce the number of cell components (the number of titanium bipolar plates was reduced from three to two) and increase the power generation area utilization rate (the manifold layout was changed from four to two sides). By providing narrow portions in the straight flow channels, a pressure loss is generated that forcibly draws in air to the electrode gas diffusion layer (GDL), thereby enhancing the water removal performance and oxygen diffusivity (Fig. 4).⁽³⁾

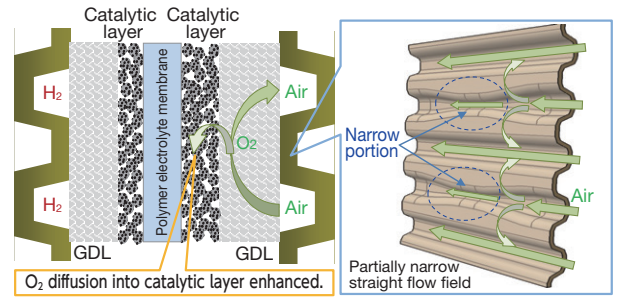


Fig. 4 Partially Narrow Straight Flow Field (Air Drawn into GDL)

With a partially narrow straight flow field, there is little residual generated water inside the electrodes. As a result, the oxygen concentration on the surface of the catalytic layers is twice as high as with conventional straight channels, which enables the same oxygen diffusivity as the 3D fine-mesh flow field (Fig. 5).

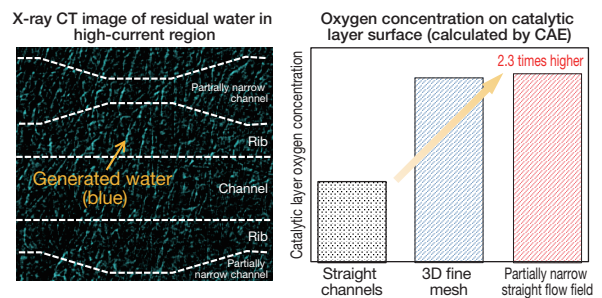


Fig. 5 Visualization of Generated Water and Oxygen Diffusivity of Partially Narrow Straight Flow Field

Fig. 6 shows the cell structure of the FC stack in the second-generation Mirai. The hydrogen flow field is wavy, which has the effect of creating a more uniform flow distribution in the cell and improving the water removal performance of the cell compared to the 2-turn, 3-step cascade flow field adopted in the first-generation Mirai. In addition, flowing the air and hydrogen in opposite directions creates a good water balance on the electrode surfaces by circulating the generated water inside the cell, thereby enabling stable power generation performance and maintaining the humidifier-free design of the FC system.

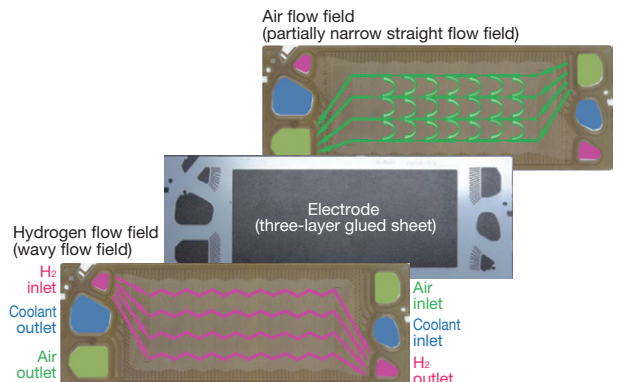


Fig. 6 Cell Structure of FC Stack in the Second-Generation Mirai

Special Feature

2.2 Innovative electrodes

As shown in **Fig. 7**, substantial improvements in physical electrode material properties were achieved for the electrodes used by the FC stack in the second-generation Mirai. These improvements increased the amount of power generation per unit area (i.e., the current density) of the electrodes.

In particular, innovative catalyst and ionomer materials were adopted in the catalytic layers. One example is the carbon support of the catalysts. Although the solid carbon adopted in the previous catalysts increased the Pt utilization rate by loading the Pt on the surface, this also had the effect of lowering activity due to sulfonic acid cover poisoning. This issue was addressed by adopting a new porous form of carbon called mesoporous carbon nano dendrites (MCND). MCND is provided with extremely small mesopores that cannot be penetrated by the ionomer. As a result, around 80% of the Pt is loaded inside the MCND, preventing direct contact between the Pt and the ionomer and suppressing sulfonic acid cover poisoning. By combining this material with a platinum-cobalt (PtCo) alloy catalyst with higher solid solubility (i.e., a material with greater dispersion), catalytic activity was increased by approximately 50% (**Fig. 8**). In addition, a new highly oxygen-permeable ionomer was adopted with an oxygen diffusion performance three times greater than the previous material. Furthermore, a new molecular structure with a higher acid functional group density was developed that increases proton conductivity by a factor of 1.2 (**Fig. 9**).

Next, raising the reinforcing layer ratio of the polymer electrolyte membrane resulted in higher strength (the yield strength was increased by approximately ten-fold), lower oxygen crossover, and allowed the adoption of a thinner membrane (approximately 29% thinner). These measures helped to increase proton conductivity by a factor of 1.4.

The gas diffusivity of the GDL was improved by 25% by lowering the density of the carbon paper substrate and increasing the diameter of the pores.

The innovative cell flow field structure and electrodes described above had the following effects: lower concentration overvoltage due to improved gas diffusion, lower resistance overvoltage due to improved proton conductivity, and lower active overvoltage due to improved catalytic activity. As a result, the maximum power of the electrode per unit area was raised by 15% (**Fig. 10**).

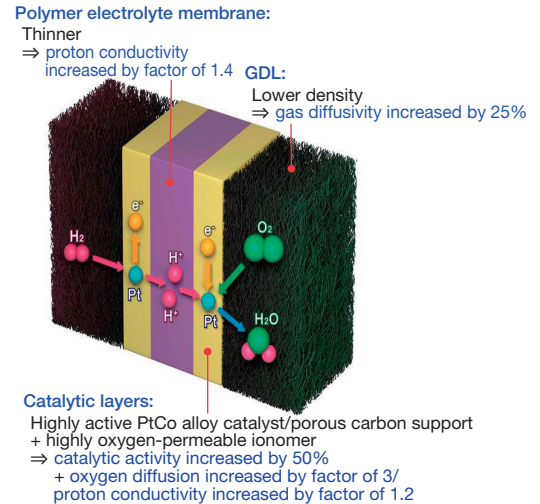


Fig. 7 Electrode Specifications of FC Stack in the Second-Generation Mirai

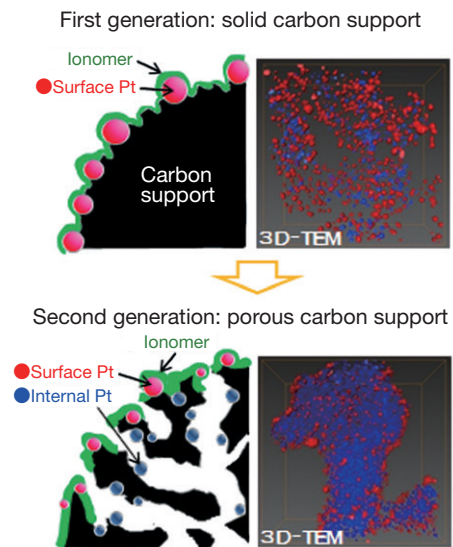


Fig. 8 Porous Carbon Support (MCND)

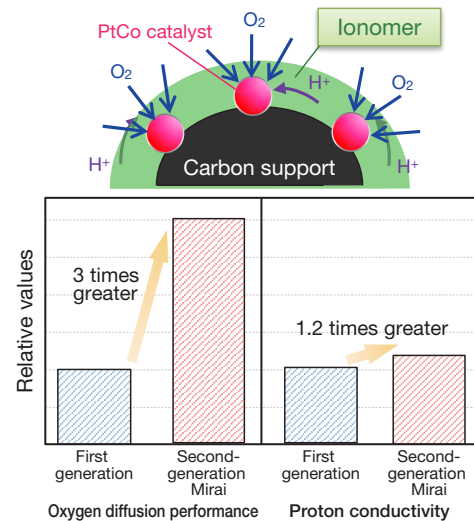


Fig. 9 Physical Properties of Highly Oxygen-Permeable Ionomer

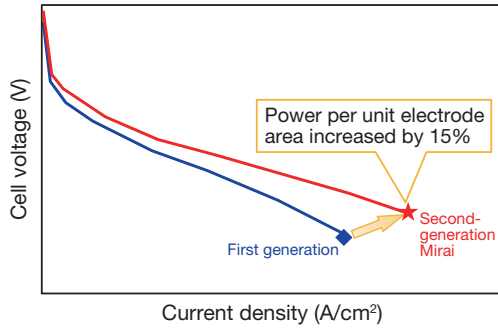


Fig. 10 Performance of FC Cells in Second-Generation Mirai (I-V Characteristics)

3. Size and Weight Reduction of FC Stack (Power Density)

By increasing the performance of the cells in the second-generation Mirai, power per cell was raised by 26%, boosting the maximum power of the FC stack from 114 to 128 kW. The size and weight of the FC stack were reduced by adopting thinner cells (the cell thickness was reduced from 1.34 to 1.11 mm, Fig. 11) as well as thinner and fewer bipolar plates (the bipolar plate thickness was reduced from 0.13 to 0.10 mm and the number of plates was reduced from 3 to 2). The number of cells in the layers was also reduced (from 370 to 330) due to the substantial 20% increase in the available sweep current. As a result, the volume of the FC stack in the second-generation Mirai was reduced from 33 to 24 liters, and the weight from 41 to 24 kg (Fig. 12).

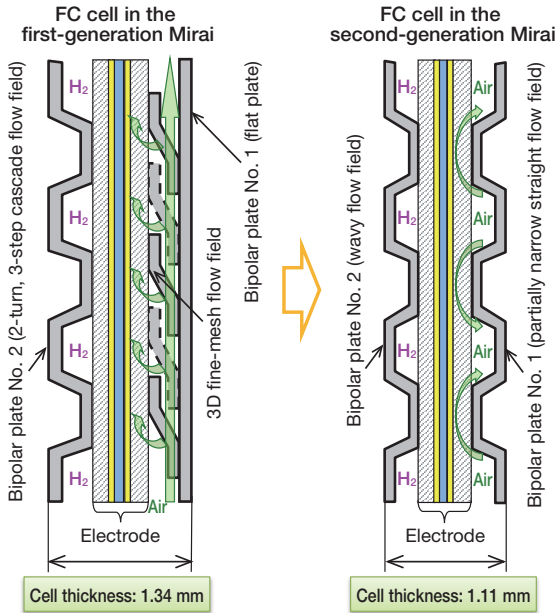


Fig. 11 Reduction of FC Cell Thickness

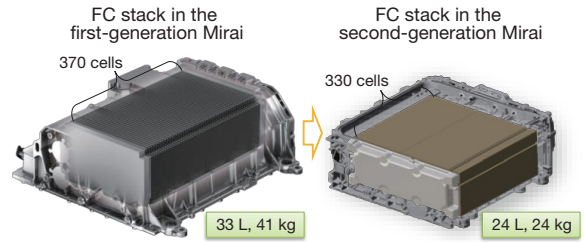


Fig. 12 Size and Weight of Stack (Excluding End Plates)

These measures to boost performance while reducing size and weight helped to realize one of the highest volumetric power density values in the world (5.4 kW/L, up from the 3.5 kW/L achieved by the previous FC stack), and a mass power density of 5.4 kW/kg, up from the 2.8 kW/kg achieved by the previous FC stack (Fig. 13).

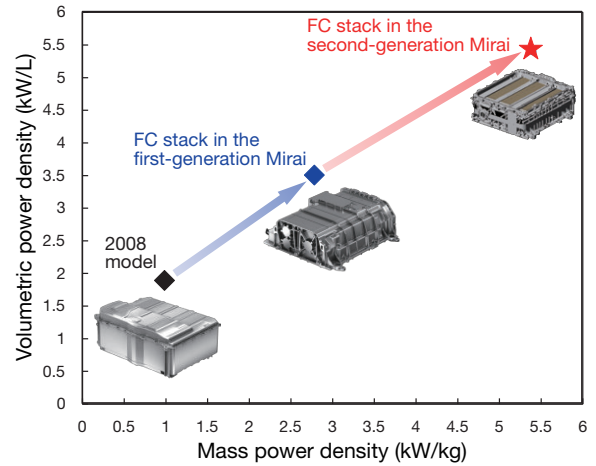


Fig. 13 FC Stack Power Density (Excluding End Plates)

4. Reliability of Under-Hood Layout of FC Stack

With the new under-hood layout, the gravitational acceleration (G)-resistant characteristics of the stack needed to be enhanced to withstand a collision.

From the standpoint of ensuring the high-voltage and hydrogen safety of the FC stack in the event of an impact, it is necessary to prevent sealing defects occurring between the cell layers due to cell layer deviation. The FC stack maintains its layered cell structure using the tightening force and the friction constraint force generated by the friction coefficient between the cells. If a major impact occurs that exceeds the friction constraint force, the external constraint force must be sufficient to restrict cell layer deviation below the required value. The FC stack in the first-generation Mirai used the inertial force of the impact to actively warp the layered cell structure and restrict cell layer deviation below the required value using the resulting reaction force created through contact with the stack case. This approach enabled the FC stack to handle a wide range of impact inputs (Fig. 14).

Special Feature

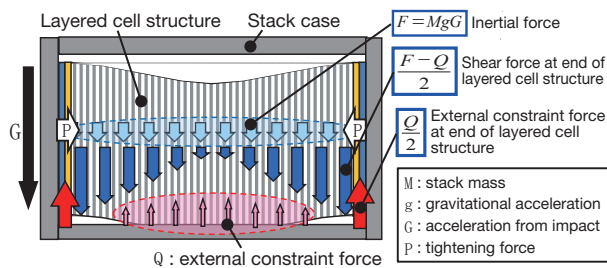


Fig. 14 External Case Constraint of FC Stack in the First-Generation Mirai

In contrast, the FC stack in the second-generation Mirai adopts a newly developed filling-based external constraint structure (Fig. 15). This filling material consists of blocks of silicone rubber highly packed with micro alumina particles, which are used to fill the gaps between the layered cell structure and stack case. Since this filling material has dilatancy characteristics that harden the material in reaction to the rapid application of force, the material can support the warping of the layered cell structure due to the impact and restrict cell deviation. This measure improved the G-resistance performance of the FC stack by a factor of 1.6 compared to the previous approach, thereby helping to ensure the reliability of the FC stack against inputs in its new location under the hood.

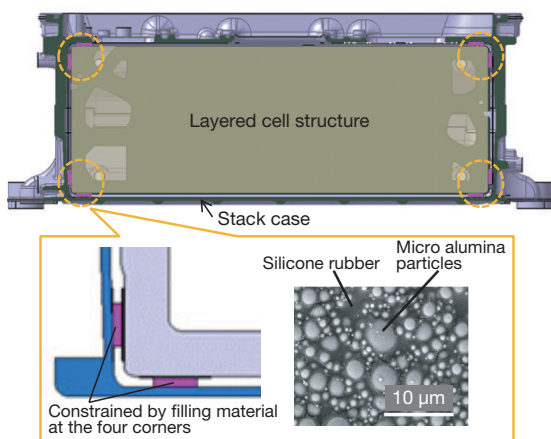


Fig. 15 Filling-Based External Constraint Structure of FC Stack in the Second-Generation Mirai

5. Cost Reduction and Mass Production of FC Stack

An important aspect of lowering the cost of the FC stack was to reduce the usage amount of high-cost special FC materials, as well as the amount of precious metal Pt in the catalyst, which does not generate an economy of scale.

The size of the cells of the FC stack in the second-generation Mirai was reduced by 20% through the adoption of an innovative cell flow-field structure and electrodes, which increased the current density and the power generation area

utilization rate. Combined with the reduction in the number of cells due to the higher current density, the thinner polymer electrolyte membrane, the reduction in the thickness and number of the Ti bipolar plates, and the increase in catalytic activity, the amount of Pt used in the FC stack was halved (Fig. 16) and the cost was reduced by three-quarters.

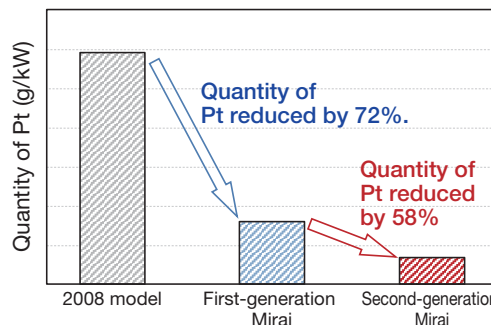


Fig. 16 Reduction in Amount of Catalytic Pt per Unit Power

In addition, the mass-production capability of the FC stack was improved by adopting an innovative cell adhesion sealing structure. The ethylene propylene rubber (EPDM) vulcanization adhesion approach of the previous FC stack was replaced by three-layer thermal plasticity adhesion and ultraviolet (UV) radiation curing, enabling an adhesion time faster by a factor of approximately 100 (a process that took several minutes can now be completed in several seconds, Fig. 17).

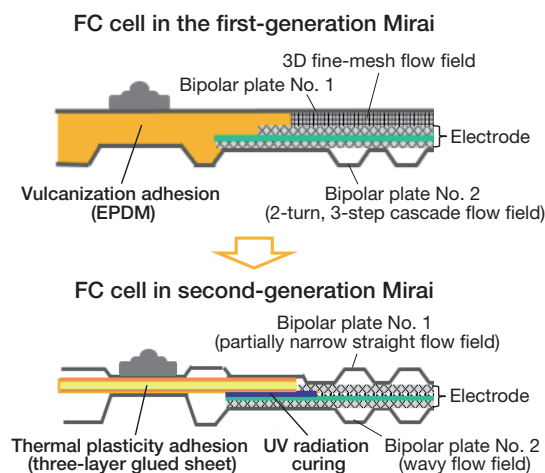


Fig. 17 Adhesion Sealing Structure of FC Cells

This three-layer glued sheet is created by laminating hot melt adhesion layers to both sides of a polyethylene naphthalate (PEN) substrate. This approach enables the optimum amount of stretching and heat fixing to restrict dimensional changes when the cells are created (Fig. 18).

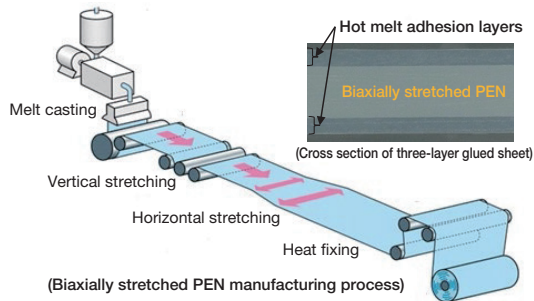


Fig. 18 Structure of Three-Layer Glued Sheet

Previously, the surface treatment of the Ti bipolar plates adopted a sheet processing technique in which a carbon nano-coating (π -conjugated amorphous carbon) called PAC was applied to the bipolar plates using plasma chemical vapor deposition (CVD) after stamping (**Fig. 19**). This was replaced by a newly developed nano composite (NC), which enabled the adoption of a continuous roll to roll process using Ti foil. The NC surface treatment layer has a composite structure of carbon and titanium dioxide (TiO_x). This layer is conductive, corrosion-resistant, and highly adhesive, which means that stamping can be carried out after the surface treatment (**Fig. 20**).

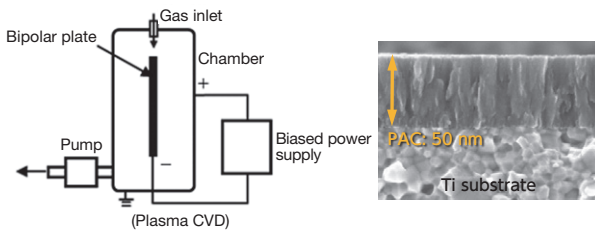


Fig. 19 Carbon Nano-Coating Surface Treatment (First-Generation Mirai)

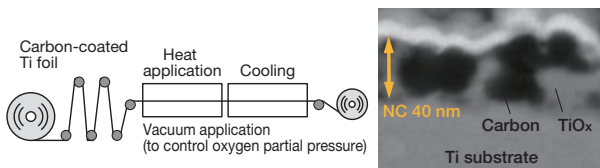


Fig. 20 NC Surface Treatment (Second-Generation Mirai)

6. Conclusion

With the aim of encouraging the further popularization of FCVs, an innovative, high performance, and compact FC stack was developed and adopted for the second-generation Mirai. This FC stack achieved one of the highest power densities in the world (5.4 kW/L, excluding end plates).

In addition, the amount of high-cost special FC materials and Pt used in the catalysts were reduced to help reduce costs and facilitate mass production. These measures lowered the cost of the FC stack by three-quarters. Rapid production with cycle

times reduced from several minutes to several seconds was achieved by adopting an innovative cell adhesion structure.

This development of a new good quality and reasonably priced (*ryohin-renka*) FC stack has enhanced the product appeal of FCVs and represents an important step toward the realization of a hydrogen-based society.

Finally, the authors would like to extend their sincere gratitude to everyone that supported this development.

References

- (1) S. Mizuno et al. "Development of High Performance and Low Cost Fuel Cell Stack." *Toyota Technical Review* Vol. 65 (2019) pp. 49-56.
- (2) M. Maeda et al. "Analysis of Water Distribution in a Fuel Cell Using X-Ray Computed Tomography." *Denso Technical Review* Vol. 13 No. 1 (2008) pp. 37-43.
- (3) A. Ida et al. "Application of CFD to the New Fuel Cell Vehicle." *Forum Text of the JSAE Annual Congress (Spring)* No. 15 Forum 14 (2015) pp. 63-66.

Authors



S. MIZUNO



T. HAYASHI



H. KUBO



M. OKUMURA



T. KURIHARA



K. MORI

Development of the High-Pressure Hydrogen Storage System for the Second-Generation Mirai

Akira Yamashita*¹
 Kotaro Nakamichi*²
 Takashi Ino*²
 Koji Kida*¹
 Hiroki Yahashi*¹
 Sogo Goto*¹

Abstract

This article describes the evolution of the high-pressure hydrogen storage system developed for the second-generation Mirai with the aim of helping to further popularize fuel cell vehicles (FCVs). New high-pressure hydrogen tanks with three different lengths were developed to store the necessary amount of hydrogen in the system without sacrificing the interior space of the sedan-type vehicle. Some of the lightest tanks in the world (weight effectiveness: approximately 6.0 wt%) were developed by adopting a new high-strength carbon fiber that reduced the fiber content of the tanks. Mass-production capabilities were increased and major cost savings were achieved by adopting a newly developed rapid-curing epoxy resin for the carbon fiber reinforced plastic (CFRP) used in the tanks, and by adopting new machining methods for the high-pressure valves and pressure regulator. The same high filling efficiency as the previous system was maintained despite the adoption of three tanks with significantly different volumes by measures such as optimizing the temperature sensor layout. In addition, the developed tanks and valves obtained certification under United Nations Regulation 134 (UN-R134), which was established to allow mutual recognition of FCVs and other vehicles.

Keywords: *high-pressure hydrogen storage system, high-pressure hydrogen tanks, carbon fiber, cost reduction, industrial innovation, high-pressure valve*

1. Introduction

Toyota is currently developing a wide range of vehicles and products to help popularize the utilization of electricity and hydrogen, which are regarded as promising energy sources to help facilitate the coexistence of vehicles with the global environment. Toyota started developing fuel cells (FCs) in 1992 and developed a new 70 MPa high-pressure hydrogen storage system for the Mirai fuel cell vehicle (FCV) sedan in 2014. This system helped the Mirai to reduce costs and achieve a driving range equivalent to that of a conventional gasoline vehicle. As a result, the Mirai can be regarded as the world's first practical mass-production FCV. A new high-pressure hydrogen storage tank system has now been developed with the aim of achieving mass-market penetration. In addition to further performance gains in weight reduction and packaging, this new hydrogen storage tank system helped to lower costs and realize higher product appeal than the system in the first-generation Mirai.

2. System Configuration

2.1 Tank installation layout

One of the advantages of an FCV is a longer driving range than an electric vehicle (EV). The driving range of the second-generation Mirai was extended further by increasing both the fuel efficiency and the hydrogen capacity (up to approximately 5.6 kg) of the FC system. **Fig. 1** shows the installation layout of the high-pressure hydrogen tanks. The second-generation Mirai makes use of the center tunnel to mount three tanks without sacrificing interior space.

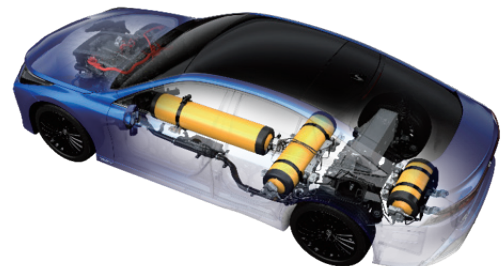


Fig. 1 Installation Layout of High-pressure Hydrogen Tanks

To ensure sufficient holding force in response to longitudinal acceleration, a new neck-mounted fixing structure was adopted for the tank mounted in the center tunnel (**Fig. 2**).

*¹ Fuel Cell Products Development Div., Toyota ZEV Factory

*² Material Engineering Div. No. 1, Advanced R&D and Engineering Company

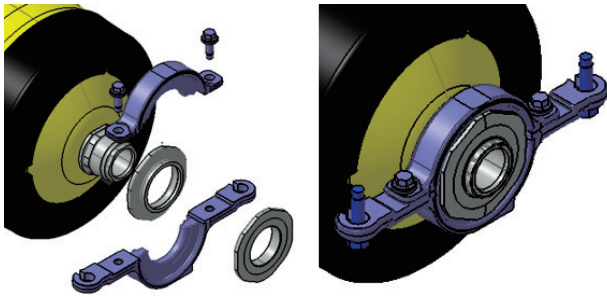


Fig. 2 Neck-Mounted Fixing Structure

Fig. 3 shows the basic outline of the high-pressure hydrogen storage system. Table 1 lists the specifications of the high-pressure hydrogen tanks. High-pressure hydrogen is supplied from three tanks with the same diameter but different lengths. The hydrogen pressure supplied from the tanks is reduced in two stages by a high-pressure regulator and injector before reaching the FC stack.⁽²⁾

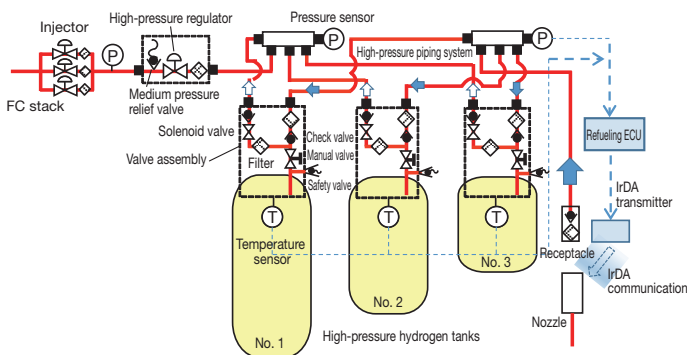


Fig. 3 Basic Configuration of High-Pressure Storage System

Table 1 Main Specifications of High-Pressure Hydrogen Tanks

Nominal working pressure (MPa)	70
Type	4 (plastic liner)
Size (mm)	Tank No. 1: diameter = 299, length = 1,467
	Tank No. 2: diameter = 299, length = 1,201
	Tank No. 3: diameter = 299, length = 683.5
Internal volume (L)	Tank No. 1: 64.9, No. 2: 52.0, No. 3: 25.3
	Tank No. 1: 43.0, No. 2: 36.7, No. 3: 22.5
	(The above figures do not include the hydrogen gas and valves.)
Effective hydrogen storage mass (kg)	Approximately 5.6 (according to Japanese Electric Vehicle Association Standards (JEVS))
Regulatory and standard compliance	UN-R134

3. Outline of Development

3.1. Mass-production technologies for longer tanks

3.1.1 Structure of high-pressure hydrogen tanks

Fig. 4 shows the structure of the high-pressure hydrogen tanks. The high-pressure hydrogen tanks are composed of a plastic liner at the innermost layer that functions to seal in the hydrogen gas, surrounded by a strong carbon fiber reinforced plastic (CFRP) layer capable of withstanding the internal pressure of the tank. This is then surrounded by a glass fiber reinforced plastic (GFRP) layer with high impact resistance. Aluminum bosses are provided at both ends of the plastic liner for valve fitting.

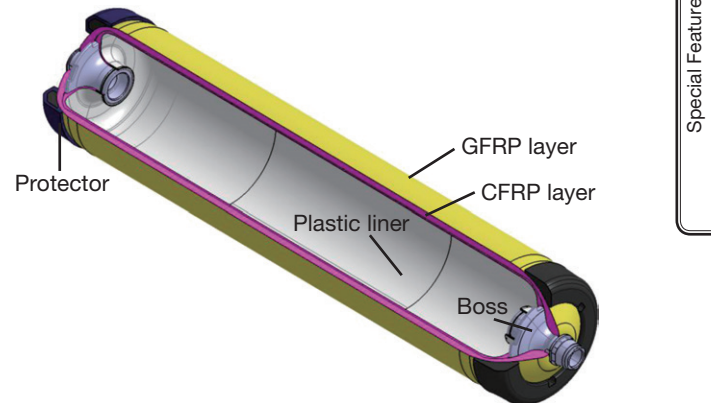


Fig. 4 Structure of High-Pressure Hydrogen Tanks

3.1.2 Development of tow prepreg

The CFRP layer is formed by filament winding (FW) tow prepreg (TPP) at high speed. TPP is a fiber bundle (called a “tow”) impregnated in advance with epoxy resin in an unhardened state. Fig. 5 shows the filament winding pattern. This article describes the carbon fiber and epoxy resin used for the newly developed TPP.

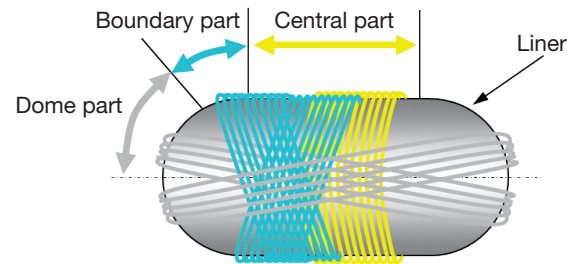


Fig. 5 Lamination Pattern of High-Pressure Hydrogen Tanks

3.1.3 Development of high-strength and highly elastic carbon fiber

The strength of the commercial type carbon fiber adopted for the tanks on the first-generation Mirai was further increased for

the second generation. Strength and elasticity were improved by approximately 4% from the previous model with the cooperation of the carbon fiber manufacturer. Using this carbon fiber reduced the number of CFRP layers by approximately 7%, thereby helping to realize smaller and lighter tanks.

3.1.4 Development of rapid-cure epoxy resin

A new epoxy resin was developed in cooperation with material manufacturers to shorten the duration of the curing process while maintaining the pot life (i.e., the usable time), which are characteristics that tend to have a trade-off relationship. To take advantage of the performance of this rapid-cure epoxy resin, the rate of temperature increase in the curing conditions was increased by approximately five times, and the soak temperature was raised by 15°C at the same time (Fig. 6).

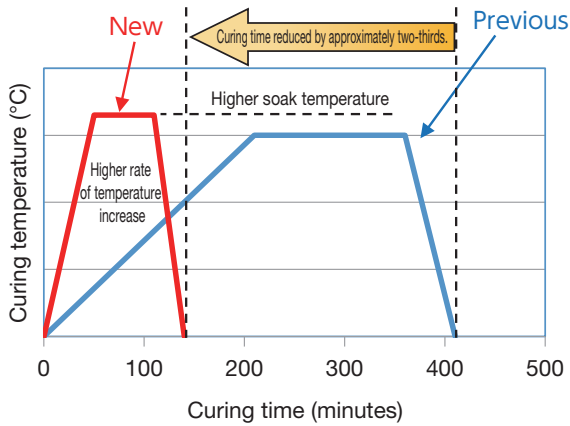
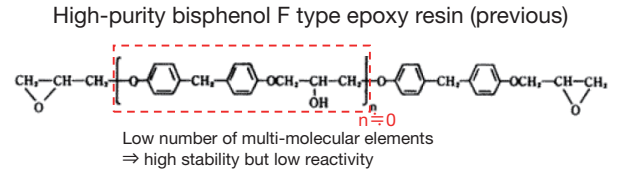


Fig. 6 Temperature Profile of High-Pressure Hydrogen Tank Curing Process

The materials-based technical approach for shortening the curing time was as follows. Previously, pot life was controlled using the main resin ingredient, which was a low-reactivity high-purity bisphenol F type epoxy resin. However, to shorten the curing time and reduce cost, the main ingredients were changed to a general-purpose bisphenol A type epoxy resin combined with a reactive diluent with an epoxy group at the end. Fig. 7 shows the differences in the chemical structure of the main epoxy resin ingredients. In addition, using the reactive diluent to reduce the initial viscosity helps to achieve an excellent balance between a short curing time and pot life (Fig. 8).



General-purpose bisphenol A type epoxy resin + reactive diluent (new)

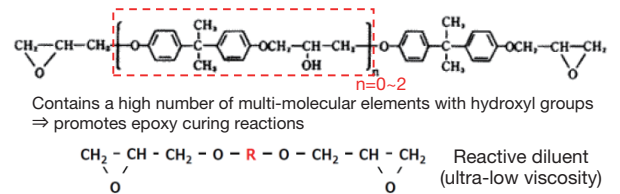


Fig. 7 Differences in Chemical Structures of Main Epoxy Resin Ingredients

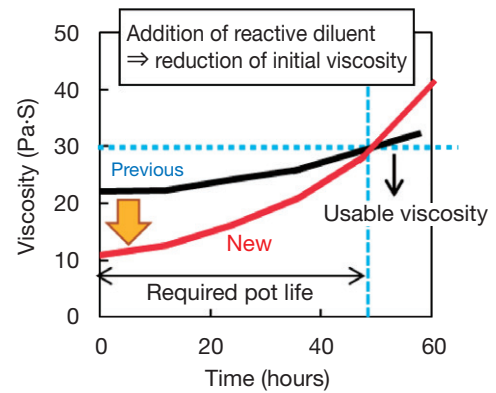


Fig. 8 Approach to Ensure Pot Life

However, it was found that the revised curing conditions shown in Fig. 6 might promote oxidative degradation (yellowing) of the inner liner surface. This oxidative degradation was restricted by changing the pressurization medium during the curing process to nitrogen and greatly lowering the oxygen concentration. By developing a new epoxy resin with a shorter curing time and optimizing the tank curing process, significant gains in productivity (the curing process duration was shortened by approximately two-thirds) and cost reductions were achieved.

3.2 Mass-production technologies for high-pressure system parts

3.2.1 High-pressure valves

A new manufacturing method was adopted for the high-pressure valves to further improve productivity and reduce cost. Continuous casting aluminum materials suitable for mass production were adopted for the valve body. In addition, the material yield was increased by 20% compared to the previous valves by adopting near net shape forging, which forms the materials into a shape resembling the final valve in advance.

Furthermore, the number of forging steps was reduced by optimizing the forging die shape.

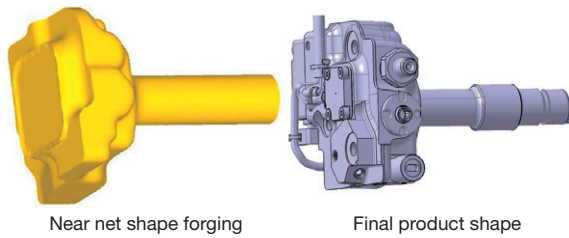


Fig. 9 Comparison of Near Net Shape Forging and Final Product Shape

To facilitate the molding of complex shapes, metal injection molding (MIM) was adopted for some of the stainless steel parts, which increased the material yield by 35%. A material called AUS316L-H2 was adopted for the in-union and out-union as a countermeasure against hydrogen embrittlement and to ensure high strength. In addition, low-frequency vibration-cutting (LFV) was adopted to resolve the issue of poor workability. LFV is a technique in which the cutting tool is brought into contact with the work over constant cycles. It helps to prevent interference from cutting chips and restricts increases in temperature, thereby shortening the machining process. Including those described above, more than 150 measures to reduce cost and boost the mass-production capability of the processes were adopted. As a result, costs were reduced by three-quarters compared to the previous model.

Assuming that the system might be refueled at a wide range of refueling stations in the future, it was necessary to improve reliability in the event that water mixed with the hydrogen gas intrudes into the valves. Therefore, the behavior of water inside the valves was visualized and performance was enhanced by both restricting the intrusion of water into the solenoid valve drive portions and preventing this water from accumulating. A crank-shaped flow path was adopted in the solenoid valve to discourage the inflow of water, and notches were added on the moving sliding parts of the solenoid valve in six locations. A gap was provided between the wall surfaces (Fig. 10) to reduce the adhesive force between the walls and the moving part in freezing temperatures, even if water intrusion occurs. As a result, the robustness of the new valves against water intrusion is approximately 2.5 times greater than the previous model (Fig. 11).

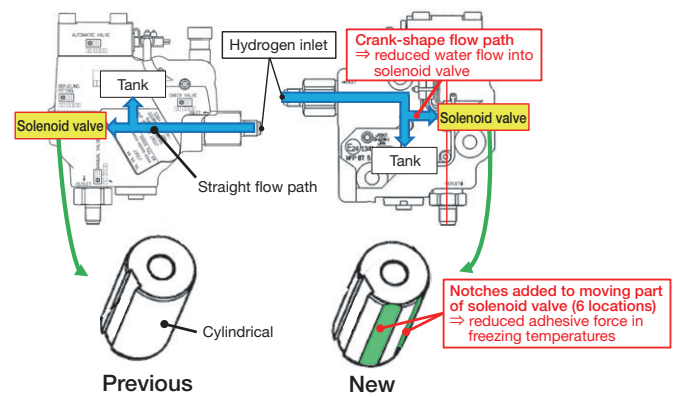
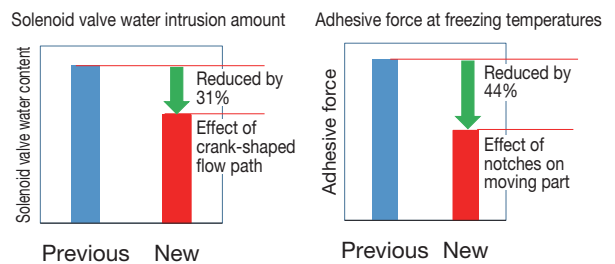


Fig. 10 Countermeasures against Water Intrusion



Robustness approximately 2.5 times higher than previous model.

Fig. 11 Effect of Valve Water Intrusion Countermeasures

3.2.2 High-pressure regulator

In the high-pressure regulator, the piston is required to slide with a stroke extending from several μm to several hundred μm in according with the opening and closing motions of the injector, which occur at intervals of 10 msec. As a result, the piston seal must slide repeatedly tens of millions of times while maintaining sealing performance with the outside. For these reasons, the sliding parts must have a surface texture that realizes an excellent balance between sealing and sliding performance, which requires micron-level precision cutting and surface treatment. This was accomplished by adopting a high-stiffness lathe to cut the piston sliding parts in the high-pressure regulator body. The structure of the piston was also simplified from three to two layers by enabling direct sliding with the regulator body (Fig. 12). As a result, total costs were reduced by one-third and weight by 15% compared to the previous model.

Special Feature

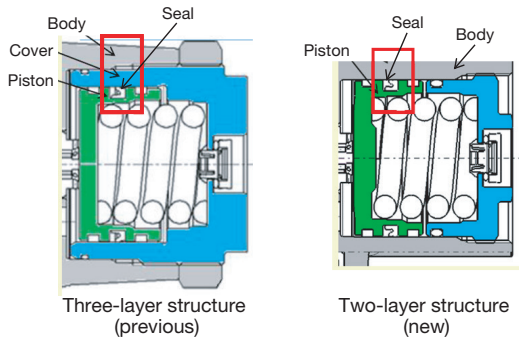


Fig. 12 Comparison of Three- and Two-Layer Pressure Regulators

Flow noise might be generated by the resonance of internal parts when gas flows in the pressure regulator. Therefore, the behavior of the internal parts (especially the pin) was visualized to identify the noise and vibration (NV) generation mechanism. The results of visualizing the internal structure under high-pressure operation found that the poppet that creates the pin angle becomes offset, creating a non-uniform flow path that generates disturbance in the hydrogen flow. This disturbance then acts as a source of vibration (Fig. 13). As a countermeasure, the length of the pin was extended and the amount of clearance was optimized to restrict the pin angle. This measure lowered the amount of flow noise by approximately 30%.

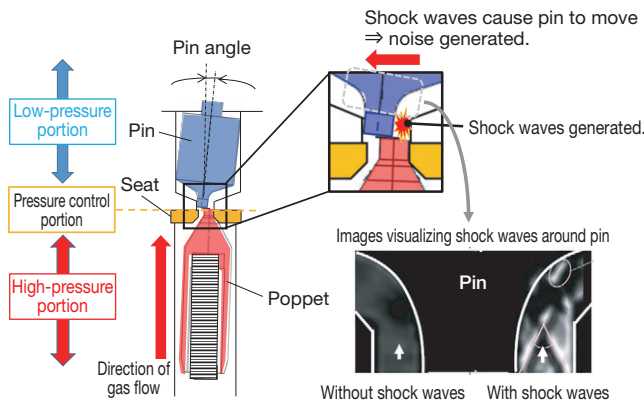

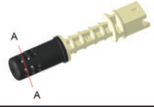


Fig. 13 Observed Images of Shock Waves around Pin when Pressure Regulator Flow Noise Occurs

3.2.3 High-pressure and temperature sensors

The high-pressure hydrogen temperature sensors installed in the tanks were simplified by revising the structural materials. The previous model adopted a stainless steel case to support the thermistors. This was changed to a plastic case with an integrated connector, which reduced the number of parts and the weight (Table 2). This lowered the cost of the sensors by one-quarter and the weight by over 90% compared to the previous model.

Table 2 Comparison of Temperature Sensor Structures

		Previous	New
			
Basic structure	Material	Stainless steel	Polyamide resin
	Mounting configuration	Bolt fastening	Bracket fastening
	Number of parts	Six	Three
	Weight	33 g	2 g

During refueling, hydrogen passes through the tank valves and into the tanks. In this process, the gas flow might exceed the speed of sound and generate a shock wave. Since the inner diameter of the tanks was reduced and smaller temperature sensors were adopted in this model, the feasibility of temperature sensor strength was confirmed and the sensors installed at the appropriate positions (Fig. 14).

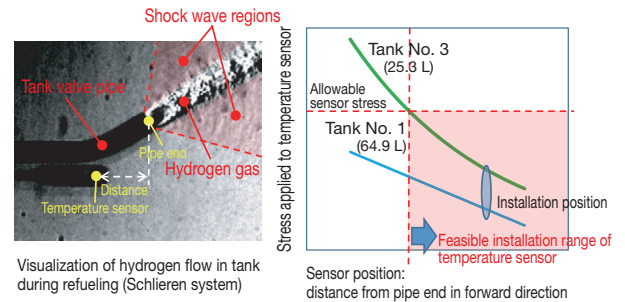


Fig. 14 Input to Temperature Sensors during Hydrogen Refueling

4. Ensuring Refueling Performance

A temperature distribution exists inside the tank during refueling with pre-cooled hydrogen, which generates a difference between the detected temperature and the average temperature of the gas inside the tank. This difference might reduce the full tank refueling amount (called the state of charge, or SOC) when the vehicle communicates with the refueling station. In addition, the developed tank system consists of multiple tanks with different capacities, and the refueling flow rate increases in proportion to the tank length (capacity). To address the temperature distribution inside the tanks, the hydrogen injection angle inside the tank was optimized, thereby enabling the average temperature of the gas inside the tank to be detected even in the longest tank with the highest flow rate (Fig. 15). As a result, the second-generation Mirai ensures the same filling rate as the previous model during communication with the refueling station.

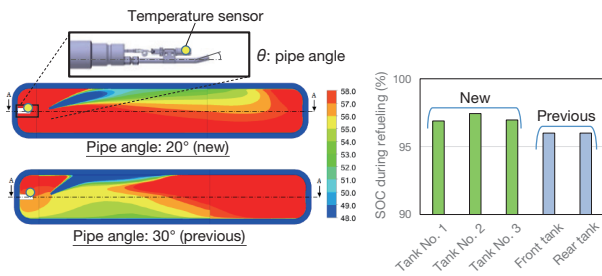


Fig. 15 Calculated Results for Internal Tank Temperature Distribution (during Refueling)

5. Certification

The previous high-pressure hydrogen tanks needed to be certified separately in each country and region around the world. The new tanks were certified under UN-R134, a United Nations Regulation (UNR) established in 2015 to allow mutual international recognition under the 1958 Agreement on harmonizing international standards.

6. Conclusion

A new high-pressure hydrogen storage tank system was developed with the aim of achieving mass-market penetration. In addition to further performance gains in weight reduction and packaging, this system incorporates innovative production engineering technologies as well as measures to further extend the driving range and lower costs.

Toyota intends to continue making progress toward the realization of a planet-friendly hydrogen energy based society through further popularization of FCVs and pioneering technical development in tune with the needs of the customer.

Finally, the authors would like to express their sincere gratitude to everyone involved in the development of this high-pressure hydrogen storage system.

References

- (1) K. Hioki, Kondo, Yamashita, Ogami. "Development of High Pressure Hydrogen Tank for New FCV." *Proceedings of the JSAE Annual Congress No. 37-15S (2015)* pp. 905-908.
- (2) A. Yamashita, Kondo, Ogami, Mitsuishi, "Development of High-Pressure Hydrogen Storage System for New FCV." *Proceedings of the JSAE Annual Congress No. 37-15S (2015)* pp. 909-913.
- (3) N. Saito, Goto, Yamashita, Inagi, Kondo et al. "Development of High Pressure Hydrogen Valve for New FCV." *Proceedings of the JSAE Annual Congress No. 37-15S (2015)* pp. 914-918.

Authors



A. YAMASHITA



K. NAKAMICHI



T. INO



K. KIDA



H. YAHASHI



S. GOTO

Production Engineering Technology for the Fuel Cell Stack of the Second-Generation Mirai

Takeshi Nagasawa*¹
 Atsushi Nogi*¹
 Teppei Ikeda*¹
 Shimpei Yano*¹
 Shinya Takeshita*¹
 Takuya Itakura*¹

Abstract

One of the objectives of the fuel cell (FC) stack developed for the second-generation Mirai was to help achieve full-scale popularization of fuel cell vehicles (FCVs) by expanding production capabilities. New mass-production technology was required to achieve this objective, including high-speed machining and inspection processes at least ten times faster than those adopted for the FC stack of the first-generation Mirai. This article describes several of the manufacturing processes that were developed to reduce costs while ensuring quality.

Keywords: fuel cell (FC) stack, cell, membrane electrode assembly (MEA), blending, intermittent slot die coating, joining, adhesion, X-ray inspection, image-based inspection, artificial intelligence (AI), break in, electricity generation, productivity

1. Introduction

In addition to size and weight reduction and greater performance, the development of the fuel cell (FC) stack for the second-generation Mirai also took on the challenge of developing production engineering (PE) technologies to achieve higher quality, lower cost, and greater productivity for completely new materials and structures.

The newly developed FC stack features innovative component materials and structures designed to enhance performance, as well as completely new manufacturing methods and technologies that aim to achieve significant improvements in productivity.

As a particular example, one FC stack contains several hundred cells, which must be manufactured in a continuous process that takes only several seconds per cell. Overcoming the difficulties of high-speed manufacturing was a major bottleneck for realizing the mass production of the FC stack.

In addition to resolving issues such as this, Toyota also incorporated simulation and analysis technologies into the development of new manufacturing methods with the objective of achieving more efficient development.

This article describes some specific examples of these innovative PE technologies.

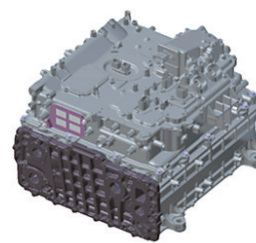


Fig. 1 External Appearance of FC Stack

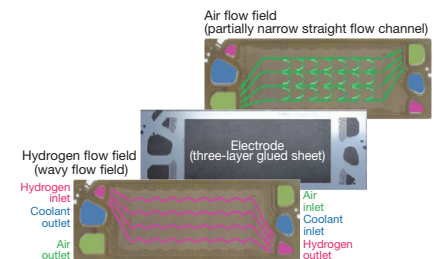


Fig. 2 Cell Configuration (Outline)

2. FC Stack Manufacturing Process

Fig. 1 shows the external appearance of the actual FC stack installed in the second-generation Mirai. The internal components of the FC stack include 330 cells arranged in layers and connected in series (**Fig. 2**). This FC stack achieves a power rating of 128 kW. **Fig. 3** shows the process flow for manufacturing this FC stack. A catalyst and an ion-conductive resin ionomer are blended together into an ink and coated on both sides of the ion-conductive polymer electrolyte membrane. This forms the catalytic layers that act as the reaction sites for power generation. The gas diffusion layer, which acts to provide a stable supply of the gas and electrons required for power generation and to efficiently discharge the water generated in the power generation process, is then joined to the outside of the catalytic layer. Finally, this is placed between bipolar plates and sealed to form a cell. The bipolar plates consist of stamped metal foil that has been surface-treated to ensure electrical conductivity. The performance of every one of the manufactured cells is tested before being layered and fixed together to create the finished FC stack.

*¹ Fuel Cell Manufacturing Div., Toyota ZEV Factory

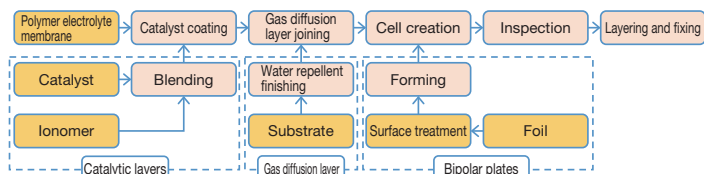


Fig. 3 Flow of FC Stack Manufacturing Process

3. Development of Catalytic Layer Forming Technologies

3.1 Method of forming catalytic layer

The catalytic layer is formed by fabricating a catalyst ink, which is coated onto a sheet by a roll-to-roll transportation process and then dried (Fig. 4). Since the catalytic layer uses expensive platinum (Pt), intermittent coating is applied so that only the portions used in the product are coated.⁽¹⁾

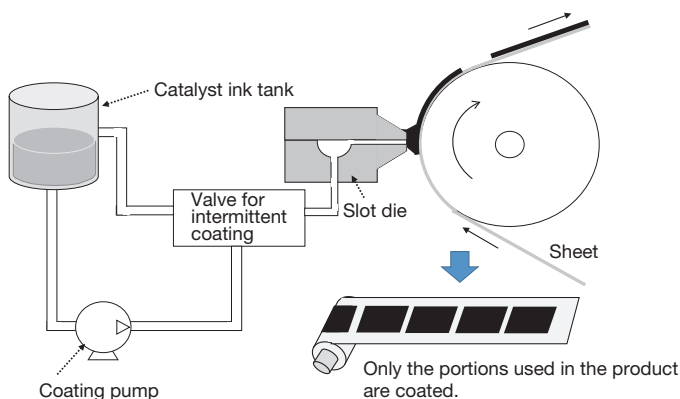


Fig. 4 Formation of Catalyst Layer by Intermittent Coating

The aim of the catalyst ink and equipment development was to speed up this intermittent coating process. To accomplish this aim, the ink pressure inside the slot die must be increased and decreased over several tens of milliseconds at the intermittent coating areas. Ink viscosity control and a high-speed intermittent coating valve are required to realize this ink pressure control.

3.2 Development to speed up catalyst ink fabrication

The catalyst ink is a blended material that consists of a catalyst and a functional resin (ionomer) for transmitting protons. Catalyst ink viscoelasticity control, which determines the coating performance of the ink, is realized by blending in the ionomer as a gel that also acts as a thickener. It was realized that a scaled-up version of the technology used for the first-generation Mirai (i.e., a single stirring blade called a dispersion blade) would cause the flow to slow down at the corners of the tank. In addition, since the ionomer gel is very light and floats at the top of the mixture, the conventional technology is also not capable of rapid dispersion.

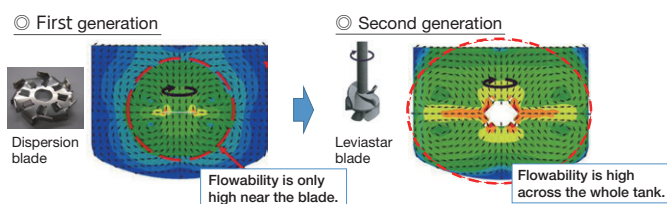


Fig. 5 Development of Ionomer Gel Dispersion Technology

Ordinarily, a disperser with an additional blade (a two-blade type disperser) would be selected to stir the whole tank and ensure flow up to the corners of the tank. However, for the second-generation Mirai, Toyota worked with Primix Corporation to develop a stirring blade capable of stirring the whole tank with a single blade. This development resulted in the stirring blade shown in Fig. 5 (the Leviastar blade). This blade is capable of stirring the whole tank up to the corners and generates sufficient shear force to disperse the ionomer gel. As a result, the dispersion time could be reduced by half compared to the first generation, while also reducing equipment costs.

3.3 Development of high-speed valve for intermittent coating

Toyota developed the intermittent valve mechanism shown in Fig. 6 to realize high-speed response in the process for the second-generation Mirai.

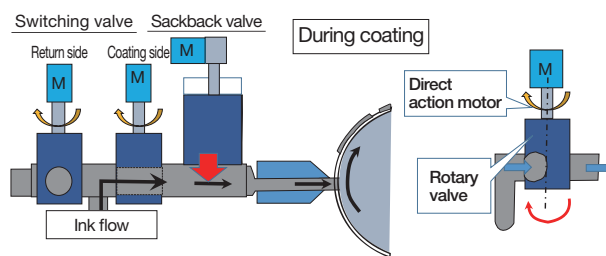


Fig. 6 High-Speed Valve Mechanism in Process for Second-Generation Mirai

This valve for intermittent coating consists of a rotary switching valve that is opened and closed directly by the rotational axis of the motor, and a sackback valve that momentarily increases and decreases the pressure of the ink inside the slot die.

The switching valve is structured with a through hole on the rotational axis and opens and closes with every 90-degree rotation. Since the valve opens and closes by direct motor action, the valve operation time is less than half that of the valve used for the first-generation Mirai. In addition, since the operation of the sackback valve can overlap with the switching valve, it can momentarily increase or decrease the pressure of the ink inside the slot die in accordance with the material properties.

4. Development of Continuous Joining Technology for MEGA

4.1 Details of MEGA joining process

The layered assembly consisting of the electrolyte membrane that forms the electrodes, catalytic layer, and gas diffusion layer is called the membrane electrode gas diffusion layer assembly (MEGA). In the first-generation Mirai, the MEGA was manufactured by joining the rolled electrolyte membrane formed with the catalytic layer called the membrane electrode assembly (MEA) to the thin gas diffusion layer by thermal pressing. To help increase productivity, a manufacturing process that joins the MEA to the gas diffusion layer using a through-process quality-oriented roll-to-roll process was developed (Fig. 7).⁽¹⁾

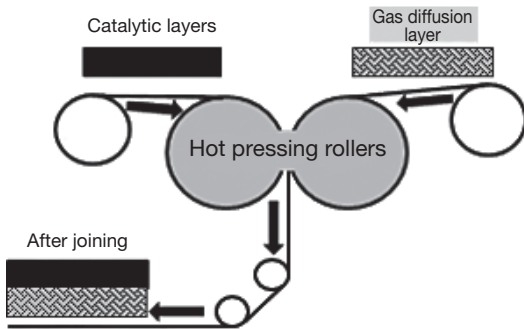


Fig. 7 Flow of Work in MEGA Joining Process

4.2 Development of rolling technology to eliminate gas diffusion layer breakage

The density of the gas diffusion layer was reduced to improve power generation performance while reducing costs. However, since this has the trade-off effect of making the material more brittle and more difficult to stretch, it is susceptible to breakage during transportation. As shown in Fig. 8, if the gas diffusion layer curves slightly outward, and that curved state is not corrected before reaching the hot pressing rollers, the longer side of the curve will rise up on the hot pressing rollers and break when pressure is applied.

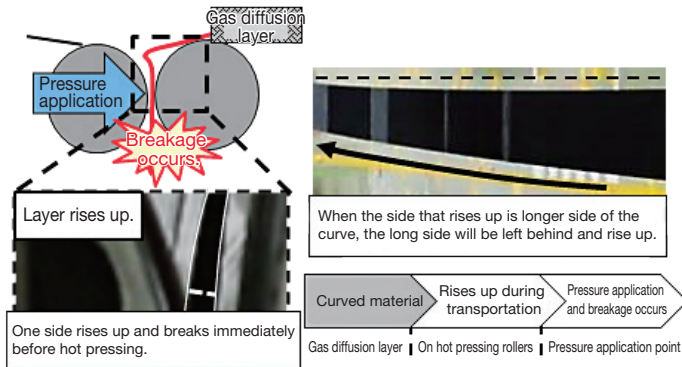


Fig. 8 Gas Diffusion Layer Breakage Mechanism

The cause of gas diffusion layer breakage is not just the curvature of the diffusion layer substrate. This development also attempted to resolve this issue by optimizing the tension control from the material manufacturer to the in-house manufacturing process. The working and joining conditions with a major impact on breakage were extracted from the entire process using multiple regression analysis. This approach identified higher tension during transportation in the joining process as an important condition for the material manufacturer, thereby helping to suppress breakage.

5. Development of High-Speed Cell Creation Technology

5.1 Details of cell creation method

The cells in the first-generation Mirai used rubber sealing materials, which required in excess of ten minutes for vulcanization. To enable a mass-production process that requires only several seconds, a thermoplastic resin seal was selected for the second-generation Mirai that can be glued instantaneously by heating and cooling. The backbone side chains and the adhesive side chains of the resin polymer were adjusted to form a thermoplastic resin with the optimum physical properties. In addition, as shown in Fig. 9, the cell creation process using this new material uses newly developed equipment that first pastes the thermoplastic resin and electrode together, layers the bipolar plates on either side, and then presses the components together by hot and cold pressing.

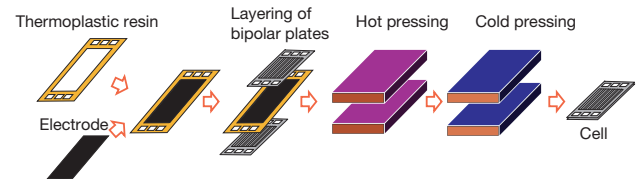


Fig. 9 Cell Creation Process Flow

5.2 Cell creation process conditions

It is widely known that a thermoplastic resin can be glued by heating and cooling. To ensure sealing performance, which is the critical function of this material, the process conditions to achieve gluing were optimized based on this heating and cooling mechanism.

The development focused on the boundary surface between the metal bipolar plate body and resin, and verified the differences between good and poor gluing performance. As shown in Fig. 10, the results found that good gluing performance was achieved when the resin had a perpendicular striped crystalline structure with respect to the bipolar plates. This is thought to be realized by the polymer side chains in the thermoplastic resin joining with the bipolar plate during heating, and the backbone chains subsequently using the side

chains as the origin point for crystallization through optimum cooling conditions. Therefore, defect-free conditions (*ryohin joken*) were defined as those that realized a striped crystalline structure at the boundary surface between the metal bipolar plate body and resin. Then, by adopting equipment capable of setting the appropriate heating and cooling temperatures, it was possible to reduce the production time for one cell to several seconds.

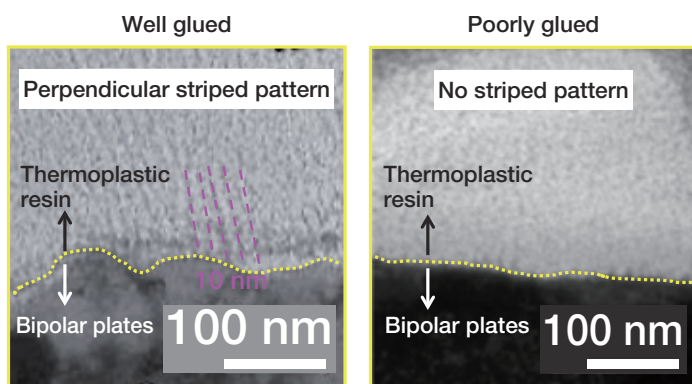


Fig. 10 Relationship between Well-Glued and Poorly Glued Metal/Resin Interface

6. Development of Cell Foreign Matter Detection Technology

6.1 Details of inspection to detect foreign matter in cells

The intrusion of ferrous metallic foreign matter into a cell can cause chemical deterioration of the polymer electrolyte membrane (Fig. 11). If this deterioration progresses, the amount of hydrogen leakage increases, resulting in lower fuel efficiency and power generation performance. Therefore, all cells are inspected to detect the presence of metallic foreign matter.

Micro-sized metallic foreign matter may potentially intrude into the cells in any manufacturing process, including at the material manufacturer. As matter that has penetrated into the cells is very difficult to detect from the outside, a transmission inspection technique using X-rays is adopted to observe the state inside the cells.

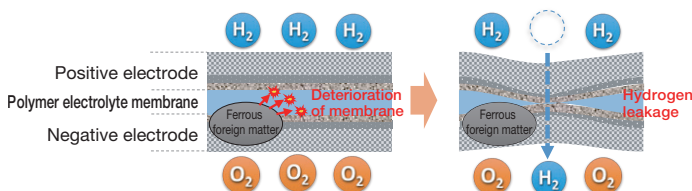


Fig. 11 Chemical Deterioration of Polymer Electrolyte Membrane

6.2 Principles and issues with transmission X-ray inspection

In X-ray inspection, metallic foreign matter and other substances with a high X-ray absorption performance show up on the obtained images as shadows. As a result, the presence and size of foreign matter can be determined quickly within several seconds. However, although this technique can identify the planar size of an object in the X-ray radiation direction, the three-dimensional size of the foreign matter is an important factor for judging whether it will be a cause of membrane chemical deterioration (Fig. 12). Although three-dimensional X-ray computerized tomography (3D-CT) exists as an analytical technique capable of measuring the three-dimensional size of foreign matter, this technique requires several hours for a single measurement. As this is not particularly suited for a mass-production line, it was necessary to develop X-ray inspection technology capable of identifying the three-dimensional size of foreign matter rapidly and accurately.

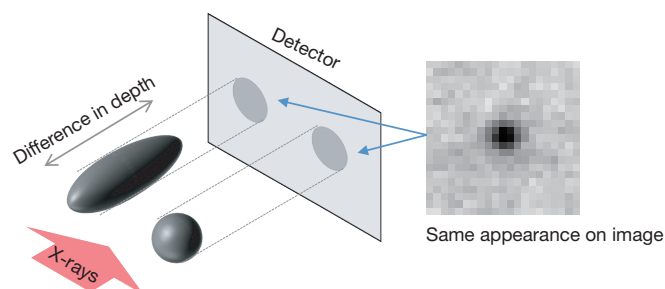


Fig. 12 Divergence between Detected Image and Actual Size

6.3 Development of high-speed three-dimensional size detection technology

To identify the three-dimensional size of foreign matter within several seconds, this development focused on the diffraction phenomenon that occurs when X-rays strike a foreign object. Since the darkness of the shadow changes depending on the diffraction, this approach had the potential to predict the three-dimensional size of foreign matter. Consequently, new inspection logic was developed based on this approach, enabling the three-dimensional size of foreign matter to be predicted and determined within an inspection time of several seconds (Fig. 13).

In addition, the resolution of this technique was substantially increased by changing the foreign matter size recognition method from camera pixel resolution to color resolution (i.e., the darkness of the shadows). Compared to measurement based on the conventional approach of using the number of camera pixels, the size measurement accuracy in repeated inspection was improved by approximately 70%.

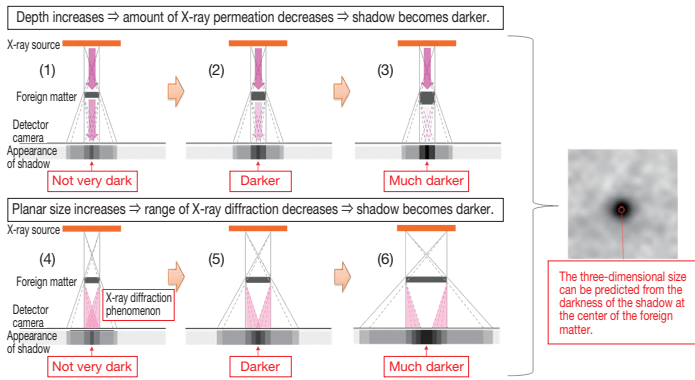


Fig. 13 Prediction of Foreign Matter Size Using X-Ray Diffraction Phenomenon

7. Development of Automatic Cell Appearance Inspection Technology

7.1 Cell appearance inspection

In the cell function inspection process, in addition to pressure loss, sealing performance, and the like, the appearance of the cells is inspected as a final guarantee of cell function. Since the second-generation Mirai is positioned as a mass-production model, the inspection speed needed to be raised to several seconds per cell. It was also necessary to automate the inspection standard judgment process (*jidoka*) for contamination (unit: several mm) and scratches (unit: 1/10 mm) on the power generation portions.

7.2 Development of imaging technology appropriate for cell defects

To help raise the accuracy of the imaging inspection process, it is important to make sure that there is a difference in contrast between defective and non-defective portions. However, since the cells are composed of fuel gas flow fields and gaskets, the resulting unevenness creates shadows that affect inspection accuracy.

Therefore, a dome-shaped illumination field was adopted for the light sources. Light from the light sources shines onto the inner walls of the illumination field and diffuses, illuminating the cell from all directions. This has the effect of producing shadows that are lighter and finer. In addition, bar illumination is applied horizontally from the side of the flow fields that produce darker shadows, resulting in a different level of brightness for defective and non-defective portions (**Fig. 14**).

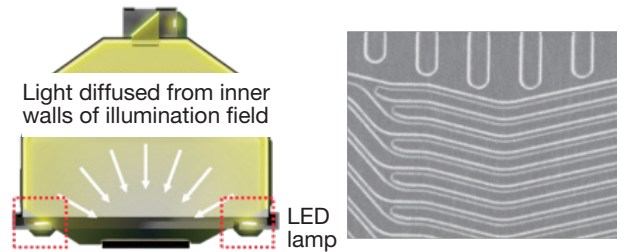


Fig. 14 Imaging Using Dome-Shaped Illumination Field

7.3 Development of AI judgment model

Surface treatment is applied to the cells to ensure electrical conductivity. However, colors on the images may change if variations in the thickness of this surface treatment result in the generation of interference colors. For this reason, defects must be distinguished with a stable degree of accuracy. Therefore, an automatic judgment system was developed using artificial intelligence (AI) machine learning.

A deep learning AI technique was applied to create a model using images with intentionally large color variations to develop the required detection capabilities (**Fig. 15**).

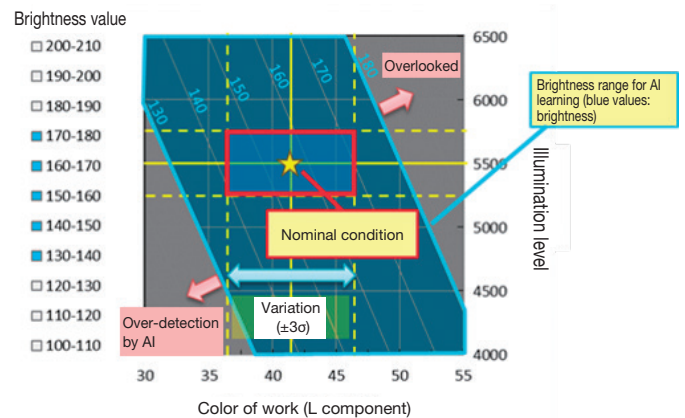


Fig. 15 Brightness Range Used for AI Learning

8. Development of Technology to Shorten Break-In Time

8.1 Definition of break-in

Immediately after manufacture, the power of the FC stack is low. Proton conductivity improves as electricity is generated, leading to an increase in power. As the battery reaction (hydrogen + oxygen \Rightarrow water + electricity) takes place on the surface of the platinum inside the catalytic layers, one reason for poor performance immediately after production is the adhesion of impurities onto the platinum during the manufacturing process that impair this reaction.

Since the vehicle cannot realize sufficient performance after production unless these impurities are removed, a break-in

process is required to trigger the inherent power generation characteristics of the FC. This process must be accomplished in a short period of time to improve productivity.

8.2 Behavior and washing of impurities

The impurities that adhere to the platinum in each process were analyzed to identify those that impair power generation. The development then aimed to find an efficient impurity detoxification and removal method for absorbed impurities.

Focusing on the fact that the surface state of the platinum changes depending on the electric potential, a technique called surface-enhanced infrared absorption spectroscopy (SEIRAS), which combines electrochemical measurement and infrared spectroscopy and was developed in a joint project with the Nagoya Institute of Technology (Fig. 16), was adopted to observe the state of the impurities on the platinum surface in-situ. As a result, this technique successfully enabled the visual confirmation of the phenomenon in which impurities are absorbed and desorbed due to electric potential fluctuations (Fig. 17).

Since water is constantly generated and discharged in the actual power generation environment, it was estimated that the application of repeated electric potential fluctuations could enable the efficient removal of impurities using the generated water. Consequently, the break-in time was reduced by 70% compared to the process for the first-generation Mirai by reflecting this information in the FC stack operation conditions.⁽¹⁾

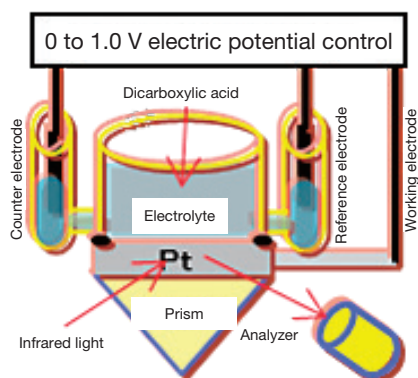


Fig. 16 SEIRAS

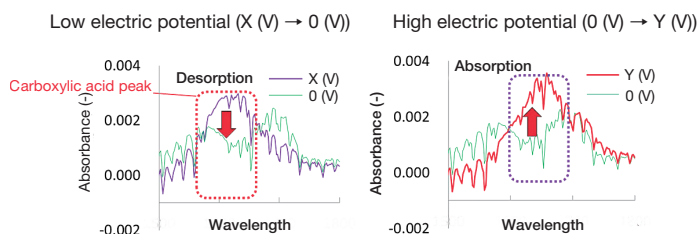


Fig. 17 Results of Impurity Behavior Observation under Electric Potential Fluctuations

9. Conclusion

This article has described the advances and newly developed PE technologies for the second-generation Mirai. Creating these technologies has improved the space productivity six-fold compared to the first generation.⁽¹⁾

Although these technologies were developed with the principle objective of expanding the mass-production potential of the Mirai, volume production has created new issues. Important knowledge has been obtained by identifying and resolving these issues one by one. Although many issues still remain to be solved before fuel cell vehicles can achieve mass market penetration, Toyota intends to redouble its efforts to develop technologies that will help to further raise quality, reduce costs, and improve productivity, and thereby lead the way to the realization of a hydrogen energy based society.

The cooperation of a wide range of people inside and outside Toyota played a critical role in the developments described in this article. The authors would like to take this opportunity to express their gratitude to everyone involved.

Reference

- (1) T. Suzuki et al. "Fuel Cell Production Technologies for the Mirai FCV." *Toyota Technical Review* Vol. 61 (2015) pp. 33-39.

Authors



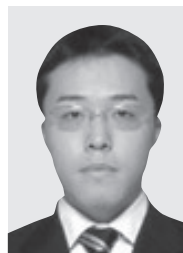
T. NAGASAWA



A. NOGI



T. IKEDA



S. YANO



S. TAKESHITA



T. ITAKURA

Production Engineering Technology for the High-Pressure Hydrogen Tanks of the Second-Generation Mirai

Yoichiro Baba*¹
 Masato Ueda*²
 Hideaki Kondo*²

Abstract

One of the objectives of the high-pressure hydrogen tanks developed for the second-generation Mirai was to provide even more reliable and safe tanks at a lower cost to facilitate the realization of a future hydrogen energy based society centered on fuel cell vehicles (FCVs). To achieve this objective, high-speed machining processes at least ten times faster than those adopted for the high-pressure hydrogen tanks of the first-generation Mirai and technology to ensure stable quality were developed. This article describes several of the manufacturing processes that were developed to reduce costs while ensuring high quality.

Keywords: hydrogen storage, high productivity, quality assurance, plastic liner, injection molding, infrared (IR) welding, carbon fiber reinforced plastic (CFRP), gas tightness test, continuous filling

1. Introduction

To realize even safer, lighter, and low-cost high-pressure hydrogen tanks (Fig. 1), Toyota is working on the development of new materials and structures, as well as the application of production engineering (PE) technologies to reduce costs while maintaining high quality and productivity.

This article describes some specific examples of the mass-production technologies that were developed to help realize the realization and expansion of a hydrogen energy based society.

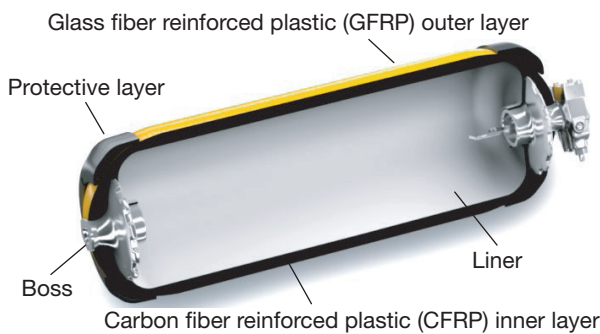


Fig. 1 Tank Structure

2. Tank Production Process

The tank production process consists of steps involving the liner, filament winding (FW), and inspection.

Specifically, the liner steps consist of injection molding and infrared (IR) welding, the FW steps consist of winding and

curing, and the inspection steps consist of water pressure and gas tightness tests (Fig. 2).

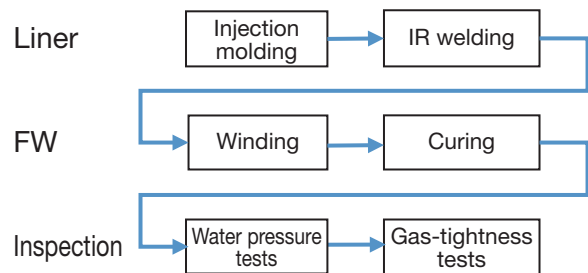


Fig. 2 High-Pressure Hydrogen Tank Production Process Flow

3. Liner Processes

The liner developed by Toyota is produced by joining injection molded plastic parts together using IR welding (Fig. 3).

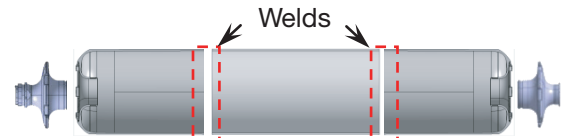


Fig. 3 Liner Configuration

3.1 Injection molding

3.1.1 Injection molder

Due to the length of the plastic parts, the molder requires a large opening. Metal rings must also be formed and inserted to the dome. Toyota developed a new injection molder that satisfies these requirements. The mold clamping machine opens and closes vertically and the lower mold can be ejected from the pressing machine. This structure allows the metal rings to

*¹ Paint and Plastics Production Engineering Div., Production Group (Vehicle Production Engineering Field)

*² Shimoyama Plant Fuel Cell Manufacturing Div., Toyota ZEV Factory

be set stably and also facilitates ejection of the long parts. The developed molder is two-thirds the size of a similar commercially available molder (Fig. 4).

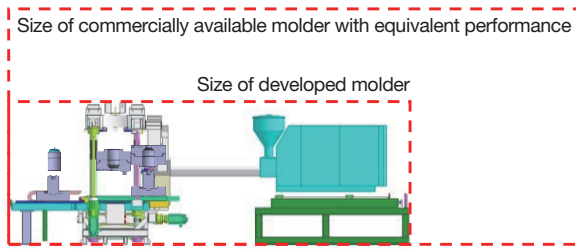


Fig. 4 Injection Molder

3.1.2 Molding conditions

Flow marks are a type of problematic molding defect. In cross-section, flow marks resemble a crack and may cause the liner to fracture at low temperatures (Fig. 5).

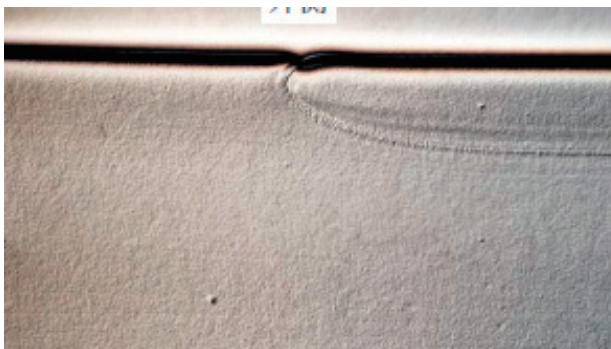


Fig. 5 Flow Mark Cross Section

Flow marks are often generated if a large speed difference occurs when the plastic passes through a portion with greatly varying thickness. The occurrence of flow marks was suppressed by adopting a control that slows the flow speed when the end of the flow reaches a portion with a large thickness difference, and returning to a higher flow speed once that portion has been passed (Fig. 6).

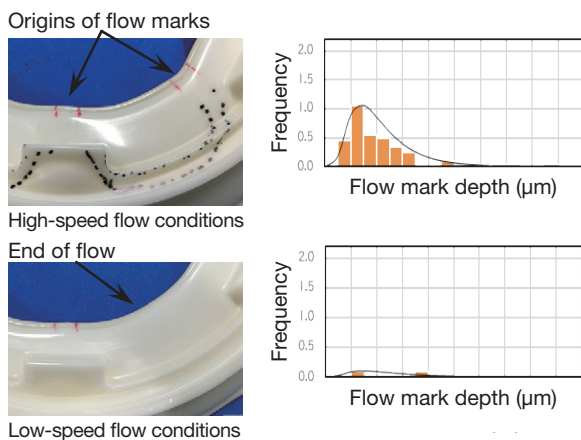


Fig. 6 Countermeasure for Flow Marks

3.2 IR welding

3.2.1 Characteristics of IR welding

IR welding is a plastic welding technique that involves the melting of the joint surfaces using infrared light and rapid application of contact between the two objects (Fig. 7).

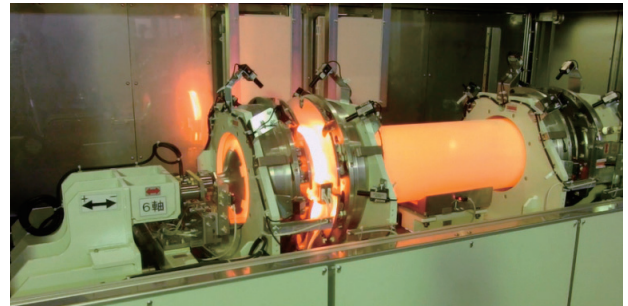


Fig. 7 IR Welding

The advantage of this technique is that the joining surfaces can be heated directly and large amounts of molten material discharged without contact between the joint and the air, resulting in a very clear joint. These characteristics make IR welding an effective technique for preventing the adhesion of foreign matter to the joining surface (Fig. 8).

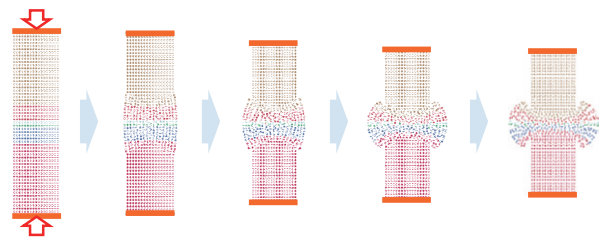


Fig. 8 Welding Process (Simulation by Particle Method)

3.2.2 Factors causing variation in joint strength

There are various factors that cause variation in joint strength. Joint strength is reduced by uneven joint thickness or large level differences caused by crooked contact between the materials. The method of sampling the test piece is also affected.

Attention must also be paid to the distribution of crystallization. When the crystallization distribution around the joint was visualized by infrared spectroscopy, a correlation was identified between the rate of crystallization change and joint strength (Fig. 9). This result shows that a smaller degree of crystallization can be realized if the temperature difference between the surface and deeper portions is reduced by heating the joint over a longer period of time at low power. These conditions are preferable for ensuring strength.

Special Feature

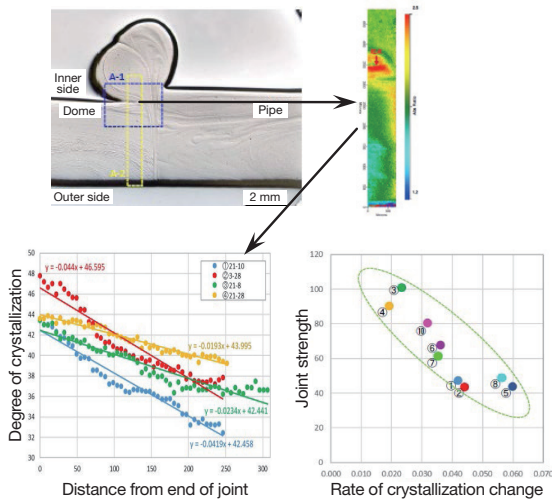


Fig. 9 Crystallization Distribution and Joint Strength

3.2.3 Quality assurance

Quality assurance is carried out by inspecting the beads generated by the welding process. The suitability of the amount of material melted by the welding process and the pressure can be evaluated by measuring the height and width all around the weld.

4. FW Steps

4.1 Outline of steps

In the FW steps, internal pressure is applied to the low-stiffness plastic liner. Approximately 3,500 meters of the carbon fiber that ensures the strength of the tank is then wound around the liner while controlling the tension (Fig. 10). In addition to shortening the process time by 50% through faster equipment operation, the measurement time was also reduced by 90% by automating the quality measurements. As a result, the production time was cut by 66% (i.e., productivity was increased by a factor of 3) (Fig. 11).

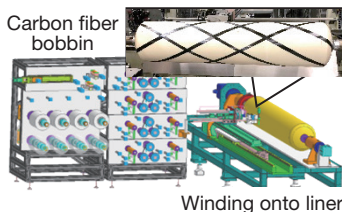


Fig. 10 Outline of FW Machine

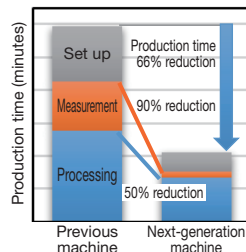


Fig. 11 FW Machine Production Time

4.2 Faster equipment operation

With the objective of shortening the process time by 50%, the weight of the fiber thread feeder, which has a wide operation range, was reduced and the drive system redesigned.

The main factor resulting in weight increase is the longitudinal shaft drive motor, which was integrated with the feeder in the previous machine. This motor was separated (Fig. 12) and the oscillating portion restricted to the end of the feeder (outlined in red in Fig. 12). This allowed the size of the oscillating shaft drive motor to be reduced. In addition, aluminum was adopted to thoroughly reduce the weight of the component materials. This measure helped to reduce the weight of the equipment by approximately four-fifths.

Since the speed of the ball screw drive system in the previous equipment could not be increased due to the effects of resonance and thermal displacement caused by friction, the drive system was changed from a ball screw to a wire drive system (Fig. 12).

As a result, the maximum speed was increased by a factor of 2.1 and acceleration was increased by a factor of 1.5, helping to shorten the processing time by 50%.

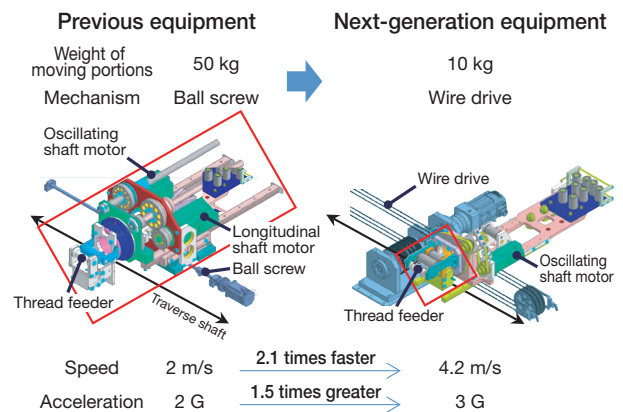


Fig. 12 Diagram of Structure around Thread Feeder (Compared to Previous Machine)

4.3 Automation of quality measurement

With the previous tanks, since the quality of each layer was measured manually, the process had to be stopped to carry out each measurement and the tanks accessed. This placed a great deal of pressure on the production time.

Therefore, a technique capable of automatically measuring the tanks without stopping the equipment was developed.

One issue with automation is the difficulty of distinguishing between previous and new layers by image processing or the like.

The dome region of the tank uses low-angle helical winding. Here, a laser deflection meter is used to measure the shape and plot the difference before and after layering (Fig. 13).

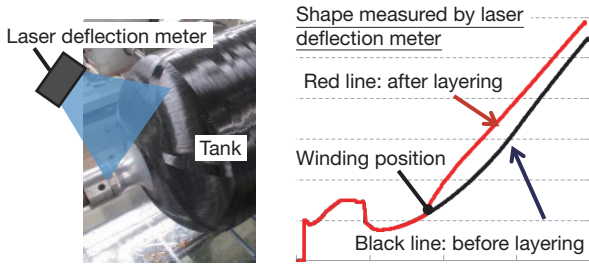


Fig. 13 Outline of Low-Angle Helical Winding Region Measurement

The central region of the tank uses hoop winding. An intense light is shone onto the new layers while winding, and the resulting light scattering is used to distinguish the upper and lower layers (Fig. 14).

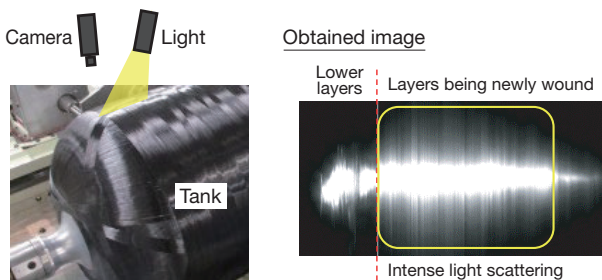


Fig. 14 Outline of Hoop Winding Region Measurement

These newly developed automatic measurement technologies helped to reduce the measurement time by 90%.

In combination with the high-speed operation measures described in Section 4.3, productivity was increased by a factor of 3 compared to the previous tanks.

4.4 Quality assurance

To make sure that safe and secure tanks are delivered to the customer, the performance of each and every tank must be assured. Therefore, quality assurance functions were adopted that constantly monitor the winding position, tension, and internal pressure. Quality is assured by measuring the winding position at each layer by the automatic measuring devices described in Section 4.3, and by constantly monitoring the tension using a tension meter installed at the feeder, which is the closest point to the processing location.

In addition to these measures, the processes are linked with a product serial number, including during equipment operation. Therefore, while constantly monitoring the product quality after the start of mass production, the resulting data is both fed back to improve the processes and applied to the next generation of manufacturing.

5. Gas-Tight Processing

5.1 Gas-tightness tests for high-pressure hydrogen tanks

To ensure that the tanks are gas-tight, a gas-tightness test is applied to all tanks at the actual usage pressure (70 MPa) before shipment.

The gas-tightness test equipment consists of a pressurization section that fills the tank with ultra-high-pressure gas, and an inspection section that tests the amount of leakage from the tank (Fig. 15). The pressurization section uses an ultra-low-temperature liquefied gas pressurization device that realizes a high filling efficiency with ultra-high-pressure gas.

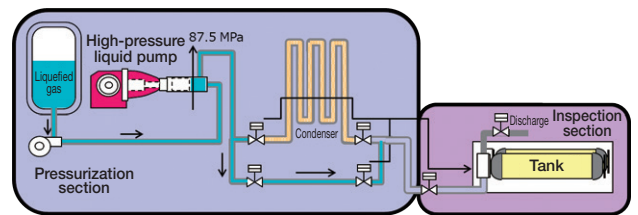


Fig. 15 Gas-Tightness Test Equipment (Outline)

The ultra-low-temperature liquefied gas pressurization device is a high-cost item of equipment since it uses special materials suitable for ultra-high pressures and ultra-low temperatures. Another issue is an increase in liquefied gas loss due to the low utilization rate of the pressurization section because liquefied gas must be consumed to maintain the pressurization section in an ultra-low-temperature state during idle periods other than when the gas is being filled, such as during the leakage tests by the inspection section, gas discharge, or tank replacement.

The utilization rate of the pressurization section must be increased and the liquefied gas loss reduced to lower the cost of the gas-tightness tests. One way that was selected to accomplish these objectives was to adopt multiple inspection sections for a single pressurization section (Fig. 16).

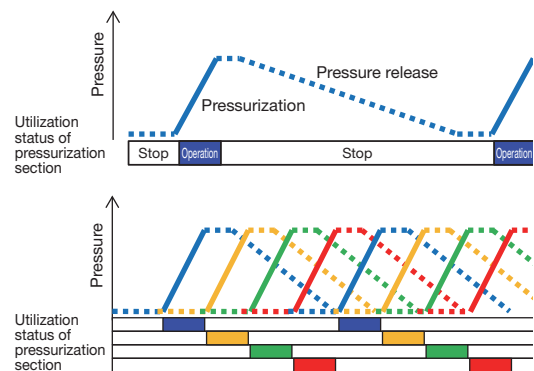


Fig. 16 Utilization of Pressurization Section by Adopting Multiple Inspection Sections

Special Feature

5.2 Development of control to continuously switch inspection section during filling

When switching from one inspection section to the next after pressurization by gas filling to each of the multiple inspection sections is completed, it requires at least 1 minute to depressurize from ultra-high to low pressure. This is to help prevent damage due to cavitation caused by localized decreases in density at narrow sections of the gas filling pipes during depressurization.

An exhaust valve was added to realize depressurization in the same short period of time required by the previous equipment configuration. In addition, a control that synchronizes this process with the pressurization device was developed. This synchronized control realizes smooth cavitation-free depressurization, and enables the switching to be completed in less than one-tenth the time of the previous method.

5.3 Development of filling time control technology

Since gas is filled into multiple inspection sections (Fig. 17), the gas filling time is not stable due to the pressure differences between the pipes. As a result, the pressurization section remains idle while the gas filling target is changed. This results in nitrogen gas loss during this idle period (Fig. 18).

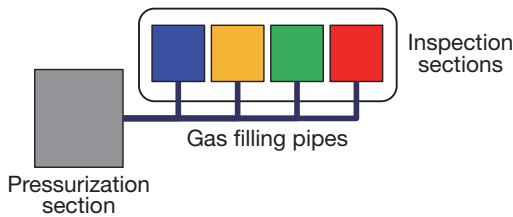


Fig. 17 Layout of Pressurization and Inspection Sections (Outline)

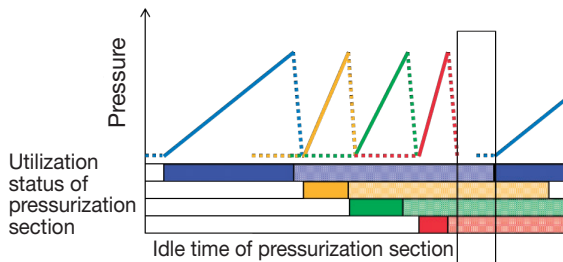


Fig. 18 Utilization of Pressurization Section during Inspection Section Switching

Under the previous control, the tanks were filled with gas using only the output of the pressurization device. Since nitrogen has a high density in ultra-high-pressure regions at or above 70 MPa, it is difficult to stably control the speed of pressure increase. To stabilize the speed of pressure increase, the output of the pressurization device with respect to the pressure during the filling of each inspection section is synchronized with the flow rate adjustment valve control. This

approach successfully stabilized the speed of pressure increase at ultra-high pressures. As a result, the variation in filling time could be restricted to 5 seconds or less, thereby reducing the idle time of the pressurization device during inspection section switching to a maximum of 10 seconds.

6. Conclusion

With the second-generation Mirai, Toyota is not simply aiming to increase production volume. The second-generation Mirai is intended to be a true mass-production model capable of facilitating the full-scale popularization of fuel cell vehicles through higher performance and quality with costs that are at least ten times lower than the previous generation. Many challenges were encountered in developing the innovative breakthrough technologies required to achieve these objectives. Toyota intends to continue developing more advanced fuel cell technology and sincerely looks forward to the advent of an Earth-friendly hydrogen energy based society.

Finally, the authors would like to express their sincere gratitude for the invaluable cooperation of everyone at Toyota's partner companies who were involved in the development.

Authors



Y. BABA



M. UEDA



H. KONDO

The Platform and Body Structure of the Second-Generation Mirai

Yasuyuki Kumazawa*¹
 Daisuke Teramoto*²
 Noboru Ogura*³
 Hiroshi Bando*¹
 Yoshiki Ishikawa*⁴

Abstract

To realize the emotionally powerful styling and fun-to-drive dynamic performance of the second generation Mirai, the platform and body structure used for the original model were wholly revised. Based on Toyota's wide-body GA-L platform, an innovative fuel cell (FC) system installation layout was combined with a highly rigid body frame and redesigned chassis components. These measures helped to achieve a roomy and user-friendly interior, while also enabling emotionally powerful styling, refined and comfortable dynamic performance, and a longer cruising range. This article describes the platform and body structure of the second-generation Mirai.

Keywords: platform, body frame, driving range, handling, large tires

Special Feature

1. Introduction

The second-generation Mirai is built on the wide-body GA-L platform, which allows the adoption of large tires to secure ground clearance, and is both roomy enough for five occupants to travel in comfort and spacious enough to enable a longer driving range by increasing the hydrogen storage capacity. Combined with the new rear-wheel drive layout, major advances have been made in driving performance. This article focuses on topics such as the mounting of the fuel cell (FC) on the wide-body GA-L platform and the realization of a highly rigid body.

2. Component Layout

Figs. 1 and 2 compare the component and hydrogen tank layout of the first and second-generation Mirai. In the second-generation Mirai, the FC stack was moved from below the front seats to under the hood. This allows a lower front seating position and vehicle height, and also helps to greatly expand the legroom of rear seat occupants. The number of hydrogen tanks was increased from two to three, including a tank located in the center tunnel, resulting in a longer driving range.

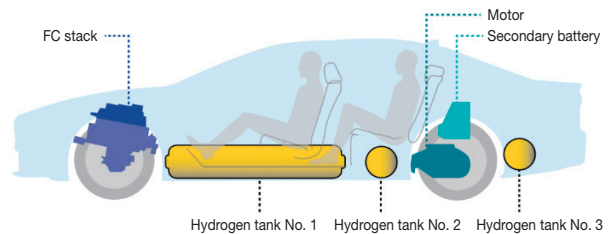


Fig. 1 Component Layout in Second-Generation Mirai

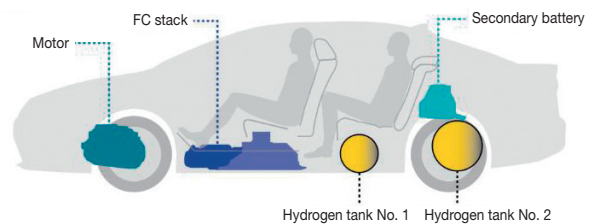


Fig. 2 Component Layout in First-Generation Mirai

3. Mounting of FC System

As fuel cell vehicles (FCVs) have a unique interrelationship between components, the wide-body GA-L platform was partially redesigned specifically to enable mounting of the FC system. The main components of an FCV include the FC stack, transaxle motor, and hydrogen tanks. The following sections focus on the areas of the platform that were modified to enable the mounting of these components.

*¹ Lexus Body Engineering Div., Lexus International Company
 *² MS Body Design Div., Mid-size Vehicle Company
 *³ MS Chassis Engineering Div., Mid-size Vehicle Company
 *⁴ MS Product Planning Div., Mid-size Vehicle Company

3.1 Mounting of FC stack

As described above, the FC stack was moved from below the front seats in the first-generation Mirai to under the hood in the second-generation Mirai (Fig. 1). To help suppress the transmission of vibration from the compressor and air conditioning compressor, which are integrated with the FC stack assembly, a support structure consisting of vibration-isolating mounts was adopted (Fig. 3)

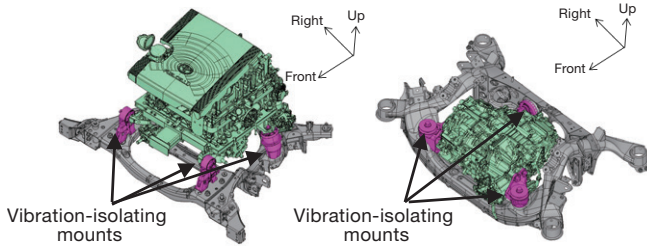


Fig. 3 FC Stack Mounting System

Fig. 4 Transaxle Motor Mounting System

3.2 Mounting of transaxle motor

In the second-generation Mirai, the motor was moved from under the hood to between the rear wheels. The intrusion of gear noise into the occupant compartment was suppressed by adopting similar vibration-isolating mounts as the FC stack (Fig. 4), and by adopting a silencer directly above the motor.

3.3 Mounting of hydrogen tanks

The first-generation Mirai adopted two transversely mounted tanks. The second-generation Mirai features a total of three tanks, including an additional longitudinally mounted tank (Fig. 5). The tank layout and mounting system was designed to achieve an optimum balance between realizing a longer driving range through higher hydrogen storage capacity and achieving a spacious occupant compartment.

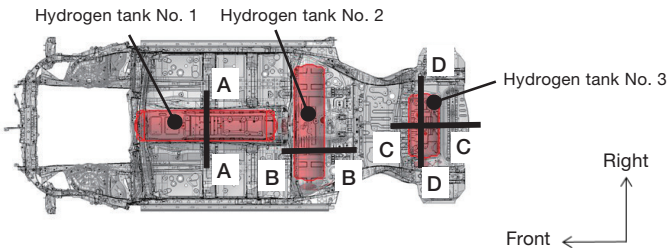


Fig. 5 Hydrogen Tank Layout

3.3.1 Mounting of hydrogen tank No. 1

To realize a roomy interior while increasing driving range, large hydrogen tank No. 1 was mounted in the center tunnel. The diameter of the tank was increased as far as possible by

widening the tunnel, while maintaining the roominess of the interior by modifying the front seat mounting position (Fig. 6). At the same time, the development focused on keeping the top edges of the tunnel as straight as possible to help enhance the longitudinal bending rigidity of the vehicle (Fig. 7).

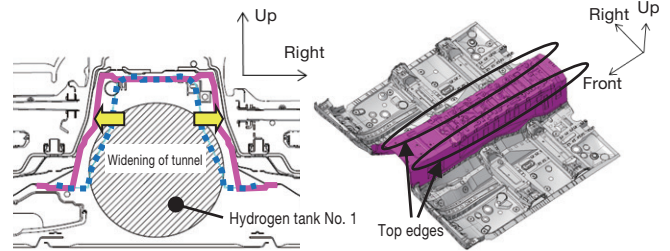


Fig. 6 Tunnel Section (A-A)

Fig. 7 Tunnel Structure

3.3.2 Mounting of hydrogen tank No. 2

Hydrogen tank No. 2 is transversely mounted under the rear seats. The tank was mounted as low and as forward as possible in this area to secure a sufficient seat cushion thickness. This approach helped to lower the vehicle height and ensure seating comfort (Fig. 8). Repeated forming simulations were carried out to maximize the left/right tank length, and the development team took on the challenge of designing a floor shape requiring the satisfaction of complex forming conditions (Fig. 9).

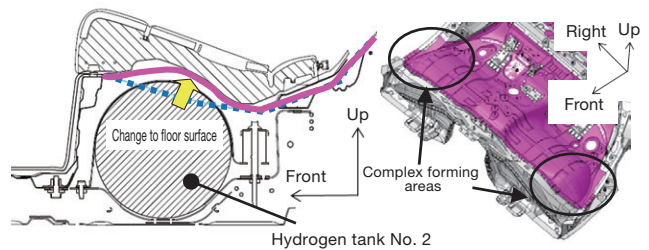


Fig. 8 Section of Area below Rear Seats (B-B)

Fig. 9 Floor Shape

3.3.3 Mounting of hydrogen tank No. 3

Hydrogen tank No. 3 is transversely mounted under the luggage compartment. The rear floor structure was divided into two parts to enable the tank to be mounted and enable tools to be stored under the deck lid (Fig. 10). In addition, the floor members in the luggage compartment that function to transfer impact loads were laid out on the floor to help further expand tank capacity and driving range, while helping to ensure performance in a collision (Fig. 11).

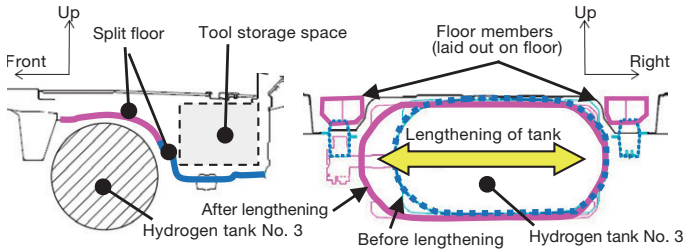


Fig. 10 Luggage Compartment Structure (Section C-C)

Fig. 11 Section of Hydrogen Tank (D-D)

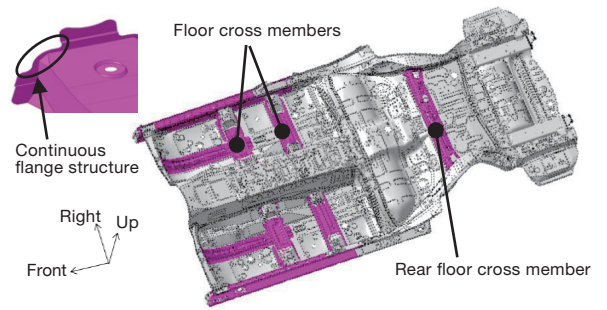


Fig. 14 Floor Frame

4. Realization of Highly-Rigid, High-Strength Body

Smooth and powerful driving performance was achieved by adopting thorough measures to increase body rigidity by approximately 25% compared to the first-generation Mirai. This was achieved by enhancing torsional rigidity, and by increasing the rigidity of the load application points and joints. In addition, the optimum adoption of aluminum and ultra-high-strength steel (hot stamped steel with a strength between 590 and 1,180 MPa) for certain main frame components also helped to increase strength and reduce weight.

4.1 Measures for the platform

The following structures were incorporated into the basic wide-body GA-L platform. Six braces were provided under the hood to substantially enhance torsional rigidity (Fig. 12). Aluminum die cast front strut towers with an optimized thickness and rib geometry were adopted. This measure enhanced the rigidity of the load application points (by approximately 70% compared to the first-generation Mirai) while reducing weight (Fig. 13).

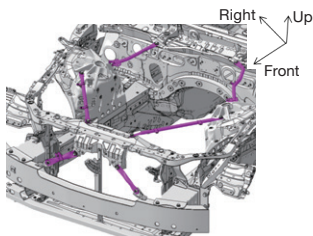


Fig. 12 Under-Hood Structure

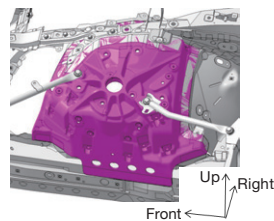


Fig. 13 Front Strut Tower

The left and right ends of the floor cross members and rear floor cross member were designed with a continuous flange structure to strengthen the frame joints and enhance both torsional and bending rigidity (Fig. 14).

Adopting an underbody shear panel is an effective way of suppressing shear deformation of the suspension members due to lateral force inputs to the suspension. Since an FCV does not require an oil replacement hole, the bead geometry and layout were optimized to maximize the rigidity of the underbody shear panel and create a lightweight and highly rigid structure (Fig. 15).

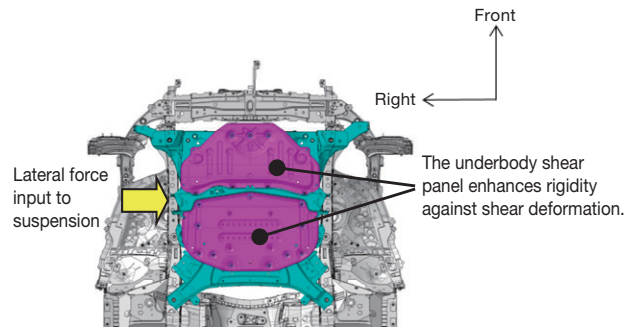


Fig. 15 Underbody Shear Panel Structure

In both full lap and offset rear-end collisions, the body is designed to suppress cabin deformation by facilitating load transfer to the opposite side, and dispersing and absorbing the impact energy (Fig. 16).

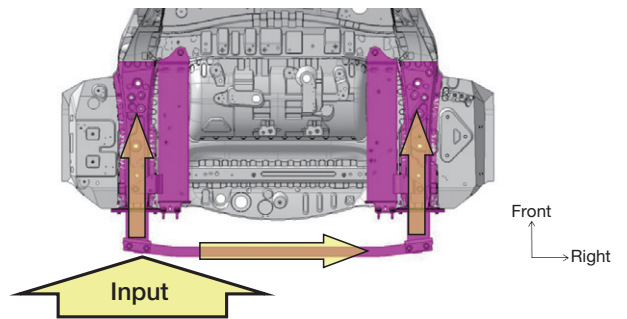


Fig. 16 Rear-End Collision

4.2 Cowl

Deformation due to force inputs to the front suspension was suppressed by eliminating the welding service hole in the cowl side and expanding the usage of arc welding (Fig. 17). The

Special Feature

cowl also passes through to the under body to enable the closed section of the cowl to be joined between the A pillars. An annular (ring) structure was formed with the instrument panel reinforcement, enabling excellent body rigidity and increasing the stiffness of the steering column support by approximately 85% compared to the first-generation Mirai (Fig. 18).

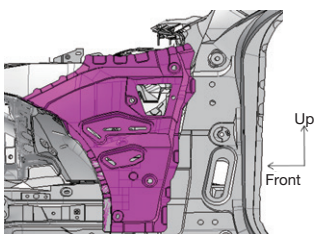


Fig. 17 Cowl Side

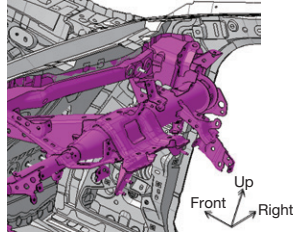


Fig. 18 Closed Section of Cowl

4.3 Rear body frame

A dedicated design was adopted for the rear strut towers. This enables a stylish design, minimizes the size of the rear strut tower attachment surfaces, and allows the addition of bead shapes. As a result, the rigidity of the vertical load application points on the strut towers was substantially enhanced by approximately 85% compared to the first-generation Mirai (Fig. 19). In addition, a shear panel was provided between the rear strut towers. In combination with the bead shapes, this configuration helps to effectively suppress deformation (Fig. 20). Finally, a closed-section frame was provided around the luggage compartment opening. This frame helps to enhance torsional rigidity, achieve excellent body rigidity, reduce vibration caused by inputs from the suspension, and lower booming noise (Fig. 21).

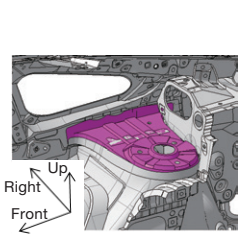


Fig. 19 Rear Strut Tower

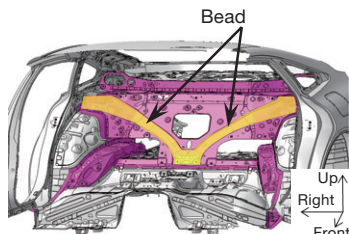


Fig. 20 Shear Panel

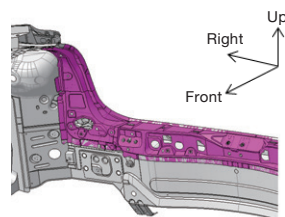


Fig. 21 Luggage Compartment Opening

4.4 Joining using structural adhesive and various welding techniques

To increase the rigidity of joints between components, structural adhesive was combined with laser welding and laser screw welding (LSW) to help communicate a strong impression of vehicle stiffness and ride comfort (Figs. 22 to 25).

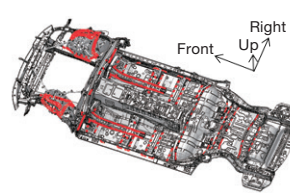


Fig. 22 Under Body

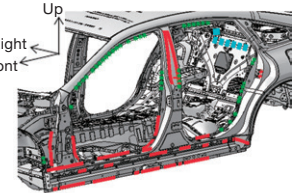


Fig. 23 Upper Body (Front Side)

* Figs. 22 to 23: red = adhesive, blue = laser welding, green = LSW

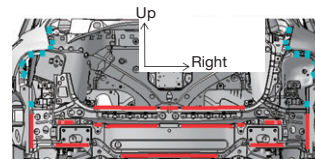


Fig. 24 Upper Body (Rear)

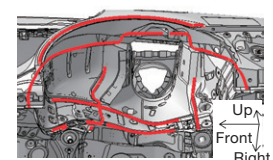


Fig. 25 Upper Body (Wheelhouse)

* Figs. 24 to 25: red = adhesive, blue = laser welding

5. Full Underbody Cover

Continuing on from the first-generation Mirai, a full underbody cover was adopted, taking advantage of the fact that an FCV has no high-temperature heat source (Fig. 26). This cover helps to help correct the airflow under the body, enhances handling, and helps to increase the driving range. In addition, the cover in the second-generation Mirai is mostly manufactured from a non-woven fabric. This gives the cover a sound-absorption effect, which helps to lower road and other noise in the occupant compartment, as well as external noise radiation from onboard components.

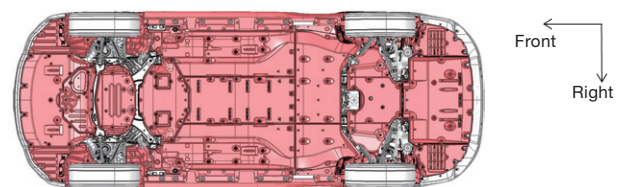


Fig. 26 Full Underbody Cover

6. Suspension

To enable both large tires and the various FC components to be mounted on the platform, the high-mounted multi-link front suspension with upper and lower ball joints from the Lexus LS and LC was adopted (a configuration that allows a lower hood due to the virtual kingpin axis) alongside a low-mounted multi-link rear suspension (Figs. 27 and 28).

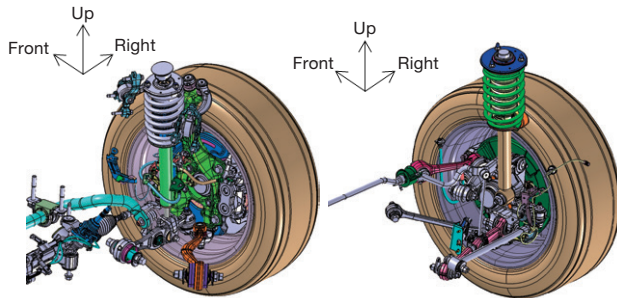


Fig. 27 Front Suspension

Fig. 28 Rear Suspension

7. Shock Absorbers

Twin-tube shock absorbers were adopted for reasons of style and performance. With the aim of achieving an excellent balance between steering response, ride comfort, and the impression of quality, a new sliding structure was adopted for the first time on the GA-L platform (Prosmooth™ shock absorbers manufactured by KYB Corporation). The rod guide bushes, piston bands, as well as the shape, materials, and blending of the shock absorber oil were optimized to obtain the most suitable shock absorber axial force (frictional force) up to extremely low speeds. This approach realized rapid response from immediately after the vehicle moves off (Fig. 29).

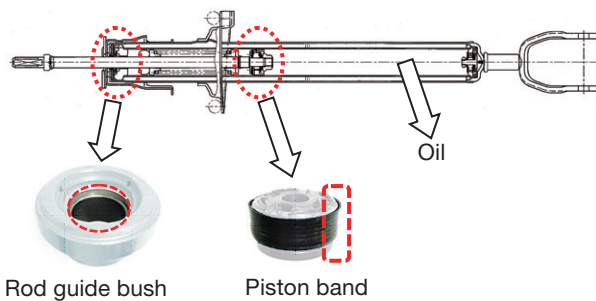


Fig. 29 Shock Absorber

8. Tires

Large tires (235/55R19) were developed to help increase the driving range, enhance handling and ride comfort, and to lower noise. An excellent balance between these requirements was achieved by optimizing the structure and materials of the tread rubber, as well as the belt reinforcement structure (Fig. 30). The upper grades of the Mirai are provided with 20-inch tires (245/45ZR20).



Fig. 30 Tire

9. Conclusion

Carrying on the legacy of the first-generation, the second-generation Mirai FCV is an attractive vehicle with global appeal. In particular, the future potential of the vehicle was boosted substantially by incorporating a number of innovations to the platform. With the second-generation Mirai still at the opening phase of its popularization, there are high hopes for further progress toward the realization of a hydrogen energy based society, including the provision of even greater infrastructure.

Authors



Y. KUMAZAWA



D. TERAMOTO



N. OGURA



H. BANDO



Y. ISHIKAWA

Special Feature

The New Character of the Second-Generation Mirai

Akira Kubota*¹

Abstract

“Design always has a reason, form always has meaning.” Tokuo Fukuichi, Toyota’s global design chief until 2019, often said this to the members of his design teams. It means that all final expressions of form must be built on the foundations of purpose, objective, function, and other elements. The design theme of the exterior styling of the first-generation Mirai was the embodiment of ingenuity as form. This theme aimed to showcase the new type of value provided by fuel cell (FC) technology. So, why was a new design adopted for the second-generation Mirai? Why was the decision made to change the outward visible character of the vehicle? This article addresses the thinking and intentions behind the decision to adopt a new character for the second-generation Mirai.

Keywords: *fuel cell vehicle (FCV), mission, popularization, character, emotion, sporty hydrogen-powered vehicle, functional/emotional design*

1. Introduction

What did you really think of the styling of the first-generation Mirai? The mission of the team in charge of styling the first-generation Mirai was to create a uniquely appealing design that communicated the arrival onto the market of the world’s first mass-production fuel cell vehicle (FCV). The theme selected by the design team was “the embodiment of ingenuity as form,” which was expressed through distinctive packaging and styling unique to an FCV. The fact that the styling of the first-generation Mirai was picked up so strongly by the media upon its launch suggests that the team achieved a powerful (and hoped-for) first impact.

So, now you have had the chance to see for yourselves, what do you make of the styling of the second-generation Mirai? It is likely that some people will be in favor of the styling, and others not. Whichever the case, it should appear that the character of the vehicle has changed.

The real thrill of day-to-day styling development differs from functional fields that measure performance in terms of numbers. Stylists revel in the creation of appeal in line with the mission of the vehicle, and giving a vehicle different aspects of character. This task is as difficult as it is exciting. Rather than discussing the resulting external form of the vehicle, this article focuses more on the background to why and how the character of the second-generation Mirai was changed.

2. New Mission

As mentioned above, the mission of the styling team for the first-generation Mirai was to create a uniquely appealing design suitable for the world’s first mass-production FCV. Building on the words of Tokuo Fukuichi, Toyota’s global design chief until 2019, the styling team adopted a function-based approach described as “the embodiment of ingenuity as form” to embody the generally unknown functions of a fuel cell (FC) in the form of a vehicle. The resulting unique proportions and large triangular side radiator grilles became new symbolic characteristics of FCVs.

Moving on from the first generation, the central mission of the second-generation Mirai is to further popularize FCVs. With the proper social infrastructure not yet fully in place, what is the role of the styling to support this mission and help popularize the Mirai?

- Should it be to create a suitable image for the ultimate environmentally friendly vehicle (i.e., as an FCV)?
- Should it reflect the expectations of customer toward the Mirai?

After tortuous debate, the conclusion was reached that the vehicle needed emotional styling with a direct appeal.

In other words, the reasoning behind the styling should not be “as an environmentally friendly vehicle...,” “as an FCV...,” or even “as the Mirai...” The styling must be powerful enough to appeal to the emotions of everyone, even those with no prior knowledge of FCVs. Only this approach has the potential to build new demand, create a following wind for building the necessary infrastructure, and invite further popularization. In this way, a strong feeling exists that the true mission of styling is to give rise to new directions (**Fig. 1**).

*¹ MS Design Div., Mid-size Vehicle Company

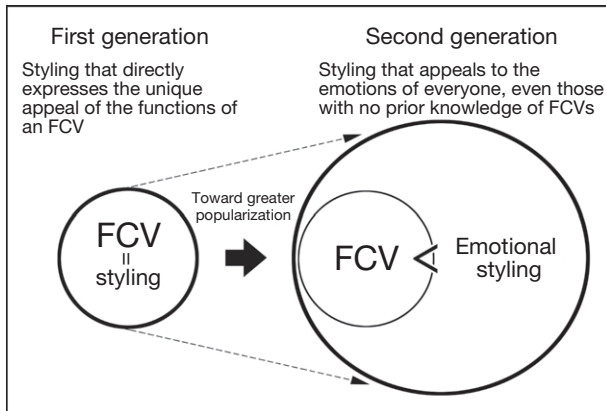


Fig. 1 How the Styling Mission Changed

3. The Creation of Appeal

People do not react with excitement when faced with something that fits inside existing categories of ideas or expectations. In fact, things or encounters that defy expectations or exceed the boundaries of existing ideas are what stimulate positive emotions and generate appeal and excitement. **Fig. 2** illustrates Tokuo Fukuichi's *Tobi-Shiro* concept (which means something like “stages of growth”) that explains the process behind creating appealing styling.

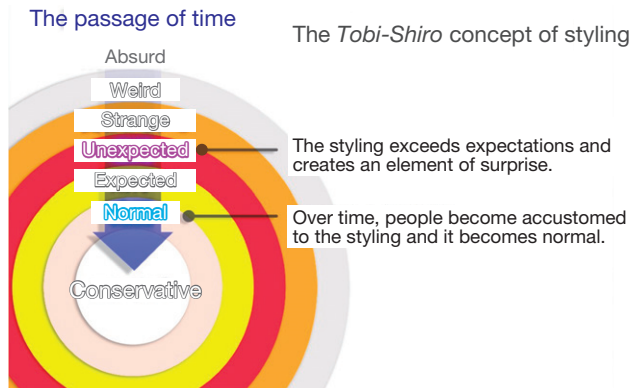


Fig. 2 Outline of the Tobi-Shiro Concept of Styling

The idea of stimulating positive emotions described above corresponds to the “unexpected” stage in the figure. However, if the stimulation is too intense, the styling becomes absurd and will no longer be interesting. In addition, styling that is stimulating at first will gradually become normal and commonplace over time. This figure also clearly illustrates the recognized idea that it is difficult to maintain the freshness of styling that is originally accepted without much resistance.

The difficulty of industrial styling lies in the creation of a styling that is appealing and readily acceptable, but that also retains its appeal to the endless variety of people’s imaginations over time.

So, how about the styling of the second-generation Mirai? Probably, most people thought that the styling of the second generation would be a continuation of the powerful image

created by the first generation, that is to say, a futuristic expression that further underlines the symbolism of the Mirai as an FCV. This would be a natural assumption if the starting point of the styling was “as an FCV....” In fact, at the beginning of the planning phase, this was the original starting point. However, with popularization as the mission of the Mirai, the team realized that very few ordinary customers were interested enough in the Mirai to enter the world of FCVs. Therefore, words expressing the role of the Mirai as an environmentally friendly vehicle or FCV were deliberately excluded from the styling mission of the new model, which was defined as emotional styling with a direct appeal. This mission was chosen because the team wanted to create a new way to reach and stimulate the interest of customers. The “direct appeal” part of the mission would be achieved through the stance of the Mirai: four large tires firmly planted at the corners of a wide and low body. The team saw this as an expression of the idea that a purely stylish car should incorporate a performance-focused sporty element.

Setting aside the function of the Mirai as FCV, the team was passionate about creating a sporty car with an emphasis on driving performance, and definitely not one with a wholly environmentally friendly image. This passion was the inspiration as the team started studying the packaging of the vehicle. One example of this can be seen in the ratio between vehicle height and external tire diameter (**Fig. 3**). Increasing the ratio of the tires to the vehicle height creates a greater awareness of driving performance and a stronger impression of agility, and results in sportier proportions. The stronger emphasis on the tire proportions compared to other vehicles should be obvious.

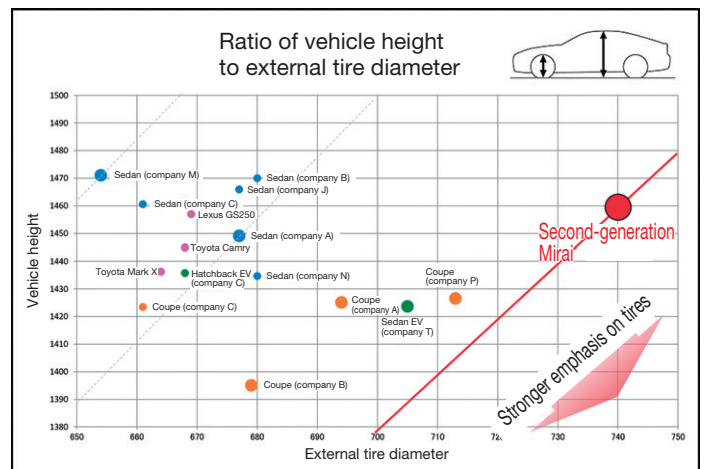


Fig. 3 Ratio of Vehicle Height to External Tire Diameter

Therefore, the team aimed to build a visually stimulating foundation by combining an assumption-busting styling mission with vehicle packaging designed to turn that mission into reality. It then considered how to create that sporty appeal described above. The following sections describe some of the specific challenges for realizing an emotional appeal through interior and exterior styling.

Special Feature

3.1 Exterior styling

The values behind the targeted performance-focused sporty appeal are different from those of sports car manufacturers such as Porsche or Ferrari.

The styling team wrestled with the following questions: how to express the new world of the second-generation Mirai, and how to translate the positive emotion generated by the Mirai into customer excitement.

It might be evident to people who have driven the Mirai that the second generation has built on the first generation to combine even quieter and smooth driving performance with a teleporter-like powerful acceleration feeling. This driving feel is a new and thrilling experience akin to flying a glider soundlessly over the surface of the Earth.

This irreplaceable and exciting sense of driving performance was defined as the very symbol of the emotion to be generated by the Mirai. Three-dimensional (3D) models were created to illustrate the embodiment of this symbol in physical forms (Fig. 4).

The top image shows the initial model, which lacks tires and is not bound in any way by the vehicle concept. The bottom image shows the final model that has been worked up into the shape of a car. From the initial to the final stages, the styling team pursued this new styling scheme without losing sight of the intentions and targets of the designers, resulting in the final target sketches shown in Fig. 5.

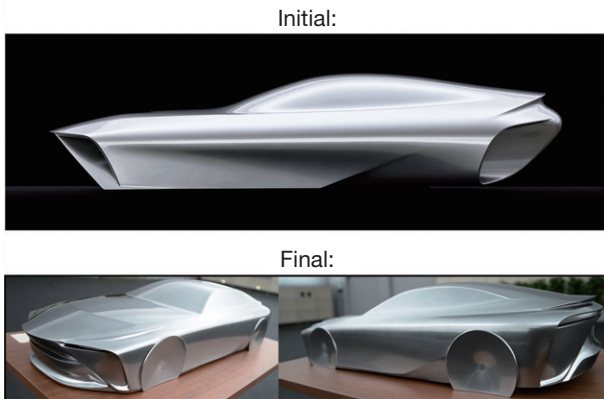


Fig. 4 3D Illustrative Models



Fig. 5 Target Exterior Sketches

In this way, the styling of the second-generation Mirai expanded the created images outward based on the new and exciting driving experience promised by the vehicle until it achieved an emotional beauty that expresses a new type of creative value.

3.1.1 Key points of the exterior styling

- (1) The rear-wheel drive layout of the Mirai combines long-nose proportions weighted toward the rear wheels with a sleek fastback design. The result is a new rear-wheel drive aerodynamic proportion that expresses a feeling of speed through every aspect of the vehicle (Fig. 6).



Fig. 6 Side View Styling Targets

- (2) The stance of the Mirai aims to express both agility and stability, like a blade cutting through the earth (Fig. 7).



Fig. 7 Stance Styling Targets

- (3) The Mirai creates a minimalistic impression using bold sectional changes without relying on conventional character lines, thereby emphasizing a silent yet powerful dynamism (Fig. 8).



Fig. 8 Bold Sectional Changes

- (4) The 20-inch wheels styled to represent jet turbine engines symbolize smooth a powerful driving performance (**Fig. 9**).



Fig. 9 20-Inch Wheels (Black Sputtering)

- (5) A new and deeply striking blue body paint that combines freshness and strength called Force Blue Multiple Layers was developed to appeal to mature sporty minded drivers (**Fig. 10**).



Fig. 10 Image of Force Blue Multiple Layers Body Color

3.2 Interior styling

For the interior, the styling team searched for an expression of emotional comfort. The moment that the driver sinks into the driver’s seat and grips the steering wheel, the moment that the driver presses the Sport mode button and feels the vehicle’s dynamism through all five senses, the moment that the occupants feel the acceleration (G) pressing on their backs in the silent cabin, the moment that, cocooned in refined materials, light, and sound, the passengers allow themselves to be taken away by the scenery flowing past the window: the styling team wanted to express comfort in all these moments through a special purity of experience that can only be realized by the Mirai.

The target image for the interior styling was a refined and exhilarating sense of driving pleasure without relying on gaudy ornamentation. This was symbolically expressed in the target sketches (**Fig.11**).

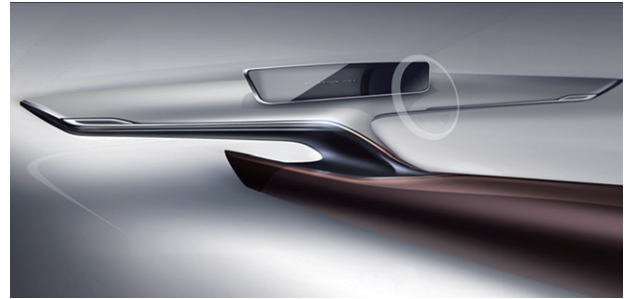


Fig. 11 Target Sketch of Interior

3.2.1 Key points of the interior styling

- (1) The new cockpit space provides the driver with an assuring feeling of being cocooned, while creating a feeling of comfort and spaciousness for the front passenger (**Fig. 12**).

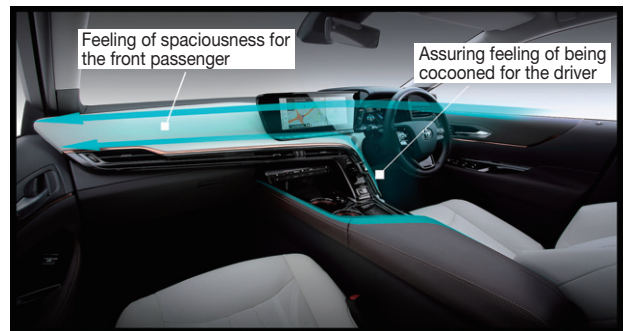


Fig. 12 Aims of the Interior Styling (1)

- (2) The front of the cockpit consists of a sweeping soft pad that wraps around the occupants and acts as a foundation for a large instrument cluster that consolidates the information functions. The styling aimed to combine a contrasting impression of concentration and relaxation (**Fig. 13**).

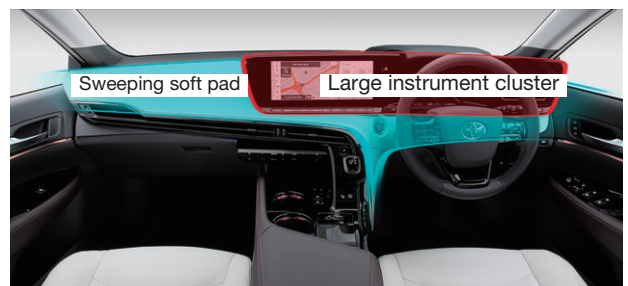


Fig. 13 Aims of the Interior Styling (2)

Special Feature

- (3) The theme of the opening movie is “flow.” The images were selected to express a silent yet dynamic sensation of the vehicle starting up (**Fig. 14**).



Fig. 14 Opening Movie

- (4) The interior illumination can be customized from the center display from a total of eight colors. The wide variety of illumination helps to create an interior space that matches the mood of the occupants (**Fig. 15**).



Fig. 15 Interior Illumination

- (5) The optional panoramic roof fills the whole interior with a soft light, creating a comfortable and airy feeling (**Fig. 16**).



Fig. 16 Airy Feeling of the Panoramic Roof

4. Conclusion

The styling of the second-generation Mirai was unveiled through the Mirai Concept model exhibited at the 2019 Tokyo Motor Show. People who saw the styling for the first time were taken aback. “Is this the Mirai?” many of them said. Some people were convinced that the styling was just for the concept model and that the actual production model would have a more “mature” design. These comments can be interpreted as surprise at how much the appeal of the second generation differs from the first generation, in other words a direct expression of the new character of the Mirai.

After the Mirai goes on sale, many people will have the chance to test drive the Mirai as well as just look at it.

The styling team hopes that people will enjoy both the new and exciting driving performance of the Mirai and its visceral styling.

The styling of the second-generation Mirai was developed with a completely different mission than the first generation. Toyota has high hopes that it will serve as a new trigger toward the realization of the hydrogen energy based society of the future.

Author



A. KUBOTA

Development of the Noise and Vibration Performance of the Second-Generation Mirai

Tepei Ishikawa*¹
 Yusaku Hamuro*¹
 Tomohisa Kato*²
 Chie Fukuhara*³
 Kazuhiro Kamei*⁴

Abstract

The second-generation Mirai was developed with the objective of achieving a refined and vibration-free driving experience from the moment that the vehicle moves off, comfortable acceleration, and fun-to-drive dynamic performance. Reflecting this objective, the noise and vibration performance of the vehicle was developed to realize a quiet and superior experience, particularly in everyday driving scenarios. In addition, to enhance the informational function of the vehicle, which is an important aspect of fun-to-drive performance and dictates how vehicle behavior is communicated in response to driver input, an acceleration sound was developed to fit the acceleration characteristics of a fuel cell vehicle (FCV) and the image of the second-generation Mirai. This article describes some specific examples from the noise and vibration development of the second-generation Mirai.

Keywords: *fuel cell vehicle (FCV), vibration, noise, noise and vibration (NV) performance, air compressor noise, acceleration sound*

Special Feature

1. Introduction

The first-generation Mirai, which was launched in 2014, was developed under the concept of realizing a torque-full and quiet driving performance.

To broaden its appeal to an even wider range of people, the development of the second-generation Mirai aimed to create a quiet driving performance that generates a sense of refinement. In addition, by realizing a particular acceleration sound, the development also aimed to achieve noise and vibration (NV) performance that expresses the fun-to-drive aspect of the Mirai.

2. Aims of NV Performance Development

Although reducing the noise and vibration felt by the vehicle occupants is a central part of creating a feeling of refinement, it is equally important to realize peak-free transient NV trends that match the changes in vehicle speed and acceleration. This development aimed to achieve a tangibly refined NV performance that makes maximum use of the lack of engine system noise.

This article describes some of the key topics related to NV in the development of the second-generation Mirai.

3. NV Performance Development Case Studies

3.1 Reduction of interior noise during constant-speed driving

Since a fuel cell vehicle (FCV) generates no engine noise, other types of noise (such as road noise, wind noise, and so on) may be more noticeable to the vehicle occupants when driving at a constant speed. Since road noise disperses into input frequencies from the suspension to the body and floor panel resonance frequencies, this was addressed by analyzing the resonance of each panel and incorporating innovations into the vehicle structure. Wind noise was addressed by adopting innovative exterior design elements to reduce exterior noise, particularly around the door mirrors, while maintaining the optimum balance with the exterior styling at the front of the vehicle.

These measures helped to reduce interior noise and realize a tangibly refined level of quietness (**Fig. 1**).

*¹ MS Vehicle Evaluation & Engineering Div., Mid-size Vehicle Company

*² Fuel Cell Products Development Div., Toyota ZEV Factory

*³ Lexus Vehicle Evaluation and Engineering Div., Lexus International Company

*⁴ Toyota Motor East Japan, Inc.

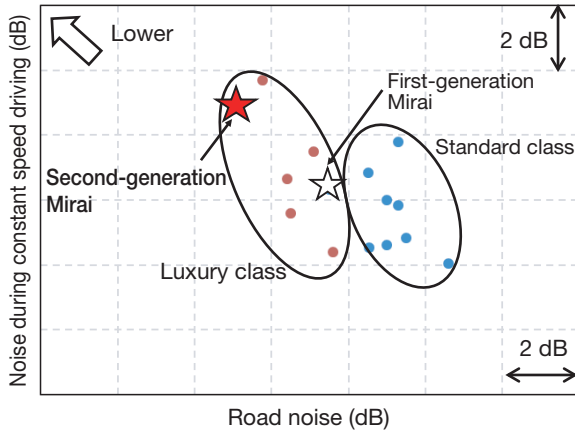


Fig. 1 Noise Level during Constant-Speed Driving

3.2 Reduction of interior noise while accelerating

An FCV includes a wide range of vibration sources, including the pump and injector used to supply the hydrogen, and the air compressor (ACP) that supplies the oxygen. In particular, the ACP used on the second-generation Mirai is a turbo pump that is equipped with a speed-increasing function. This pump generates 1st and 2nd order phenomena of motor rotation as well as a 1st order phenomenon of impeller rotation (an 11th order phenomenon of motor rotation).

This 1st order phenomenon of motor rotation is vibration that is transmitted as interior noise through the fuel cell (FC) mounts. The 2nd order phenomenon of motor rotation is an acoustic phenomenon that is transmitted between the under body and under cover. The 1st order phenomenon of impeller rotation is an acoustic phenomenon generated by the ACP and its joining parts. The measures applied to counter these phenomena were as follows.

1. Vibration insulation was applied to the ACP and all its joining parts to reduce noise generation by these parts as well as vibration transmission via the FC mounts.
2. The overall mass of the FC components was used to reduce vibration sensitivity by ensuring the rigidity of the FC frame and creating a rigid attachment to the stack.
3. Body sensitivity was addressed by drilling holes in the under cover and applying sound insulating materials inside and outside the occupant compartment.

Fig. 2 shows how much the interior noise was reduced compared to the first-generation Mirai.

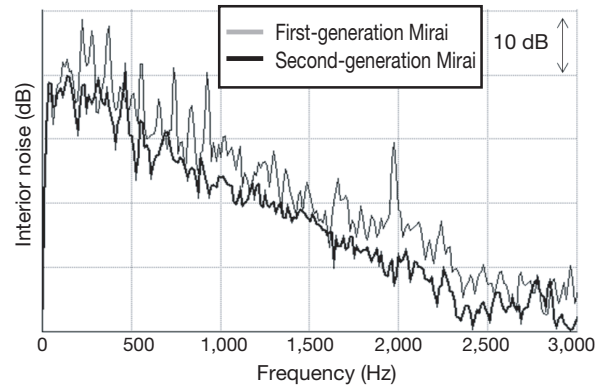


Fig. 2 Level of Noise during Wide-Open Throttle Acceleration

Fig. 3 compares the interior noise of the second-generation Mirai and a hybrid vehicle at the same speed and acceleration. These results illustrate the reduction in peak interior noise characteristics.

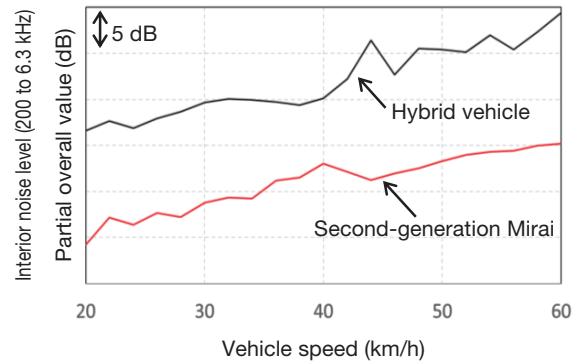


Fig. 3 Level of Noise during Acceleration

3.3 Reduction of steering vibration

In a conventional vehicle, auxiliary equipment such as the air conditioning (A/C) compressor is usually attached to the engine. The large mass of the engine has the effect of reducing the vibration of this auxiliary equipment when it operates.

In contrast, the FC stack and auxiliary equipment of the second-generation Mirai is attached to the lightweight FC frame. Therefore, to reduce vibration transmission via the FC mounts, rubber bushings were applied to the A/C mounts. Fig. 4 shows the stack mounting system and Fig. 5 illustrates the changes generated by different methods of joining the A/C and FC frame, as calculated by a two-degree of freedom spring mass model.

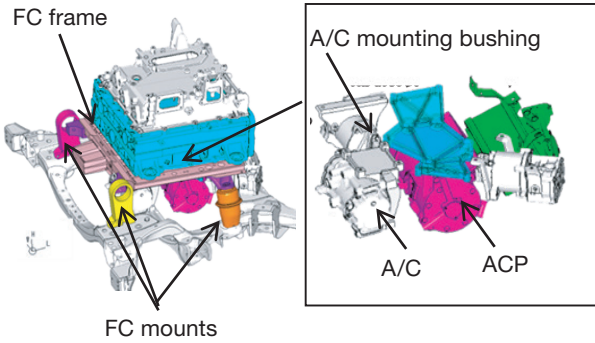


Fig. 4 Stack Mounting System and Layout of Auxiliary Equipment

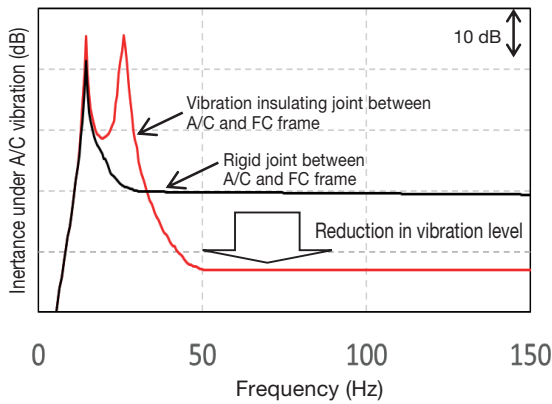


Fig. 5 Effect of Different Joining Methods between A/C and FC Frame

4. Acceleration Sound

4.1 Background of acceleration sound development

In addition to the quiet and refined performance described in the previous section, the development team was aware that the vehicle would be less fun to drive without interaction between the driver and vehicle created by sound resonant of dynamic performance as the driver depresses the accelerator, emulating the engine sound of a conventional vehicle. This is referred to as the informational function of sound. For this reason, it was decided to develop an acceleration sound specifically for an FCV.

After a long series of test drives and discussions with expert drivers inside Toyota, the informational function of the FCV sound was defined as a recognizable sound that expresses the harmony between driver operation (accelerator pedal) and vehicle behavior (acceleration).

4.2 Sound generation device

In the initial phase of sound development, the team examined the feasibility of using the sounds of various components, such as the motor and ACP that accompany operation of the power train. However, since the changes in sound pressure do not

match changes in the speed region or acceleration, it was difficult to use these to obtain an FCV sound with the necessary informational function. Fig. 6 illustrates the difference between the interior noise frequency characteristics and required interior noise during acceleration.

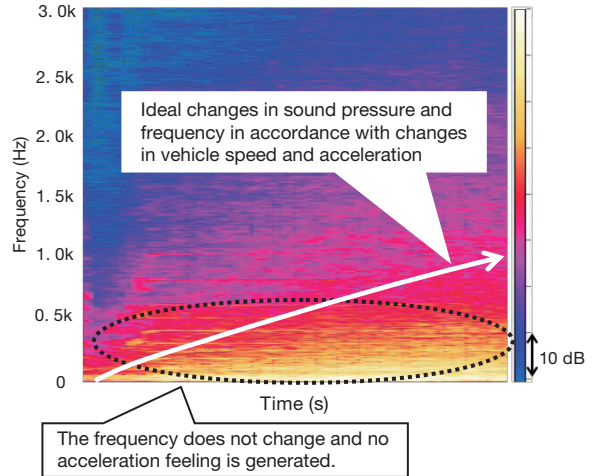


Fig. 6 Difference between Interior Noise Frequency Characteristics and Required Interior Noise during Acceleration

Therefore, it was decided to adopt an active sound control (ASC) system on the second-generation Mirai. This ASC system uses a dedicated ECU and speakers to generate a specific sound. With this system, it was possible to construct the necessary logic to realize an FCV sound with the targeted informational function.

4.3 Tonal balance of acceleration sound

In addition to the informational function, it was equally important to create an FC sound with the correct tonal balance. The development team studied how to generate the appropriate tonal balance using the key words “Nature-tech” and “Velocity,” which could also be applied to the exterior styling of the vehicle (Fig. 7).

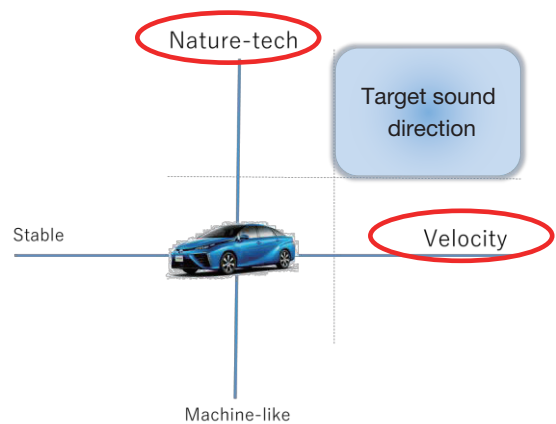


Fig. 7 Target Direction for the Acceleration Sound of the Second-Generation Mirai

First, the evaluation indices were defined using four pairs of adjectives that express tonal balance. Then, specific objective sound attributes that might affect each evaluation index were proposed (Table 1).

Table 1 Sound Evaluation Adjective Pairs and Proposed Objective Sound Attributes

Index	Evaluation adjective pairs	Proposed objective attributes
1	Powerful/strong	Sum of energy up to max. 1 kHz
2	Elegant/traditional	Harmony
3	Thick/deep	Changes in frequency band for each speed region
4	Bright/light	Sum of energy in 1 to 2 kHz bands

Based on the keyword “Velocity” (i.e., the sensation of speed of the second-generation Mirai), it was decided that the sound should emphasize evaluation index 1 (powerful/strong). In addition, to realize tonal balances in line with the expectations of the driver determined via the drive mode switch, it was decided that the sound in Normal mode should emphasize index 3 (thick/deep) and that the sound in Sport mode should emphasize index 4 (bright/light).

4.4 Acceleration sound creation and frequency characteristics

Various attempts were made to embody these tonal balances. Studies were carried out by simulating the sound generated by motor rotation. Although the informational function could be realized by changing the frequency in line with the speed, the evaluation score for tonal balance index 3 (thick/deep) remained low.

In contrast, processed ambient and white noise sounds commonly used in special effect-based movies were evaluated as having a futuristic tonal balance but a less effective informational function. These were rated as unrealistic sounds for a vehicle.

Based on these results, to achieve the desired informational function, it was decided to create an original sound that includes both motor-like rotational elements and white noise elements that create a futuristic impression.

In partnership with an external sound creator, repeated test drives were carried out with Toyota’s in-house expert drivers to produce the acceleration sound of the second-generation Mirai, a sound that realizes both the targeted informational function and tonal balances.

Figs. 8 and 9 show the interior noise frequency characteristics under wide-open throttle acceleration in Normal and Sport modes, respectively.

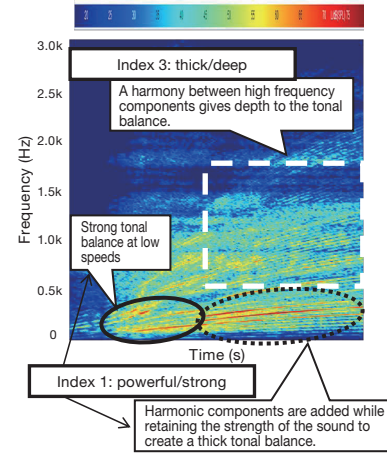


Fig. 8 Example of Acceleration Sound Generation (Normal Mode)

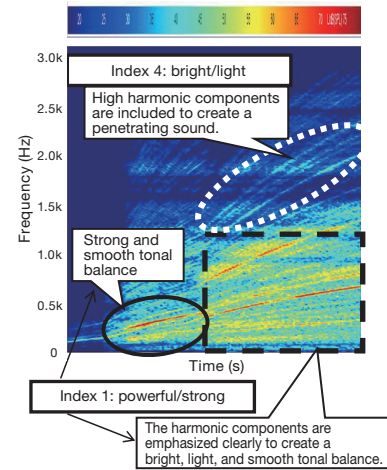


Fig. 9 Example of Acceleration Sound Generation (Sport Mode)

4.5 Verification of proposals

Fig. 10 shows the results of an evaluation carried out by 22 people, including Toyota’s in-house expert drivers and test subjects from the target user base.

The participants were asked in a questionnaire to evaluate the sound based on the adjective pair indices on a scale of 1 to 5. Although the principle speed region used by each driver differed, the results indicated that the targeted trends were achieved in each driving mode.

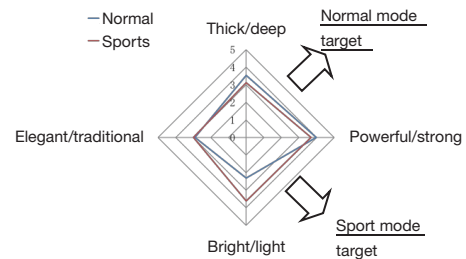


Fig. 10 In-House Evaluation Results

5. Conclusion

The NV performance development of the second-generation Mirai aimed to combine a highly refined sense of quietness with an appropriate acceleration sound. Evaluation results confirmed that this objective was achieved. It would give the development team the greatest pleasure to invite the readers of the *Toyota Technical Review* to experience the refined sense of quietness of the Mirai in daily driving, as well as its unprecedented acceleration sound when merging onto a highway or the like. The team is confident that the acceleration sound creates a recognizable harmony between driver operation and vehicle behavior.

Finally, the authors would like to express their sincere gratitude to everyone involved in the development of the ASC and to marimoRECORDS Co., Ltd. for their invaluable assistance in the creation of the acceleration sound.

Reference

- (1) H. Tajima et al. "Engine Sound Designing for Hot Hatch." *Proceedings of the JSAE Annual Congress* No. 20196155 (2019).

Authors



T. ISHIKAWA



Y. HAMURO



T. KATO



C. FUKUHARA



K. KAMEI

Development of the Dynamic Vehicle Performance of the Second-Generation Mirai

Wataru Ashikawa*¹
Shugo Okamatsu*¹
Makoto Inoue*¹

Abstract

Although fuel cell vehicles (FCVs) may be regarded as the ultimate environmentally friendly vehicle, the second-generation Mirai was not developed simply with environmental friendliness in mind. The development also aimed to achieve a refined and vibration-free driving experience from the moment that the vehicle moves off, comfortable acceleration, and fun-to-drive dynamic performance. In particular, this meant focusing on achieving easy-to-drive, confident, and natural dynamic performance by maximizing the drive motor characteristics, without fixating simply on acceleration times and critical cornering performance.

Keywords: acceleration feeling, deceleration feeling, front/rear weight distribution, body rigidity, vehicle dynamics control, suspension, resonance frequency arrangement

1. Introduction

The first-generation Mirai was well received due to the characteristic low vibration and noise performance of its electric traction motor, combined with torque-full acceleration performance that responds instantly when the driver depresses the accelerator pedal.

Additionally, the driving force of the second-generation Mirai was designed with acceleration and deceleration characteristics that help the driver to control the vehicle speed and load shifts in accordance with the driving scenario.

At the same time, the main focus of the development of the second-generation Mirai was to realize handling and ride comfort that helps to ensure a confident, natural, and enjoyable driving experience during acceleration and at high vehicle speeds.

This article describes the dynamic performance of the second-generation Mirai in terms of its acceleration and deceleration feeling, handling, and ride comfort.

2. Acceleration and Deceleration Feeling

2.1 Acceleration feeling control design

One of the merits of an electrified vehicle is highly responsive and seamless power performance. Using these characteristics, the development aimed to create a tangible fun-to-drive experience with confident and natural driving performance.

The acceleration feeling of a vehicle can be experienced via the following four physical elements with respect to the accelerator pedal stroke.

- (1) The time to perceive the vehicle starting to move
- (2) The rate that acceleration increases (gradient of the acceleration curve)
- (3) The amount of acceleration
- (4) The acceleration sustainability

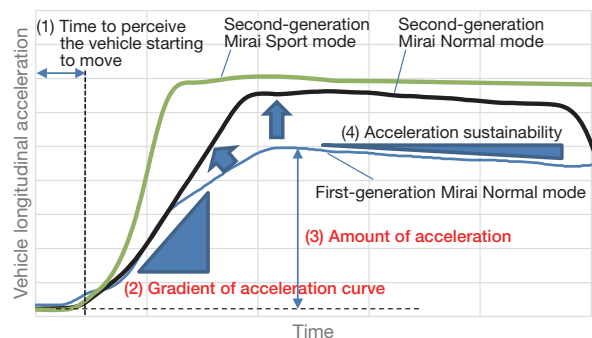


Fig. 1 Acceleration Feeling of the Second-Generation Mirai

Characteristics (2) and (3) of the second-generation Mirai were designed to exceed those of the first-generation Mirai to help generate an even better acceleration feeling.

The development also aimed to realize acceleration characteristics in tune with the driving scenario via shock-free and smooth acceleration at low speeds and sharp and smooth acceleration at medium and high speeds.

2.2 Body movement control design during acceleration

The development of the second-generation Mirai focused on controlling body movement during acceleration.

When a vehicle accelerates, the driving force is transmitted to the vehicle via the suspension. However, the amount of pitching increases in accordance with the distance between the

*¹ MS Vehicle Evaluation & Engineering Div., Mid-size Vehicle Company

suspension reaction points and vehicle center of gravity. Therefore, the pitching during acceleration was suppressed by adopting an innovative rear suspension arm layout, thereby helping to realize enjoyable acceleration that feels like being pushed from the seats in the direction of movement (Fig. 2).

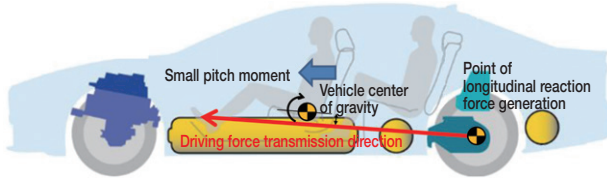


Fig. 2 Direction of Force and Vehicle Center of Gravity

2.3 Deceleration feeling control design

The deceleration feeling derives from the deceleration generated when the driver releases the accelerator pedal. In the same way as the acceleration feeling, deceleration is felt based on the deceleration amount and the gradient of the deceleration curve. If the deceleration is appropriate, the driver can control the vehicle speed more easily without having to keep depressing the accelerator and brake pedal, thereby helping to enhance vehicle stability and create a confident and natural driving feel.

The deceleration amount and gradient of the deceleration curve were refined in the second-generation Mirai compared to the first generation. A control was also adopted that increases the amount of deceleration in accordance with the driving scenario.

For example, the amount of deceleration is increased in accordance with the gradient of the road when driving downhill to restrict increases in speed. In addition, during sporty driving on winding roads, the optimum deceleration is analyzed based on the lateral and longitudinal acceleration of the vehicle to assist the driver (in Sport mode) (Fig. 3).

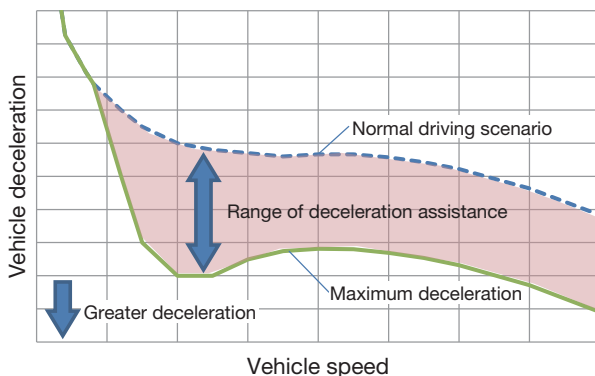


Fig. 3 Illustration of Deceleration Control in Accordance with Driving Scenario

3. Handling and Ride Comfort

3.1 Aims of handling and ride comfort

The aim of the vehicle dynamic performance development was to achieve safe, confident, and natural handling. This was accomplished by focusing on the front/rear weight distribution, body rigidity, and vehicle dynamics control.

In addition, the development also focused on reducing suspension inputs and optimizing the resonance frequency arrangement to help realize a refined and comfortable ride.

3.2 50:50 front/rear weight distribution

The development aimed to achieve a 50:50 front/rear weight distribution by identifying the optimum powertrain component layout (Fig. 4).

A 50:50 front/rear weight distribution allows a more neutral slip angle while cornering and helps to create a more natural cornering feeling (Fig. 5).

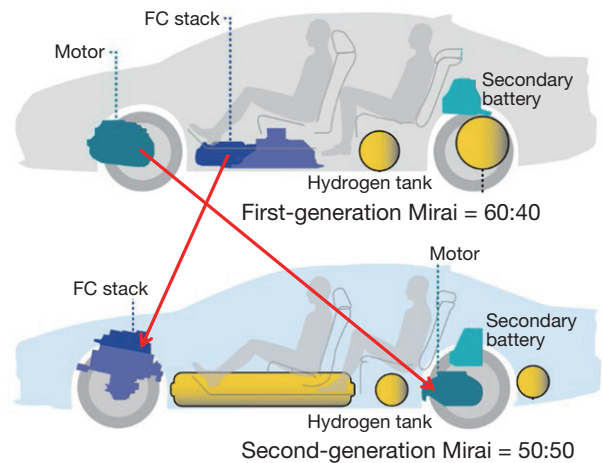


Fig. 4 Weight Distribution Comparison

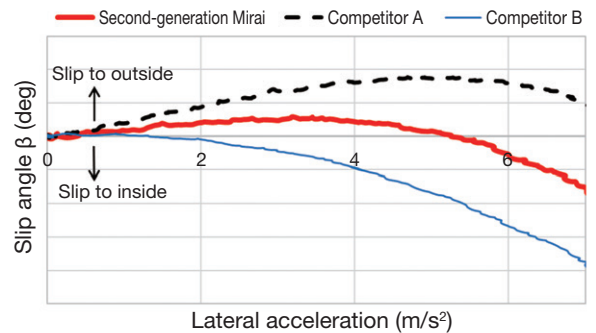


Fig. 5 Relationship between Lateral Acceleration and Vehicle Slip Angle

Special Feature

3.3 Body rigidity

A highly rigid body is a precondition for realizing excellent handling and enhancing the texture of the ride comfort.

The front body, cabin, and rear body of the second-generation Mirai were strengthened by adopting the features described below. As a result, the body torsional rigidity of the second-generation Mirai is 25% higher than that of the first-generation (Fig. 6). For details, refer to Section 4 of the article in this edition of the *Toyota Technical Review* that describes the platform of the second-generation Mirai.

- Under-hood reinforcing braces
- Shear panel and large beads between the rear strut towers
- Annular (ring) structure inside rear luggage compartment

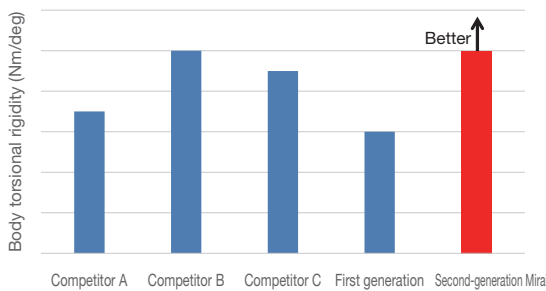


Fig. 6 Body Torsional Rigidity

Adopting a shear panel is an effective way of suppressing shear deformation of the suspension members due to lateral force inputs to the suspension. Since a fuel cell vehicle (FCV) does not require an engine oil replacement hole, the rigidity of the shear panel was increased to help create a lightweight and highly rigid structure (Fig. 7). For details, refer to Section 4 of the article in this edition of the *Toyota Technical Review* that describes the platform of the second-generation Mirai.

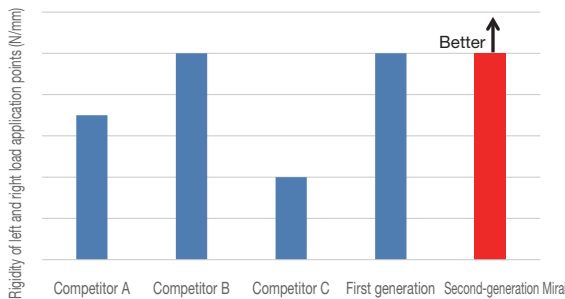


Fig. 7 Rigidity of Load Application Points

3.4 Development of vehicle dynamics control

To realize a good balance between cornering performance and stability at the performance limits, the development also focused on stability control.

Greater cornering performance tends to have a trade-off

relationship with tuck-in stability. The second-generation Mirai achieves an excellent between cornering performance and stability at the performance limits by adopting feedforward cornering performance that avoids tuck in (Fig. 8).

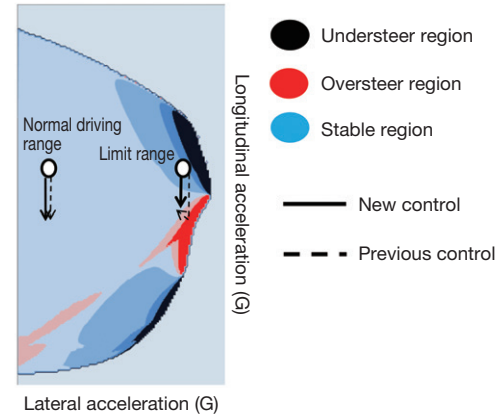


Fig. 8 G-G Diagram

In contrast to the previous control, which reduced the amount of deceleration after detecting tire slip (i.e., vehicle oversteer), the new control adopts a feedforward control that reduces the amount of deceleration in accordance with lateral acceleration.

This reduces the amount of deceleration at high speeds and helps to ensure vehicle stability.

3.5 Reduction of suspension inputs

To maintain both excellent dynamic performance and a refined and comfortable ride, a double wishbone front suspension was combined with a multi-link rear suspension (Fig. 9).

In addition, lowering the spring constant of the lower bushings helped to ensure longitudinal compliance and reduce shock when driving over bumps (Fig. 10).

Although smoother ride comfort can generally be achieved by reducing the damping force of the shock absorbers, this tends to increase movement of the sprung mass (i.e., the vehicle body), and make convergence more difficult to achieve. Therefore, in the second-generation Mirai, friction is applied to the sliding parts of the shock absorbers to facilitate sprung mass convergence. As a result, the damping force of the shock absorbers could be reduced to realize smooth ride comfort with enhanced sprung mass convergence. For details, refer to Section 7 of the article in this edition of the *Toyota Technical Review* that describes the platform of the second-generation Mirai.

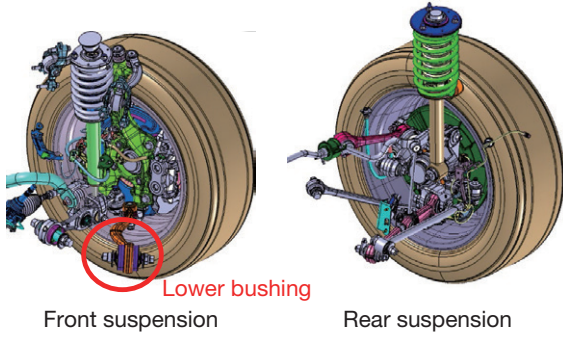


Fig. 9 Front and Rear Suspensions of the Second-Generation Mirai

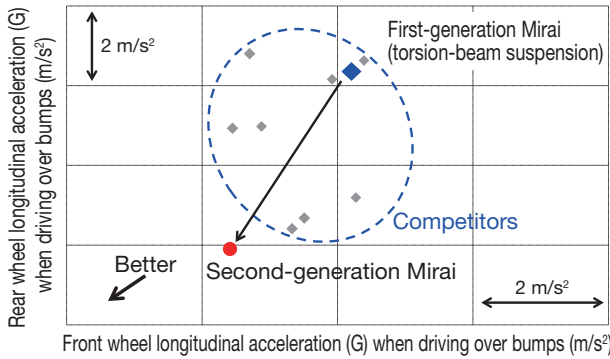


Fig. 10 Comparison of Shock when Driving Over Bumps

3.6 Suspension inputs and resonance frequency arrangement

The fuel cell (FC) components mounted under the hood of the second-generation Mirai are lighter and generate less noise and vibration than an engine. Therefore, the spring constant of the mounting system can be increased to raise the resonance frequency of the FC components (Fig. 11).

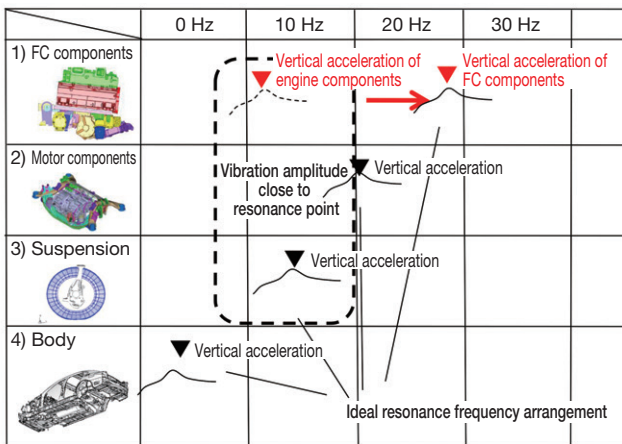


Fig. 11 Illustration of Resonance Frequency Arrangement

As a result the resonance frequency of each component was dispersed away from the large inputs of unsprung mass vibration, helping to realize refined ride comfort with little vibration (Fig. 12).

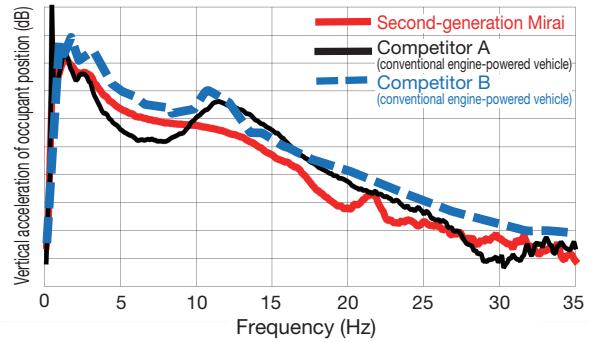


Fig. 12 Low-Vibration Ride Comfort

3.7 Body movement control

The development of body movement control adopted a new index that expresses natural motion when driving on highly undulating roads.

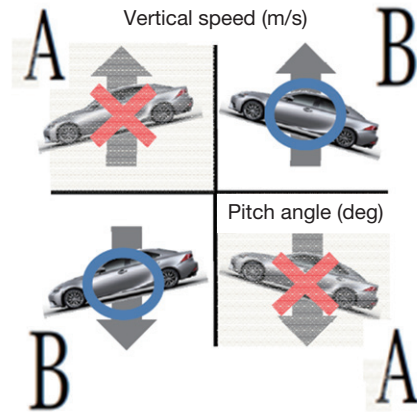


Fig. 13 New Index for Body Movement Control

Under the new index, body movement featuring minimal input from region A was defined as natural, and movement with a small pitch angle was defined as stable. The suspension of the second-generation Mirai was optimized to realize stable and natural ride comfort (Fig. 14).

Special Feature

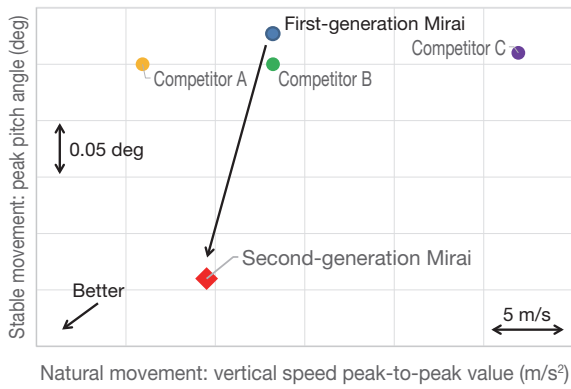


Fig. 14 Natural and Stable Body Movement

4. Conclusion

The vehicle dynamics performance of the second-generation Mirai was realized through a combination of Toyota’s engineering, manufacturing, and tuning capabilities.

The easiest way to appreciate the second-generation Mirai is to get behind the wheel, step on the accelerator pedal, and take it for a drive over all kinds of roads. This is the best way to experience and enjoy the advances that have been made in vehicle dynamics performance.

Authors



W. ASHIKAWA



S. OKAMATSU



M. INOUE

Development of the Aerodynamic Performance of the Second-Generation Mirai

Hideaki Takeda*¹
 Akihito Hosoi*¹
 Hiroshi Kuroda*¹
 Aoi Kodama*²

Abstract

Two of the important objectives for the second-generation Mirai were to substantially extend the cruising range of the vehicle and to realize emotionally powerful styling. To help realize these objectives, the aerodynamic performance development aimed to: (1) enhance underbody airflows to facilitate the installation of three hydrogen tanks, (2) optimize the shape of the exterior design, and (3) achieve a balance between the oil cooling system of the drive motor in a rear-wheel drive layout and aerodynamics. As a result, the second-generation Mirai achieved a cruising range of approximately 850 km in the Worldwide-Harmonized Light Vehicles Test Cycle (WLTC) that measures fuel efficiency. This article describes the aerodynamic performance development of the second-generation Mirai.

Keywords: fuel cell vehicle (FCV), aerodynamics, cooling, shape optimization

1. Introduction

The development of the Mirai fuel cell vehicle (FCV) started with the objective of greatly enhancing both the environmental performance and the fundamental appeal of the vehicle to facilitate its transition from a low-volume model with global sales above 10,000 units to a true mass-production model.

The latest know-how and analytical techniques were applied to the underbody and external design of the vehicle to realize the optimum balance between packaging, styling, and aerodynamic performance.

In addition, with the change in packaging from a front-wheel to a rear-wheel drive layout, it was also necessary to change the motor cooling method.

This article describes the aerodynamic performance development of the second-generation Mirai to help it lead the way toward the hydrogen energy based society of the future.

The development used both computational fluid dynamics (CFD) and wind tests with a 1/1 scale aerodynamic test vehicle.

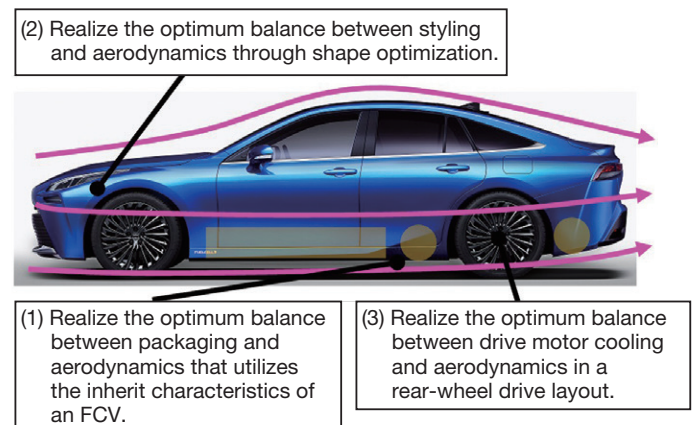


Fig. 1 Aerodynamic Development Concepts

2. Aerodynamic Performance Development Concepts

The aerodynamic performance of the second-generation Mirai was developed under the following main concepts: (1) realize the optimum balance between packaging and aerodynamics that utilizes the inherit characteristics of an FCV, (2) realize the optimum balance between styling and aerodynamics through shape optimization, and (3) realize the optimum balance between drive motor cooling and aerodynamics in a rear-wheel drive layout (Fig. 1).

3. Development of Underbody Flow Utilizing the Inherit Characteristics of an FCV

Unlike a gasoline-powered vehicle, an FCV has no exhaust pipe or other high-temperature parts. Therefore, a large cover can be adopted that creates a smooth underbody and lowers drag (Fig. 2). However, to ensure a sufficient cruising range, the second-generation Mirai is equipped with three hydrogen tanks under the floor of the vehicle. For this reason, the ground clearance of the bottom under cover surface must be partially lowered, which places major restrictions on the underbody shape for obtaining ideal aerodynamics.

Due to the effects of these restrictions, it was assumed that

*¹ MS Vehicle Evaluation & Engineering Div., Mid-size Vehicle Company

*² Mobility Evaluation and Engineering Div., Advanced R&D and Engineering Company

the airflows discharged from the engine compartment would merge with the underbody flows, form partially contracted flows, and then head toward the sides of the vehicle. In addition to impairing the main side flows, underbody flows heading toward the sides of the vehicle might also promote turbulence around the rear tires. Therefore, the development focused on the areas in front and to the inside of the rear tires, which could be modified without affecting the mounting of the hydrogen tanks. In these locations, the shape of the floor cover was partially raised to guide airflows to the rear of the vehicle (Fig. 3).

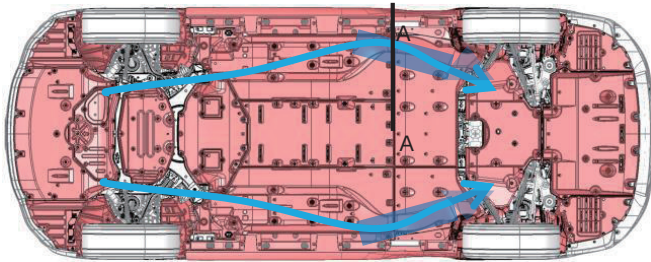


Fig. 2 Underbody Cover of the Second-Generation Mirai

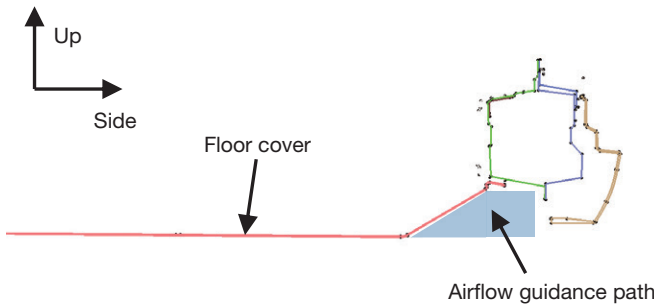


Fig. 3 Cross Section of Floor Cover (A-A)

4. Shape Optimization of Exterior Design

The aerodynamic performance development of the second-generation Mirai adopted shape optimization as a technique to realize the optimum balance between emotional styling and aerodynamic performance.

In the exterior design shape optimization process, the design variables of the applicable portions are defined. Then, by automating the shape change and CFD process by mesh morphing, it was possible to select various designs that realize a low coefficient of drag (C_D). This has the effect of increasing exterior design flexibility. This development defined the shape of the characteristic front bumper corners of the Mirai as the design variable and aimed to realize the optimum balance between styling and aerodynamic performance. This technique identified a shape that reduced airflow separation in the area shown in the figure below, which helped to reduce C_D (Fig. 4).

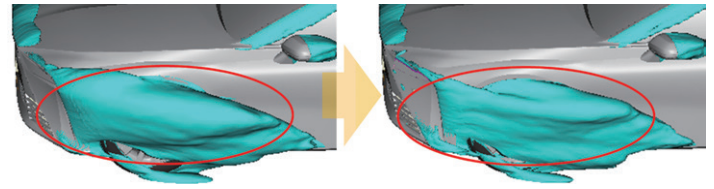


Fig. 4 Comparison Before and After Exterior Design Shape Optimization

5. Cooling of Drive Motor in Rear-Wheel Drive Layout

The second-generation Mirai has a rear-wheel drive layout with the drive motor mounted at the rear. Therefore, the air-cooled oil cooler had to be moved from the left side of the front bumper to behind the rear tires (a world first for a sedan).

Unlike the previous position near the front bumper, airflow cannot be guided to the oil cooler in this position by ram pressure. In addition, if a fan was used to guide air to the oil cooler, it would be difficult to mask the fan noise and ensure reliability at the same time. Therefore, the development focused on the pressure difference between the rear surface of the vehicle and the underbody and considered a new airflow guidance structure and cooler layout (Fig. 5).

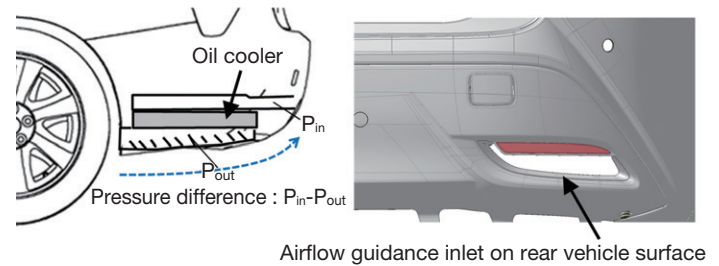


Fig. 5 Cooling Structure of Drive Motor in the Second-Generation Mirai

The layout of the vehicle rear surface and underbody was studied to prevent reverse flow. The development also confirmed that cooling performance was secured during cornering as well as when the vehicle is driving in a straight line.

The fin shape of the underbody air outlet was also optimized so that the discharge of cooling air does not adversely affect the aerodynamic performance.

6. Conclusions

The following aerodynamic technologies were developed and adopted in the second-generation Mirai. The result is an emotionally styled vehicle that achieved a cruising range of approximately 850 km in the Worldwide-Harmonized Light Vehicles Test Cycle (WLTC).

- (1) The optimum balance between vehicle packaging to mount three hydrogen fuel tanks and aerodynamics was realized

through a new underbody flow concept based on an innovative floor cover shape.

- (2) The concept of exterior design shape optimization was adopted to realize the optimum balance between styling and aerodynamics that can only be accomplished by an FCV.
- (3) The requirements for motor cooling performance were satisfied by mounting the oil cooler at the rear of the vehicle, the first time such a layout had been achieved anywhere in the world. This approach helped to realize the optimum balance between cooling performance and aerodynamics.

Authors



H. TAKEDA



A. HOSOI



H. KURODA



A. KODAMA

Development of the Passive Safety Performance of the Second-Generation Mirai

Toshihiro Fujiwara*¹
 Hiromasa Tanaka*²
 Shuji Hirakata*³

Abstract

One of the missions of the second-generation Mirai is to lead the way toward a hydrogen energy based society. The second-generation Mirai features a different fuel cell (FC) system layout than the previous model, and has an additional third hydrogen tank at the rear of the vehicle. With the passive safety performance of the vehicle given priority, work began from the initial phase of the development. In addition to achieving class-leading passive safety performance in assessments around the world, the second-generation Mirai provides high passive safety performance to protect occupants against high voltages, while also incorporating excellent hydrogen-leakage prevention performance.

Keywords: *passive safety*

1. Introduction

The second-generation Mirai was developed with the objectives of extending the driving range, and realizing emotional styling, greater comfort, and excellent handling. As part of this approach, the development also realized class-leading passive safety performance in assessments around the world, while protecting occupants against high voltages and incorporating excellent hydrogen-leakage prevention performance.

2. Occupant Protection Performance in Collisions

To achieve the objectives described above, the second-generation Mirai was built on an innovative platform based on the Toyota New Global Architecture (TNGA) design philosophy. The Mirai achieved class-leading results in passive safety assessments around the world. High-strength materials with a tensile strength of 980 MPa or higher were used in the frame to help protect the occupant compartment (Fig. 1).

In addition, to help mitigate occupant impacts, the Mirai is equipped with front seatbelts with pre-tensioners and force limiters, as well as supplemental restraint system (SRS) airbags (front, knee, and side airbags for the driver and front passenger, as well as curtain shield airbags covering the front and rear seats) (Fig. 2).

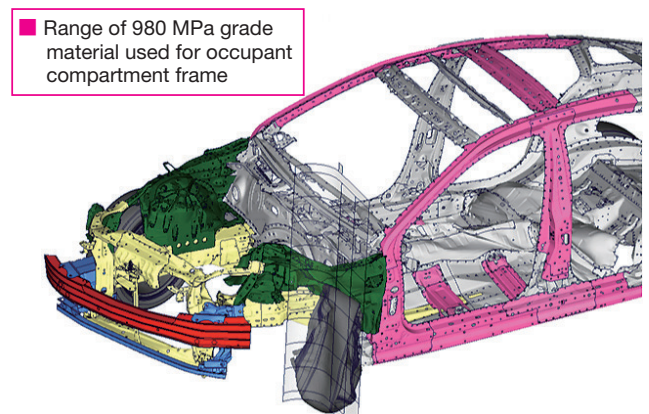


Fig. 1 Deformation Mode in Small Overlap Frontal Test Assessed by the Insurance Institute for Highway Safety (IIHS)

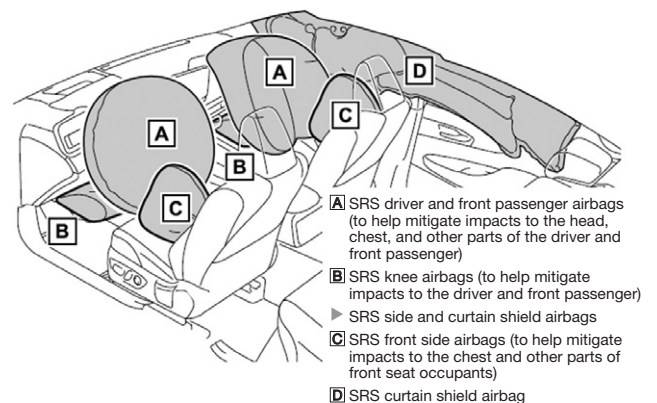


Fig. 2 SRS Airbag System

*¹ ZEV B&D Lab., Toyota ZEV Factory

*² MS Vehicle Evaluation & Engineering Div., Mid-size Vehicle Company

*³ Fuel Cell Products Development Div., Toyota ZEV Factory

3. Pedestrian Protection Performance in Collisions

In the event of a collision with a pedestrian, the Mirai is equipped with a pop up hood system that lifts up the rear of the hood in accordance with inputs from pressure sensors mounted on the front surface of the front bumper (Fig. 3). This system helps to mitigate impacts to the heads of pedestrians.

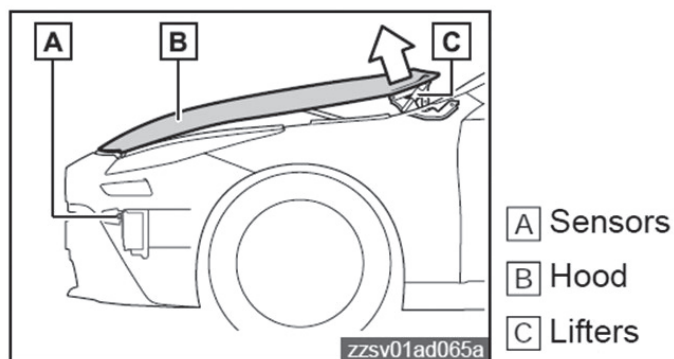


Fig. 3 Pop Up Hood System

4. Protection of Occupants from High Voltages and Hydrogen Leakage Prevention Performance

The fuel cell (FC) stack was moved from under the floor in the first-generation Mirai to under the hood of the second generation. To help protect the occupants and emergency personnel from high voltages in the event of a collision, and to help prevent hydrogen leakage, the development simulated a wide range of possible collision scenarios and analyzed the inputs to the FC stack. The FC stack and high-voltage components are protected by a strong frame (Fig. 4).

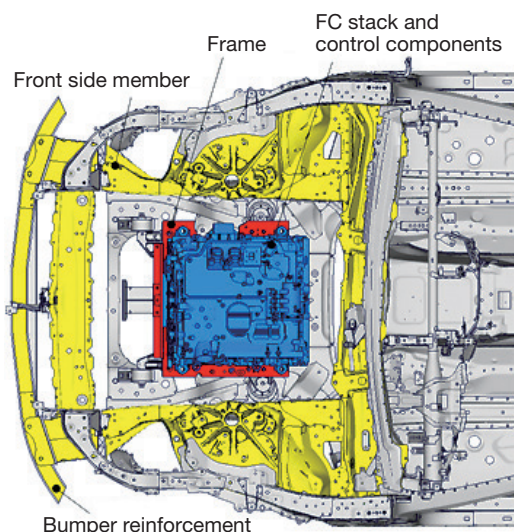


Fig. 4 FC Component Protection in Frontal Collision (Top View)

Investigations were carried out into the conditions of real-world traffic accidents to ensure that the yield strength of the tanks is greater than the yield strength of surrounding structural objects. The electric shock and hydrogen leakage performance was confirmed in crash tests (Fig. 5). In addition, the acceleration (G) generated in an impact was used to develop the controls that shut off the high voltage of the traction battery and the valves of the high-pressure hydrogen tanks, thereby helping to realize a dual hardware- and software-based approach to safety.

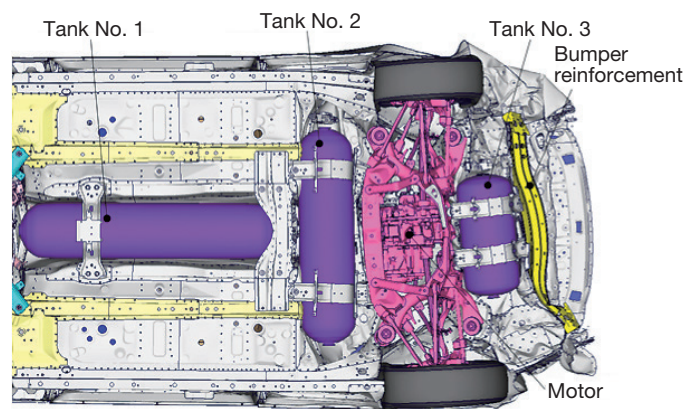


Fig. 5 Protection of High-Pressure Hydrogen Tanks in Rear-End Collision

5. Conclusion

Environmental and passive safety performance are equally critical to helping the second-generation Mirai achieve its mission of leading the way to a hydrogen energy based society. The development of the second-generation Mirai made no compromises in pursuit of achieving longer driving range, emotional styling, greater comfort, and excellent passive safety performance. Toyota intends to apply the technologies nurtured through the development of the second-generation Mirai to the development of the next FCVs with the aim of helping to realize a society based on sustainable energy.

Authors



T. FUJIWARA



H. TANAKA



S. HIRAKATA

Vehicle Production Engineering Technology to Enhance the Mass-Production Capabilities and Product Appeal of the Second-Generation Mirai

Masaru Yokoyama*¹
 Rin Masuhara*¹
 Yukinori Nasu*¹
 Hiroto Kozuki*²
 Toshimitsu Saijo*²
 Masanori Kokume*²
 Jun Matsuoka*³
 Yoji Hamamoto*²

Abstract

New production engineering technology was developed for the assembly line of the second-generation Mirai, including a painting technology called Force Blue Multiple Layers that realizes the deep, vivid, and intense signature blue color of the vehicle. This article describes the development of this technology and the activities to enable integrated installation of fuel cell (FC) components, which was necessary to achieve the step up from the low-volume production of the first-generation Mirai to full-scale mass-production.

Keywords: fill-scale mass production, end portion painting technology, uniform paint thickness application, integrated fuel cell (FC) component mounter

1. Introduction

The body color development policy of the second-generation Mirai focused on emphasizing the emotional styling and driving performance of the vehicle, rather than focusing on pure environmental friendliness. As part of this approach, a new and deeply striking blue body paint called Force Blue Multiple Layers (abbreviated in this article as “Force Blue”) was developed to appeal to mature sporty minded drivers (Fig. 1).



Fig. 1 Appearance of Force Blue Body Color

In addition, faced with growing demands to address environmental and energy-related issues, hydrogen-powered fuel cell vehicles (FCVs), which are regarded as the ultimate environmentally friendly type of vehicle, are likely to play a central role in helping to realize a hydrogen energy based society. Therefore, as part of the development of the second-generation Mirai, Toyota aimed to establish a full-scale mass-

production system to encourage wider popularization of FCVs. Consequently, it regarded the switch from the low-volume production system of the first-generation Mirai to a mixed mass-production line similar to the production lines for conventional gasoline-powered vehicles as an urgent task.

2. Force Blue Painting Technology

2.1 Characteristics

Toyota had previously created colors such as Contrast Blue Layering for Lexus. For the Mirai, the development team aimed to create an even more intense blue body color.

The development wanted to create an extremely expressive blue by applying a highly reflective and highly oriented metallic layer for the first base coat of the paint film system, complemented by a highly intense blue second base coat layer that would appear to be transparent to the eye (Fig. 2).

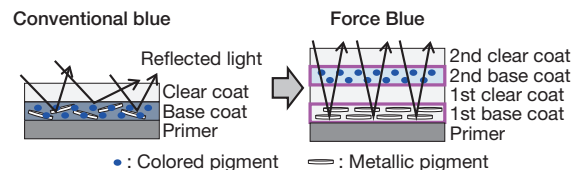


Fig. 2 Paint Film System

However, creating a highly intense blue using conventional pigments requires the use of multiple pigments, which would result in color mixing and a loss of color expression. Therefore, the development adopted a new blue pigment that expresses the required levels of both intensity and transparency (Fig. 3).

*¹ Paint and Plastics Production Engineering Div., Production Group

*² Assembly Engineering Div., Production Group

*³ Productization Engineering Div., Production Group

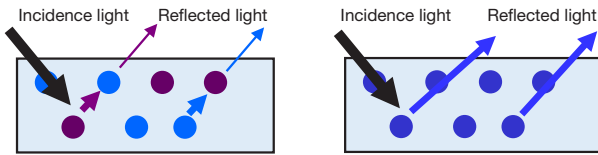


Fig. 3 2nd Base Coat Pigment

2.2 Main paint production engineering (PE) technology issues and countermeasures

The graph in Fig. 4 shows the relationship between film thickness and luminance. Force Blue changes color more extensively in accordance with the film thickness than a conventional body color. This presents two main issues. The first is the issue of color matching between the body and parts if the film thickness of individual vehicles varies at the same location (Fig. 5).

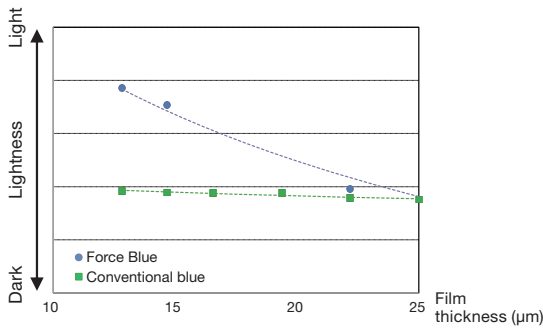


Fig. 4 Relationship between Thickness of 2nd Base Coat and Luminance



Fig. 5 Color Matching Defects



Fig. 6 color mottling

As a countermeasure, it was necessary to stabilize the film thickness at end portions close to the boundaries between the body and parts.

The second issue is differences in film thickness on the same surface, which can cause color mottling resembling uneven paint patterns (Fig. 6). This development established a manufacturing method that suppresses film thickness variations at both end and general portions.

2.3 Establishment of paint production technology for end portions

It is current practice to use an electrostatic coating method to help reduce paint loss. In this method, the painting equipment atomizes the paint and the resulting atomized paint droplets are then given a charge so that the paint will adhere more efficiently to the object being painted (such as a steel body panel). In this process, the area coated by the paint droplets atomized by the

painting equipment depends on the orientation of the electrical lines of force (Fig. 7).

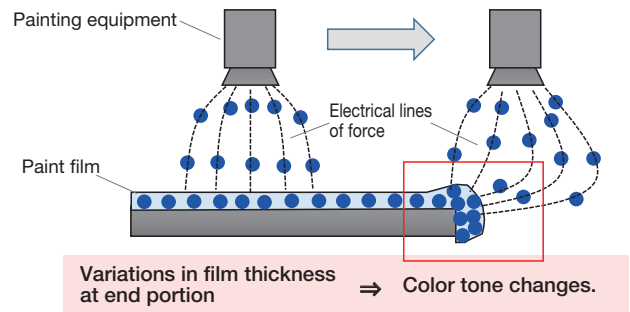
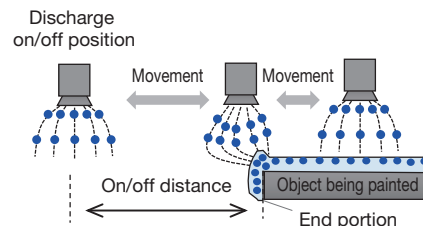


Fig. 7 Effects of Electrostatic Coating on Film Thickness

When painting an end portion, the electrical lines of force tend to concentrate at that end portion, creating a thicker film. A long end portion painting duration may induce secondary issues, such as sagging of the paint film. Therefore, to ensure that the appropriate film thickness is applied, the painting start and finish positions are switched close to the end portions. This switching operation is referred to as paint discharge on/off control and the distance from the end portion to the on/off position is referred to as the on/off distance. However, the formation of the atomization pattern is unstable immediately after the on/off control is engaged.

This has the following effects (Fig. 8). Although the roughness of the atomization pattern can be reduced by moving the painting equipment slowly, this means that the painting equipment will spend longer in the region of the end portion, which will concentrate the electric field and is a cause of film thickness variations. In contrast, the electric field is less likely to become concentrated if the painting equipment is moving quickly. However, in this case, the on/off control will affect the end portion and result in the application of a rough atomization pattern, again causing variations in the film thickness. Therefore, this development optimized the moving speed of the painting equipment as well as the paint discharge start and end positions. These measures halved the size of film thickness fluctuations and helped to reduce color variations between individual vehicles.



Fast movement → rough pattern application but low impact from electric field concentration
 Slow movement → less pattern roughness but high impact from electric field concentration

Fig. 8 Stabilization of End Portion Film Thickness

2.4 Establishment of paint production technology for general portions

The painting equipment atomizes the paint through a combination of rotating force and an air blower. The equipment then forms a uniform paint film by overlaying the paint in a pattern such as that shown in **Fig. 9**.

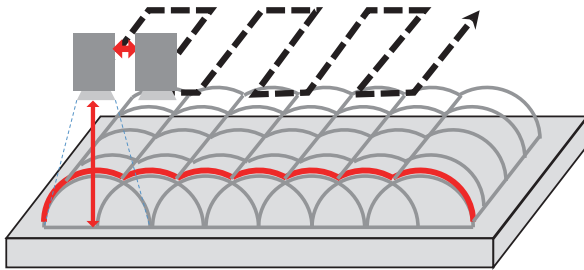


Fig. 9 Paint Film Pattern and Overlaying Application

With Force Blue, the formation of a uniform paint film thickness is even more important than with a conventional blue body color. The following conditions must be satisfied to realize a uniform film thickness: (1) the paint film must be formed using uniformly sized droplets (**Fig. 10**) and (2) the pattern formed by the paint droplets on the object being painted must have a uniform distribution (**Fig. 11**). Unless these two conditions are satisfied, a uniform film thickness cannot be applied over the whole surface, resulting in particularly noticeable differences in color density and color mottling defects.

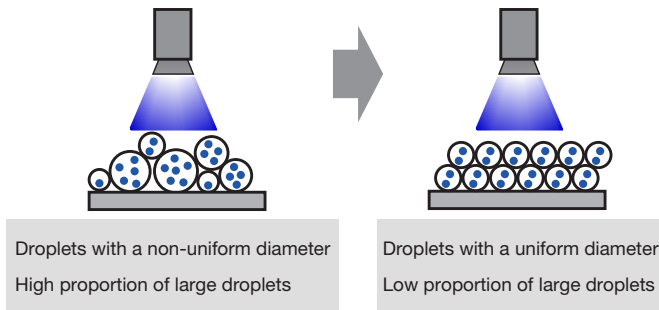


Fig. 10 Application of Uniform Paint Droplets

For condition (1), conventional painting techniques are likely to result in the formation of a paint film with non-uniform droplet sizes as shown in **Fig. 10**. This may generate a non-uniform paint film and color mottling over a surface. This development improved paint droplet size uniformity by optimizing the rotational speed of the painting equipment and the paint discharge volume.

For condition (2), conventional painting techniques use a rapid overlay speed, which tends to result in the formation of non-uniform paint film patterns. Therefore, this development studied slowing down the moving speed of the painting equipment and identified the optimum speed to form the correct

pattern. Improving these painting conditions enabled the application of more uniform paint patterns and reduced the occurrence of color mottling.

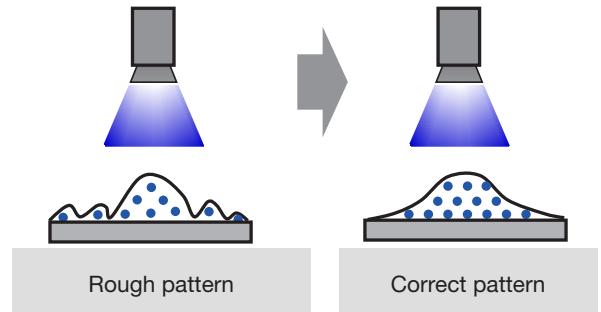


Fig. 11 Application of Uniform Paint Film Pattern

3. Mass Production Technology for Integrated FC Component Layout

3.1 Basic structure of the second-generation Mirai

The basic layout of the Mirai FCV consists of components such as high-pressure hydrogen tanks that store the hydrogen fuel, a hydrogen pressure regulator, dedicated high-pressure pipes that join the tanks with the regulator, a fuel cell (FC) stack that generates electricity from hydrogen and oxygen in the air, high-voltage cables that transmit this electricity, and a motor that generates the driving force from the electricity (**Fig. 12**).

Although the second-generation Mirai has three hydrogen tanks, the system was laid out to enable the stack to be moved from below the seats in the first-generation Mirai to under the hood. Conversely, the motor was moved from the front to the rear of the vehicle.

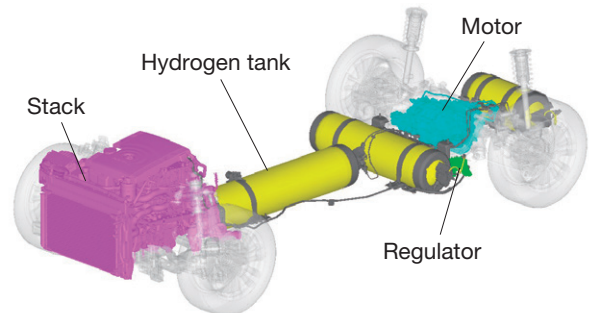


Fig. 12 Outline of Basic Structure of the Second-Generation Mirai

3.2 Production on same line as gasoline-powered vehicles

The capability to produce the Mirai on the same line as gasoline-powered vehicles was achieved by replacing the engine mounting process with the stack mounting process.

Similarly, assembly of the motor on the same line is possible since the mounting process resembles that of a rear suspension and differential assembly. In contrast, the mounting process of the hydrogen tanks does not resemble any gasoline-powered vehicle assembly process and requires a dedicated approach. In addition, since the hydrogen tanks have a high number of portions to be tightened, a dedicated mounting process would have to be added to the main production line, requiring major changes to the line. Therefore, during transportation from the painting to the assembly processes, the body of the second-generation Mirai is taken away to mount the hydrogen tanks in a dedicated process before being re-inserted into the line before the assembly processes. This reduces the scale of changes to the main production line and enables flexible adjustments to production volume.

3.3 Issues of hydrogen tank mounting

As described above, the hydrogen tanks of an FCV are joined to the pressure regulator by dedicated pipes. The relative positioning of the tanks and pipes is therefore very important. Since the amount of hydrogen leakage from the pipe joints must be restricted to an extremely small predetermined value, the shape of the sealing portion at the end of the pipes is controlled to within one-hundredth of a millimeter, and the tightening torque is assured using a dedicated tool. In addition, for the production of the first-generation Mirai, a high-precision dedicated jig was developed to position the hydrogen tanks, regulator, and pipes before the pipes were tightened in place (Fig. 13). This jig minimized the assembly strain applied to the pipes in the tightening process. This dedicated jig was positioned directly above the hydrogen tank mounter. After assembly, a leak test was carried out using helium gas and the resulting assembly was then installed into the vehicle while maintaining the same relative position determined by the jig. This approach enabled a high-quality hydrogen tank mounting process. This mounting method was only feasible because the first-generation Mirai was produced in low volumes. Considering the production volume of the second-generation Mirai, multiple mounters with the same dedicated jig would have to be prepared, which would increase the necessary capital investment and space.

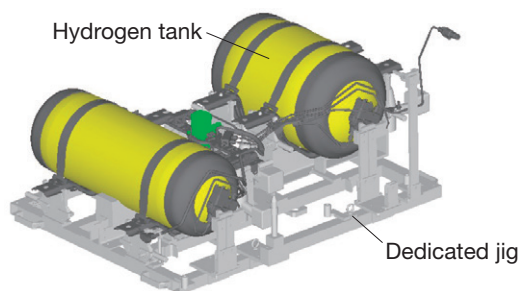


Fig. 13 Assembly Using Dedicated Jig

3.4 Hydrogen tank mounting process for the second-generation Mirai

For the second-generation Mirai, several dedicated hydrogen tank trays were prepared (Fig. 14). These trays are transferred to a position directly above the mounter and installed into the vehicle. This approach allows mass production with a single mounter, thereby helping to resolve the issues related to investment and space. The dedicated trays can be mounted on a range of automated guided vehicles (AGVs) and transported to each process. A high-precision jig is located above the dedicated trays that ensures the relative positioning between the hydrogen tanks and each tightening point. In addition, when the dedicated hydrogen system pipes are tightened, a special attachment helps to stop the pipes rotating together with the nuts, thereby increasing accuracy in the pipe tightening axis direction. The dedicated trays are transported to the hydrogen tank mounting process by AGV. The trays are then transferred to the hydrogen tank mounter with the tanks in place (Fig. 15). To ensure that the relative positioning between the hydrogen tanks, regulator, and dedicated pipes does not change, it is extremely important that the base of the trays is extremely stiff. This development focused on ensuring that vehicle mounting could be completed without affecting this relative positioning.

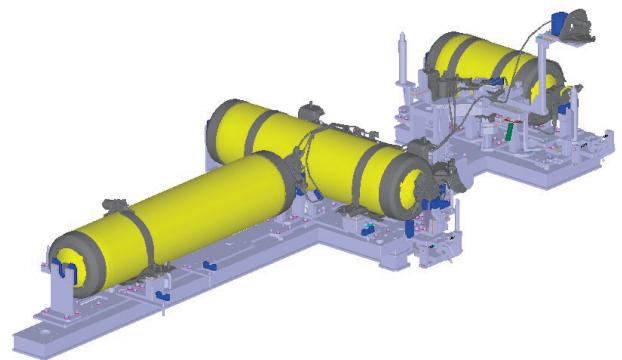


Fig. 14 Dedicated Hydrogen Tank Trays

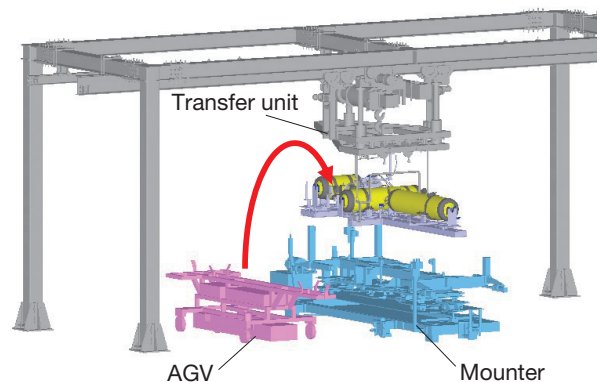


Fig. 15 Outline of Tank Transfer Process

Special Feature

After being transferred to the mounter, the dedicated hydrogen tank trays are moved together with the mounter to below the vehicle that has been raised up by a lifter (**Fig. 16**).

In this process, in addition to determining the position between the mounter and the vehicle, positioning pins are also provided on the dedicated hydrogen tank trays. This allows the relative positioning between the vehicle and hydrogen tanks to be realized highly accurately. The result is a high-quality mounting process that is also adapted to mass production.

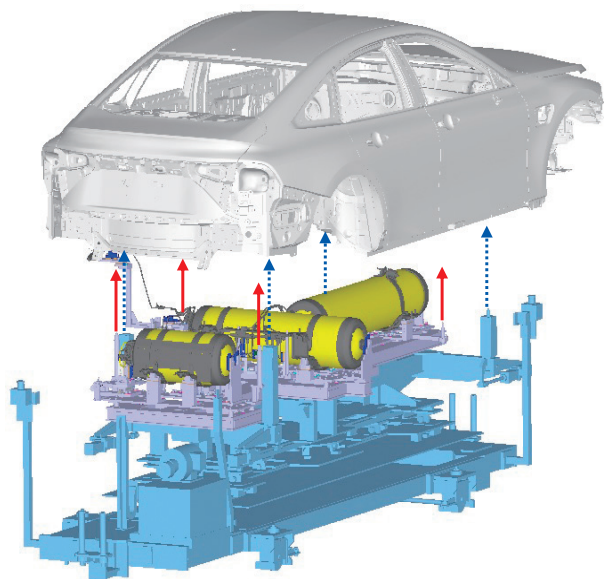


Fig. 16 Outline of Positioning for Tank Mounting

4. Conclusion

This article first discussed the PE technology that was developed to enable mass production of the Force Blue body color. Although many issues still remain, Toyota intends to apply the technical know-how gained through this project to the development of new paint colors in the future with the aim of providing users with a selection of body colors with high added value.

Next, this article mainly concentrated on describing the configuration of a hydrogen tank assembly line for mass production, assembly accuracy, and the developments carried out to realize these objectives. Measures were also taken to reduce the cycle time of leak tests. Toyota intends to continue developing PE technologies to further raise quality, reduce costs, and boost productivity to help resolve environmental and energy-related issues, and lead the way toward the hydrogen energy based society of the future.

Finally, the cooperation of a wide range of people inside and outside Toyota played a critical role in the developments described in this article. The authors would like to express their gratitude for being asked to take part in this development and for the invaluable assistance of everyone both inside and outside Toyota.

Authors



M. YOKOYAMA



R. MASUHARA



Y. NASU



H. KOZUKI



T. SAIJO



M. KOKUME



J. MATSUOKA



Y. HAMAMOTO

Development of Air Cleaner Realizing Minus Emissions

Tetsuya Ichikawa*¹
 Kuniho Kasugai*²
 Koichi Masuda*¹
 Hiroto Maruyama*¹
 Jun Goto*³
 Kimiko Yoshida*³

Abstract

This article describes the air cleaner adopted in the second-generation Mirai to help realize emissions that are cleaner than the surrounding air. Since fuel cell vehicles (FCVs) emit no atmospheric pollutants while driving, enhancing the performance of the air cleaner (the system that removes foreign objects from the external air used by the vehicle as an oxygen source for electricity generation) is an effective way of helping to clean the atmosphere around the vehicle. This new air cleaner was developed by applying electret processing to the dust filter to enhance the fine particulate matter (PM2.5) filtration efficiency, and by adding a filter that targets various chemical substances.

Keywords: *negative emissions, air purification, dust filter, chemical filter*

1. Target and Background of Development

1.1 Negative emissions

Instances of climate change are becoming more and more prevalent around the world. At the same time, environmental pollution remains a serious issue. In response, Toyota is working to develop technology and popularize environmentally friendly technologies and vehicles by broadening its focus away from individual towns and countries to encompass the entire planet.

As fuel cell vehicles (FCVs) are driven by electricity generated from the chemical reaction between hydrogen and oxygen in the air, these vehicles require an intake system that draws in and cleans the air before it can be used. Focusing on this requirement, Toyota aimed to develop a vehicle that lowers air pollution as it is driven by enhancing the filtration performance of the intake system. This vehicle goes beyond the conventional concept of zero emissions and realizes “negative” emissions that are cleaner than the air surrounding the vehicle (Fig. 1).

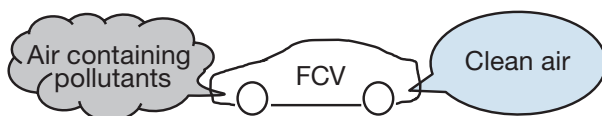


Fig. 1 Concept of Negative Emissions

2. Air Purification

2.1 Details of the air purification concept

Two target categories of air pollutants were identified: particulate matter (PM) such as PM2.5 and harmful chemical substances. PM2.5 refers to extremely small particles that are regarded as harmful to health. PM2.5 can be divided into two types, primary particles of original particulate matter and secondary particles that are generated from chemical substances in the air. As secondary particles make up around 60% of the total of PM2.5, efforts to lower air pollution must include both the direct removal of PM2.5 and the removal of the chemical substances that generate these secondary particles.

A highly efficient way to remove PM2.5 is to enhance the performance of the dust filter. This measure was supplemented by the addition of a chemical filter to remove chemical substances.

2.2 Target substances to be removed and filtration performance target

These targets were determined from the following standpoints: contribution to air purification, prevention of fuel cell (FC) power generation performance degradation, and the performance targets of the intake system.

- (1) A PM2.5 filtration efficiency of 99.5% was set after comparing conditions in regions around the world with high and low concentrations of PM2.5.
- (2) The following chemical substances were considered for removal.
 - Substances causing PM2.5: sulfur dioxide (SO₂), nitrogen dioxide (NO₂), ammonia (NH₃), and so on
 - Substances in the exhaust emissions of conventional vehicles:

*¹ Lexus Body Engineering Div., Lexus International Company
 *² TNGA Management Div., Vehicle Development Center
 *³ Toyota Boshoku Corporation

SO₂, NO₂, hydrocarbons (HCs), and so on
 - Substances that affect FC performance: SO₂ (which poisons the catalysts)

Therefore, SO₂, NO₂, and NH₃ were defined as the main target substances to be removed from the air, and a filtration efficiency target of at least 90% was set for SO₂ to help prevent FC degradation. For the other substances, the development aimed to achieve as high a filtration efficiency as possible, while maintaining the SO₂ filtration performance.

3. Methods to Lower Pollution by Air Purification

3.1 FCV intake system

Fig. 2 shows an outline of the FCV intake and exhaust system.

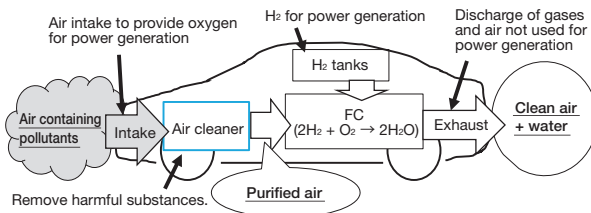


Fig. 2 Outline of Air Purification Concept for FC System

The air is filtered by an air cleaner before being used to generate power. Since substances not used for power generation are discharged from the vehicle, enhancing the performance of the air cleaner to remove pollutants from the air should help the vehicle to clean the air as it is driven.

3.2 Air cleaner components

Fig. 3 shows the configuration of the developed parts. Since substances trapped by the chemical filter might become loose, the chemical filter was installed upstream of the dust filter. Consequently, any substances coming loose from the chemical filter would then be captured by the dust filter. However, installing the chemical filter upstream of the dust filter might cause foreign matter to block the chemical filter. Foreign matter might also interfere with the dust filter and cause filter damage. In response, protective filters were provided on either side of the chemical filter. The filters in the air cleaner are assembled into a cassette, which provides a protective structure and facilitates maintenance.

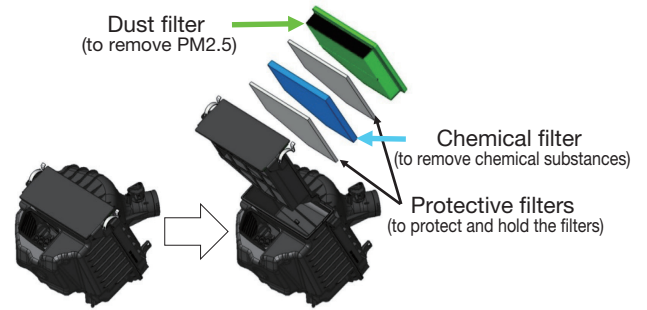
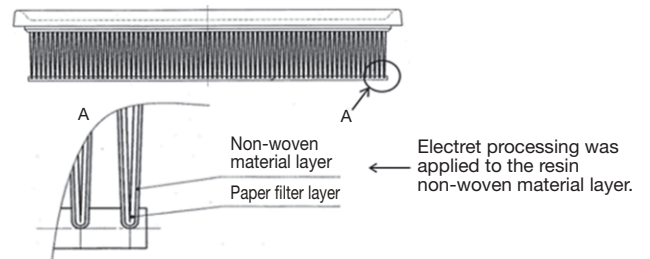


Fig. 3 Air Cleaner Structure

3.3 PM2.5 filtration performance enhancement

Electret processing was applied to the resin fibers of the dust filter to enhance the PM2.5 filtration efficiency (Fig. 4).



High voltage applied to electrically polarize the resin fibers.

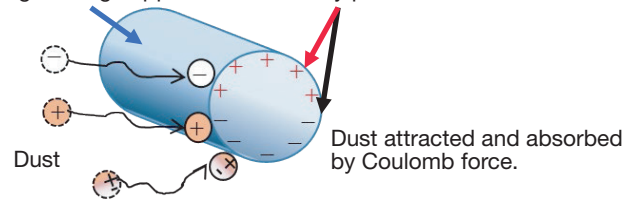


Fig. 4 Electret Processing

Fig. 5 compares the performance of the developed and existing filters. Applying the electret processing increased the PM2.5 filtration efficiency from 96.0% to 99.7%, which is above the 99.5% target. The performance of the dust filter developed for the air cleaner is among the best in the world.

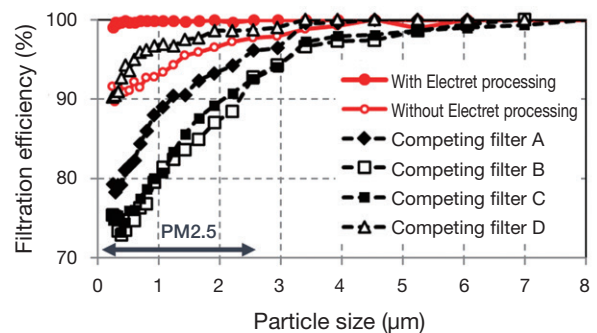


Fig. 5 Dust Filter Performance

3.4 Addition of organic chemical substance filtration function

Manganese dioxide (MnO_2) was adopted in the chemical filter since it is capable of removing SO_2 at normal temperatures as well as NH_3 , which are two substances adsorbed by the catalyst. The filtration efficiency was also enhanced by the addition of activated carbon impregnated with alkali. SO_2 and NH_3 react with MnO_2 , forming an acid that is adsorbed by the activated carbon. SO_2 and NO_2 react with the impregnated alkali, forming a salt that is also adsorbed by the activated carbon.

An aluminum honeycomb was selected for the substrate since this material causes low pressure drop and can ensure the required surface area to achieve the filtration performance target (Fig. 6). As a result, the developed filter achieved an SO_2 filtration efficiency of 94% over the vehicle lifetime in tests performed under real-world conditions. Even without the chemical filter, the air cleaner achieves NO_2 and NH_3 filtration performance of at least 40%.

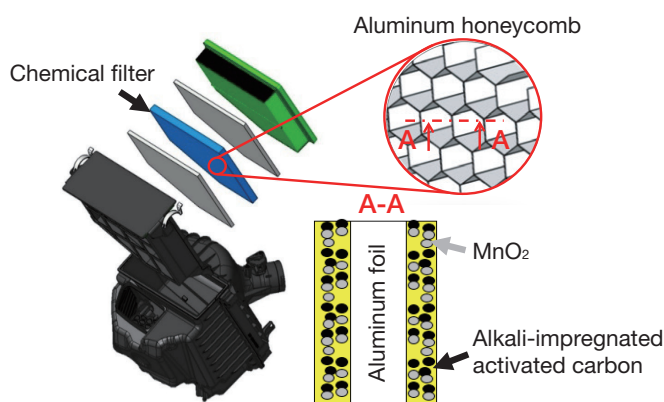


Fig. 6 Outline of Chemical Filter

4. Conclusion

A new air cleaner was developed with the aim of achieving emissions cleaner than the surrounding air by applying electret processing to the dust filter and adding a chemical filter. The developed air cleaner has a $\text{PM}_{2.5}$ filtration efficiency of 99.7% and an SO_2 filtration efficiency of 94%, above the targets set for the development. Air intake systems installed with this air cleaner should help to lower air pollution. This air cleaner also helps to prevent FC performance degradation by removing substances that affect FC performance.

The exact contribution of the air cleaner to lowering air pollution is difficult to quantify exactly since it depends on the air intake volume and the degree of pollution. However, calculations using the second-generation Mirai found that driving this vehicle for 10,000 km a year would clean an amount of air equivalent to the total annual volume of air inhaled by one person. Therefore, as vehicles capable of generating emissions lower than the surrounding air become

more widespread, it may even be possible to improve the environment along main roads and the like, which tends to be highly polluted.

The authors would like to express their sincere gratitude for the invaluable cooperation of everyone involved in this development.

Authors



T. ICHIKAWA



K. KASUGAI



K. MASUDA



H. MARUYAMA



J. GOTO



K. YOSHIDA

Development of Toyota Safety Sense

Yuto Shimbo*¹
 Yusuke Tanaka*¹
 Hiroto Katsuda*¹
 Chenyu Wang*¹
 Masami Ishihara*²
 Keiji Yamashita*²

Abstract

The ultimate wish of a mobility society is to reduce traffic accident casualties to zero. To help realize this ambition, the Toyota Safety Sense (TSS) packages of advanced safety systems are being continually enhanced to incorporate the latest safety-related technologies and know-how nurtured through vehicle development. Based on the existing monocular camera + millimeter wave radar sensor configuration, further functions have been added and the operational scope of the packages has been expanded to help further reduce traffic accidents and casualties, while lowering driver workload. The resulting impressive active safety performance of the TSS packages successfully satisfies the requirements of active safety assessments carried out around the world.

Keywords: advanced safety, pre-collision system (PCS), lane tracing assist (LTA), emergency driving stop system (EDSS)

1. Introduction

Previous Toyota Safety System (TSS) packages of advanced safety systems covered certain types of accident scenarios, such as rear-end collisions and road departures (Fig. 1). To help further reduce the number of traffic accidents and traffic accident casualties, it is important to extend this coverage to include head-on collisions as well as collisions between turning and oncoming vehicles at intersections. Furthermore, with accidents involving elderly or commercial drivers becoming a serious social issue, it has become necessary to develop safety systems capable of helping to relieve driver workload and systems that react to emergency situations.

In response to these needs, the control range of the TSS has been expanded to include a pre-collision system (PCS) and lane tracing assist (LTA), and the new emergency driving stop system (EDSS) has been added (Fig. 2). By retaining the same sensor configuration (monocular camera + millimeter wave radar) as the previous system and refining the algorithms, the objective was to swiftly realize and adopt active safety technology incorporating significant technical advances (Fig. 3).

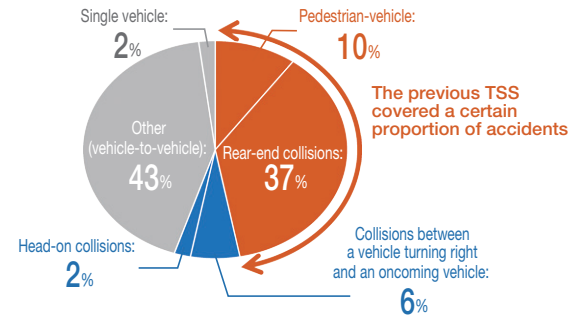


Fig. 1 TSS Accident Coverage

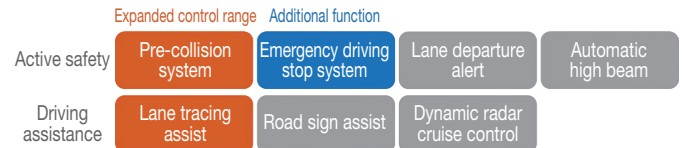


Fig. 2 TSS Functions

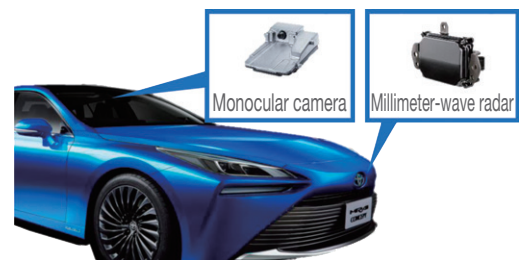


Fig. 3 Sensor Configuration

*¹ Automated Driving & Advanced Safety System Development Div., Advanced R&D and Engineering Company

*² MS Automated Driving & Advanced Safety System Development Div., Mid-size Vehicle Company

2. PCS: Intersection Left/Right Turn Assistance

2.1 Development aims

The previous PCS mainly assumed that the driver's vehicle was driving straight on. This system detected preceding vehicles and pedestrians (or bicycles) crossing a road, issued warnings to the driver and activated the brakes. The updated PCS covers oncoming vehicles when turning right at an intersection (or turning left in regions in which the vehicle drives on the right side of the road) as well as pedestrians crossing the road after the vehicle has turned left or right.

Collision judgment is more difficult when the driver's vehicle turns left or right at an intersection because the movement of surrounding objects visible to the sensors is much different from the movement when the vehicle is driven straight on. Therefore, the collision judgment logic was refined to enable the PCS to respond to oncoming vehicles during a right turn or to crossing pedestrians after a left or right turn.

2.2 Function and algorithm

Fig. 4 shows the new scenarios covered by the developed PCS. The white vehicle in the figures represents the driver's vehicle. The PCS responds to the vehicles and pedestrians shown in black. However, pedestrians that cross the road in the same direction as the driver's vehicle are not covered by the system because these pedestrians are outside the angle of view of the sensors.

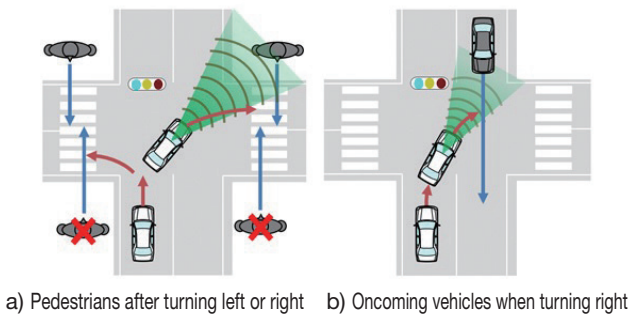


Fig. 4 Scenarios Covered by System

An outline of the collision judgment logic during a left or right turn at an intersection is described below using an oncoming vehicle when the driver's vehicle turns right as an example (Fig. 5).



Fig. 5 Flow of Collision Judgment Processing

I) Judgment that the driver's vehicle is turning

The system uses the steering wheel angle, vehicle speed, and

other information to judge whether the driver's vehicle is turning at an intersection.

II) Judgment of intersection scenario

When turning right, the paths of oncoming vehicles that might collide with the driver's vehicle (i.e. the relative path of the vehicles) look highly curved from the driver's vehicle (Fig. 6). The system traces the positions of the surrounding vehicles, judges whether oncoming vehicles are approaching on a specific path during the right turn, and calculates the collision risk to these vehicles.

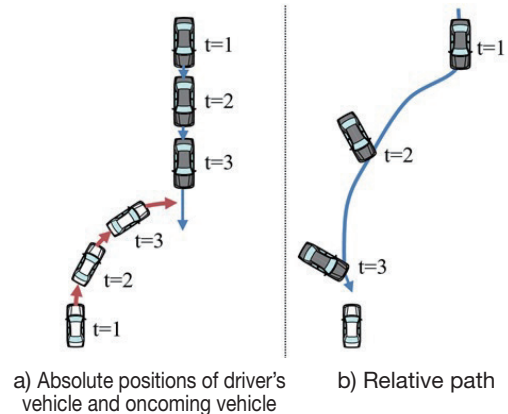


Fig. 6 Positional Relationship between Driver's Vehicle and Oncoming Vehicle (when Turning Right)

III) Calculation of collision risk

The previous PCS calculated the collision risk with target vehicles based on the time to collision with the driver's vehicle (i.e., the collision time). However, when turning right, the relative path between the driver's vehicle and the oncoming vehicle is curved. As a result, an accurate collision risk cannot be calculated from the collision time alone. Therefore, the system calculates the time required for the driver's vehicle to enter the predicted path of the oncoming vehicle (i.e., the intersection time). The system then calculates the collision risk by combining the collision time and the intersection time values (Fig. 7). If the collision risk exceeds a certain threshold, the system issues a warning and activates the brakes to help slow or stop the driver's vehicle before it enters the predicted path of the oncoming vehicle, thereby helping to avoid a collision or mitigate damage if a collision were to occur.

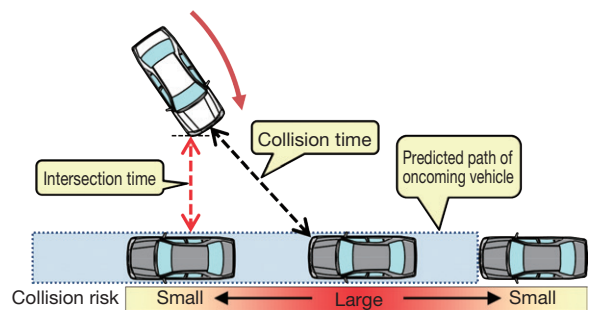


Fig. 7 Illustration of Collision Risk Calculation

Special Feature

Incorporating this logic into the system helped to realize a PCS capable of covering important accident scenarios at intersections.

3. EDSS

3.1 Development aims

Toyota has previously adopted EDSS as part of the Lexus Safety System +A (LSS+A). For the updated TSS, the system configuration was revised to enable wider adoption of the same function to various models and to realize the same functionality as the LSS+A. As an example, the data communication module (DCM), which is standard equipment on vehicles equipped with the TSS, was set to enable automatic connection to the emergency call system via EDSS regardless of the vehicle model.

3.2 Outline of EDSS

During operation of the LTA system, EDSS estimates the driver's state by monitoring whether the driver is in control of the vehicle (for example, whether the driver is holding the steering wheel). If the system fails to detect a driver operation for a certain period of time, the system slows and stops the vehicle in its lane while warning people around the vehicle to help avoid a collision or mitigate damage if a collision were to occur. There are four phases of system operation.

(1) Warning phase 1

During operation of the LTA system, if the driver is not holding the steering wheel, the driver is alerted by a warning indication on the instrument cluster. If this state continues, warning phase 1 is activated, in which the driver is alerted and encouraged to take control of the vehicle by a display and a warning buzzer.

(2) Warning phase 2

In addition to the display and warning buzzer, the system slows the vehicle down to prompt the driver to depress the accelerator. The system also automatically flashes the hazard lamps to alert the following vehicle. In addition, the audio system is muted to make the warning buzzer easier to hear by the occupants.

(3) Deceleration and stop phase

In this phase, the system automatically sounds the horn to warn people outside the vehicle that an issue has occurred. At the same time, the vehicle is slowed to a stop within the driving lane. The horn is sounded three times in short bursts to help draw the attention of other road users to the vehicle.

(4) Stop phase

After the vehicle is stopped, the brake hold function is

activated to keep the vehicle stationary. Then, the system automatically connects to the emergency call system so that an operator can contact the driver. If the operator obtains no response, emergency vehicles are called to the scene and the necessary traffic restrictions are put in place. After the vehicle stops, the system automatically unlocks the doors so that the emergency responders can reach the driver more quickly.

4. Expansion of LTA Control Range

4.1 Development aims

To expand the control range of the LTA system and to help realize deceleration around curves in line with driver expectations, deep learning was utilized to enhance the road recognition capabilities of the system and to add a curve speed reduction function.

4.2 Road recognition enhancement using deep learning

Road lane markings may be faded and difficult to see. In response, a deep neural network (DNN) was used to enhance the road recognition capabilities of the system and to enable longer continuous activation of the LTA system (**Fig. 8**). DNN-based road estimation was realized by (1) categorizing the road into different areas (green: area inside the vehicle's lane in which driving is possible, blue: areas outside the vehicle's lane in which driving is possible) and (2) extracting boundary lines (red) around the area inside the vehicle's lane in which driving is possible (**Fig. 9**).

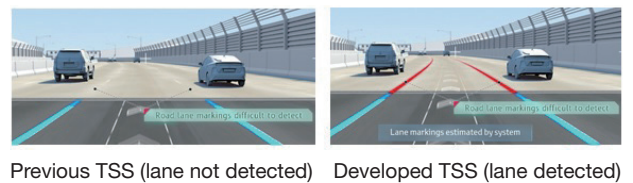


Fig. 8 LTA Operation Using DNN

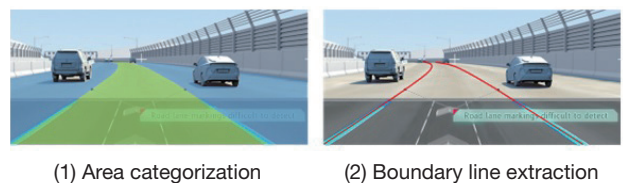


Fig. 9 Driving Lane Estimation Using DNN

4.3 Curve speed reduction function

In the LSS+A, the previous curve speed reduction function provided deceleration assistance on curves based on map data in the navigation system. For this reason, the system required relatively expensive map data. With the updated TSS, to enable

wider adoption of the same function to other vehicles, the DNN described above was adopted to help the system to recognize curves using only the monocular camera. Using DNN-based curve recognition, the system can slow the vehicle in advance in accordance with the size of the curve. This enables the LTA system to remain activated on curves.

If the vehicle enters a curve at high speed, the system slows the vehicle to the maximum lateral G that enables the LTA system to remain activated. A more natural driving feel was realized by analyzing the deceleration data for various drivers and various size curves (**Fig. 10**) and enabling the driver to customize the amount of deceleration in accordance with driving style.

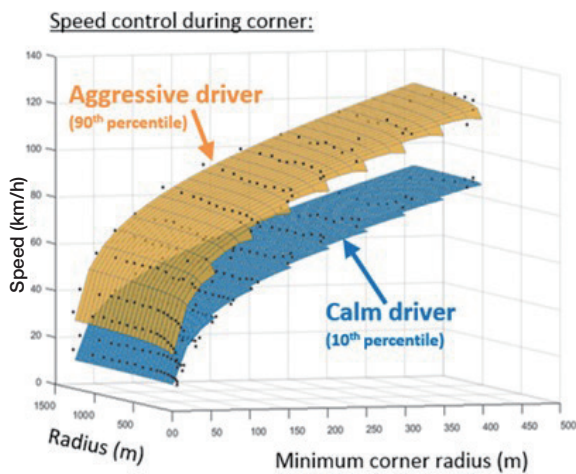


Fig. 10 Analysis of Vehicle Speed Depending on Curve Radius

5. Conclusion

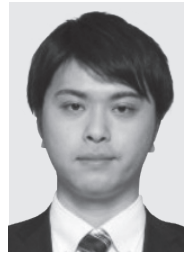
An updated version of the TSS was developed with an expanded control range and new functions with the aims of helping to both further enhance safety and relieve driver workload. This TSS is planned to be equipped on the second-generation Mirai, to be followed by a sequential rollout on new models from 2020.

Finally, the authors would like to express their sincere gratitude for the invaluable cooperation of Denso Corporation over the course of this development.

Reference

- (1) *ITARDA Information No. 133* (in Japanese).

Authors



Y. SHIMBO



Y. TANAKA



H. KATSUDA



C. WANG



M. ISHIHARA



K. YAMASHITA

Development of the Toyota Teammate Advanced Park Function

Yasutaka Matsunaga*¹

Yuki Minase*¹

Yu Hiei*¹

Abstract

Toyota Teammate is an advanced driving assistance system that was developed based on the Mobility Teammate Concept, Toyota’s unique approach to automated driving. This concept treats the driver and vehicle as partners and aims to enhance the mutual understanding between them, rather than simply taking over control and replacing the role of the driver. Toyota Teammate consists of two assistance functions called Advanced Drive and Advanced Park. This article describes the Advanced Park function of the Toyota Teammate driving assistance system.

Keywords: *Toyota Teammate, Advanced Park*

1. Introduction

The second-generation Mirai is equipped with Toyota Teammate, the latest advanced driving assistance system that operates in concert with driver perceptions. The Toyota Teammate system was developed based on the Mobility Teammate Concept, Toyota’s unique approach to automated driving. This concept treats the driver and vehicle as partners and aims to enhance the mutual understanding between them, rather than simply taking over control and replacing the role of the driver.

This system aims to help realize even more confident, natural, safe, and comfortable driving performance through mutual interaction, confirmation, and assistance between the driver and vehicle. The human driver should remain at the center of driving, even if even more advanced technology is developed. That is the core concept behind Toyota Teammate.

This article details the Advanced Park function of the Toyota Teammate driving assistance system.

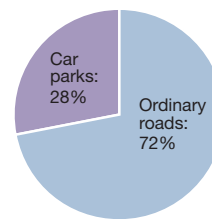
check for safety around the vehicle while simultaneously operating the steering wheel, accelerator, brakes, and so on (Fig. 4). For these reasons, it was decided to develop the Advanced Park function to support drivers during difficult driving and parking operations.

2. Advanced Park

2.1 Background

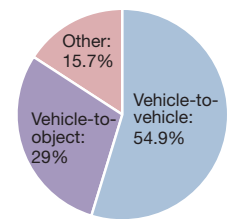
Around 30% of traffic accidents around the world occur in car parks (Fig. 1). This is probably because car parks are a complex environment containing a wide range of objects, from other vehicles, structures, and so on (Fig. 2).

Fig. 3 shows the results of a questionnaire on driving behavior that individual drivers found difficult. Parking, which was one of the most common answers, requires the driver to



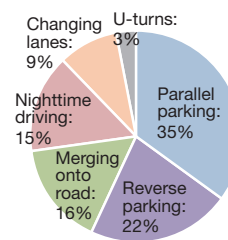
Source: Analysis of Accidents in Car Parks (in Japanese). The General Insurance Association of Japan (2012).

Fig. 1 Traffic Accident Trends



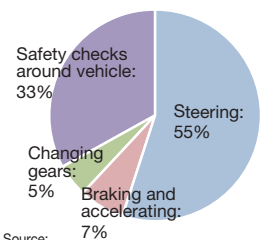
Source: Analysis of Accidents in Car Parks (in Japanese). The General Insurance Association of Japan (2012).

Fig. 2 Breakdown of Accidents Occurring in Car Parks



Source: Mynavi News (2013)

Fig. 3 Difficult Driving Operations



Source: "A Study on Reduction of Driver's Workload at Low Velocity Situation." Proceedings of the Society of Automotive Engineers of Japan (2004).

Fig. 4 Parking Operations with High Driver Workload

*¹ Automated Driving & Advanced Safety System Development Div., Advanced R&D and Engineering Company

2.2 Outline

Fig. 5 shows an outline of the scenarios supported by the Advanced Park function. These are (1) driving into an empty parking row, (2) parallel parking, and (3) exiting from a parking space after parallel parking. In the case of driving into an empty parking row, the system prioritizes reversing into the parking space (based on the results for reverse parking in **Fig. 3**). The system starts providing support when the vehicle is located immediately beside the parking space. After the vehicle is stopped alongside the space, drivers who find parking difficult can activate the support simply by pressing a switch.

If the Advanced Park function detects multiple parking spaces, it will show an optimum candidate space alongside the other viable spaces on the panoramic view monitor screen of the multi-information display, and ask the driver to select the desired space.

The Advanced Park function is a level 2 automated driving system that provides assistance under the assumption of constant driver supervision.

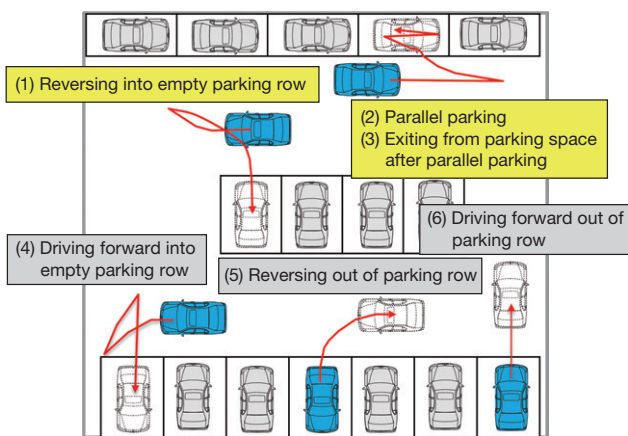


Fig. 5 Parking Scenarios Supported by the Advanced Park Function

2.3 Development concept

2.3.1 Ensure safety by recognizing the environment around the vehicle (i.e., the capability to use the function safely, naturally, and with confidence)

As described above, a large proportion of accidents in car parks involve collisions with objects such as other vehicles and structures. Therefore, it was proposed that confident, natural, and safe parking could be achieved by alerting the driver through displays and notifications when an object is detected around the vehicle, and by helping the driver avoid a collision through emergency braking if the system judges that the potential collision cannot be avoided.

In addition, it was also proposed that the workload of the driver might be lowered by providing support for steering, acceleration, braking, and gear changing operations, thereby freeing the driver to focus on safety checks around the vehicle.

2.3.2 Easy-to-understand human machine interface (HMI) (i.e., a function that is simple to use)

Table 1 lists a number of complaints about conventional parking support systems. These complaints include the difficulty of mode selection (No. 1), lack of seamless operation (No. 3), inability to activate reverse parking support (No. 4), and the system failing to display the preferred parking space (No. 5). These complaints are probably caused by requiring an over-complex operation method and procedure to activate the parking support. Therefore, it was realized that the Advanced Park function must be easy to use for all drivers and feature simple displays and a streamlined operation procedure.

2.3.3 Parking without wasting time (i.e., the capability to park smoothly)

The complaints in **Table 1** also include the time required by the system to park the vehicle (No. 6) and the large number of corrective steering maneuvers made by the system (No. 7). This suggests that drivers would probably be dissatisfied with the Advanced Park function if it parks less smoothly than a human driver. Therefore, it was concluded the Advanced Park function must be capable of parking in around the same time as an ordinary driver.

2.3.4 Using a memory function to expand the range of support (i.e., for system compatibility with unlined parking spaces)

Another complaint about conventional parking support systems is that these systems cannot be used in every type of car park (No. 2 in **Table 1**). **Table 2** lists some driver requirements for parking support in two different regions. These results show that drivers want to use the function when parking at home, as well as when driving into an empty parking row or parallel parking. Therefore, it was also concluded that the Advanced Park function must be capable of providing assistance for parking in unlined spaces, such as those at users' homes.

Table 1 Complaints about Conventional Parking Support Systems

No	Complaint	(%)
1	Cannot select mode easily.	35
2	Cannot use system in desired car park.	30
3	Cannot use system seamlessly.	24
4	Cannot activate reverse parking.	23
5	System does not display desired parking space.	23
6	Parking is too time consuming.	19
7	System makes too many corrective steering maneuvers.	17

Table 2 Region-by-Region Parking Support Requirements

Japan		North America	
Parking scenario	%	Parking scenario	%
Driving into empty parking row	80	Exiting from parking space after parallel parking	46
Parallel parking	78	Parallel parking	37
Parking at home	28	Parking at home	20

Source: MacNET analysis results (2017) Source: 2010 analysis results by The Planning Edge (2010)

2.4 Technical development

2.4.1 Omni-directional detection using fish-eye cameras and ultrasonic sonar

The Advanced Park function detects static and moving objects using fish-eye cameras by adopting a methodology based on a moving stereo and optical flow approach. Excellent detection performance was realized by utilizing the separate characteristics of ultrasonic sonar and the fish-eye cameras, and then combining the results. The function uses the detection results to help the vehicle avoid collisions with objects around the vehicle (**Fig. 6**).

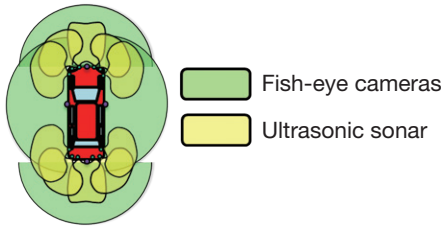


Fig. 6 Sensor Configuration and Illustration of Sensing

A highly robust process to detect parking space partitions was adopted to enable the identification of candidate parking spaces delineated by single or double lines, parking spaces drawn using crosses or diagonal lines, parking spaces indicated by methods other than white lines, faded lines, and publicly held parking spaces.

At night, since the object detection capability of the cameras drops due to insufficient light around the vehicle, infrared (IR) lamps were mounted inside the exterior mirrors close to the left and right cameras (**Fig. 7**). This helps to ensure sufficient detection performance at night.

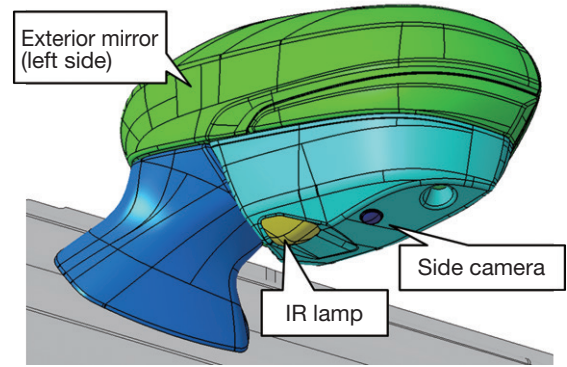


Fig. 7 IR Lamps Mounted inside Exterior Mirrors

2.4.2 Easy-to-understand HMI

2.4.2.1 Driver operation and display

To enable the function to be used with the minimum of driver operations, the function start switch and parking start switch display were designed to be operated using one hand. In addition, parking support can be started by a minimum of these two switch operations. The Advanced Park function display is also concentrated in a single location on the panoramic view screen, which helps to minimize the amount of eye movement during parking. The following sections describe the different Advanced Park function displays shown on the screen during parking.

Before parking starts:

As shown in **Fig. 8** the vehicle is shown from above in three dimensions (3D) so that the driver can identify the target parking space and the surrounding area. The viewpoint of the display changes depending on the parking space selected by the driver. The parking settings (for example, the parking method (parallel parking/drive into parking row) and the selection of alternative parking spaces) can all be changed on the same screen.

During control:

Images of the direction of movement depending on the gear selection and a panoramic view around the vehicle are displayed so that the driver can easily identify the situation surrounding the vehicle (**Fig. 9**).

After parking is complete:

The display rotates and shows the area around the vehicle. The area around the parking space and the completed parking result are also expressed on the display (**Fig. 10**).

2.4.2.2 Display of objects around the vehicle

Objects around the vehicle are shown using a panoramic view of the clearance sonar display (the whole area around the vehicle is divided into 28 segments with 10 levels of display). In addition, a clearance sonar display that simulates a solid wall

is shown on the camera image superimposed over the object so that the driver can intuitively understand that an object is present (Fig. 9).

Objects that are moving close to the driver's vehicle are shown using different sets of five arrows when moving forward or reversing to clearly emphasize the presence and direction of the object (Fig. 11).

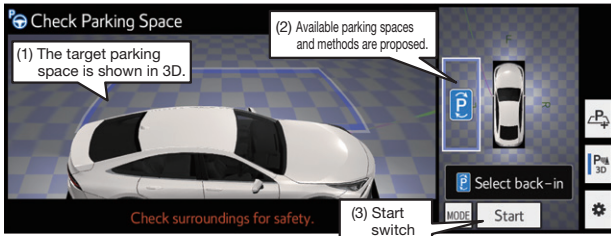


Fig. 8 Display before Parking Starts

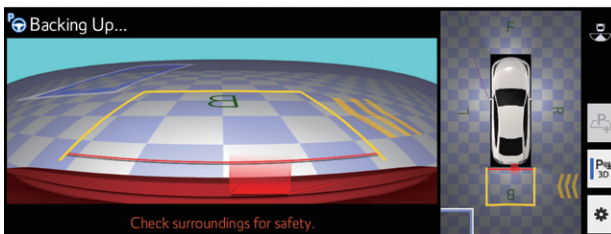


Fig. 9 Display during Parking



Fig. 10 Display after Parking Is Completed

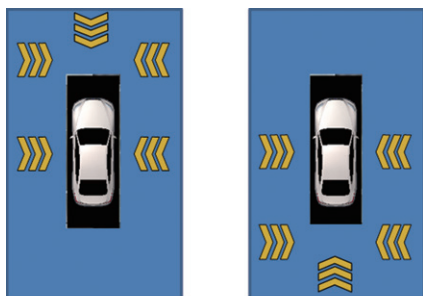


Fig. 11 Displays when Approaching Object

2.4.3 Vehicle control

2.4.3.1 Forward position when driving into empty parking row

An effective way of shortening the time required by the function to park the vehicle is to reduce the number of corrective steering maneuvers. A high number of corrective steering maneuvers increases the unnecessary distance covered by the vehicle. As a result, the process to change the course of the vehicle becomes time consuming. Fig. 12 shows how drivers that find parking relatively easy or difficult stop before reversing into a parking space. (1) Drivers that find parking relatively easy approach the parking space and stop the vehicle in a suitable position while considering the available space in the car park. These drivers point the vehicle opposite the parking space before reversing easily toward the space. As a result, the vehicle requires little adjustment when backing into the space and it is easier to enter the suitable position inside the space. (2) Drivers that find parking relatively difficult do not approach the parking space properly and tend to point the vehicle in an unsuitable direction. When reversing, the difference in the trajectories of the outer wheels means that the steering wheel cannot be turned enough to avoid hitting the vehicle next to the target space and the turn is too wide. As a result, the driver will have to stop and make a corrective steering maneuver during parking, resulting in a large loss of time. For these reasons, the Advanced Park function detects objects around the vehicle and guides the driver to an appropriate position in front of the parking space in accordance with the environment of the car park. This creates a path that requires fewer corrective steering maneuvers and helps to realize smooth parking operations.

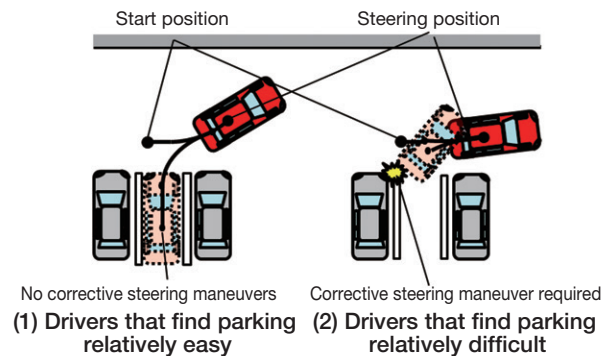


Fig. 12 Paths when Backing into Parking Space

2.4.3.2 Speed control

Although a higher vehicle speed would be required to shorten the time required for parking, the development team was concerned that this might have an adverse effect on driver confidence in the function. Away from the parking space, drivers tend to feel less concern when objects around the vehicle are further away even when moving forward at high

Special Feature

speed. In contrast, when the vehicle is inside the parking space and other parked vehicles or objects are closer, a high speed is likely to cause concern. Therefore, the function reduces speed when inside the parking space to alleviate driver concerns while still shortening the time required for parking.

In addition, individual drivers are likely to perceive the speed generated by the function in different ways, depending on the technique of the driver and whether the driver is accustomed to how the function operates. Therefore, the the speed of the function can be customized for greater user friendliness.

2.4.4 Cooperation with driver

In some situations, the driver might intervene during operation of the Advanced Park function. To verify whether the intervention was mistaken or intentional, the vehicle is stopped and the assistance paused. The driver is then asked to confirm the intention of the intervention and to check for safety around the vehicle. However, the function interprets brake operations as the driver intending to slow the vehicle down. In this case, the function will accept the intervention (**Table 3**). This approach helps to ensure that the driver's intention is reflected within safe limits, enabling the function to be used safely, naturally, and with confidence.

Table 3 Reactions after Driver Intervention

Steering	Acceleration	Braking	Shifting
Function stops.	Function stops.	Function continues.	Function stops.

2.4.5 Memory function

When parking at home or in another unlined parking space, the space can be registered in advance. This allows the Advanced Park function to park the vehicle from the next time in the same way as a regular lined parking space. Since the position and conditions of such parking spaces differs depending on the driver (distance from the road, distance from walls on the driver's side, and the like), the driver can adjust the parking space on the display at the beginning of the registration process. In this event a parking path is generated each time the space is moved and the function will not allow the setting of spaces where the vehicle cannot park. After setting the space, parking can be carried out by the Advanced Park function. However, the resulting parking position may differ from the driver's original intentions depending on the orientation of the vehicle, the unevenness of the path, the gradient, the resolution of the images, and so on when the parking space was set. Therefore, before completing registration, the driver can finely adjust the position of the parking space to ensure that the vehicle parks in the intended location (**Fig. 13**).

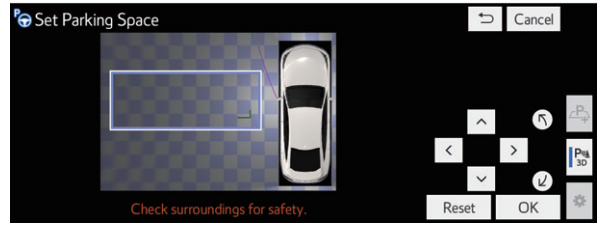


Fig. 13 Adjustment of Registered Position

After registration, the function operates in the same way as normal. The function will park the vehicle automatically in the registered space after the driver stops the vehicle in front of the space and presses the start button. As a result, the driver does not have to set the parking space every time the vehicle parks there (**Fig. 14**).



Fig. 14 Display of Parking Space in Memory Function

The memory function recognizes the parking space as follows. Compared to the parking environment when the space was registered in the memory, it is possible that the position of objects around the vehicle may change or different lighting conditions may affect the imaging conditions of the cameras. Therefore, the function memorizes road surface patterns with little variation and compares the current the memorized image with the current image. This allows the function to calculate the relative position of the driver's vehicle with respect to the position of the vehicle when the space was registered, enabling the parking space to be set automatically in accordance with the current vehicle position (**Fig. 15**).

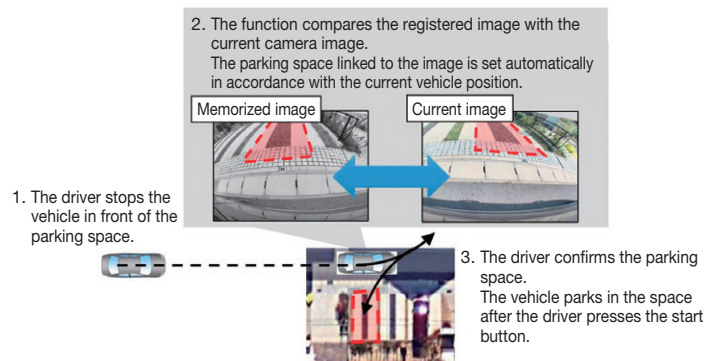


Fig. 15 Recognition Technology Adopted by the Memory Function

2.5 Conclusion

The developed Toyota Teammate Advanced Park function is a level 2 automated driving system that provides assistance under the assumption of constant driver supervision. It was developed following the following four concepts: ensure safety by recognizing the environment around the vehicle (i.e., the capability to use the function safely, naturally, and with confidence), adopt an easy-to-understand HMI (i.e., a function that is simple to use), enable parking without wasting time (i.e., the capability to park smoothly), and use a memory function to expand the range of support (i.e., for system compatibility with unlined parking spaces).

These concepts were realized by the development of an easy-to-understand HMI that synchronizes detection around the vehicle using fish-eye cameras and ultrasonic sonar with panoramic view displays, vehicle position control in front of the parking space that minimizes corrective steering maneuvers, speed control that achieves a good balance between shortening the time required for parking and driver confidence, cooperation with driver intervention, and a memory function that memorizes road surface patterns and registers parking spaces. As a result, the developed Advanced Park function realizes an optimum balance between safety and confidence.

References

- (1) Y. Sakai et al. "Development of Advanced Parking Support System" *Proceedings of the JSAE Annual Congress (Spring) (2020)*.
- (2) *Drivers under 20 Lack Confidence in Driving?! One in Four Drivers Say They Are Poor Drivers* (in Japanese). Press Release of Park 24 Co., Ltd. (2020).
- (3) *Toyota's Safety Technology - Intelligent Parking Assist 2: Steering Assistance during Reverse Parking* (in Japanese). Toyota Motor Corporation (2020).

Authors



Y. MATSUNAGA



Y. MINASE



Y. HIEI

Development of Sudden Acceleration Suppression System Using Big Data

Takuya Kaminade*¹
 Yuhi Kishimoto*¹
 Takashi Unigame*¹
 Masashi Takagi*¹
 Hiroaki Daba*²
 Masashi Oishi*³

Abstract

Accidents caused by pedal misapplication are becoming a serious social issue as Japan’s population ages. Active safety technologies are being increasingly regarded as a promising means of addressing this issue. However, systems that use clearance sonar or other object detection technologies cannot determine whether pedal misapplication has occurred when an object is present beyond the detectable range of the system. This article describes a technology that helps to prevent unintentional driver behavior that might result in an accident by determining whether pedal misapplication has occurred based on the amount and speed of accelerator depression without carrying out object detection, and then suppressing the resulting acceleration. This technology also features logic that stops the system activating in normal driving scenarios when acceleration is required, using big data obtained from actual vehicle behavior.

Keywords: safety, driving assistance, acceleration suppression, pedal misapplication

1. Introduction

Accidents caused by pedal misapplication are becoming a serious social issue as Japan’s population ages, and active safety technologies are being increasingly regarded as a promising means of addressing this issue. Pedal misapplication accidents commonly involve older drivers and are responsible for over eight times more fatalities in the 75-and-over age group than with drivers under the age of 75 (Fig. 1).⁽¹⁾

Systems that address certain cases of accelerator pedal misapplication have already been developed and widely adopted. One example is the Intelligent Clearance Sonar (Parking Support Brake (Detection of Stationary Objects)) system that detects walls and other objects and perform braking control. This system, which helps to prevent collisions with stationary objects and other accidents, has been shown to help reduce pedal misapplication accidents in car parks by approximately 70%.⁽²⁾

However, most pedal misapplication accidents that result in injury occur on normal stretches of road.⁽³⁾ In addition, a large overall proportion of pedal misapplication accidents occur at speeds higher than the top activation speed (approximately 15 km/h) of the Intelligent Clearance Sonar System (Fig. 2).⁽⁴⁾ For these reasons, appreciating the necessity of expanding the control range of pedal misapplication systems, Toyota has developed a sudden acceleration suppression system with a judgment function capable of determining whether the accelerator has been mistakenly depressed. Toyota launched this system under the name “Plus Support” for new cars.

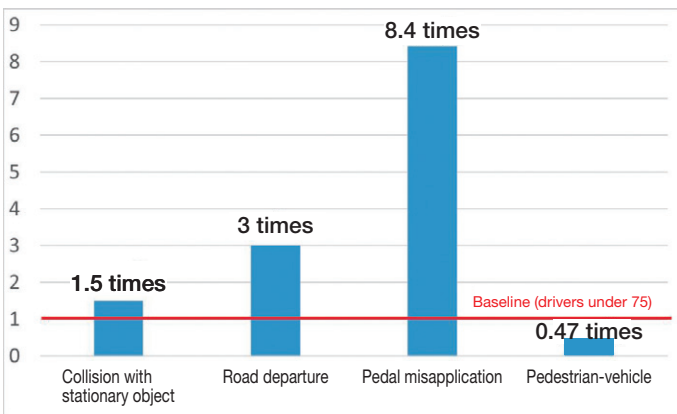


Fig. 1 Fatal Accident Rate Involving Drivers Aged 75 and Older (Drivers under 75 = 1)

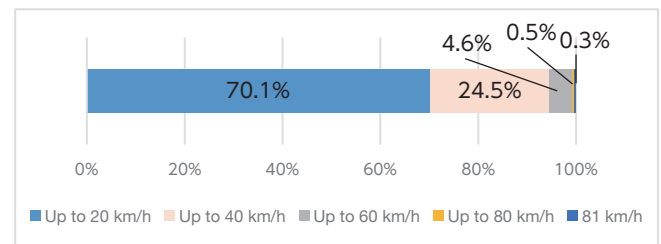


Fig. 2 Collision Risk Recognition Speed after Pedal Misapplication

*¹ Automated Driving & Advanced Safety System Development Div., Advanced R&D and Engineering Company
 *² Mobility Evaluation and Engineering Div., Advanced R&D and Engineering Company
 *³ Toyota Motor Europe S.A./N.V.

This function determines whether pedal misapplication has occurred based on the driver’s accelerator operation, regardless of whether an object has been detected. Although there is a history of research into accelerator operation, it has been difficult to analyze trends from the standpoints of both pedal misapplication accidents and ordinary driving based on sufficient data. Therefore, it was decided to adopt big data obtained from actual vehicles and develop a logic capable of analyzing driver behavior both when an accident occurs and during ordinary driving.

2. Target Performance

This development aimed to develop a system capable of identifying pedal misapplication from driver accelerator operation covering at least 90% of pedal misapplication accidents. To obtain the relationship between accelerator operation and vehicle speed when pedal misapplication occurs, around 100 pedal misapplication accidents were analyzed from nationwide data. Pedal misapplication was defined as occurring at an accelerator stroke of 90%. As shown in Fig. 3, this result is positioned slightly toward the low vehicle speed side of the collision risk recognition speed distribution in Fig. 2. Based on this result, the upper limit activation speed of the system was set to 30 km/h, which covers at least 95% of all accidents. The system was also designed to activate in either forward or reverse gears.

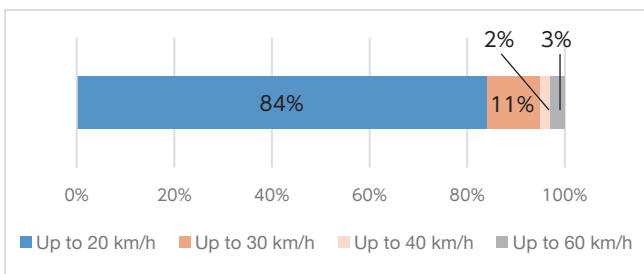


Fig. 3 Vehicle Speed when Pedal Misapplication Occurs

3. Configuration of Sudden Acceleration Suppression

The system starts up when a dedicated key is used. The vehicle recognizes the dedicated key to identify that the driver wants to use the system.

The developed system is installed as a set with the Intelligent Clearance Sonar (Parking Support Brake (Detection of Stationary Objects)) system, which has already been confirmed as helping to reduce pedal misapplication accidents in car parks. Both systems share the same ECU. When the system determines that pedal misapplication has occurred, it requests the powertrain ECU to suppress acceleration.

When acceleration suppression occurs, a message is

displayed on the meter cluster and a buzzer is sounded at the same time. Fig. 4 shows the configuration of the system.

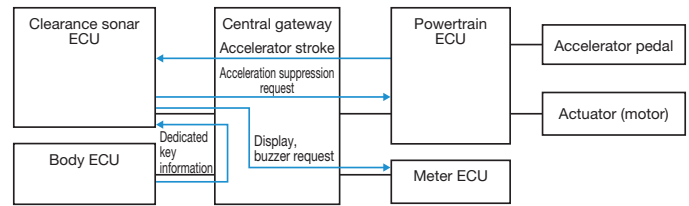


Fig. 4 System Configuration

4. Pedal Misapplication Determination Logic

4.1 Operation logic

The development analyzed around 100 pedal misapplication accidents from nationwide data. This analysis found that the accelerator stroke was at least 90% in approximately 82% of these accidents (Fig. 5). Next, Fig. 6 shows the analysis results for the maximum accelerator depression speed. In approximately 55% of the accidents, the 0 to 100% accelerator depression speed was 0.5 seconds or less. When combined with an accelerator depression speed between 0.5 and 1.0 seconds, these two ranges covered approximately 98% of all the accidents.

Since most pedal misapplication accidents occur when the vehicle accelerates suddenly, it is necessary to suppress the acceleration before the vehicle speed increases. For this reason, the acceleration suppression control was designed to rapidly stop sudden acceleration when the system determines that pedal misapplication has occurred. The operation logic is as follows.

- The system is operational up to a vehicle speed of approximately 30 km/h.
- The accelerator is depressed at a predetermined speed or faster (approximately up to a speed of 1.0 seconds).
- The accelerator stroke reaches a predetermined value (approximately 90% or higher).

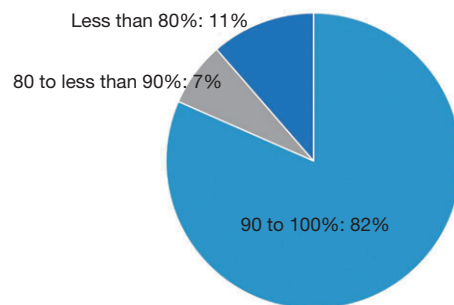


Fig. 5 Maximum Accelerator Stroke

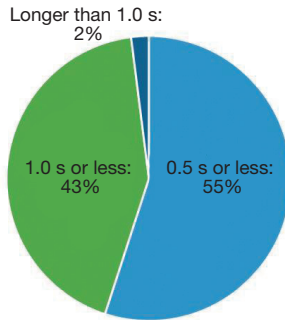


Fig. 6 Maximum Accelerator Depression Speed

4.2 Operation prohibition logic

To ensure the intended acceleration in ordinary driving scenarios requiring sudden acceleration, analysis was carried out using big data obtained from actual vehicles. Ordinary driving scenarios requiring sudden acceleration were extracted and trends other than those involving the accelerator were identified. As a result, the system is designed not to operate under the following conditions.

- During operation of the turn signals and within 2 seconds of turn signal operation ending.
- In the period approximately 2 seconds after the driver releases the brake pedal.
- When the driver's vehicle is driving up a steep gradient.

4.3 Reaction when accelerator is depressed again or continuously depressed

Assuming that the system might determine that pedal misapplication has occurred in an ordinary driving scenario requiring sudden acceleration, an upper limit speed was set and control incorporated to enable operation when both driving forward and in reverse. More specifically, if the driver depresses the accelerator again quickly and strongly immediately after acceleration is suppressed, or if the driver continues to depress the accelerator while acceleration is being suppressed, the system reduces the amount of acceleration suppression and slowly accelerates the vehicle up to the set upper vehicle speed limit.

4.4 Acceleration suppression ending logic

The system ends acceleration suppression when the accelerator is returned to a low stroke position.

4.5 Interoperability with simultaneous activation of other systems

The developed system behaves as follows when the Advanced Park and Advanced Drive systems are activated at the same time as sudden acceleration suppression.

Advanced Park (AP):

If the driver depresses the accelerator while AP is activated, the vehicle is stopped by the automatic braking control. The stopped state is then maintained until the driver depresses the brake pedal. Therefore, the developed function is not activated even when pedal misapplication occurs because safety has already been ensured.

Advanced Drive (AD):

This function will activate if pedal misapplication occurs while AD is in operation. However, the driver may feel a sense of uncertainty if the function stops operating after the accelerator is returned and the AD system starts accelerating the vehicle again. Therefore, if the function activates during AD operation, the AD system transitions to its end processing and hands over control to the driver.

5. Results

Patterns assuming a pedal misapplication accident and sudden acceleration patterns in ordinary driving were defined, and the performance of the function was confirmed in each pattern (Table 1).

Table 1 Performance Confirmation Results

No.	Evaluation pattern	Result
1	Accelerator operation corresponding to pedal misapplication	OK: activate
2	Activation while turn signals are blinking	OK: do not activate
3	Immediately after brake pedal is released	OK: do not activate
4	Steep uphill gradients	OK: do not activate

6. Conclusion

The development of this sudden acceleration suppression system used big data to create an algorithm capable of determining whether the driver has depressed the accelerator by mistake or wants to accelerate suddenly in an ordinary driving scenario. This algorithm was incorporated into the finished product in combination with a dedicated key. The upper limit activation speed of the system was set to 30 km/h, resulting in a system capable of determining that pedal misapplication had occurred in at least 90% of pedal misapplication accidents. In addition, reflecting the seriousness of pedal misapplication accidents, this technology has also been shared with other manufacturers. Toyota intends to install this system across its model lineup to enable wider use by older drivers.

References

- (1) *Special White Paper on Preventing Traffic Accidents Involving Elderly People* (in Japanese). Cabinet Office, Government of Japan (2017).
- (2) *Toyota Announces the Accident Reduction Effects of Intelligent Clearance Sonar, a Safety Support Technology for Parking*. Toyota Motor Corporation Press Release.
- (3) *Traffic Accident Analysis Report No. 124: Accelerator and Brake Pedal Misapplication Accidents - Toward Preventing Characteristic Accidents Involving Elderly Drivers* (in Japanese). ITARDA Information.
- (4) *Traffic Accident Analysis Report No. 107: Preventing Errors in Driving Behavior - Common Accidents Caused by Driving Errors by Young and Elderly Drivers* (in Japanese). ITARDA Information.

Authors



T. KAMINADE



Y. KISHIMOTO



T. UNIGAME



M. TAKAGI



H. DABA



M. OISHI

Connected Vehicle Services

Satoru Sakuma*¹
 Tetsu Yajima*¹
 Kano Asai*²
 Masaya Hizaki*²

Abstract

As automotive communication functions become more widespread, there are growing expectations about the development of connected vehicle services. Toyota is working to develop and launch new services to satisfy these expectations and respond to the evolving market environment. This article describes the outline of the system that provides these connected services and the smart phone application developed for the second-generation Mirai.

Keywords: *connected services, Mobility Services Platform (MSPF), data communication module (DCM), long term evolution (LTE), smart phone applications*

1. Introduction

The Mirai is a connected vehicle equipped with functions to provide the latest connected services. These services are designed to appeal to the user based on interaction with the vehicle using various types of information obtained from onboard systems.

2. Utilization of Vehicle Information and System Configuration

In Toyota’s lineup of connected vehicles, information is obtained from electronic control units (ECUs) mounted in the vehicle and transmitted from a dedicated onboard data communication module (DCM) to Toyota’s Mobility Service Platform (MSPF) via a long term evolution (LTE) network set up by a mobile telephone service provider.

The information to be stored in the MSPF is collected at the appropriate timings in accordance with the application. This information includes vehicle behavior while driving, driver actions, sensing data, and so on. As part of Toyota’s lineup of connected vehicles, the Mirai provides services using this information.

The onboard local area networks (LANs) used to collect this information are the controller area network (CAN), Ethernet, and universal serial bus (USB).

The MSPF is an open platform constructed by Toyota on a cloud server. Toyota is studying a range of new plans using the

collected information, in addition to the provision of mobility services, support in the event of an accident or breakdown, and functional updates. **Fig. 1** shows an overall outline of the system.

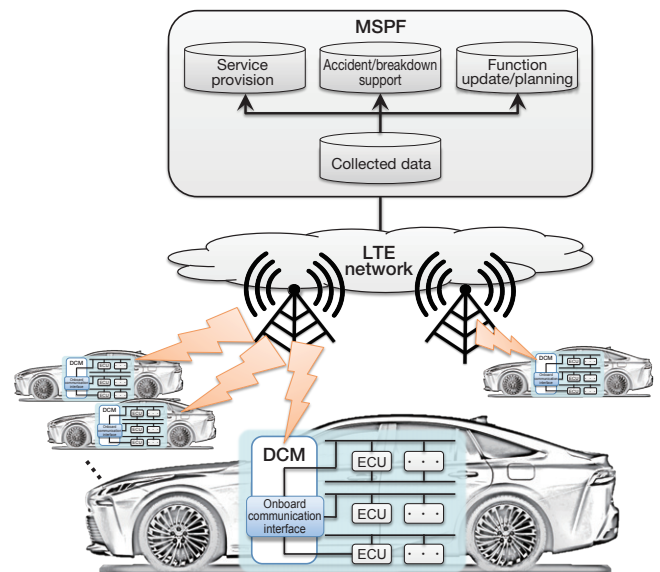


Fig. 1 System Outline

In the information collection process, Toyota protects personal information and applies various security measures so that customers can use their vehicles with peace of mind.

*¹ e-TOYOTA Div., Connected Company

*² IVI System Development Div., Connected Company

3. Services Using Smart Phone Applications

Part of the appeal of services using connected technology is the capability to supply optimum route information using constantly updated maps and real-time traffic information to navigation systems. This technology can also enable the user to perform actions through natural spoken interaction with the vehicle via a virtual agent by voice recognition.

For greater convenience and comfort in cold regions, the second-generation Mirai provides a service that allows the user to turn on the vehicle's air conditioning function remotely via a smart phone application before entering the vehicle. This service can also operate functions to defrost the windshield, rear window, and exterior mirrors. In addition, it also features functions to turn on the steering wheel and seat heaters, the first such function on a Toyota vehicle (**Fig. 2**).



Fig. 2 Remote Air Conditioning Application Screen

This function is available in the summer as well as the winter. The function can cool the occupant compartment in advance and help to prevent heat stroke. One of the merits of a fuel cell vehicle (FCV) is the capability to operate the air conditioning quietly and without engine noise so that people around the vehicle are not disturbed when the function is started remotely.

In addition, the smart phone application also shows the hydrogen fuel level and available range. Since the large-capacity battery in the Mirai can also be used to supply power after a natural disaster or other emergency, the application also shows the approximate remaining battery time (**Fig. 3**).



Fig. 3 Screen of the "Pocket Mirai" Application

4. Conclusion

This article has described an outline of Toyota's connected car system and presented some examples of the connected services provided by the second-generation Mirai.

In addition to onboard connected services, the Mirai also provides users with a range of services that can be operated away from the vehicle using a smart phone application.

Toyota intends to continue creating and updating its connected services to provide an ever-more convenient and safer vehicle experience.

Authors



S. SAKUMA



T. YAJIMA



K. ASAI



M. HIZAKI

Special Feature

Development of Low-CO₂ Recycled Aluminum Alloy

Naoki Nishikawa*¹
 Yuya Masuda*²
 Kazumi Otake*¹
 Ryo Kuramoto*³
 Yuki Yamazaki*³
 Takeshi Nagai*³

Abstract

Efforts to reduce the environmental impact of vehicles are no longer focused solely on tailpipe emissions. There are increasing demands to lower CO₂ emissions over the whole life cycle of the vehicle, including manufacturing and material production. This article describes a recycled aluminum alloy that was developed to help lower both vehicle weight and the CO₂ emissions generated during material production.

Keywords: aluminum, recycling, low CO₂, vehicle weight reduction

1. Introduction

Toyota has been working to apply aluminum alloys to automotive parts with the objective of reducing vehicle weight, thereby helping to improve fuel efficiency, reduce CO₂ emissions, and enhance dynamic performance. The first Toyota model to adopt aluminum alloy body panels was the Supra in 1993, and this technology has now been extended to the hood of the second-generation Mirai (Fig. 1).



Fig. 1 The Second-Generation Mirai

To help achieve its sustainable development goals (SDGs), Toyota has announced the Toyota Environmental Challenge 2050, part of which describes targets for lowering CO₂ emissions throughout the entire vehicle life cycle. The new recycled aluminum alloy used for the inner hood component of the Mirai, which is a vehicle that was designed with a specific focus on environmental performance, is a fruit of this initiative. This is the first application of this recycled material to an automotive body panel stamping, and it helped to lower CO₂ emissions in the aluminum manufacturing process by approximately 50%. This article describes the background and characteristics of the development of this recycled material.

2. CO₂ Emissions in Aluminum Manufacturing Process

Fig. 2 shows the process that converts the raw aluminum material (bauxite) to the rolled coils of aluminum used in vehicle manufacturing. It should be noted that rolled aluminum coil is simply flat sheets of aluminum that have been rolled up. These coils of aluminum are delivered from the material manufacturer to the automaker as the raw material to manufacture body panels. Aluminum is manufactured as virgin metal from raw bauxite by electrolytic smelting. As this smelting process consumes large amounts of power, aluminum is often referred to as “canned electricity.” Approximately 90% of the CO₂ generated during the aluminum manufacturing process occurs during smelting. If, for example, an aluminum drink can is manufactured from recycled aluminum can scrap, no smelting is required and the CO₂ emissions of the aluminum manufacturing process can be substantially reduced. However, because vehicles have a long service life and the amount of sheet aluminum alloy used in a vehicle is increasing in line with greater demands for weight reduction, the amount of recovered scrap has not been able to keep up with the demand for aluminum alloy for body panels.

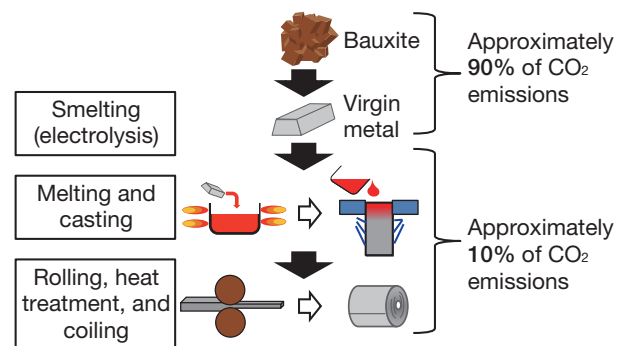


Fig. 2 Outline of Aluminum Manufacturing Process and Proportions of CO₂ Emissions

*¹ Material Engineering Div. No. 1, Advanced R&D and Engineering Company
 *² Tahara Plant Engine Manufacturing Div.
 *³ UACJ Corporation

3. Raw Material for Recycling

As shown in **Fig. 3**, Toyota has conventionally re-used stamping scrap from vehicle manufacturing processes as part of its efforts to recycle aluminum alloy for body panels. First, the stamping scrap generated during body panel manufacturing is sorted and recovered, and transported to the aluminum manufacturer. The aluminum manufacturer melts and casts the stamping scrap, converting it back into the same alloy products. This material can then be used to reduce the amount of virgin metal required to manufacture a component, thereby helping to lower CO₂ emissions by several percent.

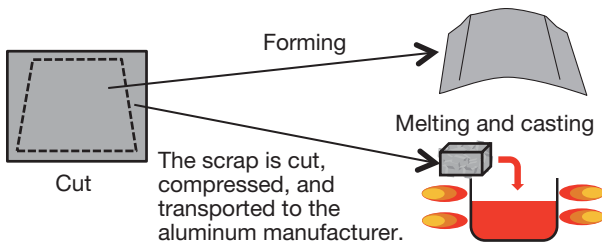


Fig. 3 Recycling of Vehicle Stamping Scrap

To help further reduce the amount of virgin metal used (i.e., to raise the proportion of recycled material), this development focused on the types of aluminum alloy scrap generated by the aluminum manufacturer. As shown in **Fig. 4**, this scrap is generated on a daily basis during the aluminum manufacturing process. Most of this is re-melted, cast, and rolled into products by the aluminum manufacturer. However, as shown in **Fig. 5**, a type of aluminum alloy scrap called clad sheets, which consists of layers of different alloys, cannot be returned to its original product since the composition of each layer becomes mixed together after re-melting. This material is difficult for the aluminum manufacturer to use and is often adopted for engine blocks and other castings with a relatively large tolerance for impurities. Therefore, this development studied the feasibility of recycling aluminum alloy scrap including these clad sheets with the aim of reducing the amount of virgin metal used in aluminum alloy material for body panels.

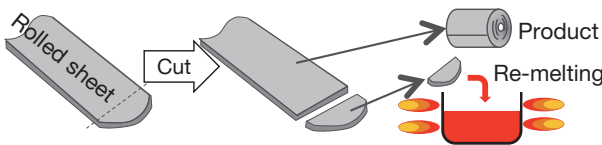


Fig. 4 Generation of Aluminum Scrap

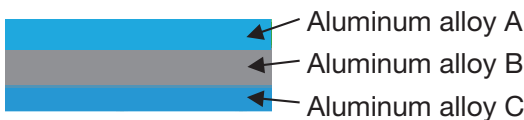


Fig. 5 Illustration of Clad Sheet

4. Study of Application of Recycled Material to Parts

4.1 Recycled material composition

Conventional aluminum alloy body panels in Toyota are manufactured from 6,000 series aluminum alloy that contains magnesium (Mg) and silicon (Si) as alloying elements (Al-Mg-Si alloy). In contrast, as shown in **Fig. 6**, recycled material contains a higher proportion of impurity elements derived from the original aluminum alloy scrap, such as manganese (Mn) and iron (Fe). One of the most effective ways of reducing CO₂ emissions is to raise the proportion of scrap used to manufacture the aluminum alloy. However, a high proportion of impurity elements tends to result in the formation of larger amounts of intermetallic compounds (Al-Fe-Mn-Si compounds, eutectic Si, and so on), as shown in **Fig. 7**. These intermetallic compounds tend to act as the origin points or propagation paths of fractures, thereby reducing the ductility of the material and raising the concern that recycled material will have worse formability than the conventional material.

In response to this issue, this development aimed to reduce the size of intermetallic compounds by raising the rolling temperature and increasing the rolling reduction ratio during the rolling process. **Fig. 7** shows images of the microstructure of the recycled material before and after this material improvement measure was adopted.

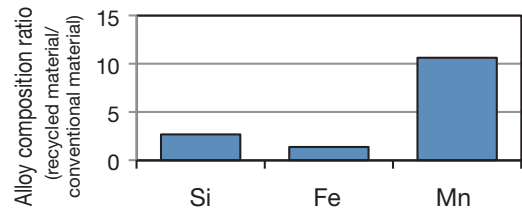


Fig. 6 Example of Composition Ratio of Conventional and Recycled Materials

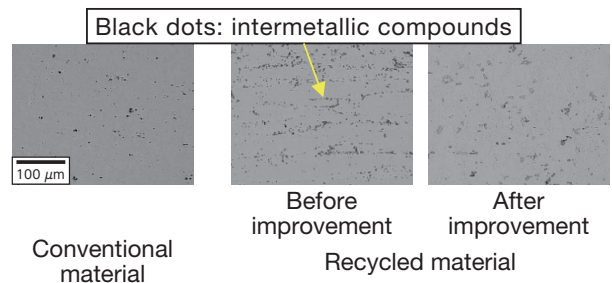


Fig. 7 Images of Microstructure of Conventional and Recycled Materials

Special Feature

4.2 Sheet metal forming performance

Despite the measures taken in the manufacturing process as described in Section 4.1, the recycled material still does not elongate as easily as the conventional material. Therefore, the study examined revising the material requirements for elongation. Forming simulations were carried out to identify the optimum shape to offset the lower material elongation, without sacrificing the performance requirements of the inner hood. As a result, measures were adopted to relax the required characteristics for elongation by increasing the bead radius and lowering the forming height requirement (**Fig. 8**). This enabled the proportion of recycled material to be increased to 50% (**Fig. 9**). In addition, the same 0.2% yield strength after bake hardening (a heat treatment using the temperature of the painting process) as conventional 6,000 series alloy was realized by identifying and adding optimum amounts of components that contribute to strength, despite the higher impurity element content of the recycled material.

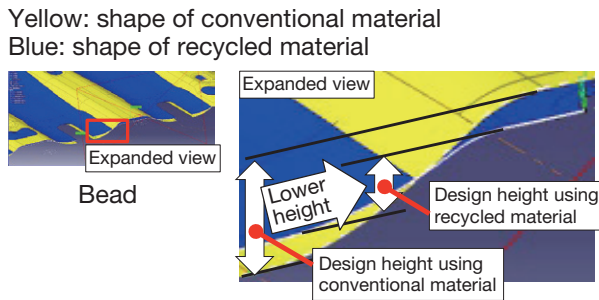


Fig. 8 Optimum Design of Inner Hood

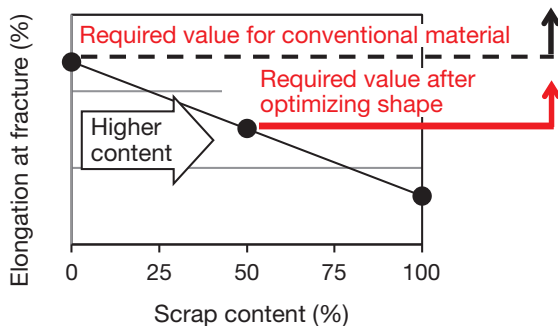


Fig. 9 Relationship between Proportion of Aluminum Scrap Content and Elongation at Fracture

4.3 Paint film adhesion

Two requirements for an inner hood manufactured from recycled material are corrosion resistance and appearance. Therefore, the development studied whether the recycled material could achieve the required performance, including whether the paint adhesion performance and corrosion resistance were equivalent to the conventional material. **Fig.**

10 shows the surface states of the chemical conversion coating, which is a paint surface pretreatment applied to the inner hood. The results found that the pretreatment state satisfied the criteria and confirmed that the surface state of the recycled material was equivalent to that of the conventional material.

Next, after the pretreatment, the paint was applied to the surface and the adhesion of the paint film was confirmed. A grid pattern of cracks was applied to the paint film, which was then completely immersed in water for a set time. Tape was then applied to the surface and peeling force applied using tape.

Fig. 11 shows sample images of the results of this test. The test confirmed that peeling did not occur on the recycled material, and that equivalent paint film adhesion as the conventional material was achieved. Further verifications were carried out on the mass-production line to verify corrosion resistance and confirm the suitability of the material for use in the real world.

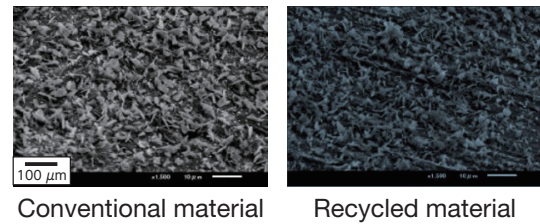


Fig. 10 Surfaces of Conventional and Recycled Materials after Pretreatment

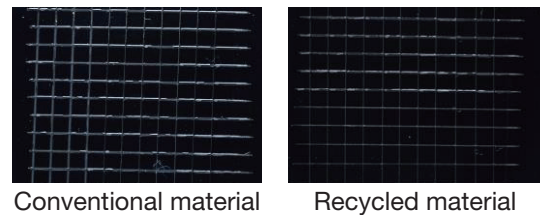


Fig. 11 Surfaces of Conventional and Recycled Materials after Adhesion Confirmation

5. Summary

This newly developed recycled aluminum alloy material for body consists of approximately 50% of aluminum alloy scrap generated by an aluminum manufacturer. As a result, the CO₂ emissions of this material in the aluminum manufacturing process are roughly 50% lower than that of conventional aluminum.

6. Conclusion

With the reduction of CO₂ emissions over the entire vehicle life cycle being increasingly regarded as an important issue, the development and adoption of this recycled material represents a major step toward the realization of this objective. To continue

addressing this issue in the future, it will be necessary to overcome the limitations of acting alone and work in partnership with other companies, such as the aluminum manufacturer described in this article. Toyota intends to continue these initiatives and promote development that will help to further reduce CO₂ emissions and alleviate the environmental impact of vehicle manufacturing.

Authors



N. NISHIKAWA



Y. MASUDA



K. OTAKE



R. KURAMOTO



Y. YAMAZAKI



T. NAGAI

Born from the World Rally Championship –Introduction to the GR Yaris–

Naohiko Saito*¹
Takashi Doi*¹

Abstract

Since re-entering the World Rally Championship (WRC) in 2018, Toyota has dedicated itself to building cars that are even more competitive under a wide range of driving environments. The lessons learned and the technologies developed through these efforts were incorporated into the GR Yaris, which was launched in September 2020. This article describes the various challenges that were overcome in the development and production of the GR Yaris.

Keywords: GR Yaris, World Rally Championship, sports car, sporty four-wheel drive, GR Factory

1. The World Rally Championship

The World Rally Championship (WRC) is a car racing world championship run by the International Automobile Federation (FIA). It consists of races between mass-production cars that have been specially modified into rally cars based on a set of technical regulations. The races are held on various surfaces, including paved tarmac, extremely rough unpaved gravel, and snowy roads (Fig. 1).



Fig. 1 The GR Yaris Rally Car in Action on Various Road Surfaces

Toyota has a long history of participation in the WRC, taking part from 1973 to 1999 (Fig. 2), before rejoining the competition after a short hiatus in 2017 under the Toyota Gazoo Racing-World Rally Team banner. The goal of participating in the WRC is to gain knowledge and experience that can be fed back into future production vehicle development. The GR Yaris was born directly from this concept.



Fig. 2 Historic Toyota Rally Cars

2. The GR Yaris

The GR Yaris is Toyota's first independently developed and produced true four-wheel drive (4WD) sports car in almost twenty years. It is a mass-market car that features a wide range of technologies nurtured through the development of sports cars, starting with cars for the WRC (Fig. 3).



Fig. 3 The Exterior of the GR Yaris

In this day and age, developing this kind of car is no easy matter. A critical driving force behind its development was the President of Toyota, Akio Toyoda, under his pseudonym "Morizo."

From the initial phase of development to the current day, Morizo invested a large amount of time in the development and testing of the GR Yaris as a master test driver. Morizo was the inspiration for the development team and constantly led the project from the front (Fig. 4).

Aside from leadership, Morizo's skill in driving 4WD cars is highly rated within Toyota. These skills identified various issues that the development team had overlooked, which

*¹ GR Project Operation Div., GAZOO Racing Company

Morizo then worked as part of the team to help overcome.

While the development team seemed almost too overawed to approach Morizo at the beginning of the development, after working together on the car right up to the launch, Morizo had become simply another member of the team.



Fig. 4 Morizo Testing the GR Yaris

3. The Two Challenges in Developing the GR Yaris

The development team faced two major challenges in the development and production of the GR Yaris.

3.1 Building a car bred from motor sports

In its history, Toyota has developed and built many cars that excelled in motor sports. However, the approach for these vehicles was generally to first develop a car for the mass-market, and then to refine it for a particular category of racing.

The GR Yaris was developed under the exactly opposite approach, that is, to build a mass-market car bred from motor sports. Specifically, Toyota planned to first develop a racing car, and then further develop, test, and manufacture that car for the regular market. To accomplish this, racing drivers were drafted in from the early phases of development to carry out repeated and thorough assessments (Fig. 5).



Fig. 5 Assessments by Professional Drivers

3.2 Low-volume production of large amounts of parts

Sports cars are a highly niche product and do not sell in the quantity of an SUV or minivan. Another attraction of sports cars is the regular application of performance upgrades and the addition of new specifications. Therefore, the feasibility of producing low volumes of a wide range of parts was a major

challenge, not only for the GR Yaris, but to enable Gazoo Racing to continue producing sports cars at all.

Therefore, a new dedicated sports car production line called the GR Factory was built inside the Motomachi Plant (Fig. 6) with the aim of making the production of low volumes of a wide range of high-performance parts feasible.



Fig. 6 GR Factory (Assembly Process)

As low-volume production generally results in higher costs, Toyota worked closely with its partner companies to reduce the cost of every component through a thorough *genchi-genbutsu*-based approach to continuous improvements (*kaizen*).

4. The Development of the GR Yaris

With these two major challenges in mind, the team began the development of the GR Yaris in high spirits. However, with the GR Yaris being Toyota's first true 4WD sports car in almost twenty years, the complete lack of know-how and experience meant that the development was extremely difficult. Virtually none of the development team from twenty years was still at the company and almost no records had survived.

Therefore, the development team decided to bring in and learn from the expertise of Tommi Mäkinen Racing (TMR), which played a major role in the development of the current WRC car (Fig. 7).

TMR has a wide range of expert knowledge and experience in how to set up a car to drive quickly on various road surfaces in the WRC. The development team tapped this know-how and applied it to the development of the GR Yaris. The team also asked actual WRC drivers to test the car and incorporated much of this professional expertise particularly in the settings of the 4WD system.



Fig. 7 Joint Development Activities with TMR

The following sections provide an overview of some of the technologies that were incorporated into the GR Yaris. The subsequent articles in this edition of the Toyota Technical Review describe these technologies in more detail.

4.1 Styling that emphasizes performance

The styling of the GR Yaris was designed with a clear emphasis on performance.

In the exterior styling process, individual style and shape elements were determined by putting performance first. For example, the side silhouette was designed to prioritize downforce and aerodynamics and the front was designed to prioritize cooling performance.

As a result, the rear end of the roof has a large taper (Fig. 8) and an extremely sporty low and wide styling was achieved.

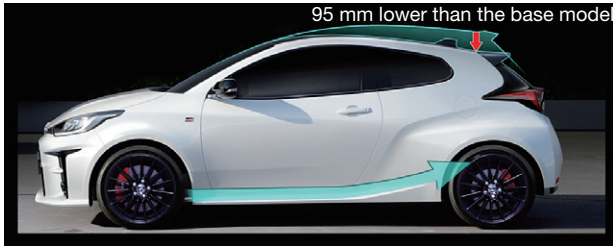


Fig. 8 Side Silhouette of the GR Yaris

4.2 Lightweight body

It has been long-appreciated that lightness is the ultimate weapon of any sports car. Since the rules of the WRC and other rally series state that the materials and shapes of competing cars must be unchanged from the base cars, the development of the GR Yaris focused strongly on reducing the weight of the body.

Although generally an exception for vehicles in this class, innovative materials were adopted in various areas of the GR Yaris, such as carbon fiber for the roof, and aluminum for the hood and doors (including the back door) (Fig. 9). In fact, the carbon fiber roof is the world's first example of a sheet molding compound (SMC) adopted for a vehicle roof. As a result, the body of the GR Yaris is approximately 30 kg lighter than the body of the base model.

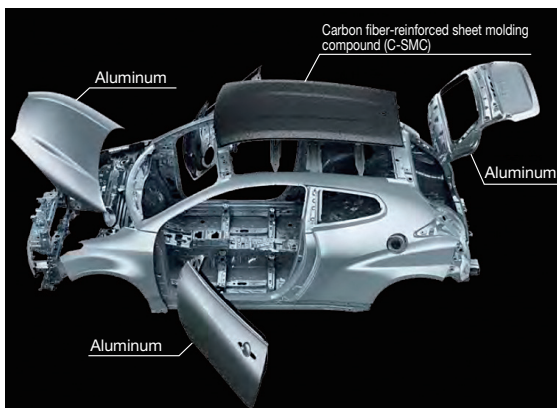


Fig. 9 Locations of Innovative Upper Body Materials

4.3 Optimized inertial characteristics

The optimization of vehicle inertia generally involves lowering the center of gravity. In addition, the GR Yaris development team worked to optimize the front/rear and left/right weight distribution. The optimum layout for each component was realized through a process that identified the mass and center of gravity position of several tens of thousands of separate parts. For example, the front/rear weight distribution was optimized with the auxiliary battery mounted under the trunk at the rear of the vehicle. However, since this position is slightly offset to the left, the left/right weight distribution was also optimized (Fig. 10).

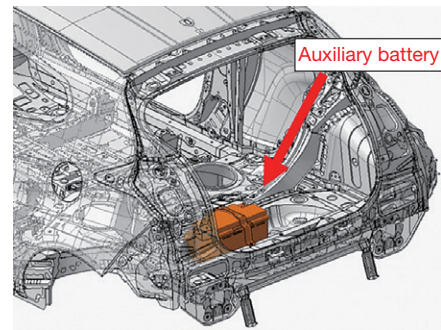
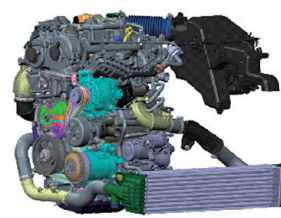


Fig. 10 Layout of Auxiliary Battery

4.4 New 1.6-liter turbocharged engine

A new 1.6-liter inline 3-cylinder turbocharged engine (model code: G16E-GTS) was developed for the GR Yaris. To achieve a lightweight and compact engine with high-power and rapid response, virtually all the component parts were completely redesigned, and a wide range of motor sports technologies were incorporated. The result is an engine with class-leading power performance (Fig. 11).



Outline of G16E-GTS engine

Number and alignment of cylinders	Turbocharged inline 3-cylinder
Total displacement	1,618 cc
Bore diameter × stroke	87.5 × 89.7
Maximum power	200 kW/6,500 rpm
Maximum torque	370 Nm/3,000 to 4,600 rpm

Fig. 11 Outline of G16E-GTS Engine

Through a combination of the weight reduction described above and the G16E-GTS engine, the GR Yaris is substantially quicker than other subcompact B segment hot hatches. It realizes equivalent performance to compact C segment 4WD sports cars, while being substantially lighter (Fig. 12).

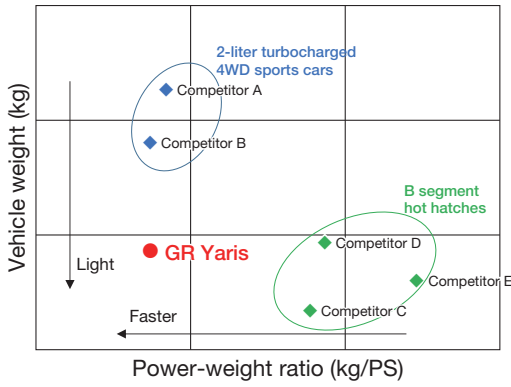


Fig. 12 Comparison of Power-Weight Ratios and Vehicle Weights

4.5 New sporty 4WD system

A new sporty 4WD system was developed and adopted for the GR Yaris to achieve exhilarating acceleration by transmitting the power of the 1.6-liter turbocharged engines firmly to the road and to realize stable and safe performance on any surface.

A rapid-response, electronically controlled multi-plate clutch is mounted in front of the rear differential. The system uses the rotation differential before and after the clutch (rotational speed before clutch > rotational speed after clutch) to enable an unprecedentedly wide front/rear driving force distribution range (Fig. 13).

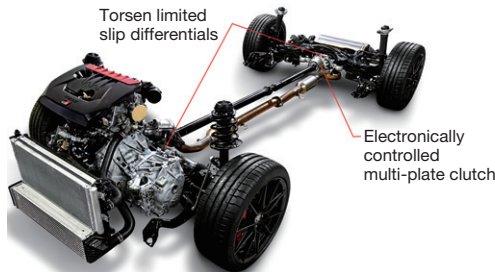


Fig. 13 Appearance of 4WD System

In addition, a triple mode selection switch is provided in the cockpit that allows the driver to select the optimum torque distribution in accordance with the driver's preference or driving scenario (Fig. 14).

Mode selection switch	Mode	Basic front/rear distribution ratio
	Normal	Basic front/rear distribution ratio: 60:40 F ██████████ R ██████████
	Sport	Basic front/rear distribution ratio: 70:30 F ██████████ R ██████████
	Track	Basic front/rear distribution ratio: 50:50 F ██████████ R ██████████

Fig. 14 Outline of 4WD Modes

4.6 Chassis for the GR-Four 4WD system

To realize the highest level of dynamic performance while supporting the exhilarating power delivered by the engine, the GR Yaris adopts a MacPherson strut front suspension and a trailing-arm type double wishbone rear suspension (Fig. 15). Although the basic configuration is shared with the current platform, the suspension features a number of dedicated components, such as the steering knuckles and carriers, which were designed to optimize the suspension geometry and increase stiffness.

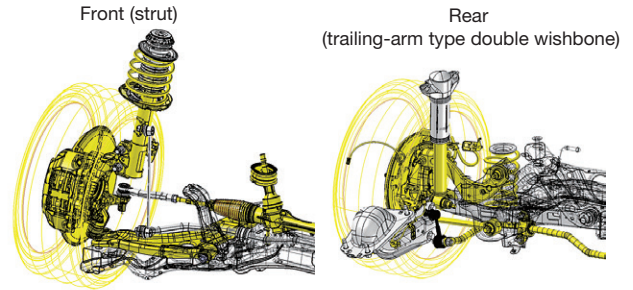


Fig. 15 Outline of Suspension

Designed with fade-resistant performance for high-speed racetracks such as the Nürburgring Nordschleife, the brake system uses newly developed 18-inch discs at the front and 16-inch discs at the rear (Fig. 16).

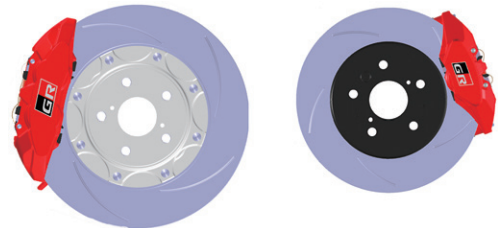


Fig. 16 Appearance of Front and Rear Brakes

In addition, the parking brake was not designed simply for use after the vehicle has been parked. The capability of the parking brake to change the orientation of the car in gymkhana-style races and the like was also assessed during the development. As a result, a drum-in-hat type parking brake with excellent response was adopted and the brake lever was laid out in an easily accessible location.

4.7 Development of driving performance

In addition to Toyota's own proving grounds, the GR Yaris was assessed by both internal and external test drivers on a wide range of surfaces, including racetracks, snowy roads, gravel, and other conditions. Racing drivers have a particular keen sense of perception and demanded a level of performance that was far higher than that envisioned at the start of development. To respond to these demands, the development emphasized the following three points.

Special Feature

a. Use of data

Although data was obviously used to analyze phenomena under various conditions, it also became the common language of the drivers and development team.

Fig. 17 shows an example of driving data (braking during cornering) obtained from two drivers during the development process. Despite both drivers being professionals in the same racing category in Japan, both drive in completely different ways. Driver A depresses and lifts off the brake pedal very quickly, before subsequently using the brakes to control the vehicle. In contrast, driver B depresses the brake more gradually while feeling for the optimum dynamic behavior. The development team aimed to build a car capable of accommodating both driving styles, while factoring in different techniques as shown in the figure.

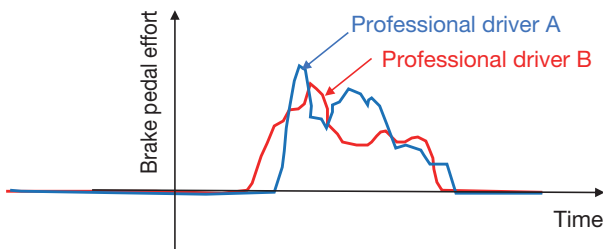


Fig. 17 Differences in Driving Styles

b. Evaluations of complex driving operations

Normally, dynamic performance development tends to evaluate single aspects of driving (such as 0.8 G straight-line braking or 100 km/h steady-state sine wave steering) since these are easier to quantify. However, as these situations are rarely encountered in actual driving, the development of the GR Yaris focused on more realistic complex driving operations.

Fig. 18 shows a G-G diagram illustrating the driving characteristics of a professional driver on a racetrack in Japan. The regions outlined in blue show instances of high G in which the driver was steering while braking at the same time. The driving performance settings of the GR Yaris were optimized focusing on these regions.

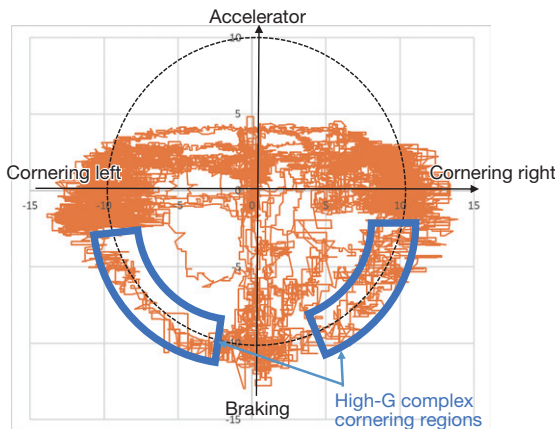


Fig. 18 G-G Diagram

c. Development structure that crosses functional boundaries

Although technical fields are becoming increasingly segmented as a way of increasing developmental efficiency, the GR Yaris used a development team structure that crossed these functional boundaries. This allowed, for example, the engineer in charge of the suspension to learn about the 4WD system and for the engineer in charge of the 4WD system to make proposals for engine controls on a routine basis. This approach was adopted from the standpoints of both effective development and the development of human resources (**Fig. 19**).

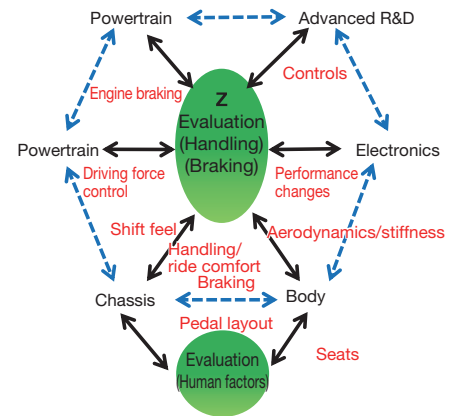


Fig. 19 The GR Yaris Development Team

4.8 Cooling performance

Since the GR Yaris combines a compact body with a powerful engine, cooling performance is extremely important. In particular, the cooling performance has the greatest impact on sporty driving. As shown by the openings at the front of the car (**Fig 20**), each component was designed to perform multiple roles while considering the overall airflow around the vehicle.

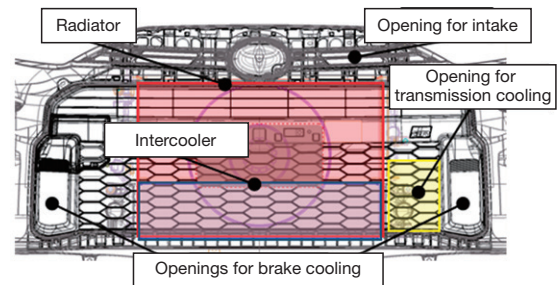


Fig. 20 Appearance of Front Openings

In addition, to ease the rise in intercooler temperature during driving and realize the full performance of the engine, an intercooler spray (**Fig. 21**) is adopted in some specifications of the GR Yaris.

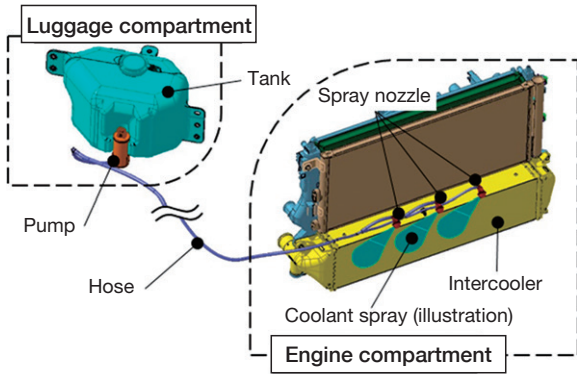


Fig. 21 Outline of Intercooler Spray

adhesive to be applied to areas that are difficult to reach with conventional techniques, thereby resulting in a more rigid body (Fig. 23).

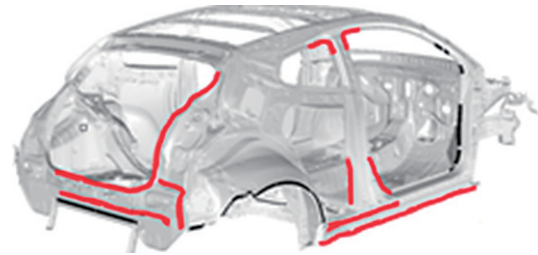


Fig. 23 Structural Adhesive Application Ranges

4.9 Sound

As a sports car, the most important element of the sound of the GR Yaris is to audibly transmit vehicle information. As a result, the sound must have an informational function that prompts the driver about shift timings and other driving operations (“Info” in Fig. 22), and must also be consistent with the driving performance of the vehicle (“Match” in Fig. 22). The development aimed to satisfy these requirements (Fig. 22). Active noise control (ANC) was adopted in some vehicle grades to help achieve the optimum sound for various driving scenarios and to help optimize the basic sound characteristics.

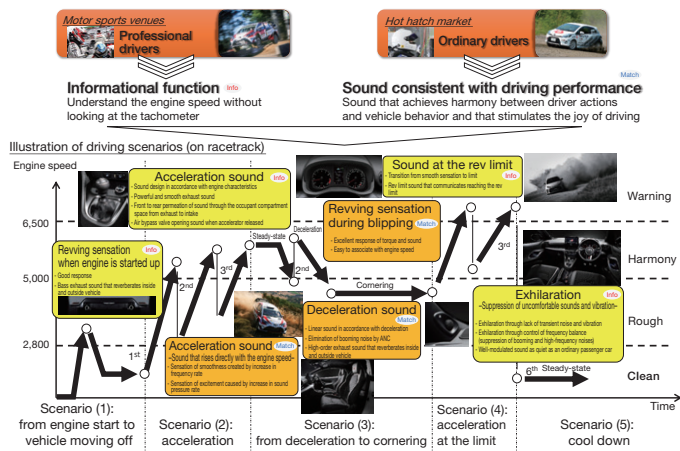


Fig. 22 Sound Concept of the GR Yaris

4.10 The GR Factory

A new dedicated sports cars production line called the GR Factory has been established inside the Motomachi Plant in Toyota city. The GR Yaris is the first model to be produced on this line. The line adopts a cellular layout for the body production and assembly processes and can be adjusted to produce different models and different volumes (Fig. 6).

The GR Factory is also designed to enhance driving performance. For example, virtually all the structural adhesive is applied manually by skilled craftspeople, which allows the

In addition, the development identified the components that make the most significant contribution to dynamic performance. These components are all measured before assembly so that the items with the least variation are used on the line (Fig. 24).

This approach is exactly the same as that adopted by a racing team when building a racing car. As a result, every GR Yaris is built with extremely low variation, enabling vehicles of the highest quality to be delivered to customers.

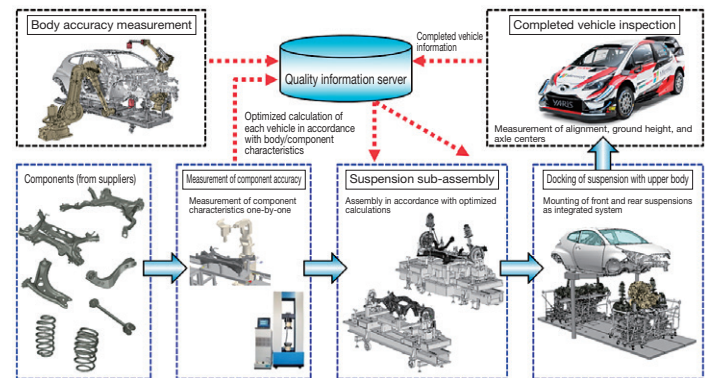


Fig. 24 Highly Accurate Suspension Assembly System

5. Conclusion

After the GR Yaris was unveiled at the Tokyo Auto Salon in January 2020, it has attracted widespread attention and, to the delight of the development team, an increasing number of orders from potential customers. In addition to the feelings of gratitude for the invaluable cooperation of everyone at Toyota’s partner companies, this is a sobering reminder for the development team of the high expectations that customers are placing in this car.

Although the development and manufacturing teams worked on the GR Yaris without compromise, the finishing touches to a car are carried out by the customer. It would be extremely gratifying to see the GR Yaris being customized according to the tastes of customers in their own fields. To facilitate this process, various groups of parts are being prepared (Fig. 25).

Special Feature

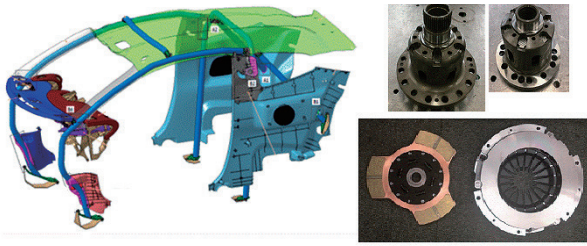


Fig. 25 Racing Parts for the GR Yaris

Finally, the application of the concept of building ever-better cars to the GR Yaris remains an ongoing process. Various fields are still gaining valuable experience and Morizo is still taking the wheel himself.

The first round of the Super Taikyu endurance race series was held at Fuji Speedway on the day of the launch of the GR Yaris. The GR Yaris entered by the Rookie Racing team took victory in its debut race (**Fig. 26**).

In addition to showcasing the potential of the GR Yaris, this result was a massive present from Morizo to everyone involved in the development and manufacturing of the car.



Fig. 26 Round One of the Super Taikyu Race Series

The development team intends to take the results of this experience and the opinions of customers on board and continue providing appealing products that meet the highest expectations.

Authors



N. SAITO



T. DOI

Designed for Driving Performance –Styling that Emphasizes the Performance of the GR Yaris–

Yoshiharu Nakajima*¹
Tatsuhide Hoshi*²
Kosuke Taniguchi*³
Kiyotaka Yoshida*⁴
Satoshi Nishikatsu*⁴

Abstract

As car sharing and other forms of shared mobility become more popular, Toyota has recognized a growing demand for vehicles with a personalized appeal and is developing mass-production models with distinctive characteristics that make an emotional connection with customers. The GR Yaris was designed to participate in the World Rally Championship (WRC), a series of races over a wide range of road surfaces contested primarily by cars based on mass-production models. The development of the GR Yaris was inspired by Toyota’s philosophy of building ever-better cars.

Keywords: *Born from the World Rally Championship*

1. Introduction

The concept of being born from the World Rally Championship (WRC) refers to the idea of developing a mass-market vehicle from a racing car. This is the polar opposite to the conventional idea of building a racing car from an existing mass-market vehicle as a way of developing a next-generation rally car. Toyota regards this concept as its inspiration to make the company a permanent fixture in the world of rallying. From an early phase of development, various material requirements, such as the adoption of an aluminum hood, trunk lid, and door panels, as well as a carbon fiber reinforced plastic (CFRP) roof panel were incorporated with an aerodynamically enhanced silhouette and wide body designed to maximize the potential of its four-wheel drive (4WD) system. The vehicle also features a dedicated Gazoo Racing (GR) front face to enhance cooling performance, and was designed as a three-door hot hatch with the aim of strengthening its competitiveness to win races.

2. Exterior Styling

2.1 Aims of the exterior styling

Toyota worked extensively with Tommi Makinen Racing (TMR) from the packaging phase to integrate the racing-based know-how of both companies into the styling to maximize downforce and aerodynamic performance (**Fig. 1**).

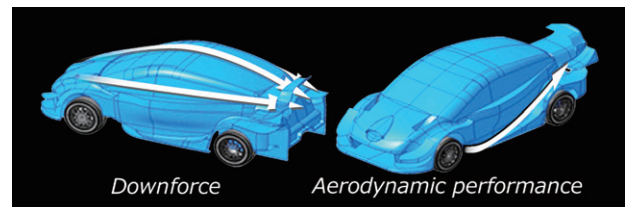


Fig. 1 Feedback of Know-How from Racing

2.1.1 Side silhouette

The roof of the GR Yaris was lowered from the base model to increase the volume of airflow reaching the rear spoiler. In addition, racing-car methodology was used to maximize downforce and enhance aerodynamic performance by guiding the airflow from the front wheelhouse along the body (**Fig. 2**).

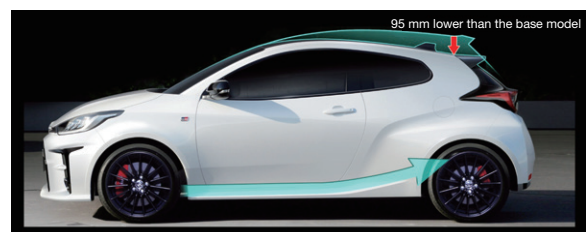


Fig. 2 Maximization of Downforce and Aerodynamic Performance

2.1.2 Front styling

The front face of the GR Yaris was styled in accordance with the Functional Matrix concept, which is the unified approach to front face styling in GR models. This styling emphasizes the functional aspects of driving performance while creating a uniform brand image. The lower spoiler section was designed to provide downforce and integrated seamlessly with the low corners, which are provided with vortex-generating canards at the top and bottom. The aim was to create a sporty impression that reinforces the low and wide stance of the vehicle. In

*¹ GR Design Group, GAZOO Racing Company

*² MS Design Div., Mid-size Vehicle Company

*³ Color Management Dept., Vehicle Development Center

*⁴ Toyota Motor East Japan, Inc.

addition, brake ducts were added to the large functional lower grille opening to create an impression closer to the typical characteristics of a GR model (Fig. 3).



Fig. 3 Functional Styling that Emphasizes the Brake Ducts

2.1.3 Rear styling

The cabin tapers toward the rear to enhance downforce and aerodynamic performance. In addition, the rear fender flares were emphasized to create an even lower and wider silhouette (Fig. 4).



Fig. 4 Rear Styling Emphasizing Low and Wide Stance

2.2 Wheel styling

2.2.1 Aims of wheel styling

World-leading ultra-lightweight and highly stiff wheels were designed based on the GR wheel scenario to emphasize both

beauty and form (beauty). The resulting wheel styling makes a significant contribution to the brand image. In particular, the forged wheels for the top model grades were styled to convey feelings of flexibility and stiffness using the stylishness of a Japanese sword as a motif. The development aimed to create wheels that grip the road smoothly and with agility, regardless of the state of the surface (Fig. 5).

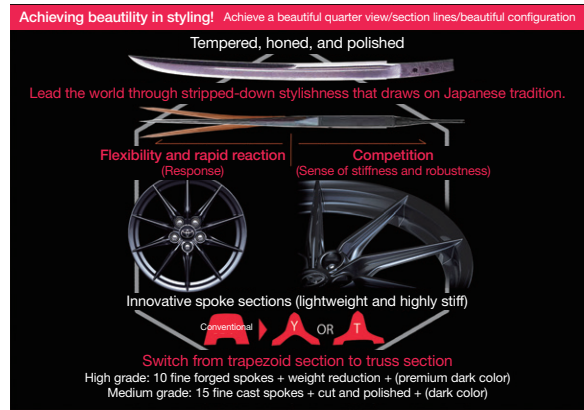


Fig. 5 The Achievement of Beauty

2.2.2 The GR wheel guidelines

The GR Yaris wheel lineup consists of two levels: the high and medium grade wheels that are designed to project an image of a true sports car, and the low grade wheels that project a simpler sporty image (Fig. 6).

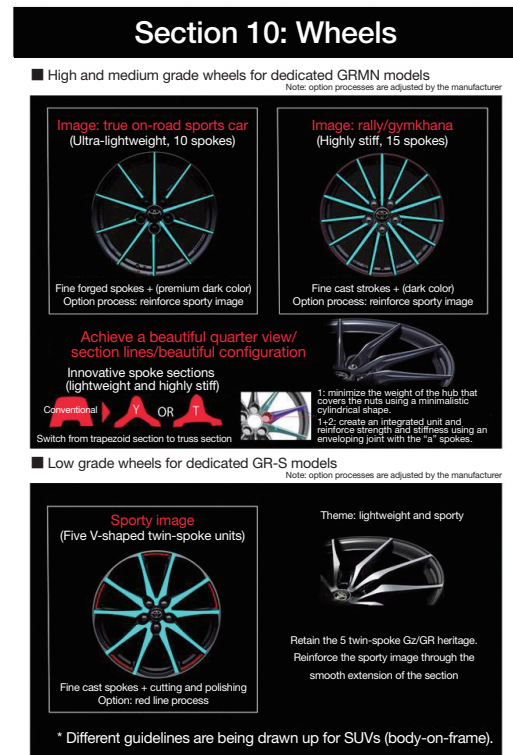


Fig. 6 GR Wheel Guidelines

2.2.3 Wheel lineup

The high grade models of the GR Yaris are equipped with forged 18-inch wheels manufactured by BBS. These wheels were designed with a focus on beauty to convey an image of a true grand tourer (GT) or on-road sports car. The styling prioritizes balance with ten equally spaced spokes.

These are ultra-lightweight wheels that were designed using the stylishness of a Japanese sword as a motif. The styling expresses an overwhelming sense of agility and a genuine presence, while providing a showcase for the genuine race-car brakes. The styling aims to stimulate a sense of closeness and ownership in the user.

The engravings normally located at the rear of the spokes are cast on the front rims to express a sportier image (Fig. 7).



Forged 18-inch aluminum wheels manufactured by BBS: highly polished dark metallic color with dedicated forged center ornament and black nuts

Fig. 7 Forged 18-Inch Wheels Manufactured by BBS (Medium Grade)

The customer can also select lightweight and highly stiff wheels to convey an image suitable for a rally or gymkhana series race car. These wheels emphasize a sense of stiffness with fifteen equally spaced spokes. The styling aimed to realize true sports car wheels that express the capability of the vehicle to respond with agility to rough road surfaces and quick steering operations.

The engravings are the same as the forged wheels (Fig. 8).



Cast 18-inch aluminum wheels manufactured by BBS: glossy black

Fig. 8 Cast 18-Inch Wheels Manufactured by ENKEI Corporation (Low Grade)

Another wheel option is the sporty five twin-spoke design. These wheels continue the heritage of Gz and GR-s models.

The engravings are the same as the forged wheels (Fig. 9).



Cast 17-inch aluminum wheels manufactured by ENKEI Corporation: cut and polished + glossy black

Fig. 9 Cast 17-Inch Cut and Polished Wheels Manufactured by ENKEI Corporation

3. Body Colors

3.1 Aims of body colors

Three body colors are available for the GR Yaris: white, red, and black. These colors are based on the GR color guidelines and are designed to evoke Toyota's racing activities and reinforce the brand image (Fig. 10).

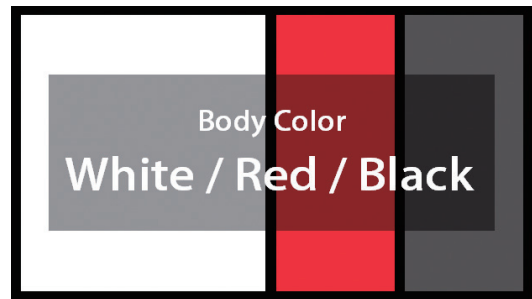


Fig. 10 GR Body Color Guidelines

3.2 Body color lineup

The three colors are available in four tones intended to create a direct connection with a racing image: Super White 2, Platinum White Pearl MC, Emotional Red 2, and Precious Black. This lineup was chosen carefully as the best way to promote the GR brand (Fig. 11).



Fig. 11 Body Color Lineup

Special Feature

4. Interior Styling

The instrument panel of the base model was redesigned centered on the driver seat, and dedicated parts were adopted for the meter cluster, steering wheel, the area around the shift lever, and the pedals. This is the same methodology as used by racing cars to enhance operability and visibility during sporty driving (**Fig. 12**).



Fig. 12 Enhancement of Operability and Visibility Centered on the Driver Seat

4.1 Seats

Both the front and rear seats of the GR Yaris are exclusive to the model. Sporty seats with excellent holding performance were adopted in the front. The sporty image of the seats was enhanced by incorporating a special mesh-textured covering material, synthetic leather, convex stitching, and ornamentation showing the GR logo (**Fig. 13**).



Fig. 13 Sporty Seats with Excellent Holding Performance

4.1.2 Meter cluster

Red needles and a red zone display were adopted to make the information in the meter cluster easier to read during sporty driving. All the information necessary for sporty driving (such as the 4WD mode, boost pressure, shift position, warnings, and so on) is indicated together in the center liquid crystal thin-film-transistor (TFT) multi-information display, creating a premium sporty experience for the driver (**Fig. 14**).



Fig. 14 Analog Meter Cluster and Liquid Crystal TFT Display

4.1.3 Steering wheel and area around shift lever

The dedicated steering wheel was designed with a ring sectional shape that emphasizes the quality of contact with the driver's palm and creates a closer grip feeling. The steering wheel features dedicated styling with the GR logo on the center spoke, which adds to the premium sporty experience.

The position of the shift knob was optimized and a shorter shift stroke was adopted to enhance the sporty driving feel (**Fig. 15**).



Fig. 15 Dedicated Steering Wheel and Optimization in Area around Shift Lever

4.1.4 4WD mode selection switch and aluminum pedals

The 4WD mode selection switch is located in front of the

shift lever to make it easier to operate while driving. In addition, aluminum pedals were adopted for the same reason during sporty driving (Fig. 16).



Fig. 16 4WD Mode Selection Switch and Sporty Aluminum Pedals

5. Interior Colors

5.1 Aims of interior colors

The customer can choose from two color options called Core Coordination and Emotional Coordination that were designed to emphasize the GR brand image (Fig. 17).

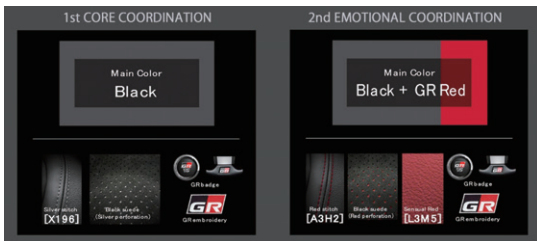


Fig. 17 GR Interior Color Guidelines

5.2 Interior colors

Regardless of the color coordination option, the area within the driver's eye line has a uniform black tone to help the driver maintain concentration. Color inserts are present only in the lower area and on the seat to reflect the spartan design perspective of the high-performance models from Gazoo Racing (Figs. 18 and 19).



Fig. 18 Core Coordination Interior Color Combination



Fig. 19 Emotional Coordination Interior Color Combination

5.3 Seat materials

Parts of the seats that contact the occupants are covered in a suede-like fabric with excellent grip. The holding performance of the seats is good enough under the most spirited driving conditions (Figs. 20 and 21).



Fig. 20 Seat Material (High Grade Seats)



Fig. 21 Interior Surface Treatment

Special Feature

Authors



Y. NAKAJIMA



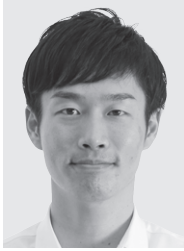
K. YOSHIDA



S. NISHIKATSU



T. HOSHI



K. TANIGUCHI

Development of a High-Performance Engine for the GR Yaris

–The New 1.6-Liter Turbocharged Engine–

Kenji Yamanari*¹
 Kazunori Yamaji*²
 Takeshi Hagiwara*³
 Atsunori Kumagai*⁴
 Hiroyasu Koyama*⁵

Abstract

A new inline 3-cylinder 1.6-liter turbocharged engine was developed for the GR Yaris. Incorporating extensive measures to reduce weight and size, increase power, and improve response, this newly developed engine realizes an exhilarating and smooth sensation of acceleration, while also delivering impressive environmental performance. The new engine was designed with the optimum structure to maximize power under normal rallying conditions. High-speed combustion was adopted to enhance knocking resistance, thereby helping to achieve the targeted power increase. In addition, rapid response and the desired acceleration feeling were achieved by increasing the efficiency of each turbocharger component and enhancing the engine control. This article describes the technologies of this newly developed 1.6-liter turbocharged engine.

Keywords: *high power, ultra-lightweight, rapid response*

1. Introduction

The GR Yaris was developed to be Toyota’s first independently-developed and produced true four-wheel drive (4WD) sports car for almost twenty years with the purpose of bringing the joy of driving to customers all around the world. Under the completely new concept of building a car bred from motor sports, the development aimed to achieve exhilarating dynamic performance. To realize this level of dynamic performance, it was not sufficient simply to deliver overwhelmingly superior performance to other cars in the subcompact B segment. Targets were also set for engine power and weight to ensure that the GR Yaris would be competitive with cars in the large compact C segment.

This article describes the G16E-GTS engine that was developed for the GR Yaris, and how it incorporates technologies from motor sports to help realize the highest levels of power and response, as well as to reduce size and weight.

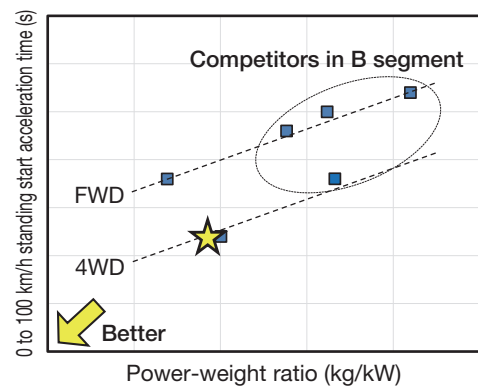


Fig. 1 Development Targets for the GR Yaris

2. Outline of Engine

Fig. 2 shows the external appearance of the G16E-GTS engine and Table 1 lists its specifications.

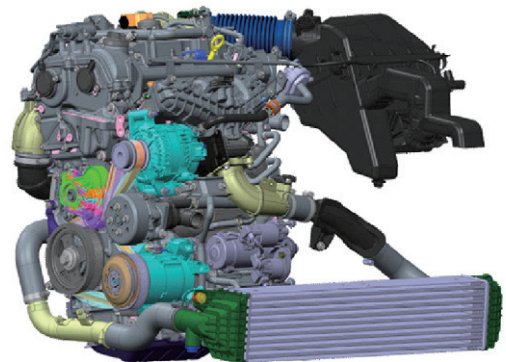


Fig. 2 External Appearance of G16E-GTS Engine

*¹ Powertrain Development Div. No. 1, Powertrain Company
 *² Electric Powertrain Performance Development Div., Powertrain Company
 *³ GR Powertrain Development Div., GAZOO Racing Company
 *⁴ Advanced Powertrain Engineering Div. No. 2, Powertrain Company
 *⁵ Powertrain Product Planning Div., Vehicle Development Center

Table 1 Main Specifications of G16E-GTS Engine

Number and alignment of cylinders	Inline 3-cylinder
Valve train	4-valve duel overhead cam (DOHC) with roller rocker
Displacement (cc)	1,618
Bore diameter x stroke (mm)	87.5 x 89.7
Compression ratio	10.5
Fuel	High-octane
Fuel injection system	D-4ST
Maximum power (kW/rpm)	200/6,500
Maximum torque (Nm/rpm)	370/3,000 to 4,600

To realize high power and rapid response, a 3-cylinder engine that generates no exhaust interference was selected. Then, through detailed analysis of the engine operating regions used by R5 category cars in the World Rally Championship (WRC), the main engine specifications were determined to achieve maximum power performance under normal rallying conditions.

With a set displacement, maximum power is achieved at a certain cylinder bore diameter (**Fig. 3**). **Fig. 4** shows two approaches for increasing power. First, as the bore diameter increases, a larger valve area can be secured and pumping loss reduced. At the same time, the set displacement realizes a short stroke, which reduces the piston speed and lowers friction loss. In contrast, **Fig. 5** indicates that strong turbulence is necessary to shorten the combustion duration, which suggests that the bore diameter should actually be reduced to increase power. As a result of this trade-off relationship, there is an optimum bore diameter to produce maximum power. In this development, a one-dimensional (1D) engine model incorporating a predictive combustion model was combined with an optimization tool (called an “optimizer”) as shown in **Fig. 6**. Then, the optimum design specifications were identified from more than 4,000 possibilities to produce the most effective specifications before the completion of the engine.

The same methodology was adopted for the diameter of the intake and exhaust valves to determine the optimum valve diameters for power. Simultaneously, state variables such as the in-cylinder pressure and exhaust temperature were predicted to help determine the performance requirements for the intake port design specifications. Then, the knock tolerance of the engine was enhanced and the exhaust temperature lowered by adopting the same high-speed combustion approach as the Toyota New Global Architecture (TNGA) design philosophy. This approach helped to realize high boost pressure and satisfy the targeted high power performance (**Fig. 7**).

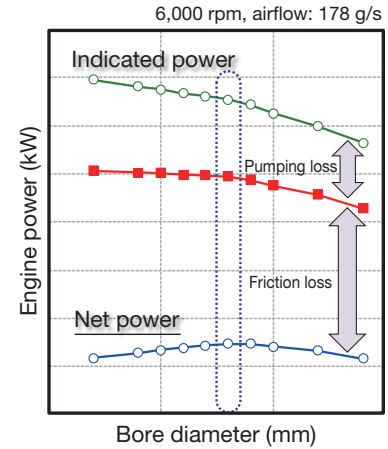


Fig. 3 Relationship between Bore Diameter and Engine Power

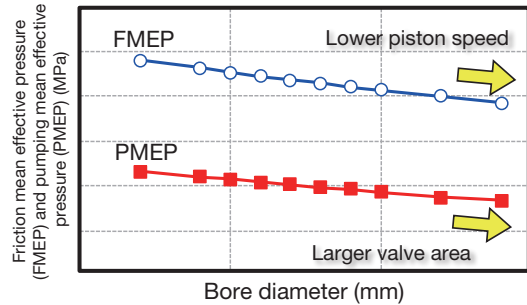


Fig. 4 Relationship between Bore Diameter and Pumping and Friction Losses

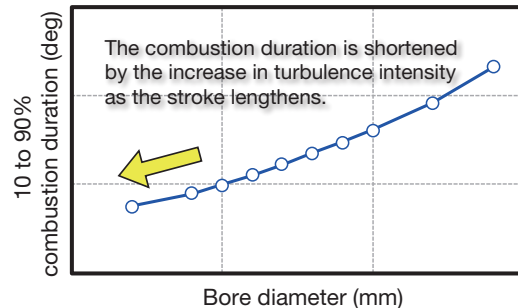


Fig. 5 Relationship between Bore Diameter and Main Combustion Period

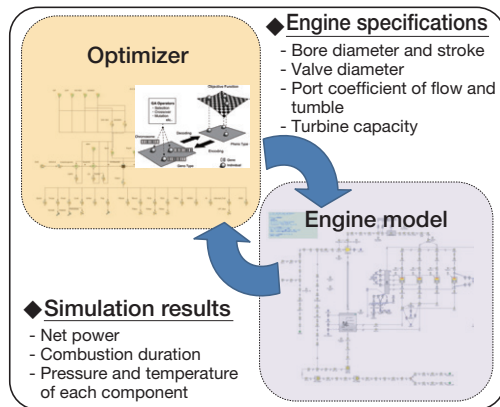


Fig. 6 Optimization of Design Specifications

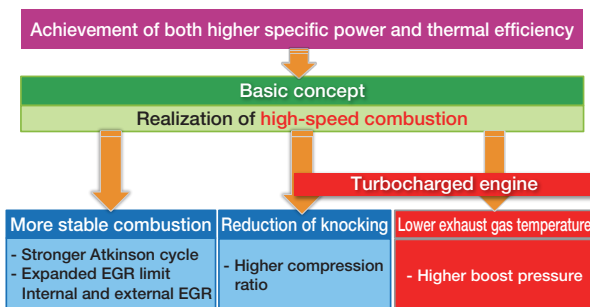


Fig. 7 Effects of High-Speed Combustion in Turbocharged Engine⁽¹⁾

3. Technologies Adopted in the Engine

3.1 Highly efficient intake ports with high tumble

To increase the knock tolerance and lower the exhaust temperature under normal rallying conditions, newly designed intake ports were adopted to realize both the intense tumble flow and intake airflow rate required to achieve the targeted combustion speed.

The included angle between the intake and exhaust valve was expanded and a hydraulic lash adjuster (HLA) was positioned inward of the valves to achieve a linear port shape. This design helps to suppress airflow separation and maintain the flow rate. The valve diameters described above were optimized and an eccentric press-fit intake valve seat was adopted. In addition, the geometry of the combustion chambers and the multi-hole injector nozzles in the direct injection system was also optimized, resulting in highly efficient intake ports that achieve high tumble flows without airflow control valves or any other control devices (Fig. 8).

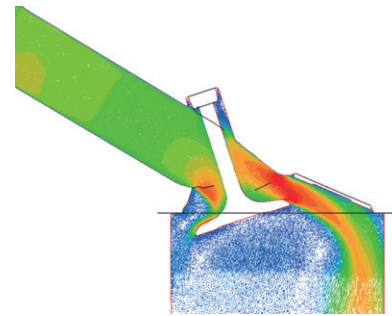


Fig. 8 Intake Port and In-Cylinder Flow

3.2 Turbocharger system

To achieve both high power and rapid response, turbocharger blades compatible with high levels of boost were adopted and the efficiency of each component of the turbocharger was enhanced. As shown in Fig. 9, overall turbocharger efficiency ahead of the leading trend was achieved by adopting ball bearings on the turbocharger shafts, reducing friction, providing abradable seals on the surface of the compressor housing, shortening the tip clearance, and enhancing the flow at the ends of the blades.

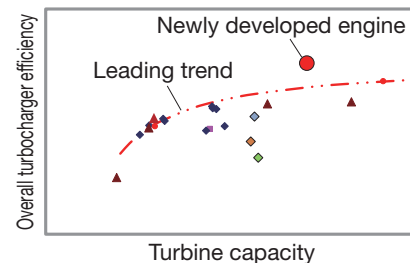


Fig. 9 Relationship between Turbine Capacity and Overall Turbocharger Efficiency

Furthermore, rapid response was realized by refining the drive control of the wastegate valve (WGV). In general terms, a large turbine capacity is required to achieve high power. However, in this case, it takes time for the impeller to reach the necessary rotational speed to provide boost. As shown in Fig. 10, the boost pressure response was improved by approximately 15% by closing the WGV before acceleration commences and starting the turbine rotation in advance. This enhances acceleration response by increasing the charging efficiency more quickly during acceleration.

Special Feature

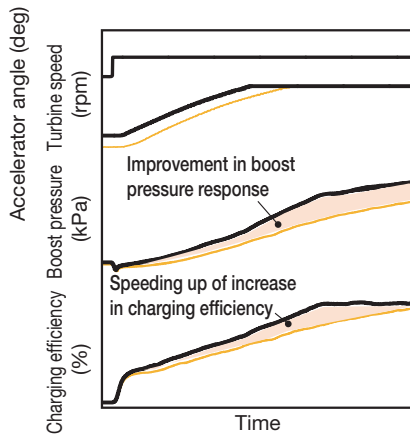


Fig. 10 Improvement in Boost Pressure Response by Refining WGV Control (Thick Lines: After Control Refinement, Thin Lines: Before Control Refinement)

In the WGV control described above, the pressure applied to the valve must be accurately controlled in accordance with the exhaust energy. However, since the exhaust energy changes in accordance with the driving conditions, this control requires the definition of a massive operation map. This development determined the pressure to be applied to the WGV for realizing the appropriate boost pressure using the exhaust energy calculated in the engine model.

3.3 Weight reduction

As shown in **Fig. 11**, the thickness of the exterior walls of the aluminum die cast cylinder block was reduced by adopting a shallow water jacket and lower diameter head bolts to optimize stiffness. Weight was also reduced by adopting a high-strength aluminum cylinder head and a hollow assembled camshaft. Thorough weight reduction was achieved by using computer aided engineering (CAE) to design moving parts such as the pistons and crankshaft. This approach helped to achieve the world's lightest engine within the group of engines with equivalent power, and also made a major contribution to both the wide-open throttle (WOT) acceleration performance and rapid response of the vehicle.

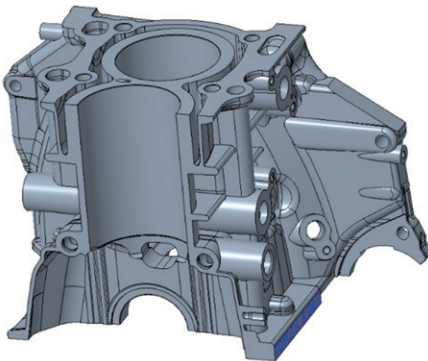


Fig. 11 Shallow Water Jacket Structure of Engine Block

3.4 Cooling performance

The water jacket inside the cylinder head has a dual-level structure. The flow of coolant is concentrated in the lower water jacket to achieve low pressure loss and intensify the cooling of the combustion chambers. A columnar structure that connects the top of the combustion chambers to the walls of the upper water jacket was adopted to reinforce the combustion chambers in response to the higher in-cylinder pressures and heat loads. Furthermore, the cooling performance of the combustion chambers was ensured by increasing the flow rates of the drilled passages between the cast iron liner bores by approximately 30% compared to a conventional engine and by the adoption of the shallow water jacket. Reducing the pressure loss and capacity of the cooling system in this way helped to improve the heater performance and increase fuel efficiency during the engine warming up process.

3.5 Lubrication performance

The specifications of the lubrication system were determined to tolerate high G values, based on the targets set for the longitudinal and lateral G applied to the vehicle during driving on a racetrack by professional drivers. The oil pump was provided with a compact cycloid rotor driven coaxially by the crankshaft. Reliability was then enhanced by optimizing the structure. Additionally, an oil pan with an integrated baffle plate was adopted to ensure the lubrication performance of the oil surface even under high G values.

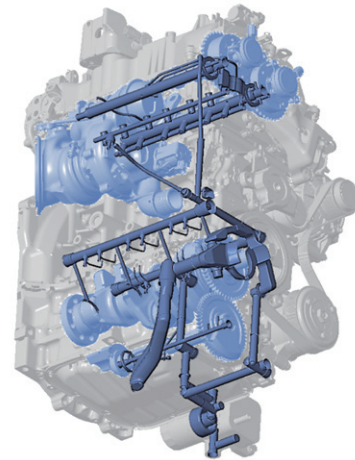


Fig. 12 Layout of Engine Lubricant Passages

3.6 Technologies for exhaust system

This engine was developed to achieve both high power and excellent environmental performance. An integrated exhaust manifold and turbocharger was adopted to reduce weight and enhance mountability. This also helped to lower the surface area of the exhaust system components and reduce the waste heat from the exhaust gas. In addition, the geometry of the

manifold branches and exhaust flow path of the WGV were optimized to achieve uniform exhaust gas flows to the catalyst. These measures reduced the waste heat and ensured cold start catalytic performance. Optimizing the geometry of the flow paths also helped to lower exhaust interference and ensure turbocharger efficiency.

High-flow injectors are generally required to achieve high engine power. However, the resulting increase in penetration tends to increase the amount of fuel wetting on the walls of the combustion chambers. Therefore, as shown in **Figs. 13** and **14**, the geometry of the multi-hole injector nozzles in the direct injection system was optimized to suppress fuel wetting on the bore and lower the particle number (PN) in the emissions. In addition, a gasoline particulate filter (GPF) with a newly developed substrate was adopted. This filter combines low pressure loss with high particle trapping efficiency, and enables the vehicle to achieve the target set for power while complying with the Euro 6d emissions standards.

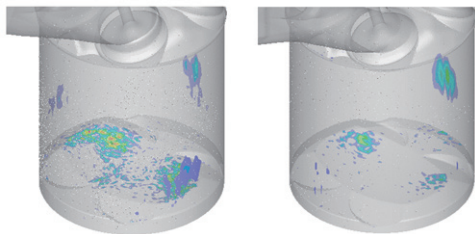
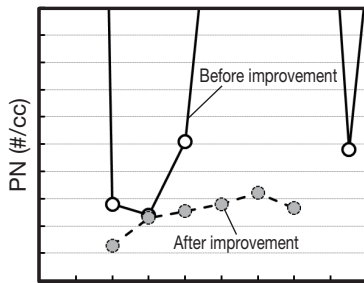


Fig. 13 Reduction in Fuel Wetting by Optimization of Nozzle Hole Geometry (Left: Before Improvement, Right: After Improvement)



Injection timing (degrees before top dead center (BTDC))

Fig. 14 Relationship between Fuel Injection Timing and PN in Emissions

4. Engine and Vehicle Performance

4.1 Engine performance

Incorporating the technologies described above resulted in engine characteristics with exhilarating torque across a wide range of engine speed regions (**Fig. 15**).

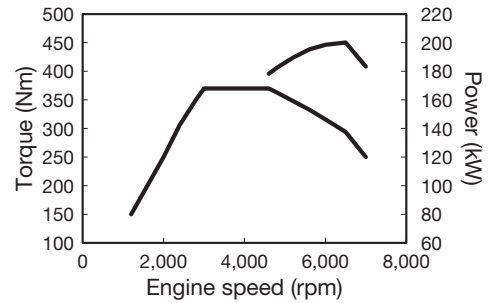


Fig. 15 Engine Power Performance

4.2 Vehicle performance

Fig. 16 shows the acceleration performance of the vehicle. The measures to ensure exhilarating engine torque and thorough approach to weight reduction across the whole vehicle helped to realize an acceleration feeling far beyond that of other competing B segment vehicles with the same response. The 0 to 100 km/h WOT acceleration performance of the GR Yaris is 5.2 seconds.

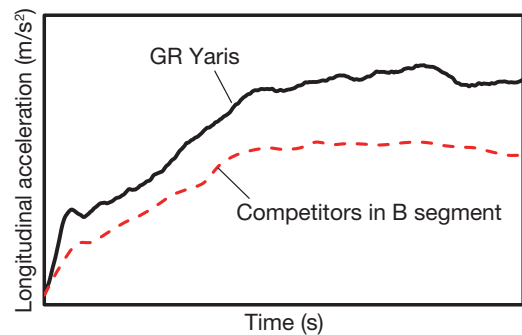


Fig. 16 Vehicle Acceleration Performance

5. Conclusions

To realize the exhilarating dynamic performance required of the GR Yaris, a new inline 3-cylinder 1.6-liter turbocharged engine was developed with a total focus on achieving high power, rapid response, and weight reduction.

(1) High power and rapid response

The new engine was designed with the optimum structure to maximize power under normal rallying conditions. High-speed combustion was adopted to enhance knocking resistance, thereby helping to achieve the targeted power increase. In addition, overall turbocharger efficiency ahead of the leading trend was achieved by adopting ball bearings and abradable seals. Combined with refinements to the WGV control, these measures helped to realize both rapid response and an exhilarating acceleration feeling.

Special Feature

(2) Weight reduction

The world's lightest engine within the group of engines with equivalent power was achieved by adopting an aluminum die cast cylinder block, high-strength aluminum cylinder head, and a hollow assembled camshaft, as well as by applying thorough weight reduction measures to moving parts.

(3) Environmental performance

Compliance with the Euro 6d emissions standards was achieved by optimizing the design of exhaust gas flows and the geometry of the multi-hole injector nozzles in the direct injection system.

Finally, the authors would like to express their sincere gratitude for the invaluable assistance and cooperation of everyone involved in the development of this engine.

Reference

- (1) T. Yuasa, Yamazaki, Nogawa, Mori. "The New V6 3.5L Turbocharged Gasoline Engine." *Proceedings of the JSAE Annual Congress*.

Authors



K. YAMANARI



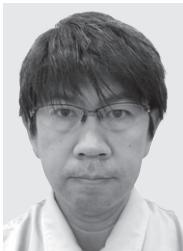
K. YAMAJI



T. HAGIWARA



A. KUMAGAI



H. KOYAMA

GR-Four –The 4WD System of the GR Yaris–

Masayuki Arai*¹
Naoaki Maeda*²
Shinichiro Ishikawa*²

Abstract

A new high-capacity, responsive, and highly accurate four-wheel drive (4WD) system was developed for the lightweight high-power engine of the GR Yaris with the aim of delivering exhilarating acceleration performance and handling on any road surface. This system features a new electronically controlled multi-plate clutch that enables a wide range of front/rear torque distribution ratios and high-response driving force transmission by adopting different gear ratios for the transfer case and rear differential. In addition, front and rear Torsen® limited-slip differentials (LSDs) were adopted to maximize the driving force at the four wheels.⁽¹⁾ Furthermore, a mode control switch was adopted that allows the driver to select the optimum driving force distribution in accordance with preference and the driving scenario. This flexibility contributes greatly to the creation of exciting driving performance suitable for a sporty 4WD system. This article describes the development of this new 4WD system, including the development aims, the details of component development, and the 4WD control technology.

Keywords: four-wheel drive (4WD), electronically controlled multi-plate clutch, differential, front/rear driving force distribution, 4WD control mode

Special Feature

1. Introduction

As the GR Yaris is Toyota’s first 4WD sports car in almost twenty years since the Celica GT-Four, it was decided to design and develop a 4WD system with a completely new configuration and control, which would be suitable for a model directly descended from the Yaris competing in the World Rally Championship (WRC). In addition, the development also aimed to perfect the 4WD system through extensive testing by professional drivers from outside Toyota with experience of racing in various series including the WRC, and then feeding back the analysis results from this driving data into the development.

This article describes the configuration of this 4WD system, the development of its components, and control.

2. Development Aims

The GR Yaris was developed under the concept of building a car from motor sports. In accordance with this concept, the 4WD system was developed with the dual aims of achieving competitiveness (i.e., the capability to win races) and a fun-to-drive experience regardless of the level of the driver.

To achieve these performance objectives, the 4WD system was constructed with a particular focus on achieving high capacity, response, and accuracy.

3. Structure

3.1 System configuration

Fig. 1 shows an outline of the developed 4WD system.

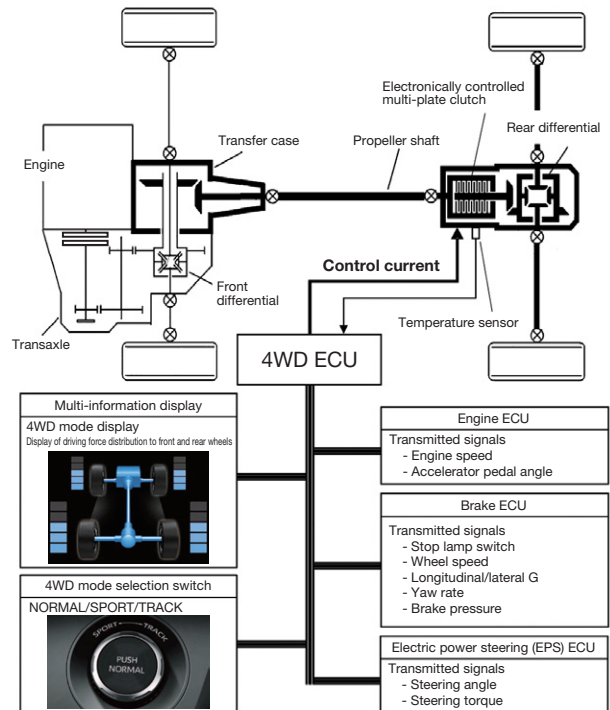


Fig. 1 Outline of 4WD System for the GR Yaris

*¹ Electric Powertrain Control Function Development Div., Powertrain Company

*² Powertrain Function Development Div., Powertrain Company

A lightweight electronically controlled multi-plate clutch was adopted to transmit power between the front and rear. This clutch was mounted immediately in front of the rear differential to optimize the front/rear weight distribution. Different gear ratios were adopted for the transfer case that divert the driving force to the rear wheels and the rear differential. This structure allows the rotational speed of the propeller shaft to be increased to maintain a constant difference in rotational speed between the front and rear of the electronically controlled multi-plate clutch. As a result, driving force can be distributed rapidly to the rear wheels even when the front wheels are not slipping, and allows the front/rear driving force distribution range to be expanded to between 0:100 and 100:0 (**Fig. 2**). In addition, front and rear Torsen® limited slip differentials (LSDs) were adopted to maximize the tire performance of the outer wheels during cornering.

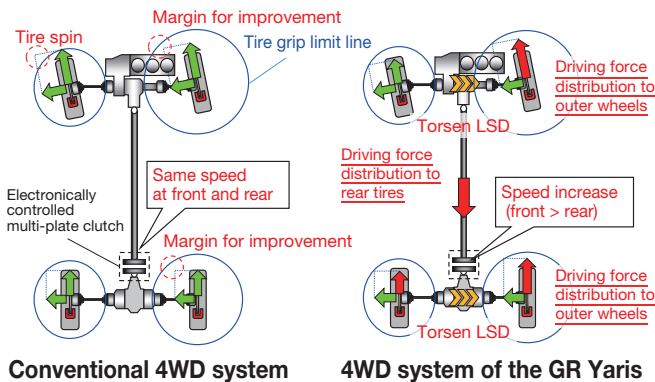


Fig. 2 Comparison of 4WD Systems

3.2 Electronically controlled multi-plate clutch

A new lightweight, high-capacity, and rapid-response electronically controlled multi-plate clutch was developed for use with the powerful engine installed in the GR Yaris (**Fig. 3**).

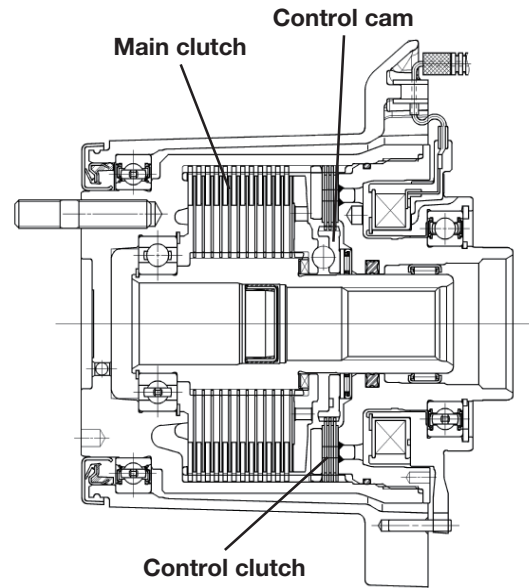


Fig. 3 Electronically Controlled Multi-Plate Clutch

This new clutch was developed to increase capacity and speed up response. Carbon friction materials were adopted for the main clutch to ensure stiffness, and the control cam angle and number of control clutch plates were optimized. As a result, response was improved by approximately 50% compared to a conventional electronically controlled multi-plate clutch (**Fig. 4**).

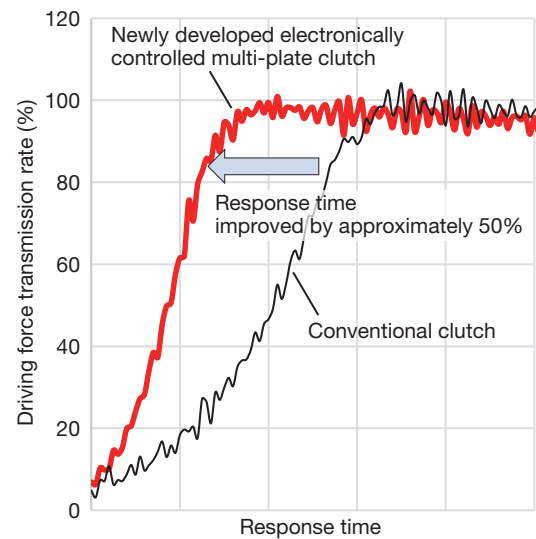


Fig. 4 Comparison of Electronically Controlled Multi-Plate Clutch Response Time

To achieve highly accurate driving force distribution, the power transmission characteristics of every electronically controlled multi-plate clutch was measured and stored in the electronic control unit of the 4WD system (4WD ECU). This allows the 4WD control to factor in the transmission characteristics of individual electronically controlled multi-

plate clutches and realize precise driving force distribution across the whole production run of the GR Yaris.

Since the clutch will be used under high load environments such as motor sports, a hollow shaft was adopted to ensure sufficient oil capacity and optimize airflows around the clutch. In addition, highly accurate driving force control in any environment, from extremely low temperatures to the high temperatures that occur when driving around a racetrack, was achieved by incorporating a temperature sensor into the system.

3.3 Transfer case and rear differential

3.3.1 Setting of gear ratios

The electronically controlled multi-plate clutch adopted in the 4WD system of the GR Yaris uses the rotation differential between the front and rear of the clutch (rotational speed in front of clutch > rotational speed at rear of clutch) to transmit driving force to the rear wheels. The GR Yaris adopts different gear ratios for the transfer case and rear differential. This realizes rapid driving force distribution response and a wide driving force distribution range.

These gear ratios are also affected by the vehicle state. For example, as shown in **Fig. 5**, if a larger gear ratio difference is set, the difference between the turning paths of the front and rear wheels can also be increased, allowing the driver to drift the rear wheels when cornering, in the same way as in a rear-wheel drive (RWD) vehicle. However, the vehicle behavior becomes unstable the moment that the rear begins to slide out more quickly and the amount of slide exceeds the turning path due to the gear ratio difference. Therefore, various gear ratios were repeatedly manufactured, evaluated, and verified to determine the optimum ratios to realize natural vehicle behavior (**Table 1**).

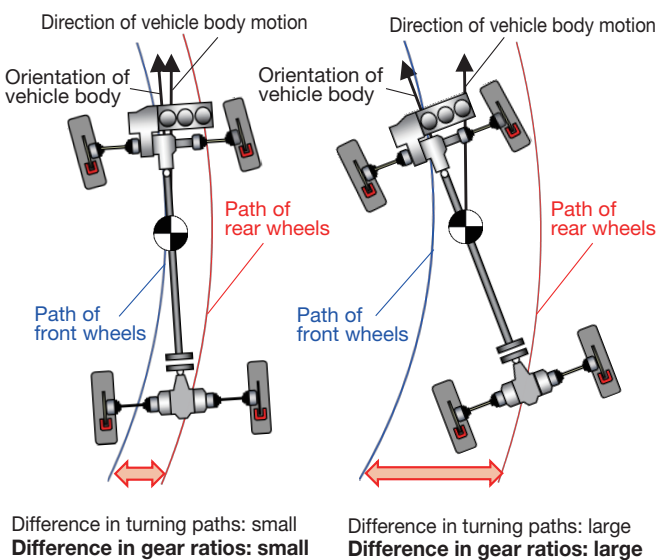


Fig. 5 Illustration of Difference in Turning Paths due to Different Gear Ratios

Table 1 Front/Rear Gear Ratios of GR Yaris

		Transfer case	Rear differential
Model		GF1A	FD15FE
Speed reduction device	Type	Hypoid gear	Hypoid gear
	Gear ratio	0.436 (17/39)	2.277 (41/18)

3.3.2 Hypoid gears

The specifications of the hypoid gears adopted in the transfer case and rear differential were revised to reduce the heat generated during driving force transmission, and to ensure sufficient strength and durability for use with the powerful GR Yaris engine.

3.4 Driveshafts

Similarly, the powerful engine also prompted the adoption of stiffer driveshafts. This involved reducing the amount of wheel spin by optimizing the stiffness ratio of the front and rear driveshafts while minimizing increases in weight, and ensuring high standing start acceleration performance up to the maximum four-wheel driving force (**Fig. 6**).

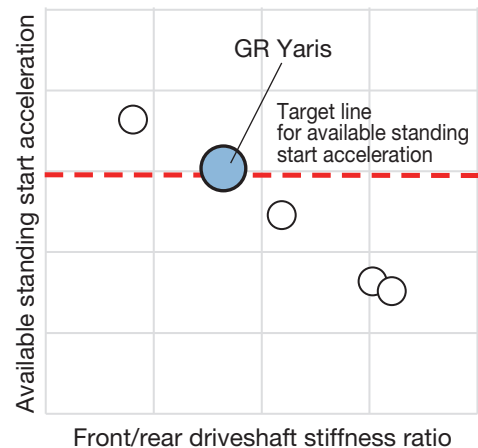


Fig. 6 Correlation between Front/Rear Stiffness Ratio and Available Standing Start Acceleration

3.5 Torsen® LSDs

The Circuit Pack grade of the GR Yaris is provided with front and rear Torsen® LSDs to ensure that grip is transmitted firmly from the four wheels to the road surface. The left/right torque bias ratio was optimized to ensure an excellent balance between grip and cornering performance on all road surfaces.

Special Feature

3.6 Effects of weight reduction

In addition to the various technologies that were adopted in the GR Yaris, the dynamic performance described above is a result of a thorough approach to weight reduction, which is one of the most important elements in motor sports. The 4WD system of the GR Yaris was developed to ensure a wide front/rear driving force distribution ratio within a simple structure. As a result, the developed 4WD system is approximately 20% lighter than a 4WD system with a center differential (**Fig. 7**).

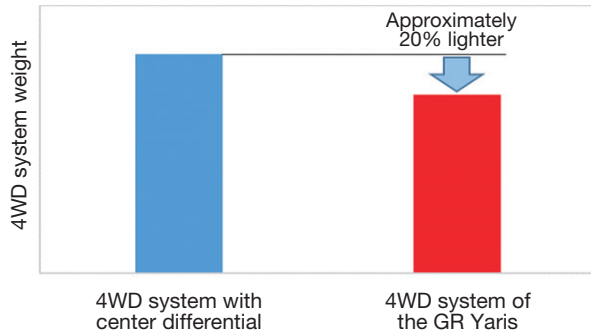


Fig. 7 Comparison of 4WD System Weights

4. 4WD Control Technology

This section describes the control technology that was adopted to achieve the development concept of the 4WD system of the GR Yaris, i.e., competitiveness and a fun-to-drive experience.

4.1 Rapid response and highly accurate control technologies

To realize equivalent performance using an electronically controlled multi-plate clutch instead of a center differential, the electronically controlled multi-plate clutch that transmits the driving force to the rear wheels requires faster and more accurate control than a conventional 4WD system. As described above, more accurate control was achieved by storing the output characteristic information of each electronically controlled multi-plate clutch in the 4WD ECU.

The power response of the G16E-GTS engine installed in the GR Yaris is extremely rapid. Therefore, if conventional 4WD control that uses engine power values based on the intake air volume and ignition timing is used, the transmission of driving force to the rear wheels might be delayed. For this reason, in addition to this engine power information, the developed 4WD control also uses the engine power demand calculated from the accelerator pedal angle. The driving force command transmitted to the rear wheels is generated from both these items of information to bring the response forward. **Fig. 8** shows an outline of the control. The delay in transmitting driving force to the rear wheels was reduced by combining the electronically controlled multi-plate clutch, which incorporates mechanical response-improvement measures such as the optimized control

cam angle, and the stiffer driveshafts. As a result, rapid control response capable of accelerating all four wheels at the same time in accordance with accelerator operation was realized.

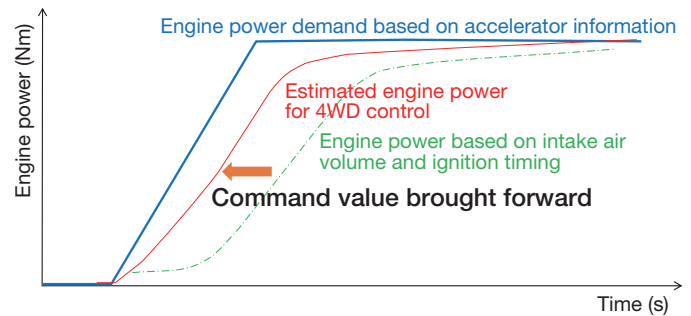


Fig. 8 Outline of Engine Power Information Estimation for 4WD Control

4.2 4WD control modes

As part of the efforts to optimize 4WD performance, one of the aims of the new 4WD control was to make it easier for the driver to predict vehicle behavior. To accomplish this, brake pressure was added to the driver operation information used by conventional controls (accelerator pedal angle, steering angle, stop lamp signals, and the like) to enhance the accuracy of driver intention estimation. This operation intention information is then combined with vehicle state information (wheel speed, acceleration, yaw rate, and the like) to realize optimum 4WD control based more closely on driver intention.

The GR Yaris is provided with a mode selection switch that allows the driver to select from three different front/rear driving force distribution ratios depending on preference or the road surface (**Fig. 9**). In Normal mode, which is the default mode when the engine is started, the basic front/rear distribution ratio is 60:40. This mode provides balanced dynamic performance from urban to snowy roads.

The basic front/rear distribution ratio in Sport mode is 30:70. By biasing the driving force distribution toward the rear wheels, this mode aims to achieve a fun-to-drive experience with brisk vehicle behavior as the driver steers through a winding road.

Finally, the basic front/rear distribution ratio in Track mode is 50:50. This mode aims to transmit the entire driving force of the four wheels to the road surface. This mode was designed to realize the “competitive” aspect of the development concept by converting the results of evaluations by professional drivers on racetracks into precise control.

In addition to the basic front/rear distribution, each mode also incorporates control variables for when the driver releases the accelerator and feedback controls for when wheel slip occurs. These variables are based on the driver operation and vehicle behavior information described above. This approach enabled the realization of optimally designed modes that communicate different vehicle behavior to the driver the moment that the mode is selected.


Mode selection switch	Mode	Basic front/rear distribution ratio
	Normal	Basic front/rear distribution ratio: 60:40 F ██████████ ██████████ R
	Sport	Basic front/rear distribution ratio: 30:70 F ██████████ ██████████ R
	Track	Basic front/rear distribution ratio: 50:50 F ██████████ ██████████ R

Fig. 9 4WD Mode Selection Switch

Fig. 10 shows the differences in vehicle behavior in each mode when the driver accelerates from a steady-state turn on a snowy road.

By expanding the controllable front/rear distribution range, a different turning path and vehicle posture can be achieved for each mode. In Sport mode, directing most of the driving force to the rear wheels realizes a vehicle posture that facilitates drifting.

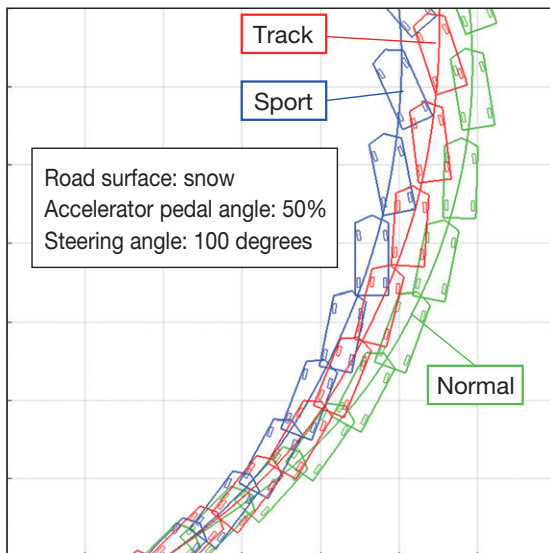


Fig. 10 Differences in Vehicle Turning Paths in 4WD Modes

4.3 Focus on driving performance

The GR Yaris was developed under the concept of building a car bred from motor sports. In accordance with this concept, the development of the 4WD system needed to identify and incorporate how this system is used in motor sports as well as what drivers want from such as system.

When the control was constructed, the development team concentrated on how to make vehicle behavior more predictable at the performance limits (i.e., in the non-linear ranges of performance). Easily predictable vehicle behavior allows the driver to interact with the vehicle at all times, resulting in greater controllability and helping to reduce lap times.

With the GR Yaris, the basic driving force distribution control was regarded as the central element in achieving more

predictable vehicle behavior at the performance limits. With the aim of realizing ideal vehicle behavior, the development team also considered adopting constantly variable specifications that would allow the distribution ratio to change in accordance with the driving situation, such as whether the vehicle was being driven on a straight or through a corner. Although this would not be an issue in ordinary driving scenarios, vehicle behavior at the performance limits of the tires, such as on a racetrack, is difficult for the driver to read.

To address this issue, the control was completely reconceived as a feedback control with the driver as the central controlling element to support the driver's actions and ensure grip.

As an example, the following section describes how the control operates in accordance with actual driving actions in Track mode (Fig. 11).

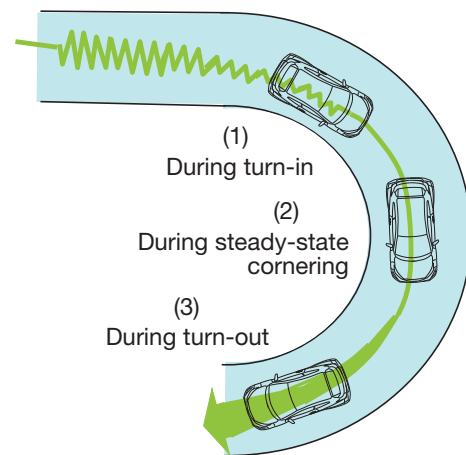


Fig. 11 Different Scenarios during Cornering

(1) During turn-in

When the driver enters the corner while braking, the driver turns the front wheels inward. As a result, the vertical load on the rear wheels lightens and actions are required to stabilize vehicle behavior. In this case, although increasing the driving force to the rear wheels will intensify the sensation of contact with the road and ensure stable vehicle behavior, increasing the driving force too much will make it more difficult to complete the turn.

Therefore, to help identify the optimum value, rather than test the vehicle on ordinary roads, a series of thorough evaluations were carried out on various racetracks, including the Nürburgring Nordschleife in Germany.

The results of these evaluations were then used to realize an excellent balance between cornering performance and stability. In this case, the development defined the settings of Track mode to be different from other modes in terms of the amount of driving force transmitted to the rear wheels under braking and vehicle behavior in response to driver actions. In addition, the Circuit Pack grade also provides even greater vehicle stability through the additional effects of the Torsen® LSDs.

(2) During steady-state cornering

When the driver lifts off and depresses the accelerator again, the sudden application of driving force might cause the vehicle behavior to become unstable. As a result, full acceleration might not be available in the lead up to the turn-out phase. Therefore, so that the vehicle can respond to the fast accelerator reactions of a professional driver, this mode distributes an optimum level of driving force to the rear wheels when the driver lifts off the accelerator, which helps to ensure driving force from the deceleration to the acceleration phases.

(3) During turn-out

The basic front/rear driving force distribution during acceleration is set to 50:50. This control aims to maximize the grip of the four wheels and make the vehicle behavior easier to predict in response to driver actions.

In addition, to minimize time loss and help ensure acceleration performance, control to suppress wheel slip is applied as soon as slight levels of slip occur. The Circuit Pack grade uses the Torsen[®] LSDs to generate turning yaw moment when acceleration occurs, which helps to realize even greater cornering and acceleration performance.

Fig. 12 shows the results of the further performance enhancements achieved in cooperation with professional drivers after the unveiling of the GR Yaris at the Tokyo Auto Salon.

After the driving force distribution was refined in the period from the driver lifting off to depressing the accelerator again (phases (2) to (3) above), the difference in rotational speed between the front and rear wheels was greatly reduced and drivers commented that it was possible to apply full acceleration.

The data also shows an improvement in the speed of accelerator pedal depression, resulting in even greater acceleration after exiting the corner.

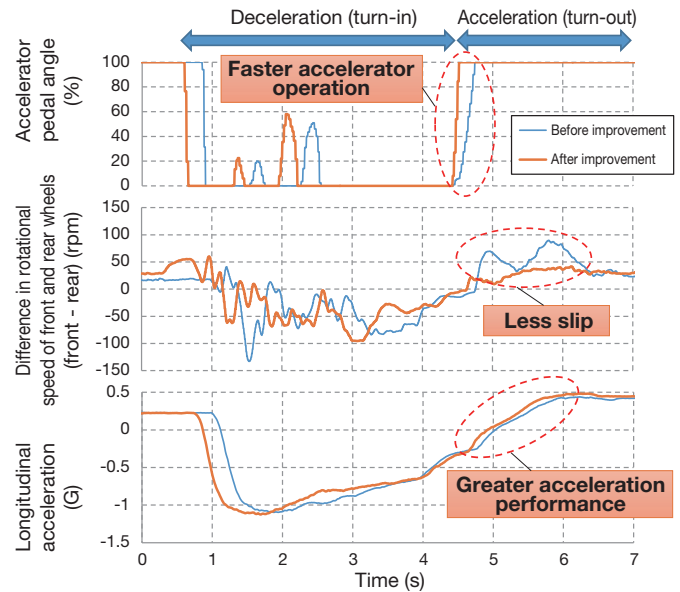


Fig. 12 Comparison of Cornering Performance before and after Refinement of 4WD Control

5. Conclusion

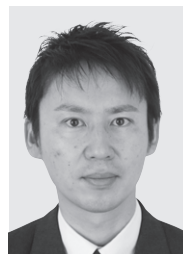
The ideal system for a sporty 4WD vehicle was developed through a process of thorough driving performance evaluations, driving data analysis, and feedback. The authors would like to express their sincere gratitude for the invaluable cooperation of everyone at Toyota's partner companies who were involved in the development of this 4WD system.

Toyota intends to continue the development of 4WD systems to provide as many customers as possible with a confident, natural, safe, and fun-to-drive experience.

Note

(1) Torsen[®] is a registered trademark of JTEKT Corporation.

Authors



M. ARAI



N. MAEDA



S. ISHIKAWA

Realization of Superlative Driving Performance

–Development of the Chassis and Dynamic Performance of the GR Yaris–

Takaaki Nagata*¹
 Keita Oba*¹
 Masahiro Ogane*¹
 Yosuke Iwata*¹
 Masanori Horie*¹
 Kohei Kozono*¹

Abstract

The chassis of the sporty four-wheel drive (4WD) GR Yaris was developed to facilitate handling from normal driving conditions to the limits of performance, and to become the fastest vehicle in its class. Based on the Toyota New Global Architecture (TNGA) design philosophy that focuses on enhancing the fundamentals of driving performance, a wide range of modifications were adopted to emphasize the sporty dynamics of the GR Yaris. These included further enhancing fundamental performance aspects such as mass and inertia, changing the front and rear suspensions, developing new brakes, and adjusting the shift layout. In addition, to facilitate handling in all situations, from every-day to sporty driving scenarios, and to refine the vehicle dynamics, the chassis was tuned under various conditions, including on a racetrack by top-level racing drivers.

Keywords: *handling, suspension, brakes, shift, pedal, tuning*

1. Outline of Development

Driving faster than everyone else is the essence of motor sports. To win, a car must accelerate more quickly, corner at higher speeds, and stop over shorter distances. Easy control and the ability to interact with the car are essential for driving continuously at the limits of performance. The GR Yaris was born to be driven in this world. It is the result of the thorough design and implementation of fundamental performance and specifications, followed by tuning to maximize the vehicle's potential, all at a price that puts the GR Yaris within the reach of as many people as possible. This article describes how the chassis and dynamic performance of the GR Yaris were developed.

2. Enhancement of Fundamental Mass and Inertia-Performance

It is impossible to drive more quickly than the physical limits. Therefore, this development studied the ideal configuration to raise the fundamental performance limits of the GR Yaris above its rivals. The focus of the Toyota New Global Architecture (TNGA) design philosophy is to lower the center of gravity, increase body rigidity, and equalize the weight balance between the left and right sides of the vehicle. Based on this approach, the GR Yaris realized further enhancements by optimizing the body shape, replacing the materials of components located away from the center of gravity, and so on.

2.1 Low center of gravity

To ensure tire grip and overturning immunity, it is important to reduce the lateral load shift when cornering. In other words, this means increasing the gravity center height – tread ratio (= tread ÷ gravity center height). In the GR Yaris, a low center of gravity was achieved by adopting a low roof, reducing weight, and mounting components as low as possible. This approach successfully realized fundamental performance attributes superior to other four-wheel drive (4WD) sports cars (**Fig. 1**).

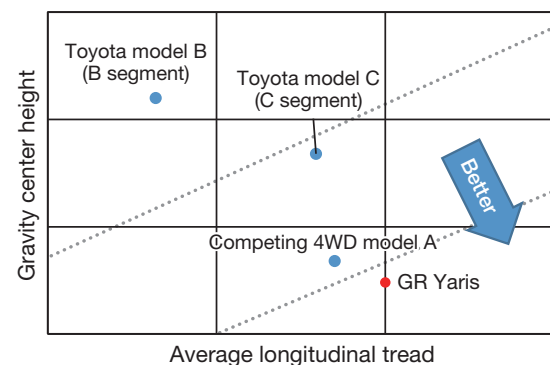


Fig. 1 Gravity Center Height – Tread Ratio (Values Measured by Toyota)

2.2 Lightness, yaw inertia, and front/rear weight distribution

To enhance cornering response, it is necessary to reduce the normalized yaw inertia moment (= yaw inertia moment ÷ (mass × wheelbase² × front axle weight ratio × rear axle weight ratio)). The normalized yaw inertia moment was reduced by 5%

*¹ TC Vehicle Development Div. No. 1, Toyota Compact Car Company

compared to a competing 4WD vehicle by reducing the size of the overhangs and replacing body panel materials (**Fig. 2**). An ideal front/rear weight distribution can be difficult to obtain with a hatchback type vehicle. For the GR Yaris, a front/rear weight distribution of 59:41 equivalent to competing 4WD vehicles was realized by moving the battery toward the rear of the car, which helps to ensure stability while braking in a turn.

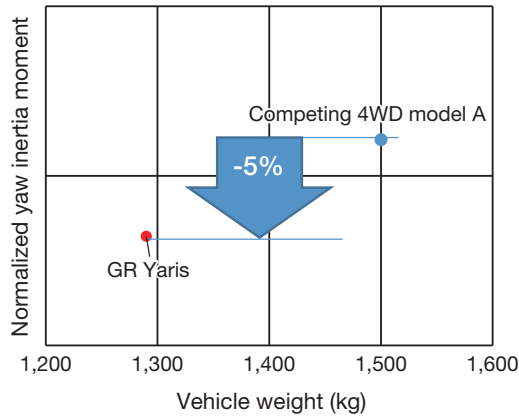


Fig. 2 Normalized Yaw Inertia Moment (Values Measured by Toyota)

2.3 Body rigidity

A highly rigid body is essential for maximizing the potential of the powerful engine and responding to high turning inputs. This was achieved by increasing the number of spot welds, expanding the use of special structural adhesives, and adopting high-rigidity urethane adhesive to secure the windshield and quarter glass. As a result, the torsional rigidity was increased by 23% compared to the base Yaris.

2.4 Aerodynamics

Vehicle stability at high speeds was enhanced by optimizing the roof shape to strengthen the competitiveness of the World Rally Championship (WRC) car, by providing fins on the fender liners to guide the airflow inside the front wheelhouse as well as airflow correction fins on the rear wheel bumper seals, and by shaping the lower end of the rear bumper to bend backward and guide airflow to the rear of the vehicle.

2.5 Tire size selection

A low tire load rate is advantageous for maintaining grip. The regulations of gymkhana-style races and other motor racing series place restrictions on the amount that tire width is permitted to change. Therefore, a tire size of 225/40R18 was selected, which has a lower load rate than competing 4WD vehicles (**Fig. 3**). (Here, the load rate is expressed as the external tire diameter \times nominal width.)

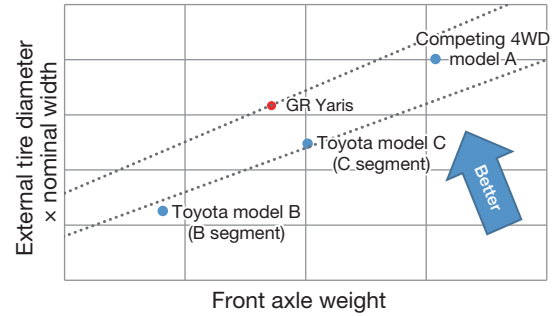


Fig. 3 Tire Size Plot (Values Measured by Toyota)

3. Suspension

3.1 Expansion of camber angle of ground plane

An important way of maximizing tire performance is to set an appropriate range for the camber angle of the ground plane. In a turn, the vehicle roll creates a positive camber angle, which degrades tire performance. To cancel this effect, the initial camber angle was increased (**Fig. 4**). This was realized by changing the steering knuckles in the front suspension and the length of the upper suspension arms in the rear suspension.

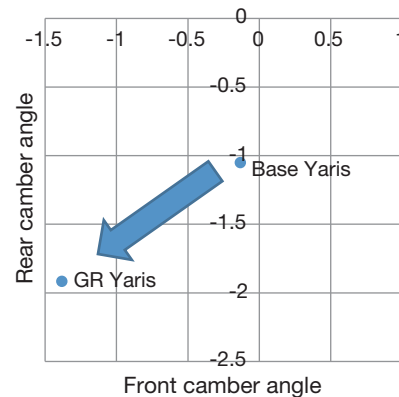


Fig. 4 Initial Camber Angle Settings

3.2 Special measures for production processes

Special production processes were prepared to enable the mass-production of the desired components. The details are described in the GR Factory article later in this edition of the *Toyota Technical Review*.

3.3 Front suspension

A lightweight and highly stiff front suspension is necessary from the standpoints of the front/rear weight distribution and controllability. The geometry of the front suspension in the GR Yaris was modified based on the Macpherson strut suspension from the GA-B platform and optimized for a 4WD sports car.

The dedicated components adopted for the GR Yaris are shown in yellow in **Fig. 5**.

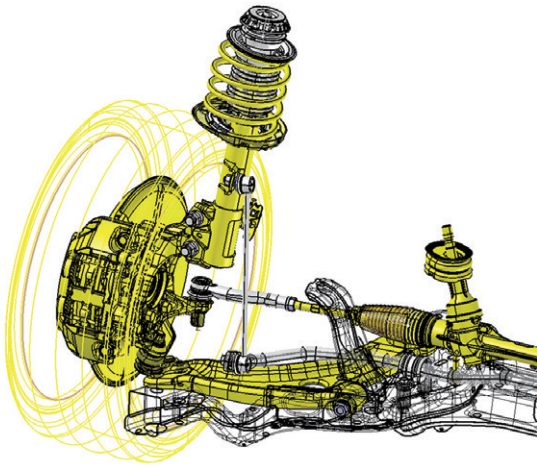


Fig. 5 Front Suspension

To lower the frequency of steering wheel grip adjustments while cornering and realize agile steering responses, the overall steering gear ratio (OA gear ratio) was set to 12.3 (standard grade). The steering knuckles were redesigned to optimize the roll center height, reduce the OA gear ratio, and enlarge the initial camber angle.

To enhance response and controllability, the lower suspension arm bushes and hub bearings were stiffened and redesigned. Prosmooth shock absorbers manufactured by KYB Corporation were paired with size C35 pistons to ensure rapid response characteristics. This combination held to realize excellent body controllability and driving line tracing performance.

In addition, the world's first front hub bearing grease with conductive and static electricity suppression properties was adopted to help enhance steering feel and aerodynamics.

3.4 Rear suspension

To ensure the stiffness and geometrical characteristics required by a 4WD sports car, the trailing-arm type double wishbone rear suspension from the GA-C platform was adopted (**Fig. 6**).

Ball joints were used for the two joints on the carrier side of the lower arm in combination with a newly designed dedicated rear carrier. Controllability at the limits of performance was greatly enhanced by increasing the torsional stiffness around the Z axis.

Rapid response characteristics were ensured by pairing size C32 pistons with the shock absorbers.

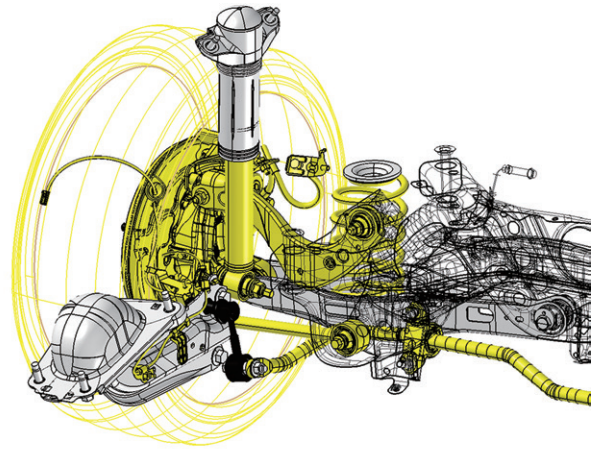


Fig. 6 Rear Suspension

3.5 Measures for low-volume suspension production

To make the vehicle as affordable as possible, the development team aimed to maintain the required performance while minimizing tooling investment. This is because tooling accounts for a large proportion of component costs in low-volume production.

For the front suspension, the GA-B platform was developed alongside the GR Yaris, which enabled the development team to incorporate the requirements of the GR Yaris into components such as the lower arms, upper supports, and struts. The lower suspension arm bushes share the same metal couplings as the base model and were redesigned using a rubber mold. For the rear suspension, a wide variety of TNGA components were used as the basis for characteristics optimization. Typical examples include the trailing arm bushes and rear hub bearings.

4. Brakes

4.1 Calipers and disc rotors

To ensure fade resistance and brake feeling when driving on racetracks such as the Nürburgring Nordschleife, new 18-inch front brakes and 16-inch rear brakes were developed (**Fig. 7**).

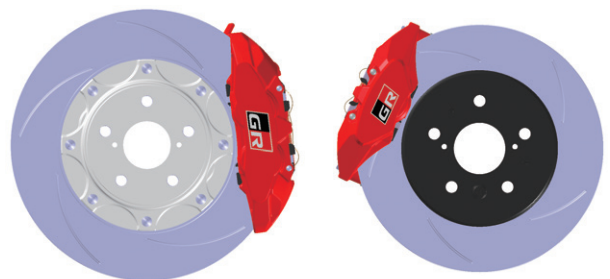


Fig. 7 Front Brakes (Left) and Rear Brakes (Right)

Special Feature

Disc rotors with an outside diameter of 356 mm at the front and 297 mm at the rear were adopted to ensure sufficient heat capacity (**Fig. 8**). The front brakes are provided with spiral fins to enhance cooling performance and a two-piece aluminum bell housing to reduce weight. In addition, the fade resistance of both the front and rear brakes was enhanced by adding slits to the sliding surfaces (**Table 1**).

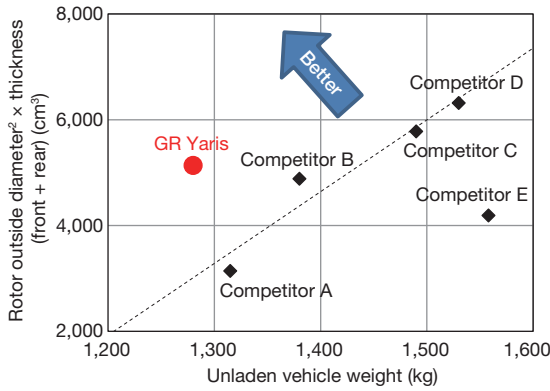


Fig. 8 Comparison of Disc Rotor Heat Capacity

Table 1 Disc Rotor Specifications

	Front	Rear
Type	Spiral fin type ventilated 2-piece discs with slits	Ventilated discs with slits
Outside diameter (mm)	Diameter: 356	Diameter: 297
Thickness (mm)	28	18

Aluminum opposed monoblock type calipers were adopted for both the 4-pot front brakes and 2-pot rear brakes. This approach helped to reduce the weight of the brakes and restrict uneven brake pad wear. Low steel brake pads were adopted to ensure the effectiveness and fade resistance of the brakes.

The front brakes of some grades are also provided with standard brake ducts to further enhance cooling performance.

4.2 Brake feeling

The brakes in sports cars require an excellent balance between effectiveness, stiffness, controllability when releasing the brake pedal, and ease of heel-and-toe operation. This balance was realized by tuning the pedal effort weighting and matching it to a short pedal stroke. As shown in **Fig. 9**, the pedal effort is controlled from low acceleration. In addition, the fade resistance of the developed brakes helps to minimize changes in brake feeling when driving on racetracks (**Fig. 10**).

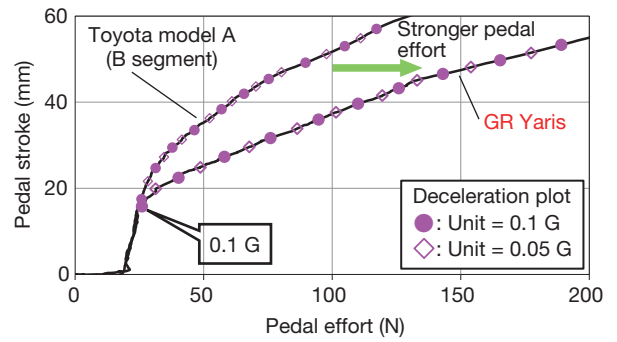


Fig. 9 Deceleration Plotted on Relationship between Pedal Effort and Stroke

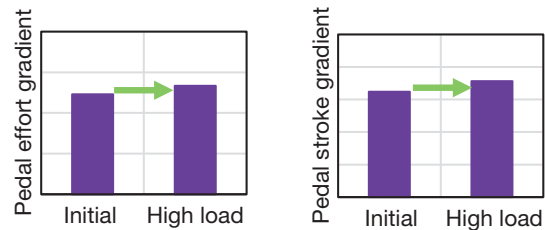


Fig. 10 Changes in Pedal Effort and Stroke Gradients with Respect to Deceleration

4.3 Brake control

To further heighten driving enjoyment, an Expert brake mode was set that mitigates unstable vehicle behavior while retaining driver control in the region close to the performance limits. Expert mode functions to facilitate even sportier driving. In ranges of possible intentional oversteer, intervention by the vehicle stability control (VSC) system is reduced to enhance vehicle controllability. In contrast, when understeer occurs, the brake control intervenes to emphasize line tracing performance (**Fig. 11**).

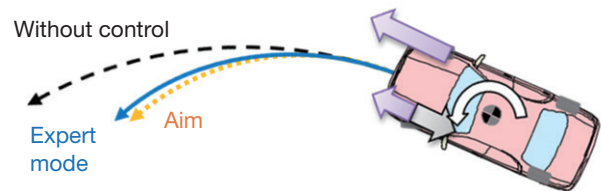


Fig. 11 Illustration of Control when Understeer Occurs

4.4 Parking brake

A drum-in type manual parking brake lever was adopted to ensure the required effectiveness and operability for a parking brake in a sports car.

4.5 Measures for racing

Smaller wheels must be fitted when racing on the gravel and dirt surfaces commonly found in rally events. Therefore, as shown in **Fig. 12**, the calipers were separated from the attachment brackets, allowing the brackets to be changed.

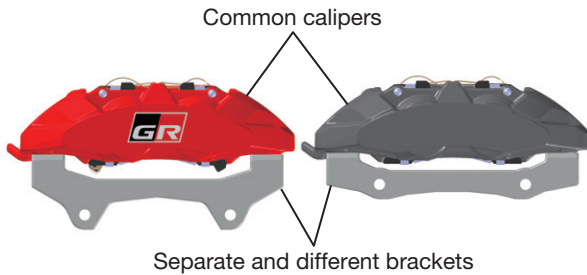


Fig. 12 Standard Front Caliper Configuration (Left) and Configuration for Smaller Wheels (Right)

5. Driving System Components

5.1 Shift system

Toyota’s unique shift-clutch simulator (**Fig. 13**) was used to lay out the shift knob in a position appropriate for sporty driving, and to define and enhance the load and stroke characteristics of the shift lever to enable accurate and fast shifts. The target performance of the shift lever was set with an emphasis on driver perception. An excellent balance between the shift knob position and shift feeling was realized by adopting a newly designed dedicated mounting bracket, shortening the length of the shift lever shaft (i.e., the distance from the center of rotation to the knob) by 50 mm, and enhancing the feeling of stiffness by reducing the shift stroke by 30% compared to the base Yaris and optimizing the lever ratio allocation (**Fig. 14**). The routing and characteristics of the shifter cable were completely revised to enhance efficiency and stiffness. Since this routing brought the cable close to the high-temperature exhaust manifold, a new highly heat-resistant cable was developed.

The newly designed six-speed manual transmission features a triple-cone synchronizer from first to third gear (first and second gear use a carbon synchronizer) and a double-cone synchronizer for fourth gear. The mass of the redesigned shift knob was increased by 250 g and specific performance targets were set by treating the system as an integrated unit.



Fig. 13 Shift-Clutch Simulator

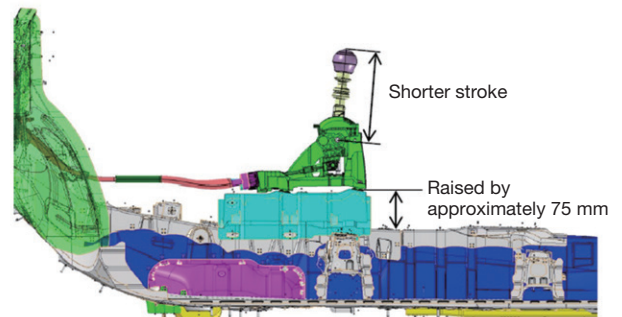


Fig. 14 Shift System Layout

5.2 Brake pedal

To facilitate heel-and-toe operations, the interval between the accelerator and brake pedals was reduced. In addition, for this reason, special measures were adopted for part selection during assembly on the production line to reduce variation.

5.3 Clutch

In the same way as the shift system, the optimum load and stroke characteristics for the clutch were defined and enhanced using the shift-clutch simulator. Similarly, the target performance of the clutch was set with an emphasis on driver perception (**Fig. 15**).

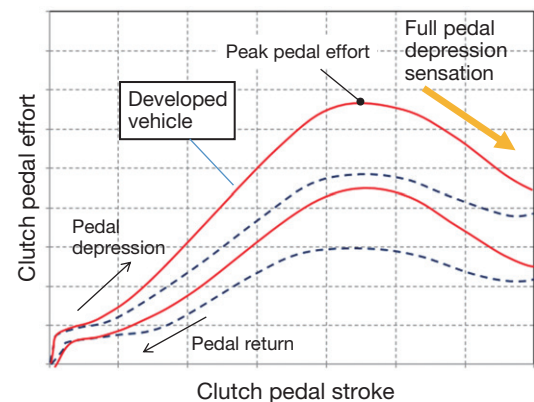


Fig. 15 Target Characteristics for Clutch Pedal Effort

Special Feature

The newly developed clutch and the clutch pedal assist characteristics designed specifically for the GR Yaris enhance the feeling of stiffness, pedal feel, and gradient after the peak pedal effort in line with the requirements of sporty driving. These measures enhance the feeling of arrival at the end of the pedal stroke and make the clutch system easier to use. In addition, to handle the high torque delivered by the new engine, the structure of the newly developed clutch restricts increases in pedal effort due to clutch disc wear. The contact surface of the aluminum pedal pad was also re-shaped to make the pedal easier to depress.

6. Tuning and Determination of Specifications

The development concept for the GR Yaris was to build a car bred from motor sports, completely opposite to the development concept of a conventional vehicle. The method of tuning the chassis and dynamic performance was changed to fit this approach.

Normal dynamic performance development is mainly carried out through testing at the Higashifuji Technical Center. For the GR Yaris, the main aspects of development were shifted to the Shibetsu and Shimoyama Proving Grounds, and dynamic performance was enhanced under complex vehicle speed and acceleration conditions on circuits, high speed oval tracks, winding country roads, and the like. Evaluations were also carried out on racetracks such as the Nürburgring Nordschleife, Fuji Speedway, Suzuka, and Tsukuba (**Fig. 16**).



Fig. 16 Scene from Racetrack Testing

Vehicle development is also normally carried out mainly using drivers from inside Toyota. In contrast, the GR Yaris was developed using professional drivers right from the initial development phase. **Fig. 17** shows a G-G diagram that plots the relationship between cornering, acceleration, and deceleration G values to illustrate the difference between normal drivers driving at high-speed driving and race drivers driving to achieve a fast lap.

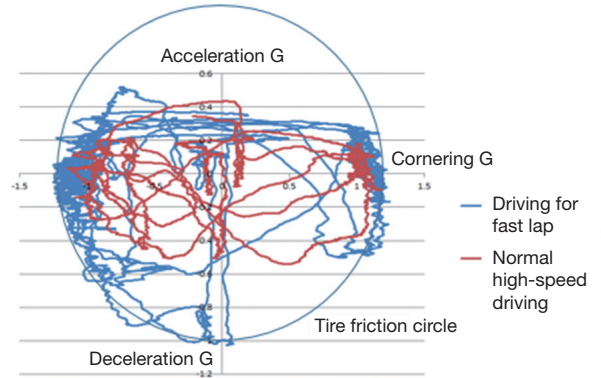


Fig. 17 G-G Diagram

The diagram shows that, when driving to post a fast lap time, the driver is continuously at the limits of the tire friction circle. The chassis specifications, electronically controlled coupling torque, and VSC control were optimized to enhance controllability. These were reflected in the settings to realize rear stability under braking, and the heavier-than-normal steering effort required to feedback information about the front tire grip.

The wealth of motor sports-related knowledge of Toyota GAZOO Racing Europe (TGR-E) was also used during the tuning process. The suspension stroke was measured alongside conventional parameters such as vehicle speed, acceleration, yaw rate, and so on (**Fig. 18**). Driver comments were used to define quantitative phenomena. Countermeasures were then studied via desktop calculations and tested. Repeated iterations of this development cycle were carried out. The test team included members from a wide range of departments, who were gathered together in the same place. The cycle of performance enhancements was carried out immediately there and then by the team based on both the comments from professional drivers and measurement results from on-board data loggers and instruments. As a result, the specifications and vehicle characteristics were determined by a process closely resembling that of an actual race team.

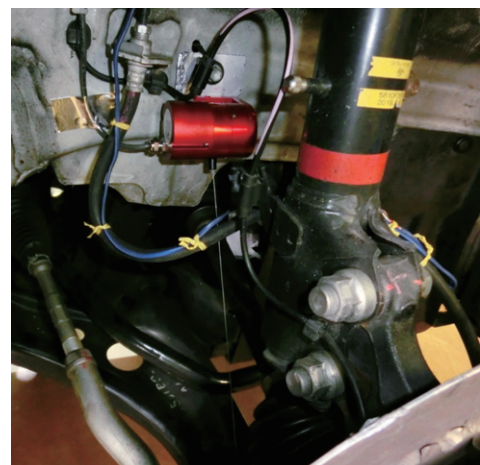


Fig. 18 Suspension Stroke Measurement

The settings for the standard grade were defined to enable as many drivers as possible to enjoy a fun-to-drive experience.

In contrast, the settings for the Circuit Pack grade were defined to help drivers take on the challenge of even higher performance limits.

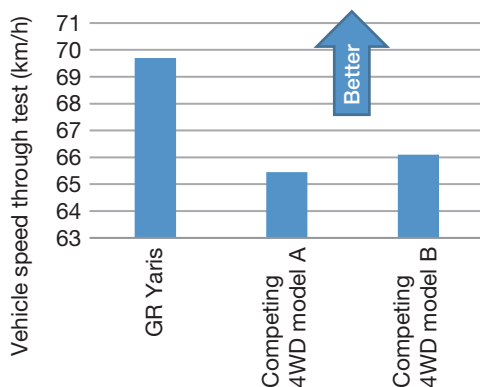
Optimum settings were determined for the tires, differential, coil springs, shock absorbers, and anti-roll bars (**Table 2**).

**Table 2 Typical Specifications
(Differences Highlighted in Bold Text)**

	Standard	Circuit Pack
Tires	Dunlop SP SPORT MAXX 050	Michelin Pilot Sport 4S
Wheels	Castings manufactured by ENKEI Corporation	Forgings manufactured by BBS
Front and rear limited slip differentials	Open	Torsen
Front	Spring constant 34 N/mm Coil spring specifications Diameter: 23.2, thickness: 3.6 Shock absorber damping force: extension/contraction at 0.3 m/s 1,550/880	36 N/mm Diameter: 24.2, thickness: 4.0 1,610/890
Rear	Spring constant 36 N/mm Coil spring specifications Diameter: 21, solid type Shock absorber damping force: extension/contraction at 0.3 m/s 1,130/870	Same as left Same as left 1,440/860
Roll stiffness (total of front and rear)	2,360 Nm/deg	2,540 Nm/deg
Roll stiffness front distribution	61%	64%
Electric power steering (EPS) constant	For standard grade	For Circuit Pack grade

7. Results

This section describes the results measured in an 18-meter slalom test carried out inside Toyota as an example of dynamic performance. The results confirmed that the GR Yaris is faster than its competing models (**Fig. 19**).



**Fig. 19 Vehicle Speed through 18-Meter Slalom Test
(Values Measured by Toyota)**

8. Conclusion

Toyota has developed its first 4WD sports car for twenty years. Despite the arduous nature of the development, excellent performance was achieved over a short period of time by learning from motor sports. The authors would like to express their sincere gratitude for the invaluable cooperation of everyone at Toyota’s partner companies who were involved in the development. Toyota intends to continue developing vehicles with even greater performance and appeal to bring the joy of driving to as many people as possible.

Authors



T. NAGATA



K. OBA



M. OGANE



Y. IWATA



M. HORIE



K. KOZONO

Special Feature

Weight Reduction for Exhilarating Performance

–Weight Reduction Technology for the Body of the GR Yaris–

Tomohisa Kanamori*¹
 Haruki Nakamura*¹
 Kazuhiro Morita*¹
 Kyohei Yamaji*²

Abstract

One of the development aims of the GR Yaris was to realize a car that can be driven purposefully and with confidence by anyone on any road throughout the world. To enhance the fundamental specifications affecting the inertial characteristics of the vehicle, which have a close relationship with dynamic performance, the layout of components was carefully optimized and a wide range of weight reduction technologies was examined. Weight reduction technologies adopted on the GR Yaris include an aluminum hood, side doors, and rear hatch, as well as roof panels that are made from carbon fiber reinforced plastic (CFRP) and formed using sheet molding compound (SMC) processing for excellent geometrical flexibility. Further weight reduction was also achieved by incorporating high-strength steel at optimum locations throughout the body frame. This article outlines the component layout and weight reduction technologies adopted to enhance the inertial characteristics of the vehicle body.

Keywords: inertial characteristics, aluminum, sheet molding compound (SMC), carbon fiber reinforced plastic (CFRP), high-strength steel, Yaris

1. Introduction

One of the development aims of the GR Yaris was to realize a car that can be driven purposefully and with confidence by anyone on any road throughout the world. To accomplish this, the development focused on enhancing the fundamental specifications affecting the inertial characteristics of the vehicle, which have a close relationship with dynamic performance. **Fig. 1** illustrates the relationships between vehicle performance and inertial characteristics. This article describes some of the specific development approaches that were followed to optimize the layout of the battery, which helped to enhance these inertial characteristics, and to reduce the weight of the vehicle by adopting aluminum and carbon fiber reinforced plastic (CFRP).

2. Enhancement of Fundamental Specifications Affecting Inertial Characteristics

In general, projects to enhance vehicle performance tend to focus on engine, drivetrain, and chassis components. In addition to this conventional approach, the development of the body of the GR Yaris also aimed to enhance vehicle performance by focusing on the key performance-related inertial characteristics. Although much of this focus on inertial characteristics was directed on the mass of the vehicle, these

mass reduction efforts also examined the center of gravity height, front/rear weight distribution, left/right weight distribution, and the moment of inertia. The mass and center of gravity of every body component was estimated and modeled. The components with the largest contribution ratio were then identified so that the fundamental characteristics could be enhanced efficiently. In addition, the component layout was changed so that the battery, which has major impact on the front/rear and left/right weight distribution was moved from its normal position in the engine compartment to inside the luggage compartment. This measure helped to lower the center of gravity of the vehicle (**Fig. 2**).

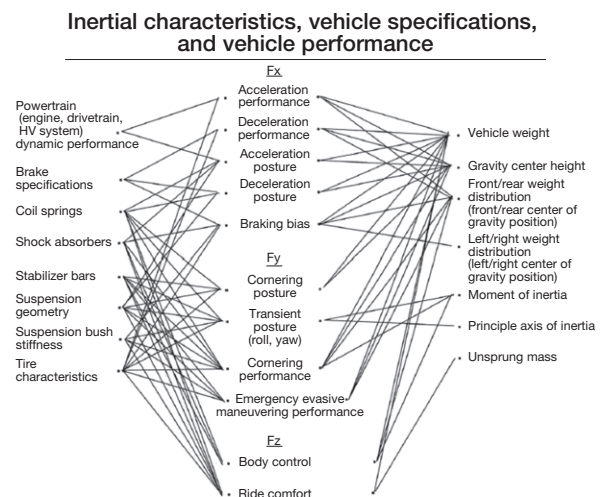


Fig. 1 Relationships between Inertial Characteristics and Vehicle Specifications

*¹ TC Vehicle Development Div. No. 2, Toyota Compact Car Company

*² Toyota Motor East Japan, Inc.

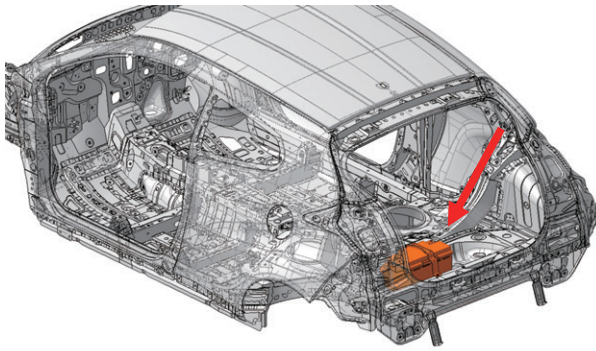


Fig. 2 Battery Layout

The development also focused on reducing the weight of the body panels. The moment of inertia and front/rear weight distribution can be enhanced by reducing the weight of components further away from the vehicle center of gravity. Aluminum and CFRP were actively adopted to reduce weight.

3. Outline of Locations Adopting Lightweight Materials

Aluminum, CFRP, and high-strength steel were used for many body panels and body frame components in the GR Yaris. Fig. 3 shows the locations that these materials were used. The use of these materials reduced the weight of the vehicle by approximately 38 kg compared to the previous 3-door Yaris.

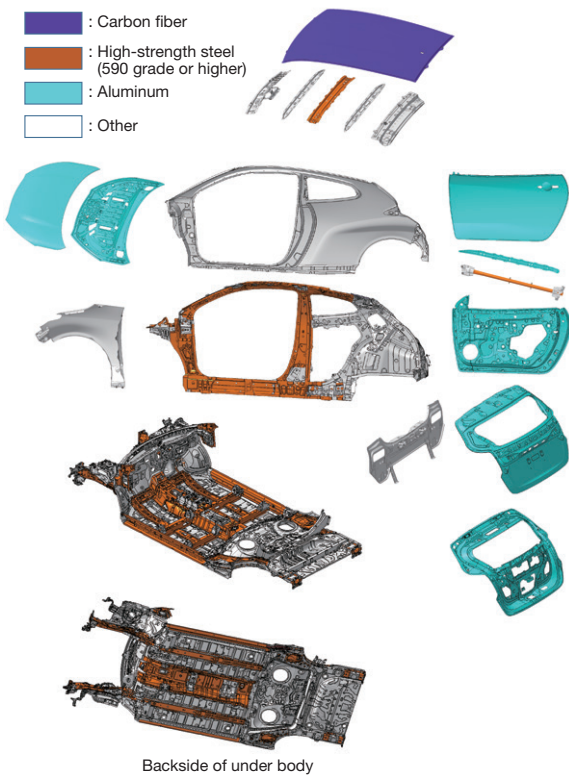


Fig. 3 Outline of Materials Used to Reduce Body Weight

4. Use of Aluminum

Aluminum, which is rarely used on conventional compact cars, was adopted for the hood, back door, outer side door panels, and the inner panels. In addition, aluminum was also adopted for all the components in the side doors, except the impact beams (Fig. 4). The use of aluminum reduced the weight of the vehicle by approximately 23 kg compared to the previous 3-door Yaris.

In addition to the widespread use of aluminum in the side doors, a sash-free structure was also adopted. Compared to the frame structure of the previous Yaris, this approach reduced the size of the step around the door glass (Fig. 5), thereby creating a more uncluttered impression and enabling a more sports car-like appearance.

This sash-free structure uses the weatherstrip around the door to ensure sealing performance when the door is pushed outward by the negative pressure applied to the door glass at high speeds. This helped to reduce weight since a door with a frame structure usually requires a reinforced belt molding to prevent the door from being pushed outward.



Fig. 4 Aluminum Side Door Components (Highlighted in Light Blue)

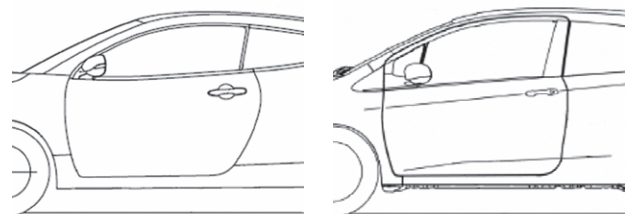


Fig. 5 Comparison of Side Door Structures (Left: Sash-Free Structure, Right: Frame Structure)

Special Feature

5. Use of CFRP

Instead of a component manufactured by resin transfer molding (RMT), sheet molding compound (SMC) CFRP was adopted for the roof panel to reduce both weight and cost (**Fig. 6**). Although this method had previously been adopted for the back door of the Prius, this was its first application to the roof panel of a Toyota model. The use of a CFRP roof panel reduced the weight of the vehicle by approximately 5 kg compared to the conventional steel roof of the previous Yaris.



Fig. 6 CFRP Roof Panel

6. Optimization of Steel Components

In addition to replacing conventional materials with aluminum and carbon fiber to reduce weight, high-strength steel was also adopted in the optimum locations of the body frame to ensure performance (i.e., crash performance, strength, or the like) while lowering the weight of the vehicle. **Figs. 7** and **8** show the locations of high-strength steel in the upper and under body, respectively. In addition, the thickness of the fender panels and side outer panels was reduced by 0.05 mm compared to the previous 3-door Yaris, which helped to reduce weight further.

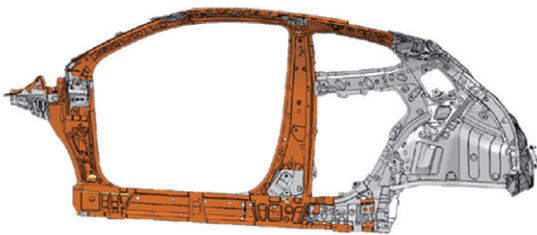


Fig. 7 Locations of High-Strength Steel in Upper Body

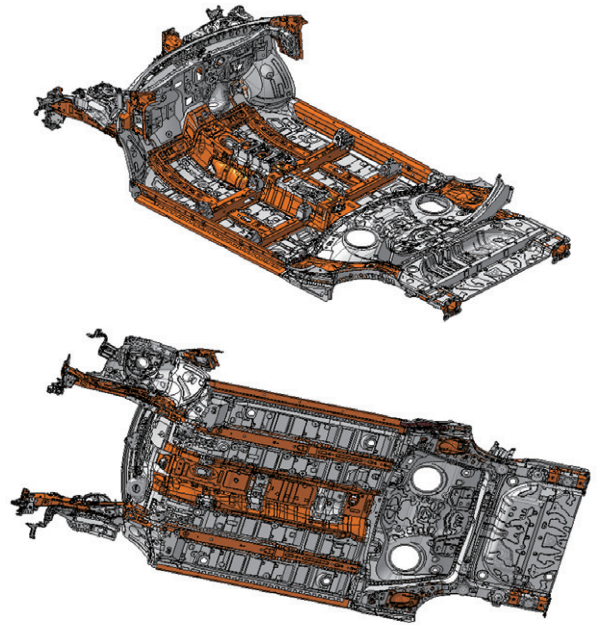


Fig. 8 Locations of High-Strength Steel in Under Body (Top: Top View, Bottom: Bottom View)

7. Summary

The fundamental specifications affecting the inertial characteristics of the vehicle were enhanced by optimizing the layout of components and incorporating a wide range of weight reduction technologies. The development team took on the challenge of reducing the weight of body components, primarily by adopting CFRP for the roof panel and actively applying aluminum throughout the body. These measures reduced the weight of the vehicle by approximately 38 kg.

The development team confirmed the positive effects of these enhanced inertial characteristics in test drives of a prototype vehicle incorporating the measures described in this article.

8. Conclusion

The authors would like to express their gratitude to everyone that assisted in the component layout optimization and helped to incorporate the weight reduction technologies, as well as to everyone that contributed to this article as a member of the production team. The activities described in this article made a major contribution to enhancing the dynamic performance of the vehicle and realizing the development concept of the GR Yaris.

Authors



T. KANAMORI



H. NAKAMURA



K. MORITA



K. YAMAJI

Expressing Driving Performance through Sound

–Development of the Sound of the GR Yaris–

Hisashi Tajima*¹
 Chie Fukuhara*²
 Hideyuki Kasamatsu*¹

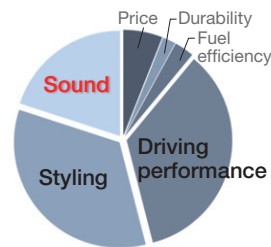
Abstract

Sound is a key aspect of motor sports and the creation of the appropriate sound was emphasized during the development of the GR Yaris. The development aimed to use sound as an information source to audibly communicate the engine speed to the driver, and to create a sound consistent with vehicle performance and in harmony with driver operation and vehicle behavior to intensify the enjoyment of driving. This article describes how the frequency balance was designed to emphasize the order arrangements and sound of the engine, as well as the linearity of the sound pressure with respect to the engine characteristics, acceleration, and deceleration. It also discusses the development of the particular sound characteristics that distinguish the GR Yaris, such as the tonal balance at the rev limit and the transient sound when the driver blips the throttle.

Keywords: *sound, hot hatch, motor sports, informative function, driving performance matching*

1. Introduction

The GR Yaris is a car bred from motor sports, a world in which winning and driving quickly are more important than anything else. Since these represent completely different values from those of an ordinary passenger vehicle, the approach to noise and vibration (NV) development was completely reconsidered. First, the sound concept for the GR Yaris was identified by repeatedly riding alongside and interacting with professional drivers, and with reference to competing vehicles in the same hot hatch segment. As a result, it was concluded that the most important function of sound in motor sports is to provide information that audibly communicates the engine torque and allows the driver to determine the optimum shift timings. This is called the “informative function.” Customers also have high expectations for sound in the hot hatch segment (**Fig. 1**). After analyzing customer comments, a sound consistent with driving performance was identified as a key concept. The sounds identified in these comments help to provide an adrenaline-filled experience that conveys the type of vehicle performance that exceeds normal limits.



Exhilarating and nimble driving performance and the engine sound have the most important appeal.

A sound consistent with the driving performance is highly enjoyable.

A good sound when shifting down is important.

Hot hatches are quite noisy, but that is part of the appeal.

Fig. 1 Key Points for Customer Satisfaction in the Hot Hatch Segment and Sample Comments

The GR is installed with a highly responsive three-cylinder turbocharged engine. However, the reputation of three-cylinder engines with regard to vibration sensation and tonal balance is far from positive. In addition, restrictions on vehicle noise emissions are making it increasingly difficult to adopt engines and intake and exhaust systems that intentionally generate sound. Despite this background, the development aimed to create a sound suitable for a car bred from motor sports, which is consistent with the driving performance of the vehicle and provides an excellent informative function. This article describes this sound development in more detail.

*¹ Vehicle Engineering Development Div., Vehicle Development Center

*² Lexus Vehicle Evaluation and Engineering Div., Lexus International Company

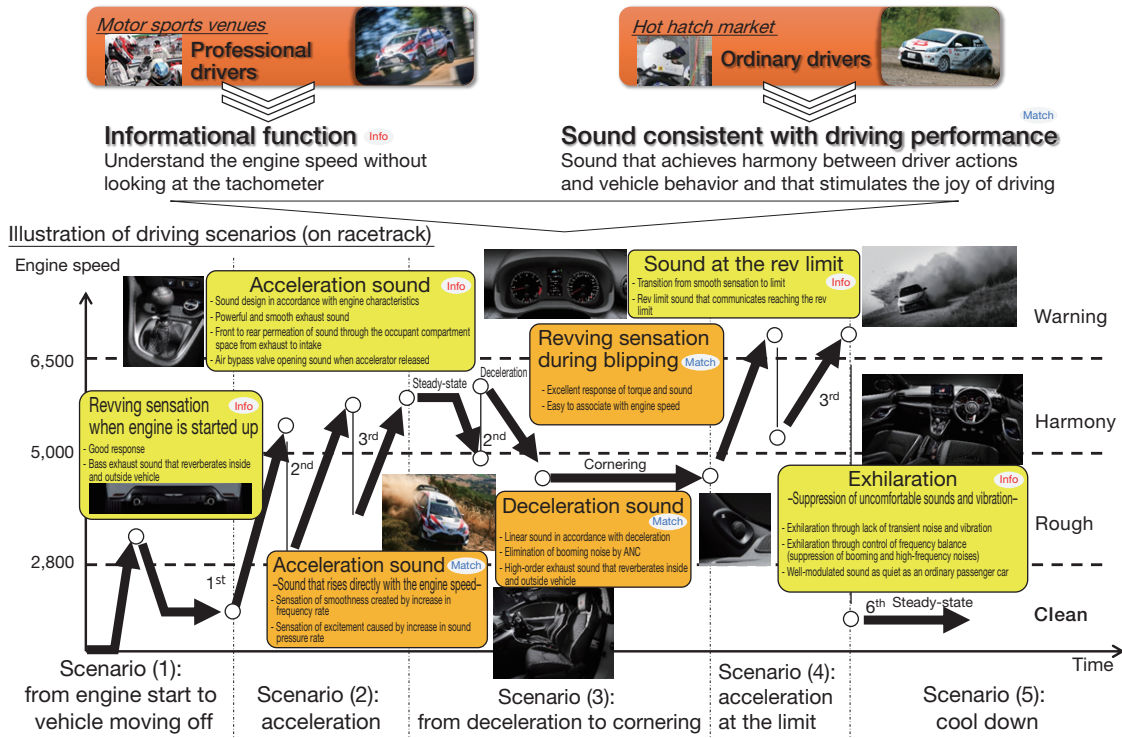


Fig. 2 The Sound Concept of the GR Yaris

2. Sound Concept

This section describes the sound concept of the GR Yaris. In addition to conventional market surveys, the sound concept was created while riding alongside experts at actual motor sports venues. As a result of these test drives, the informative function was defined as the capability to understand the engine speed without looking at the tachometer. In addition, a sound consistent with driving performance was defined as a sound that achieves harmony between driver actions (acceleration and shifting) and vehicle behavior (engine speed and acceleration) and that stimulates the joy of driving. **Fig. 2** illustrates the sound concept of the GR Yaris in terms of the envisioned racetrack driving scenarios and individual target sensations. These envisioned scenarios are described in more detail below.

(1) From engine start to vehicle moving off

As soon as the engine starts, the exhaust creates a pleasant deep-bass note that bubbles upward and acts to build expectations about the vehicle’s driving performance before the vehicle even starts to move. The exhaust bass sound also responds sharply if the driver revs the engine.

(2) Acceleration

Here, with expectations building about the performance of the vehicle, the driver puts the car into first and starts to move off silently before suddenly accelerating with the throttle wide open. The engine sound responds in a linear fashion to the engine speed and delivers a steadily mounting sense of

excitement. The exhaust sound is enough to communicate the fact that a GR Yaris has joined the track. When the driver shifts up, the sound of the turbocharger opening is clearly audible, as if a build of boost pressure has been released. The rhythmic sensation as the driver shifts through the gears is created by the transient tonal balance between the torque and smooth acceleration sensations generated following the cross ratios of the newly developed manual transmission. After a short amount of time behind the wheel, the driver will be able to identify the engine speed from the sound alone. The interaction between exhaust and intake sounds creates a sensation of further dynamism.

(3) From deceleration to cornering

Shifting down before a corner can be carried out rapidly and without any wasteful actions because the driver can read the engine speed from the sharp blipping sound. The changes in sound pressure as negative G is generated create a sensation of deceleration, enabling the driver to concentrate on driving using the ideal level of sound reverberation.

(4) Acceleration at the limit

When the driver lets the car loose and accelerates to the limit, the resulting tonal balance creates sensations of smoothness and lightness bred from rallying. The driver is warned that the rev limit is approaching by a natural modulating sound. The driver can be guided by the sound to interact with the vehicle right up to the performance limit.

Special Feature

(5) Cool down

Here, the driver has finished a hot lap and has reduced speed. The driver can look back over the driving performance of the hot lap while enjoying a contrasting and exhilarating tonal balance within a quiet space equal to that of a well-modulated passenger vehicle. In this space, the driver can then build up to the next lap.

3. Characteristic Sounds in each Driving Scenario

This section describes the sound development for each driving scenario outlined in Section 2.

3.1 Exhaust sound: scenarios (1) and (2)

A powerful exhaust sound is one of the major appeals of motor sports. The tonal balance of this sound is part of the distinguishing character of the car. However, as noise restrictions become increasingly stringent, it is becoming more difficult to create loud sounds. In addition, three-cylinder engines tend to generate muddy rough sounds, even at high engine speeds. In contrast, the highly responsive three-cylinder engine in the GR Yaris has its own distinguishing low and powerful character. Using this, the development created a smooth tonal balance at high engine speeds. An even more powerful sound was created by setting the pipes of the exhaust manifold to the same length, thereby generating a uniform pressure pulsation in each exhaust stroke and emphasizing the combustion order components. In addition, the resonant sound of the exhaust end pipe was used to intentionally generate a sound in the 315 Hz band. This helps to emphasize high-frequency (3rd and 4.5th order) sounds at high engine speeds, thereby realizing an exhaust sound that maintains the sensation of smoothness (Fig. 3).

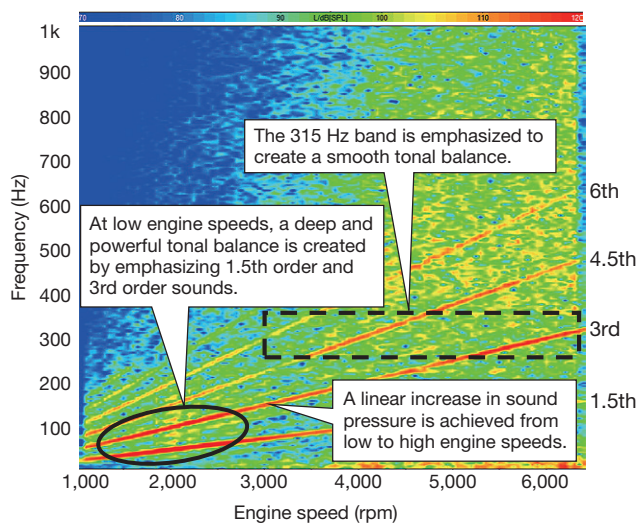


Fig. 3 Order Arrangement of Exhaust Sound (during Acceleration)

3.2 Tonal balance at each engine speed: scenario (2)

A characteristic and distinct tonal balance at each engine speed is necessary to enable the driver to audibly distinguish the engine speed instantaneously without looking at the tachometer. In addition to the natural changes that occur as the volume and frequency rises in accordance with the engine speed, the GR Yaris expresses these distinct characteristics through extensive changes in the order arrangement at each engine speed. Fig. 4 illustrates this concept.

At close to maximum engine torque (between 2,800 and 5,000 rpm), a tonal balance full of torque and power is expressed by creating an excellent blend and balance between first and half order engine combustion sounds. In this range, the tonal balance is changed by adding ± 0.5 th order sounds to the 3rd order sound at lower engine speeds (2,800 to 4,000 rpm) and ± 0.5 th order sounds to the 4.5th order sound at higher engine speeds (4,000 to 5,000 rpm). When the driver revs the vehicle to the highest engine output point (5,000 to 6,500 rpm), the order arrangement consists of just the combustion orders. This evokes an agile tonal balance that reminds the driver of the rallying origins of the vehicle. Adding high-frequency orders (6th and 7.5th order sounds of engine speed) expresses smoothness through the seemingly quadratic increase in frequency.

3.3 Blipping sound: scenario (2)

The blipping sound must adhere strictly to the engine speed in the selected gear. If this cannot be achieved, the driver may be distracted by the generated transient vibration and loss of acceleration. In addition to the tonal balance trends for each engine speed described in Section 3.2, the sound pressure level (SPL) is increased when blipping occurs.

As an intermediate parameter to express this phenomenon,

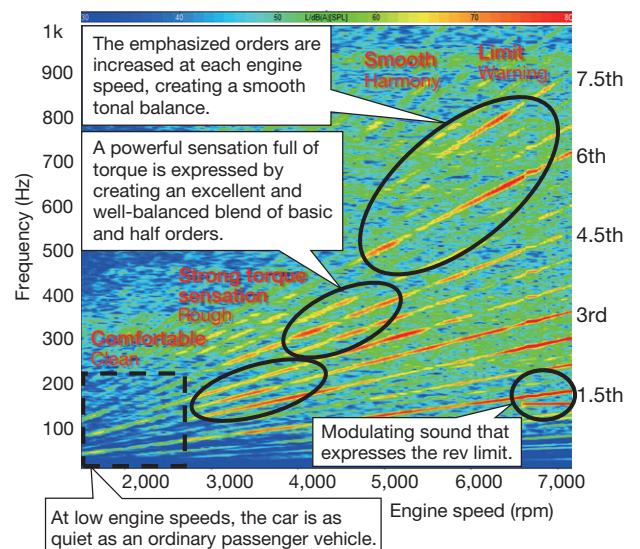


Fig. 4 Order Arrangement of Interior Sound (during Acceleration)

the crest factor (CF) is used to express the size of the higher peak values before and after blipping compared to the effective value (Equation 1).

$$CF = \frac{\text{Peak sound pressure}}{\text{Effective value}} = \frac{\text{Peak SPL}}{\sqrt{\frac{1}{N} \sum_{i=1}^{N-1} (x_i - \bar{x})^2}} \quad (1)$$

The results of subjective evaluations equated larger CF values with “sharper” sounds. The target CF value for the GR Yaris was 1.06 (Fig. 5)

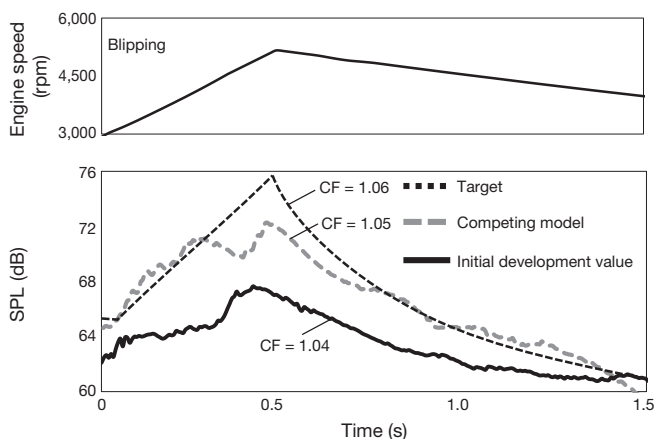


Fig. 5 CF Before and After Blipping

3.4 Deceleration sound: scenario (3)

When controlling the vehicle speed before entering a corner, the driver judges the deceleration by ear. Vehicles with a larger and linear SPL gradient with respect to the longitudinal acceleration were rated as “more direct” in a subjective evaluation (Fig. 6). The GR Yaris carries out order control in accordance with deceleration to realize a more direct deceleration sound with a linear and large SPL gradient.

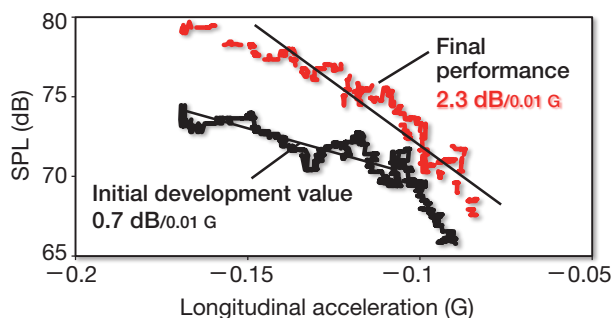


Fig. 6 Relationship between Longitudinal Acceleration and SPL

Furthermore, to create a sound that reverberates well in the ear during deceleration, a simple order arrangement consisting of simply combustion orders was created (Fig. 7).

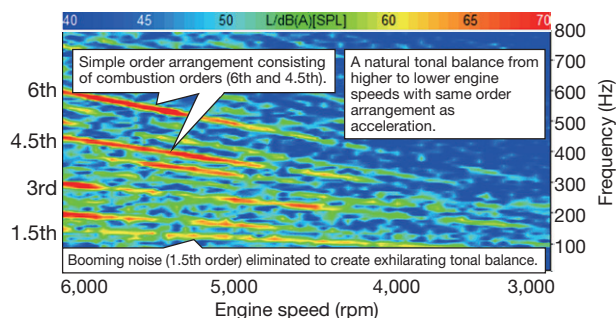


Fig. 7 Order Arrangement during Deceleration

3.5 Sound at the rev limit: scenario (4)

The rev limit is the maximum speed at which the engine is allowed to rotate. Above this limit, the engine is protected by cutting the fuel supply and reducing torque. In addition to the conventional means of determining when this limit is reached through physical sensations (i.e., by feeling the acceleration) or visibly (i.e., by looking at the tachometer), the driver of the GR Yaris can also intuitively sense the limit audibly (i.e., by listening to the sound). At the initial phase of development, it was difficult to sense when the prototype vehicle was close to the rev limit. As a result, many drivers tended to exceed the limit during test drives. Therefore, the development team aimed to create a sound that uses the engine speed to directly communicate the approach of the rev limit. The rev limit itself generates a distinctive modulating rumbling sensation as the fuel supply is cut off. First, this sound was analyzed (Fig. 8). This modulating sound was analyzed at the rev limit (the red line) and immediately before the rev limit (around 7,000 rpm: the black line). The results identified a large sound modulation between 20 and 30 Hz, and particularly at 27 Hz. Therefore, the sensation of approaching the rev limit was realized by increasing the modulation frequency toward 27 Hz in the engine speed range between 6,600 and 7,200 rpm (the blue lines in Fig. 8).

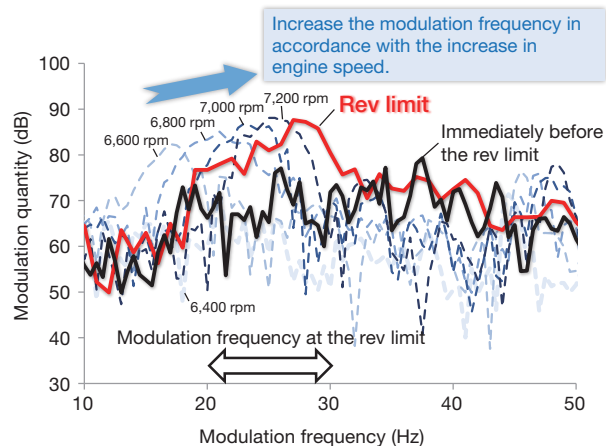


Fig. 8 Analysis of Modulating Sound Close to Rev Limit

3.6 Frequency balance: scenario (5)

In a conventional sports car, in addition to the engine sound, booming noise caused by the drivetrain and engine mounts, road noise from the tires, wind noise, and the like is often not addressed in the same way as an ordinary passenger vehicle since weight reduction is prioritized to emphasize driving performance. In the GR Yaris, to realize the targeted informative function (i.e., to enable the driver to instantaneously recognize the engine speed order), unnecessary noises other than those related to engine speed orders were thoroughly eliminated. First, in addition to countermeasures applied to the engine frame and drivetrain, the vehicle was equipped with active noise control (ANC)* to suppress booming noise. Next, wind noise and other high-frequency noise was reduced to prevent interference with driving performance by preventing leakage through the body and adding lightweight acoustic trim in the optimum locations. As a result, a refined sound balance was achieved that combines distinctive sporty driving sounds with quiet performance equal to an ordinary passenger vehicle (Fig. 9).

* ANC is a system that controls uncomfortable interior booming noise using opposite-phase frequencies.

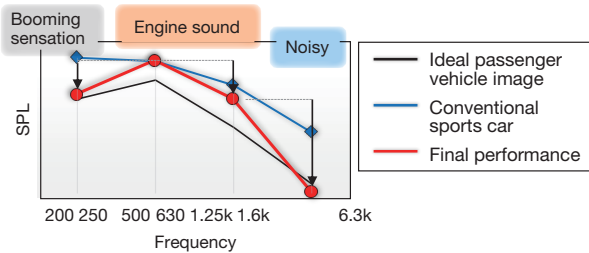


Fig. 9 Frequency Balance while Driving

3.7 Volume control: scenarios (2), (4), and (5)

To achieve good sound modulation in the three scenarios of acceleration, acceleration at the limit, and cool down, the development focused on the volume as well as the frequency balance of the sound. Fig. 10 shows the relationship between engine speed and SPL in the GR Yaris. A different SPL is set for each scenario and, so that extremely small changes in the engine speed can be audibly recognized without fail, the SPL increases in accordance with the engine speed.

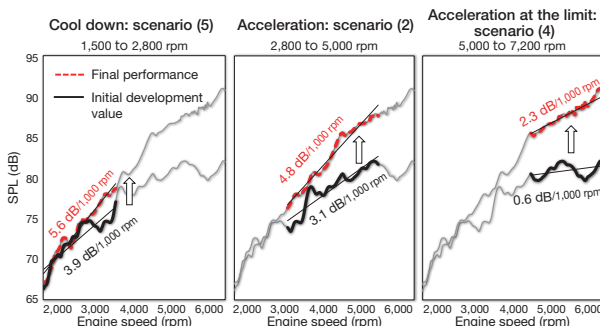


Fig. 10 SPL in each Scenario

4. Verification of Hypothesis

Fig. 11 shows the results of an evaluation using twenty-five people with many years of experience of driving sports cars, who were regarded as close to the target customers for the GR Yaris. Most of the evaluation panel stated that the sound of the GR Yaris was consistent with its driving performance. Even when the frequently used engine speed region differed depending on the driver, this suggests that the GR Yaris closely maintained the targeted informative function due to the characteristic tonal balance set for each engine speed region.

Q: Do you think that the sound of the GR Yaris matches its driving performance?

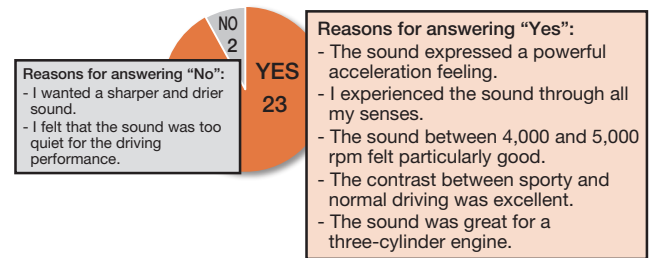


Fig. 11 Results of Driver Subjective Evaluation

Fig. 12 shows the score awarded by Toyota's internal experts using the company's own subjective evaluation index. The target scores were roughly achieved in the five categories of particular importance to the GR Yaris: sharpness, smoothness, modulation, lightness, and directness.⁽²⁾

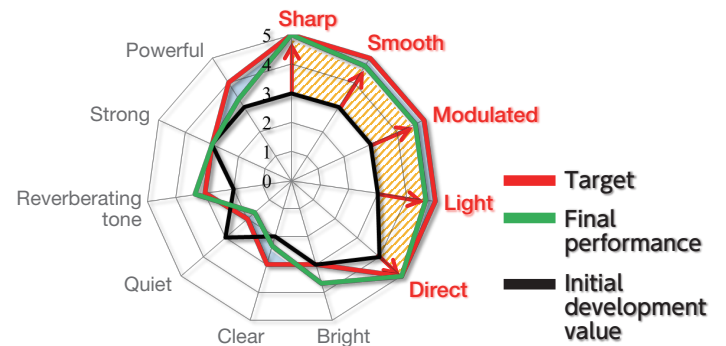


Fig. 12 Results of Subjective Evaluation by Experts inside Toyota

Professional drivers from outside Toyota were asked to test drive the GR Yaris and comment on how far the sound is suitable for a car bred from motor sports. Two of these comments are as follows.

- The sound is exciting and the sound that accompanies shifting makes coordinating the timing of shifts and driving easier.
- I have never experienced an engine sound like this before, and it feels good. The sound makes me want to drive the car.

5. Conclusion

The development successfully created a sound suitable for the GR Yaris as a car bred from motor sports, which provides an excellent informative function and is consistent with the driving performance of the vehicle. The authors would like to express their sincere gratitude to everyone at Toyota's partner companies who were involved in this sound development. It would also give the authors the greatest pleasure to invite all the readers of the Toyota Technical Review to drive the GR Yaris and enjoy its characteristic sound for themselves.

References

- (1) The Technical Information Institute Co., Ltd. *Development and Evaluation of Products in Accordance with People's Perceptions* (in Japanese) (2012).
- (2) H. Tajima et al. "Engine Sound Designing for Hot Hatch." *Proceedings of the JSAE Annual Congress* No. 20196155 (2019).

Authors



H. TAJIMA



C. FUKUHARA



H. KASAMATSU

Cooling to Support Driving Performance –The Cooling Performance of the GR Yaris–

Keisuke Ishita*¹
Masaru Matsuda*¹
Atsushi Murakawa*¹
Yoshifumi Nishio*¹
Shinichiro Hattori*¹

Abstract

Based on the newly developed GA-B platform, the GR Yaris is a compact sports car with exhilarating driving and dynamic performance that is designed to be driven vigorously. Consequently, this vehicle required a cooling structure capable of efficiently managing the heat generated by the newly developed 1.6-liter turbocharged engine and a cooling performance capable of handling heavy loads at high speed, on racetracks, and under similar situations. This article describes case studies from the cooling performance development of the GR Yaris.

Keywords: cooling, sporty driving, heat exchanger, duct

1. Introduction

The GR Yaris is a compact sports car developed from the standpoint of winning the World Rally Championship (WRC).

To realize this objective, the GR Yaris features a wide range of enhancements and changes to the dynamic performance and handling of the base Yaris, including a newly developed powerful engine and four-wheel drive (4WD) system.

Development of the cooling performance was planned around the sporty driving concept of the vehicle. The development team took on the challenge of maximizing the high potential of the GR Yaris, including its confident and natural driving performance, safety, and engine power.

2. Cooling Performance Development Concept

2.1 Outline

The GR Yaris is installed with a newly developed 1.6-liter turbocharged engine with a maximum power of 200 kW. It was necessary to develop a cooling system capable of efficiently dissipating the heat generated by this powerful engine.

Fig. 1 compares the cooling systems of the base model and the GR Yaris.

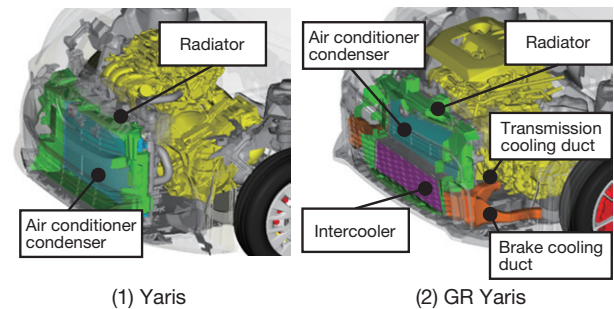


Fig. 1 Cooling System Comparison

Compared to the base model, the GR Yaris features a larger radiator and a large air-cooled intercooler mounted at the front of the vehicle to support the increased engine power. In addition, to maximize the stability of sporty driving performance, the GR Yaris also features ducts to efficiently cool the transmission and brakes.

2.2 Concept of sporty driving

During the initial phase of development, the heat load during sporty driving was investigated on racetracks around Japan. During this process, to ensure coverage of a wide range of conditions, a wide variety of racetracks, from internationally sanctioned to local circuits, were selected. Running data was obtained from these tests and analyzed.

This data was used to identify the severest racetrack conditions that frequently occur at both low speeds and under high load conditions. A local circuit with a relatively low average speed was selected as a representative racetrack (**Fig. 2**).

*¹ TC Vehicle Development Div. No. 2, Toyota Compact Car Company

	Racetrack comparison			
	Racetrack A	Racetrack B	Racetrack C	Racetrack D
Average speed	High speed	>>		Low speed
Cooling air	High	>>		Low
	(Internationally sanctioned racetrack)			(Local racetrack)

Fig. 2 Illustration of Representative Racetrack Selection

3. Engine Cooling

3.1 Heat load estimation

The engine heat load of the GR Yaris on the racetrack selected as described in the previous section was compared with the heat load of the base Yaris (TNGA 1.5-liter engine) identified during the development of that vehicle. The results showed that the GR Yaris required a heat transfer capacity approximately two times higher than the base Yaris (Fig. 3).

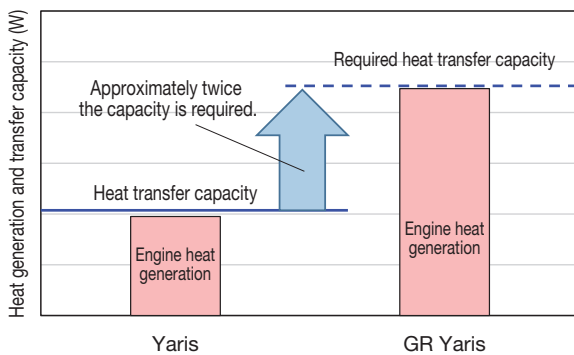


Fig. 3 Engine Heat Generation and Required Heat Transfer Capacity

3.2 Study of heat exchanger layout

Next, the development studied the optimum layout to satisfy the required heat transfer capacity described in the previous section, considering the temperature rise caused by the waste heat generated by the intercooler and air conditioner condenser.

Another aim of the layout was to maintain the optimum balance between engine power (intercooler) and air conditioning performance (air conditioner condenser) with respect to the heat transfer capacity (radiator).

After studying a wide range of proposals, layout (3) in Fig. 4 was selected as providing the best balance of all the elements within the limited space of the GA-B platform.

	Front view	Side view	Heat transfer capacity	Engine power	Air conditioning performance	Installation
(1) Base model			×	×	○	×
(2) Studied proposal (extract)			×	○	○	×
(3) Final proposal			○	○	○	○

Fig. 4 Study of Heat Exchanger Layout (Extract)

3.3 Component cooling performance design

(1) Radiator and fan

The radiator of the GR Yaris is larger than that adopted in the base model. In terms of the frontal projected area, it is 27% larger, and in terms of the fin area, it is approximately 110% larger than the base model (specifications for the Japanese market). The intake ducts located above the radiator in the base model were redesigned for the GR Yaris to create the space for the taller radiator.

The radiator in the GR Yaris is also thicker than in the base model. The motor output of the electric fan was also substantially increased to counteract the higher drag of cooling air due to the presence of the intercooler. These measures ensured the required heat transfer capacity for the greater heat generated by the engine of the GR Yaris.

Fig. 5 shows the external appearance of the heat exchangers and fan.

Special Feature

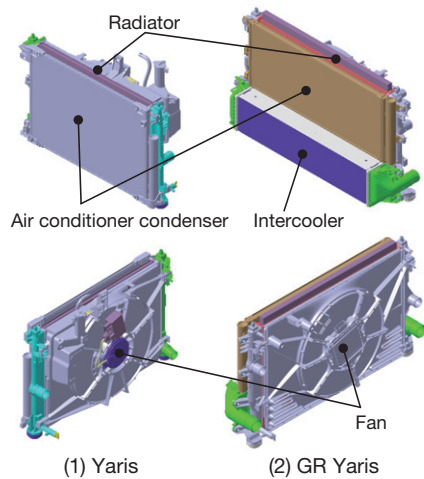


Fig. 5 Heat Exchangers and Fan

(2) Intercooler

An air-cooled intercooler with large cross flows was selected for the GR Yaris.

The intercooler features straight inner fins to reduce the pressure drop inside the intake paths. The cooling capacity of the intake air required to achieve maximum engine power was ensured by maximizing the core length (Fig. 6).

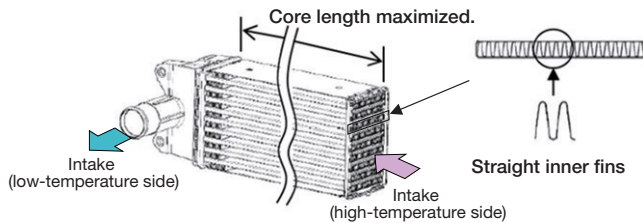


Fig. 6 Intercooler Structure

(3) Front grille opening

The cooling grille opening was aligned with the mounting locations of the heat exchangers to efficiently guide the airflow generated by the vehicle speed. The grille opening was also designed to realize both functionality and stylishness (i.e., beauty) in accordance with the styling concept of the GR brand (Fig. 7).

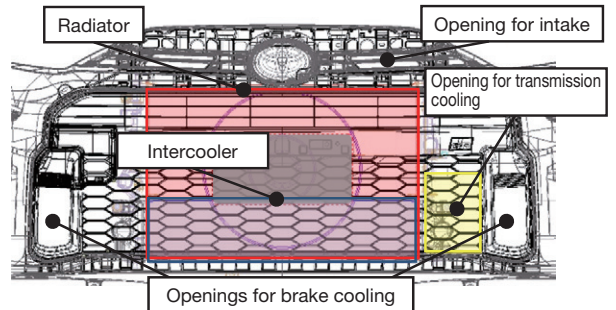


Fig. 7 Front View of Front Grille

4. Transmission Cooling

4.1 Outline of study

The top speed of the GR Yaris is 230 km/h (European specifications). When driving at high speeds like this, the temperature rise of the transmission fluid (six-speed manual transmission) must be restricted.

Although this can be accomplished by an oil cooler, the extra space required for piping and a pump and the resulting increase in weight would have a negative effect on the desired vehicle characteristics. Therefore, rather than relying on an oil cooler, this issue was resolved by increasing the heat transfer capacity of the air-cooled transmission surfaces.

4.2 Enlargement of case surface area

First, the heat transfer capacity was enhanced by adding fins to enlarge the area of the case. Fig. 8 shows the external appearance of the transmission case.

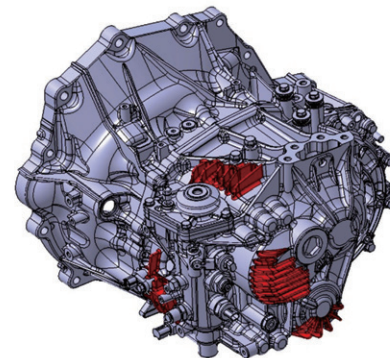


Fig. 8 Clutch and Transmissions Case (Extra Fins Shown in Red)

To increase the heat transfer area, the temperature distribution of the case surface in high-speed driving was measured in tests using a prototype vehicle. Heat transfer fins were provided on the case after repeated studies with the design department focusing on the high-temperature portions capable of effectively promoting heat transfer from the case surface.

As a result, this approach enhanced the heat transfer surface area of the case by approximately 9%.

4.3 Transmission cooling duct

The next study examined methods of lowering the transmission fluid temperature by promoting forcible heat transfer from the case surface. This can be accomplished by increasing the airflow speed across the case surface and by lowering the temperature of the cooling air. As the most effective way of achieving this is to bring in cool air through the front grille opening, a cooling duct was added to guide airflow to the front of the transmission. **Fig. 9** shows the location of this cooling duct.

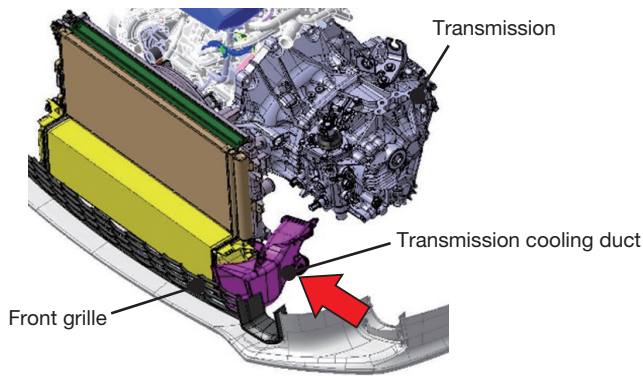


Fig. 9 Transmission Cooling Duct

The geometry of the cooling duct was studied using computational fluid dynamics (CFD) to maximize the effect of the duct within the limited available space.

The duct has to take in a sufficient volume of cooling air at the inlet, increase the speed of the airflow guidance by adopting a narrower sectional area at the outlet, and guide the cool air to the target locations. This was accomplished by adjusting the temperature, velocity, and position of the cooling air reaching the transmission case surface. The duct geometry (sectional area and outlet orientation) was determined to maximize the effect of these parameters. **Figs. 10** and **11** show the results of the CFD study. It should be noted that the heat-transfer coefficient is expressed as a non-dimensional number for comparison purposes.

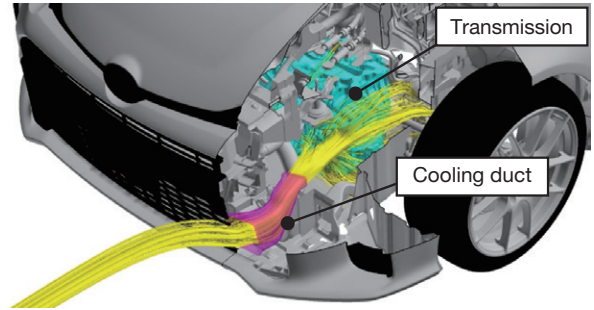
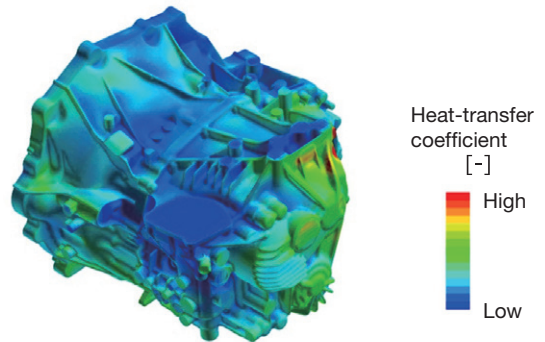
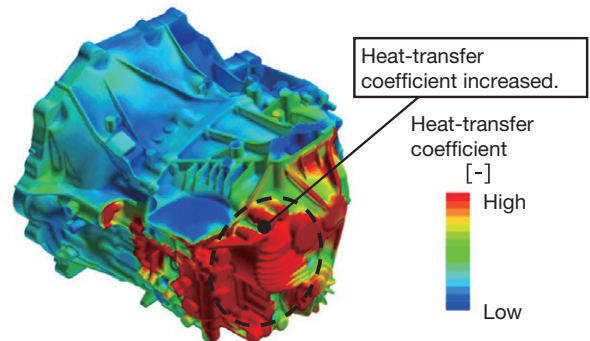


Fig. 10 CFD Results (Stream Lines)



(1) Without cooling duct



(2) With cooling duct

Fig. 11 CFD Results (Surface Heat-Transfer Coefficient Distribution)

Adopting this cooling duct raised the heat-transfer coefficient of the case surface by approximately 18% (**Fig. 12**).

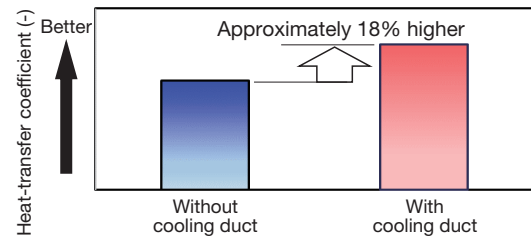


Fig. 12 Effect of Cooling Duct

The targeted improvement in heat transfer capacity was achieved by enlarging the case surface area and adding a cooling duct as described above (Fig. 13).

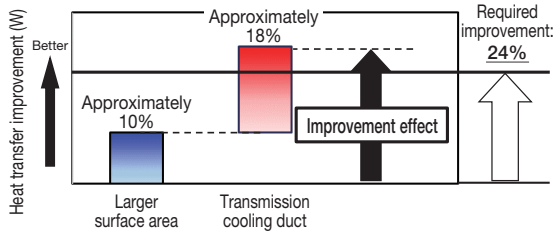


Fig. 13 Case Surface Heat Transfer Capacity Improvement Effect

5. Study of Intercooler Spray

5.1 Outline of development

With an air-cooled intercooler, engine power tends to depend on the ambient temperature. To maintain high power and prevent power loss during the summer or at other times with a high ambient temperature, an intercooler spray system was installed and optimized.

5.2 Component configuration and mounting position

The intercooler spray system mainly consists of a coolant tank and pump, spray nozzles, and a connecting hose (Fig. 14). The tank was mounted in the rear luggage compartment in consideration of the front/rear weight distribution of the vehicle. The tank capacity was set to 3.7 liters.

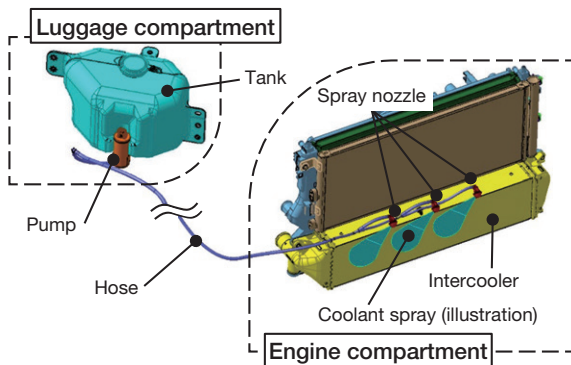


Fig. 14 Configuration of Intercooler Spray System

Three spray nozzles were located on the front surface of the intercooler behind the license plate so that the cooling air entering the grille opening is not blocked (Fig. 15).

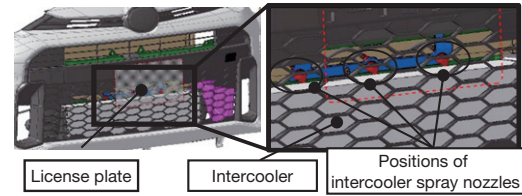


Fig. 15 Mounting Positions of Spray Nozzles

5.3 Optimization of spray nozzles

The spray nozzles were optimized to achieve the maximum cooling effect with the minimum spray volume.

The mounting interval and angle were set to maximize the area wetted by the spray on the intercooler front surface, and the spray direction was targeted toward the high-temperature side of the intake inlet. In addition, the optimum spray volume and timing were identified. An intermittent pattern of five-second sprays interposed with five-second intervals was adopted.

5.4 Confirmation of effect in actual driving

The intercooler outlet temperature was compared with and without the intercooler spray system under wide-open throttle acceleration. Fig. 16 shows the measured results.

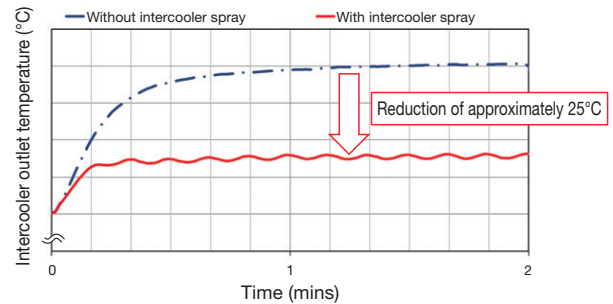


Fig. 16 Effect of Intercooler Spray System

The comparison results showed that the air temperature at the intercooler outlet was approximately 25°C lower with the spray, which would make a major contribution to maintaining engine power under high ambient temperatures.

6. Summary

(1) Engine cooling

The performance of the heat exchangers was ensured within the limited available space, thereby enabling sufficient cooling performance to achieve approximately twice the heat transfer capacity as the base Yaris.

(2) Transmission cooling

The development took on the challenge of enhancing the air-

cooling performance of the vehicle without relying on an oil cooler. Cooling performance that enables driving at high speeds up to 230 km/h was achieved while minimizing increases in mass.

(3) Intercooler spray system

Optimizing the spray system made a major contribution to minimizing decreases in engine power during the summer.

7. Conclusion

The team developing the cooling performance of the GR Yaris faced a number of completely new hurdles. Each of these hurdles was overcome by a united spirit to build an even-better car and bring a smile to the faces of as many customers as possible.

The development team is delighted to have contributed to Toyota's philosophy of building ever-better cars by delivering the type of confident, natural, and safe driving performance that supports the driveability of the GR Yaris.

The authors would like to express their sincere gratitude for the support of the development team that worked to overcome these hurdles, the readers of the *Toyota Technical Review*, and everyone that contributed to this development.

The year 2020 is likely to linger in the minds of many people. The GR Yaris is being launched as the world fights an invisible enemy and restrictions in its freedom. It is hoped that the GR Yaris can play even a small role in bringing freedom back to mobility and demonstrating the joy of driving a vehicle exactly according to the desires of the driver.

Authors



K. ISHITA



M. MATSUDA



A. MURAKAWA



Y. NISHIO



S. HATTORI

The Dedicated Sports Car Production Line –The GR Factory–

Motoyasu Machino*1
Hiroyuki Kitagawa*1
Yuya Arai*1
Hidetsugu Kitaori*2

Abstract

The GR Factory is a new dedicated production facility for GR models that was established to help build ever-better cars under the philosophy of Toyota Gazoo Racing, and is an important part of efforts to revitalize the legacy of pure-Toyota sports cars designed and produced first-hand by Toyota team members. The GR Factory incorporates the essential elements of a sports car, ensuring that each and every model is produced to the highest quality and finish.

Keywords: building ever-better cars, monozukuri, high rigidity, high accuracy, short-pitch welding, alignment, ground height, wheel load, thin plastic bumper, sheet molding compound (SMC)

1. Introduction

The inspiration to build a new dedicated production facility for the GR Yaris comes from the desire to recover the capability to produce sports cars inside Toyota, something that had been lost twenty years ago. The aims of building this facility were to build sports cars that would satisfy customers, use this experience to train and nurture Toyota’s team members, and to redefine the GR brand for the future (Fig. 1). Toyota has a strong motivation to produce and sustain sports cars by applying its own production engineering (PE) technologies to build ever-better cars and realize ever-more competitive manufacturing capabilities (*monozukuri*).

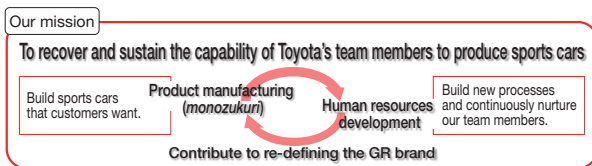


Fig. 1 Mission of the GAZOO Racing Company

2. The GR Factory Concept

To build ever-better cars, can customer satisfaction be achieved by disassembling completed cars in a racing team garage and increasing body rigidity by adding welding points (Photo 1), or by measuring each and every component, making the finest adjustments, and realizing customer needs by building ever-better cars ourselves? The GR Factory is the answer to this question. In the GR Factory, Toyota can take on

the challenge of planning new processes under the concept of building racetrack-ready cars that are available to ordinary customers.



Photo 1 Japanese Rally Championship (JRC) Car

Twenty years ago, Toyota brought its long history of sports car production to an end. To restart and sustain its capability to build sports cars, the GR Factory combines this challenging spirit with competitive *monozukuri* capable of realizing groundbreaking cost reductions even with low-volume production.

Ever-better cars are built on the three foundations shown in Fig. 2. The first foundation is drawings. Drawings are an indispensable part of the planning of cars with universally-acknowledged performance. The second foundation is the equipment capable of bringing these drawings to life. This equipment must be capable of building ever-better cars without restriction. The third foundation is the technical skill and passion upon which the building of ever-better cars depends. Passionate people are the driving force behind the building of ever-better cars, and craftspeople with sophisticated skills are a vital part of Toyota Gazoo Racing.

The GR Factory was established to help realize these ever-better cars under the philosophy of Toyota Gazoo Racing.

*1 GR Project Operation Div., GAZOO Racing Company

*2 Vehicle Quality & Production Engineering Div., Vehicle Production Engineering Field

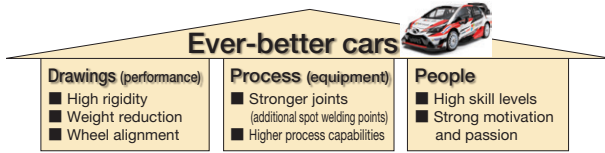


Fig. 2 Three Foundations of Building Ever-Better Cars

3. High Rigidity and High Quality

At a race car manufacturing facility, additional arc welding points are added to the body and various vehicle alignment parameters are adjusted. In these processes, body installation points and suspension components are measured one-by-one, selected, assembled, and tested.

At the GR Factory, Toyota aimed to realize the same methods as adopted for race cars within a full-scale manufacturing process.

3.1 Development of high body rigidity

To realize a highly rigid and high-quality body, the following three changes were made to conventional vehicle structures and manufacturing methods.

(1) Addition of spot welding points

As shown in **Fig. 3**, higher rigidity was achieved by shortening the spot welding pitch and increasing the number of spot welding points by 187 compared to the base Yaris. As a shorter welding pitch usually lowers the strength of each weld, new welding conditions and control methods were adopted to ensure sufficient welding strength. The red dots in **Fig. 4** show the areas in which the welding pitch was shortened.

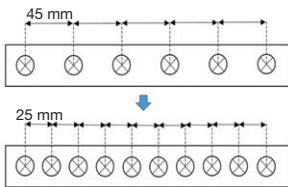


Fig. 3 Shorter Pitch Welding

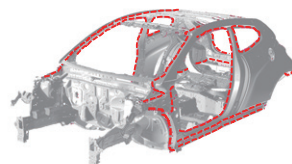


Fig. 4 Additional Spot Welding Points

(2) Addition of structural adhesive

Rigidity was also increased by increasing the coating area of structural adhesive, which is cured in a paint drying oven at a temperature of approximately 200°C, by 11 meters compared to the base model. Unlike welding, adhesive enables the formation of linear joints. It can be combined with welding to achieve even higher rigidity.

Structural adhesive was added primarily in the locations shown by the red lines in **Fig. 5**. These are locations at which high rigidity is particularly important and include joints between the under and upper body as well as around suspension member attachment points. This adhesive is carefully applied manually by the craftspeople on the line (**Photo 2**).

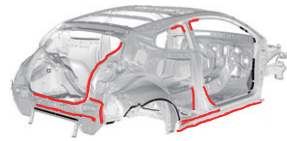


Fig. 5 Locations of Additional Structural Adhesive



Photo 2 Craftsperson at Work

(3) Completion of spot welding using single jig

This development focused on using a single welding jig as a way to enhance body accuracy. The assembly process was designed to complete welding without unclamping. This approach is an effective way of minimizing product variation (**Photo 3**), and makes a major contribution to improving quality (especially alignment) in the assembly process (described in more detail below).



Photo 3 Completion of Spot Welding Using Single Jig (General-Purpose Cell)

3.2 Highly accurate suspension assembly

To guarantee basic vehicle dynamic performance, a new system for assembling and securing the axle centers of the four wheels (i.e., the tire centers) in accordance with the drawings was adopted. The suspension attachment points are measured in the body production process (**Fig. 6**). In addition, every suspension component (suspension members and arms) is measured in the assembly process (**Fig. 7**). Each vehicle is then assembled and calculated on a computer and the results are fed back as instructions to every process. This approach enables extremely accurate assembly and results in variation-free completed models.

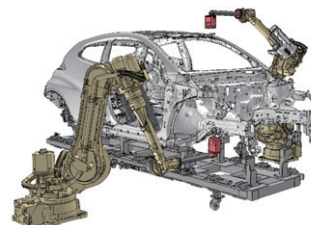


Fig. 6 Measurement of Suspension Attachment Points

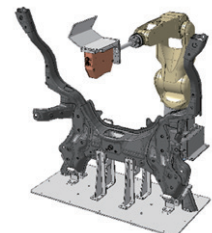


Fig. 7 Measurement of Suspension Components

Fig. 8 shows the concept for assembling the axle centers of the four wheels in accordance with the drawings.

The assembly jig uses the measured body and accuracy data

to automatically adjust the position and angle of each component so that the axle centers of the four wheels match the normal dimensions on the drawings in the completed vehicle state. As a result, the line workers are able to assemble the vehicle as normal. The suspension can be assembled to the vehicle with high accuracy by fixing the adjusted suspension jig to the surface plate and mounting the body on top.

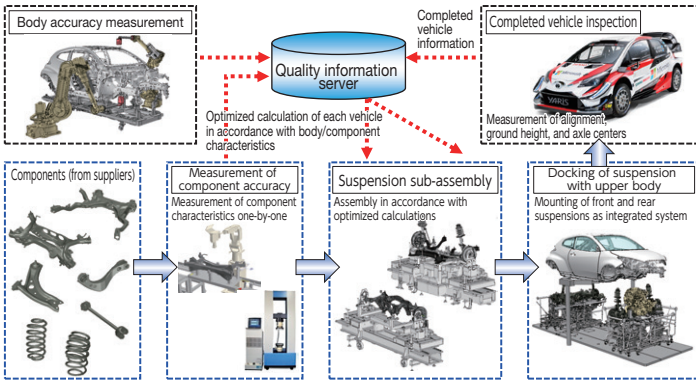


Fig. 8 Highly Accurate Suspension Assembly System

Fig. 9 shows the measured results of the front camber angle (i.e., the tire inclination angle when view from the front of the vehicle) as an example of a parameter requiring alignment. These results indicate that variation has been minimized, realizing accuracy close to the normal dimensions on the drawings for any vehicle.

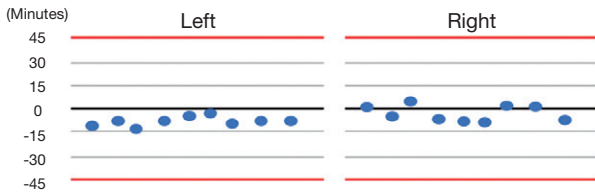


Fig. 9 Measurement Results for Front Camber Angle

3.3 GR Factory vehicle inspection process

The GR Factory applies the adjustment technologies learned from race cars to the vehicle inspection process to realize suspension quality that can be used in races without any further adjustment.

(1) Highly accurate alignment adjustment

Before carrying out adjustment, the car is placed on a low-stress turntable and moved across a wavy road to run in the chassis by the application of the appropriate amounts of vertical and lateral vibration (Photo 4). As a result, the car can be taken to the alignment tester (Photo 5) in the optimum state.

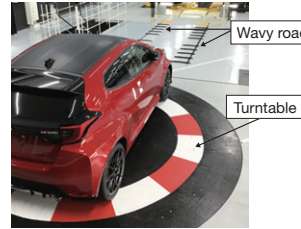


Photo 4 Turntable + Wavy Road



Photo 5 Alignment Tester

In the alignment adjustment process, the adjustment is carried out with weight equivalent to two occupants placed in the vehicle, simulating the state of a race car (Photos 6 and 7). After the adjustment is completed, the alignment is measured to ensure highly accurate suspension quality.

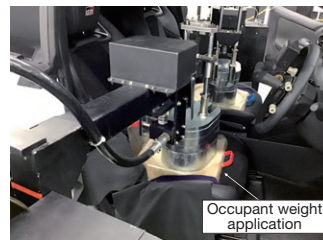


Photo 6 Weight Application



Photo 7 Alignment Adjustment

(2) Measurement of vehicle specifications

The ground height, wheel load, and brakes are important elements for race cars. Each individual component is measured and precisely assembled. In the final process, these elements are then measured and confirmed using the completed vehicle. For the ground height and wheel load, the wheels on opposite corners are measured and confirmed in addition to the front and rear and the left and right wheels (Photo 8). Furthermore, axle center measurement, which is a process that can be carried out most easily at the production plant, is used to measure whether the tires (wheel hubs) are located in the correct position with respect to the body, thereby confirming the assembly accuracy that affects alignment (Photo 9).

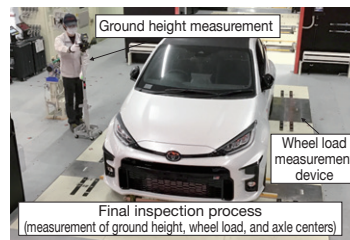


Photo 8 Ground Height and Wheel Load Measurement

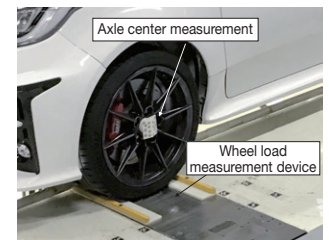


Photo 9 Axle Center Measurement

For brake performance, the hydraulic brake pressure in reaction to pedal inputs (pedal effort and stroke) are measured to confirm that there are no vehicle-to-vehicle differences in brake feeling (Fig. 10).

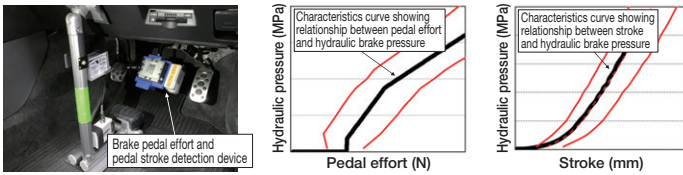


Fig. 10 Hydraulic Brake Pressure Characteristics Measurement

4. Weight Reduction

The weight of key components of the GR Yaris was reduced with the aim of realizing racing car-like performance.

For example, the weight of the body was reduced by adopting aluminum for the doors, hood, and back door, and carbon fiber reinforced plastic (CFRP) for the roof. In addition, the world's lightest front and rear bumpers were developed through the application of PE technologies (Fig. 11).

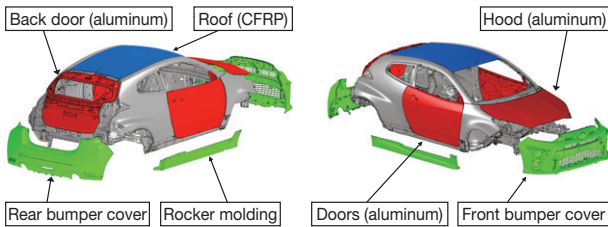


Fig. 11 Locations Adopting Lightweight Materials

4.1 Aluminum panels

Since the vehicle uses aluminum panels, a dedicated aluminum welding cell was added to the body production process. Instead of aluminum friction stir welding (FSW), aluminum spot welding was adopted since this process results in superior shear and peeling fracture load properties. Photo 10 shows the cross sections produced by each type of welding. The images clearly demonstrate the high strength provided by aluminum spot welding.

Adopting this welding process reduced running costs by 60% while improving productivity by 55% due to the shorter welding time required.



Photo 10 Cross Sections (Left: Spot Welding, Right: FSW)

4.2 Thin plastic bumpers

To help enhance vehicle dynamic performance, PE technologies were developed to form thin front and rear bumpers, which are large external components forming part of the front and rear overhangs, and rocker moldings. The developed technology can be adopted in a wide range of vehicle components.

The development target was to reduce enough weight to be noticeable when the car is driven. In specific terms a weight reduction target of 25% was set. This was accomplished by lowering the average sheet thickness by 25% from 2.6 to 1.9 mm. However, since changing materials has a major effect on production models and requires a long development leadtime, the GR Yaris aimed to reduce the thickness of the sheets through the development of PE technologies.

To ensure sufficient surface stiffness, the sheet thickness distribution was optimized by adopting thicker sheets for areas without character lines and thoroughly reducing the thickness in other areas.

The greatest concern with thin sheets is a deterioration in moldability. Therefore, the optimum molding conditions were established using computer aided engineering (CAE) after greatly enhancing analysis accuracy. This development also optimized the molding conditions to enable the mold to be filled in an extremely short amount of time by boosting the filling rate during the initial flow-in.



Fig. 12 CAE Flow Analysis for Front Bumper



Fig. 13 CAE Flow Analysis for Rear Bumper

Figs. 12 and 13 show the CAE flow analysis results using the developed technology. In the case of a thin product, the mold tends to absorb heat from the plastic more quickly, thereby increasing the viscosity of the plastic and reducing flowability at the product ends. However, the development made use of this phenomenon to greatly reduce the cooling time in the mold. A molding cycle time of less than 25 seconds was achieved, including an injection time of between 1.4 and 1.7 seconds, and a cooling time of 4 seconds. This technology also helped to lower costs by reducing the amount of plastic used by 25%.

4.3 CFRP roof manufactured using SMC

As a component located far from the vehicle center of gravity, the weight of the roof was reduced to help further enhance dynamic performance.

The carbon fiber molding technology developed in the past for the Lexus LFA was applied to the GR Yaris to produce a

Special Feature

CFRP roof using SMC, a process that combines excellent productivity with low weight and high stiffness.

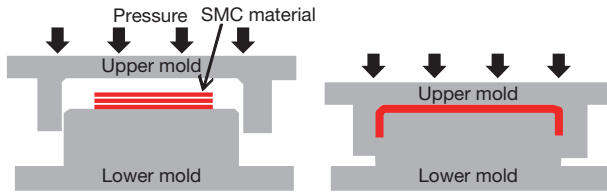


Fig. 14 CFRP Molding Method Using SMC

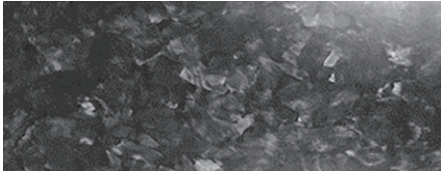


Photo 11 External Appearance of CFRP Molded Using SMC

As shown in Fig. 14, the CFRP molding process using SMC involves cutting the carbon fiber sheets into the specified shape, placing the cut sheet into a mold, and stamping the sheet at high pressures and temperatures. The result is an extremely strong molded product with a marbled pattern as shown in Photo 11.

Fig. 15 shows the results of an investigation into the relationship between molding time and material viscosity with the material and thickness used by the GR Yaris.

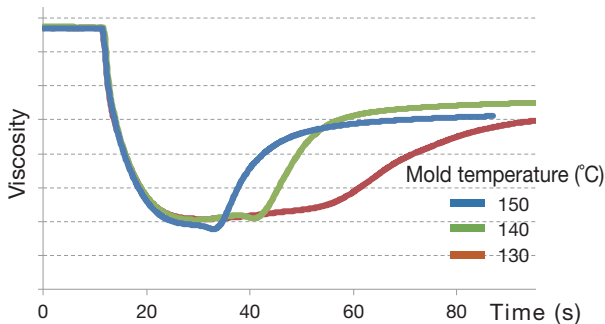


Fig. 15 Viscosity of CFRP Molded Using SMC

After incorporating these results, the material input size was studied using CAE (Fig. 16). By stamping the sheet at the timing of the lowest viscosity, moldings with excellent properties can be obtained within a short cycle time.

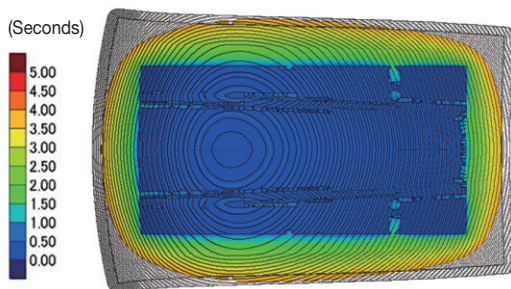


Fig. 16 Results of Molding CAE for CFRP Molded Using SMC

5. Actions for the Future: Changes to Model Type and Production Volume

To homologate the GR Yaris for participation in the WRC or Rally2 category in Japan, it must have an annual production volume of 25,000 units. Stable production to achieve this standard is guaranteed for the first year after launch. However, the production volume of a sports car from the second year is extremely difficult to predict, and is likely to fall to several hundred units per month or even less. In addition, Toyota is aiming to launch a succession of new GR models to help build the GR brand. As mentioned above, to support the building of ever-better cars with competitive *monozukuri*, the GR Factory was constructed on a cell basis to enable rapid responses to changes, such as fluctuations in production volume or additional models, while strictly following the guidelines of the Toyota Production System (TPS), and to maintain high productivity.

The cell-based approach for the body production process involves the adoption of so-called general-purpose cells. Transportation to these cells is carried out by automated guided vehicle (AGVs, Photo 12).

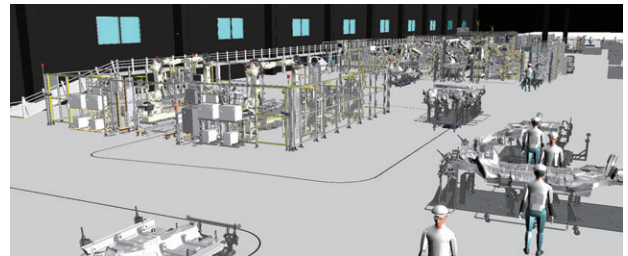


Photo 12 Body Production Process

The process is divided into general-purpose and dedicated sections. In the general-purpose section, all the cells are the same. By adopting common cells like this, any cell can perform any sub-assembly process and models can be added simply by adopting a new dedicated section. In addition, flexible response to changes in production volume can be achieved by increasing or decreasing the number of general-purpose cells. Furthermore, if new technology is introduced, this can be accommodated by adding a dedicated cell for that technology.

The assembly process uses cells for mounting the engine and chassis to ensure high suspension quality. The component assembly process uses AGVs for transportation without any conveyor belts (Photo 13).



Photo 13 Assembly Process

In the engine and chassis mounting process, high quality is realized by stopping the assemblies and working in fixed positions. Transportation is also carried out by AGVs, which are flexible enough to be compatible with the different number of work hours required by different models, thereby enabling high productivity.

6. Conclusion

Twenty-seven vehicles were manufactured in the GR Yaris production trial and tested on Toyota's Higashifuji, Shimoyama, and Motomachi Plant proving grounds by the professional race drivers Hiroaki Ishiura and Kazuya Oshima, who acted as the test drivers for the GR Yaris. These tests confirmed that the variation of the vehicles is substantially less than previous models.

It might be stated with some confidence that the GR Factory is capable of building sports cars that satisfy customer requirements. However, Toyota intends to continue developing ever-better PE technologies and nurturing the skills and craftsmanship of its team members to achieve even greater heights in the future.

Authors



M. MACHINO



H. KITAGAWA



Y. ARAI



H. KITAORI

Development of Teammate Advance Drive –An Advanced Driving Assistance System Using Automated Driving Technology–

Masaki Matsunaga*¹
Osamu Ozaki*²
Koichiro Kimura*²
Koichi Hara*²
Shinya Okawa*²
Takeshi Sasuga*¹

Abstract

Teammate Advanced Drive is the latest advanced driving assistance system developed based on the Mobility Teammate Concept, Toyota’s unique approach to automated driving technology. This system is capable of performing the following actions on highways and other vehicle-only roads under driver supervision: maintaining lanes and vehicle-to-vehicle distances, branching off, changing lanes, and overtaking. This article describes an outline of this system, as well as the characteristics and details of the technologies involved.

Keywords: advanced driving assistance, automated driving, LiDAR, high-precision map, over-the-air (OTA), human machine interface (HMI), redundancy design

1. Introduction

Toyota is developing automated driving technologies with three main aims: to help enhance safety, increase the freedom of mobility, and preserve the environment (**Fig. 1**), all with the objective of helping to realize a society in which everyone can move safely and freely.⁽¹⁾

Toyota Teammate is an advanced driving assistance system that was developed based on the Mobility Teammate Concept (**Fig. 2**), Toyota’s unique approach to automated driving technologies. This concept treats the driver and vehicle as partners and aims to enhance the mutual interaction between them, rather than simply taking over control and replacing the role of the driver.

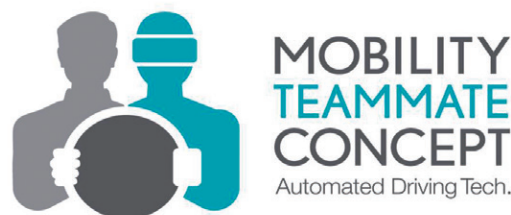


Fig. 2 The Mobility Teammate Concept Logo

2. Outline of the Teammate Advanced Drive System

Teammate Advanced Drive is a system that provides the appropriate support for the cognition/decision making/operation process during driving on highways and other vehicle-only roads under driver supervision. Under these conditions, it is capable of maintaining lanes and vehicle-to-vehicle distances, branching off, changing lanes, and overtaking (**Fig. 3**). Constantly prioritizing safety in the decision-making process encourages driver trust in the system and facilitates driving operations and the creation of a driving experience in concert with driver intentions that also reflects the characteristics of the manufacturer. By doing so, the system helps to reduce the workload created by accelerating, braking, and handling during long drives, and helps to enhance safety by freeing the driver to take even greater care of the traffic environment around the vehicle. Furthermore, the system is also equipped with state-of-the-art hardware that allows new maps, functions, and performance aspects to be added even after sale through a new over-the-air (OTA) software update function.



Fig. 1 Aims of Automated Driving Technology Development

*¹ Automated Driving & Advanced Safety System Development Div., Advanced R&D and Engineering Company

*² Toyota Research Institute - Advanced Development, Inc.

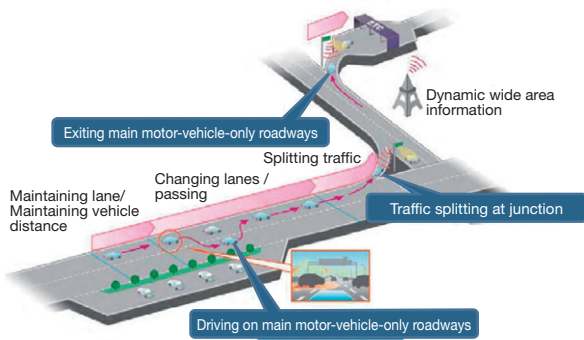


Fig. 3 Illustration of Advanced Driving Assistance

2.1 System outline

This system is equivalent to a level 2 automated driving system as defined by the Society of Automotive Engineers (SAE).⁽²⁾ The principle system configuration and control flow are as follows.

This system is an extension of the Lexus Safety System +A (LSS+A) that was launched in 2017. In addition, it supplements the existing sensors of other advanced driving assistance systems (ADAS) with the additional sensors, electronic control units (ECUs), and actuators required to realize the functions and performance of the Teammate Advanced Drive system. The result is a robust system that provides a full range of existing safety functions while also offering an even more confident, natural, and safe driving experience (Fig. 4, Tables 1 and 2).

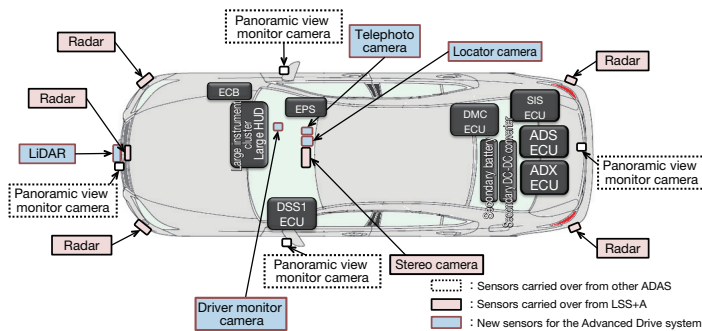


Fig. 4 Advanced Driving System Configuration Diagram

Table 1 Main ECUs and ECU Functions

ECU	Function
ADS ECU	Recognition/localization/vehicle dynamics control
ADX ECU	Recognition by AI/future functional expansion
SIS ECU	Output of high-precision map information
DMC ECU	Driver recognition/monitoring
DSS1 ECU	LSS+A functions

Table 2 Other Main Component Parts and Functions

Component part	Function
Secondary battery	Redundant power supply
Secondary DC-DC converter	DC-DC inverter for the redundant power supply
Instrument cluster/HUD	Instrument cluster/head-up display
ECB	Braking for the system control
EPS	Electronic power steering for the system control

In addition, Fig. 5 illustrates the Teammate Advanced Drive system control. The system replaces and realizes the cognition → decision making → operation process of the driver with an automated driving planning → control/human machine interface (HMI) process based on surrounding environment recognition/localization → prediction and judgment technology.

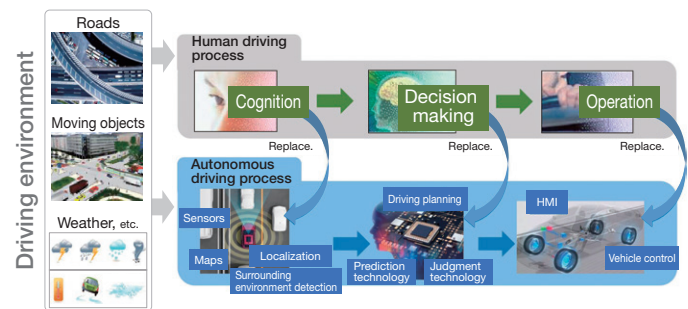


Fig. 5 Flow of Advanced Drive System Control

3. Technical Characteristics of the Teammate Advanced Drive System

The five technical characteristics of the Teammate Advanced Drive system can be defined as perceptive, intelligent, interactive, reliable, and upgradable.

This section describes each of these characteristics in turn.

3.1 Perceptive (sophisticated detection performance)

Highly reliable and accurate 360-degree coverage around the vehicle is achieved by combining sensors with different characteristics, such as light detection and ranging (LiDAR) systems, cameras, radar, and high-precision maps (Fig. 6). This combination is capable of detecting and identifying the surrounding traffic environment. The high-precision maps are capable of recognizing the road farther ahead of the vehicle by looking ahead to areas beyond the range of the sensors mentioned above. In addition, the position of the driver's vehicle can be identified with a high degree of accuracy by combining the camera and LiDAR detection functions with high-precision map and global positioning system (GPS) information (Fig. 7).⁽³⁾ In total, these sensors and systems have a far greater detection performance than previous ADAS.

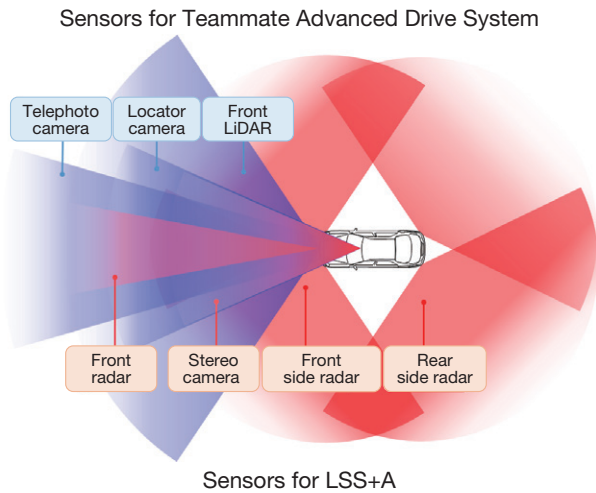


Fig. 6 360-Degree Sensing

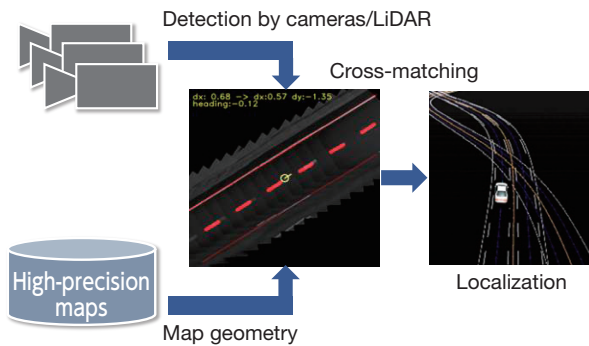


Fig. 7 Localization Using High-Precision Maps

3.2 Intelligent

To help realize the early detection of hazards, formulate the appropriate driving plans, and facilitate smooth control in a constantly changing traffic environment, this system is equipped with artificial intelligence (AI) technology centered on deep learning. This technology helps to increase the number of scenarios that can be predicted and handled by the system under various conditions that might be encountered while driving. This helps to ensure safety and driving stability in complex road environments. These functions are realized through high computing power achieved by combining massive amounts of data obtained from driving with multiple high-performance system-on-a-chip (SoC) integrated circuits.

To provide more confident, natural, and comfortable driving assistance for all vehicle occupants, the system features a control that smoothly combines longitudinal and lateral acceleration (Fig. 8). In addition to scenarios such as lane changing and branching off, the vehicle is driven in its own lane while considering the surrounding vehicles (i.e., the position of the driver's vehicle and how it gives way to merging vehicles, Fig. 9) to realize confident, natural, and safe controls as an integrated system.

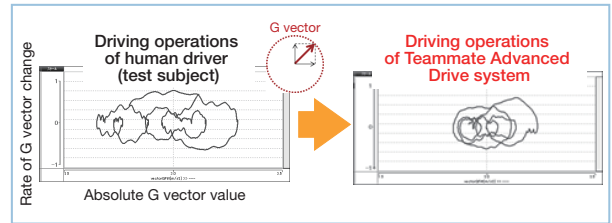


Fig. 8 Longitudinal and Lateral Acceleration Control

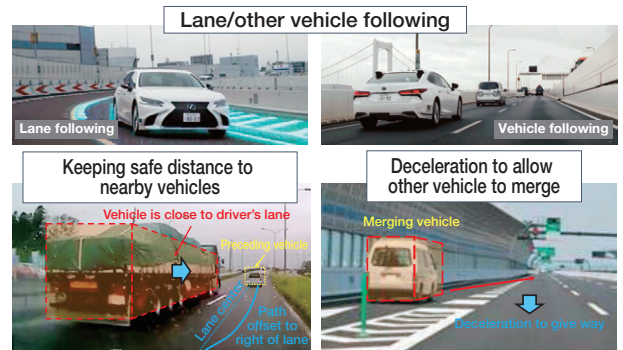


Fig. 9 Controls to Realize Basic Functions and Confident, Natural, and Safe Driving

3.3 Interactive (interaction between driver and vehicle)

This section presents an example of the sophisticated driver-centric driving assistance HMI of the Teammate Advanced Drive system. The Teammate Advanced Drive system features a specialized HMI that communicates between the driver and vehicle so that each has a correct awareness of each other's status at all times. Fig. 10 shows an example of a prototype display.

Fundamentally, the vehicle uses a simple easy-to-read display to communicate the driving situation (e.g., the surrounding vehicles, structure of the road ahead, and future actions of the driver's vehicle) to the driver. If a scenario arises that the system is not fully capable of handling, the HMI is designed to give the driver adequate time to provide support to the vehicle. The system also incorporates innovative functions to facilitate confident, natural, and comfortable driving over long distances, such as audible cues generated by the vehicle depending on the state of the driver (Japanese market only).

If the vehicle judges that the driver is incapable of continuing to drive due to a sudden change in the driver's physical condition or the like, the vehicle will slow down and stop on the road shoulder if possible, thereby helping to reduce the possibility of causing or becoming involved in an accident, or mitigating the damage if an accident should occur (Fig. 11).



Fig. 10 Intuitive and Easy-to-Read Instrument Cluster Display

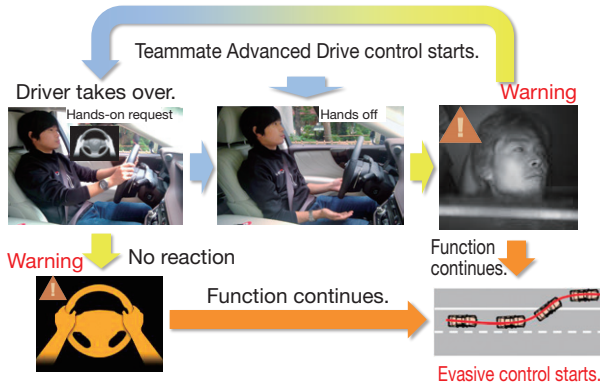


Fig. 11 Interaction with Driver and Emergency Evasive Actions

3.4 Reliable

To realize a comfortable, confident, natural, and safe system, thorough testing and evaluation was carried out under various environments. This involved actual vehicle driving tests and simulated large-scale data tests carried out from both real and virtual standpoints.

The system design also incorporates redundancy into the power supply systems, steering systems, sensors, on-board networks, ECUs, calculation devices, algorithms, and the like (Fig. 12) to help realize a highly reliable system configuration capable of handling unforeseen circumstances.

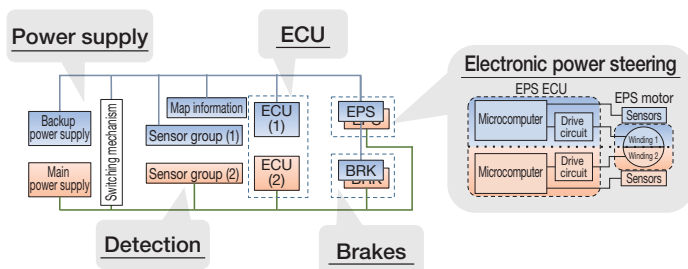


Fig. 12 Redundancy Design

3.5 Upgradable (software updates)

This system incorporates Toyota’s first OTA control system, which is one method of enabling software updates. The system also collects data on vehicle usage and control results after purchase by the customer.

The accumulated data can be used to continuously provide enhanced or additional functions. The OTA system also allows control and high-precision map software to be updated after purchase. This enables constant access to the latest driving assistance technology as well as the confident, natural, and safe driving performance that this technology provides, while also enabling the vehicle to be continuously updated.

This technology represents an important attempt by Toyota to transform its conventional concept of vehicle development and to swiftly meet the needs of customers in the coming software-first age.

4. Future Direction

The Teammate Advanced Drive system that was introduced in this article is not yet ready for adoption on a wide range of vehicles.

To help realize an accident-free society and enhance the quality of life (QOL) for everyone around the world, it will be necessary to further and more smartly integrate and simplify sensors, ECUs, and other components. However, Toyota is confident that the knowledge and system infrastructure obtained during the course of this development will provide the foundation for more widely available systems in the future.

Toyota is aiming to provide safe forms of mobility to all, even those who cannot drive, and the establishment of fully automated driving technologies will be extremely important to finally realize this objective. With this in mind, Toyota Research Institute - Advanced Development, Inc. intends to continue facing up to and overcoming the challenges of the future.

References

- (1) K. Koibuchi et al. “Overview of the Latest ADAS & Automated Driving Technologies to Achieve Zero Traffic Fatalities.” *JSAE Journal* Vol. 74 (2020) pp. 10-16.
- (2) Guideline Regarding Safety Technology for Automated/Autonomous Vehicles. Road Bureau of the Ministry of Land, Infrastructure Transport and Tourism (2018).
- (3) M. Matsunaga et al. “Research into Automated Driving System on Highway.” *Toyota Technical Review* Vol. 63 (2017) pp. 40-45.

Authors



M. MATSUNAGA



O. OZAKI



K. KIMURA



K. HARA



S. OKAWA



T. SASUGA

Research into Generation of Atmospheric Secondary Organic Aerosols from Gasoline Vehicle Emissions Using Photochemical Reaction Experiments Simulating Solar Radiation

Daisuke Hayashi*¹
Tetsuya Yamashita*¹

Abstract

Air pollution caused by fine particulate matter (commonly known as PM_{2.5}) has become a global issue. This particulate matter (PM) contains secondary organic aerosols (SOA) that are generated from gaseous hydrocarbons by photochemical reactions. A wide range of photochemical reaction experiments have been conducted to study SOA generated from gasoline vehicle emissions. It has been reported that the amount of SOA generated in this way is at least ten times higher than tailpipe PM emissions. However, most of these experiments have used light sources with different spectra and intensity than actual solar radiation. Therefore, this research created a light source simulating the spectra and intensity of solar irradiation and examined the SOA formation potential of the main hydrocarbons. The results found that the estimated amount of SOA generated from gasoline vehicle emissions is between 0.3 and 1.7 times the amount of tailpipe PM emissions.

Keywords: secondary organic aerosol (SOA), photochemical reaction, smog chamber, SOA formation potential, solar radiation, gasoline vehicle, emissions, hydrocarbon

1. Introduction

The non-attainment of air quality standards for fine particulate matter (commonly known as PM_{2.5}) is an issue faced by urban areas around the world. In Japan, the Ministry of the Environment set up the Technical Committee on Fine Particulate Matter in 2014 as an ongoing forum for experts to discuss countermeasures for PM_{2.5}. In 2015, this committee issued a report entitled “Countermeasures to Suppress Emissions of Fine Particulate Matter in Japan (Interim Report),”⁽¹⁾ which summarized the discussions of the committee to date. One of the medium- to long-term issues that this report highlighted was the secondary generation of PM_{2.5}. The report particularly emphasized the importance of identifying the mechanism behind the generation of secondary organic aerosols (SOA). SOA are particles formed via the photooxidation of gaseous volatile organic compounds (VOCs) by solar radiation, and have been recognized as a major component of PM_{2.5}. These VOCs, which act as precursors for SOA, are emitted from vehicles and other mobile sources, as well as from point sources such as paints and fuel evaporative emissions. In particular, it is well known that hydrocarbon (HC) emissions from gasoline vehicles increase under cold-start conditions. Such emissions are seen as a major source of SOA precursors in urban areas. While many studies on SOA formation from

gasoline vehicle emissions have been conducted, most of these studies have used a type of experimental apparatus called a smog chamber to simulate atmospheric photochemical reactions. Some results of these studies have suggested that SOA generated from gasoline vehicle emissions is at least ten times higher than particulate matter (PM) emitted from tailpipes.⁽²⁾

However, most of these studies were conducted using light sources, precursor concentrations, and other conditions that differ from actual atmospheric conditions. The light source and spectrum are two of the most important of these experimental conditions. Many of these studies used a type of lamp called a black light, which has a spectrum that peaks at a certain wavelength in the ultraviolet (UV) light range.⁽²⁾⁽³⁾ This might cause different reactions than those that occur in the actual atmosphere because the spectrum of the light source affects the formation and decomposition of the radical components that cause photooxidation.

Therefore, the study described in this article aimed to estimate the SOA formation potential of gasoline vehicles under conditions closely resembling the actual atmosphere and gain new findings that might contribute to understanding the actual effect of SOA generated from gasoline vehicle emissions. The SOA formation potential of HCs contained in gasoline vehicle exhaust gas was estimated using a smog chamber with a light source that simulates the actual spectrum of solar radiation. The results found that the SOA formation potential of

*¹ Advanced Powertrain Planning & Management Div., Powertrain Company

aromatic HCs, which are regarded as the primary SOA precursors, is less than conventionally thought, and that the SOA formation potential of the gasoline vehicle emissions investigated in this study is between 0.3 and 1.7 times the amount of tailpipe PM emissions. These results underline the importance of obtaining a deeper understanding of the effects of experimental conditions, such as the light source spectrum of the smog chamber, through identifying the actual behavior of SOA.

2. Methodology

2.1 Smog chamber experiment

A smog chamber is a type of experimental apparatus used to investigate the formation and decomposition of gases and particles due to photochemical reactions by exposing gases and particles in a chamber (a reactor vessel) to the light from a UV lamp instead of actual sunlight. **Fig. 1** illustrates the configuration of the smog chamber created for this study. This smog chamber consists of a chamber, light source, thermoregulator, and various measurement apparatus arranged inside a closed container.

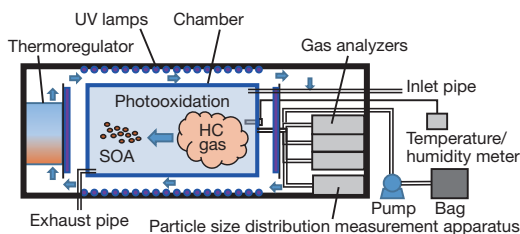


Fig. 1 Component Parts of Smog Chamber (Manufactured by Ceric Corporation)

The chamber is an enclosed space constructed using a Teflon film (Toyoflon FEP film with a thickness of 50 μm), which is highly permeable to UV light and less susceptible to HC adsorption, and supported by an aluminum frame. The chamber volume is approximately 2 m^3 (approximate dimensions: length = 2 m, width = 1 m, height = 1 m).

The light source of the smog chamber was designed to approximate the standard average daytime solar radiation of a mid-latitude region (AM1.5) through the spectrum and intensity of the ultraviolet band (wavelength: from 300 to 400 nm), which have a large impact on photochemical reactions. Type 40 (length: 1,198 mm) fluorescent UV lamps with different spectra were laid out around the chamber on six sides. The lamps consisted of 12 UVA-340 lamps manufactured by Q-Lab Corporation and 120 FL40SB lamps manufactured by Mitsubishi Electric Corporation. **Fig. 2** shows the composition of the resulting synthetic light source spectrum.

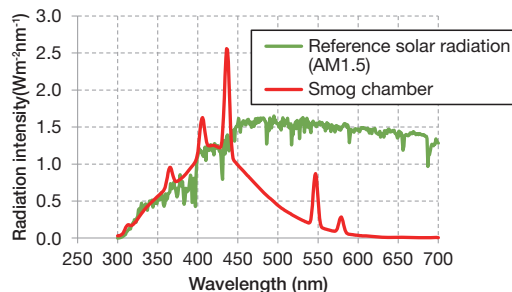


Fig. 2 Light Source Spectrum of Smog Chamber

The average of values measured at five points (the center point of the chamber and points at the same height at the four corners) was calculated. The measured values for each point consisted of the totals at the upper and lower surfaces sides as measured by an S-2440 solar spectroradiometer manufactured by Soma Optics, Ltd.

The thermoregulator functioned to prevent the gas temperature inside the chamber rising due to the heat generated by the UV lamps by circulating and cooling the air outside the chamber to maintain a constant temperature. This was sufficient to maintain a constant temperature inside the chamber.

The PM inside the chamber was measured by a model 3080 scanning mobility particle sizer (SMPS) manufactured by TSI. This apparatus is capable of measuring the distribution of particle sizes from 15 to 640 nm and calculates the mass concentration of the particles by multiplying the volume concentration (assuming that the particles are spherical) by the common particle density of 1.2 g/cm^3 used for particle measurement. In addition, the rate of particle concentration decrease due to adsorption by the chamber walls was assumed to be proportional to the particle concentration. The calculations compensated for this rate of particle concentration decrease using actually measured data showing the rate of particle concentration decrease in the chamber with the UV light turned off.

The concentrations of gaseous substances (NO_x , non-methane hydrocarbons (NMHC), and ozone) were respectively measured by the APNA-370, APHA-370, and APOA-370 atmospheric gas component concentration analyzers manufactured by Horiba, Ltd. (these are collectively called “gas analyzers” throughout this article). To measure individual HC components, the gas inside the chamber was sampled by the pump into the bag (the Smart Bag PA with a volume of 10 liters manufactured by GL Sciences Inc.). Quantitative analysis of the concentration of each HC component was carried out using a GC-2010 gas chromatograph (GC) manufactured by Shimadzu Corporation via an HP764 gas sample condensation system manufactured by GL Sciences Inc.

The procedure of the SOA generation experiment carried out in the smog chamber was as follows.

First, to remove the residue of the previous experiment, the chamber was filled with moist purified air and irradiated with the UV light for 6 hours at a temperature of 40°C and a relative

humidity of 50%. This has the effect of vaporizing and oxidizing the residue in the chamber. Then, the UV light was turned off, and the chamber was purged and cleaned overnight using purified air.

On the day of the experiment, moist purified air was introduced into the chamber with the UV light turned off. After adjusting the temperature to 25°C and relative humidity to 50%, the background concentrations of the chamber were confirmed to be sufficiently low using the gas analyzers and the SMPC and GC apparatus. Next, the gases and particles were introduced into the chamber through the inlet pipe at levels corresponding to the experimental conditions. The UV light was then turned on to start the photochemical reactions. The temperature and relative humidity in the chamber with the UV light turned on were adjusted to remain steady at 25°C and 50%, respectively. The generation of SOA by these photochemical reactions was measured using the SMPS at five-minute intervals after turning on the UV light. The decrease in gaseous components regarded as precursors was measured using the GC immediately after turning on the UV light (initial conditions), and then after 0.5, 2, 3, and 4 hours. The UV light was turned off after 4 hours to stop the photochemical reactions.

2.2 Measurement of SOA formation potential of HC components

The exhaust gas of gasoline vehicles contains a large number of HC components. This study investigated the SOA formation potential of aromatic HCs with a carbon number of 7, 8, or 9 (abbreviated below as C7, C8, and C9), which are regarded as having a high SOA formation potential. The following components were selected to represent each of these aromatic HCs: toluene, *o*-xylene, and 1,2,4-Trimethylbenzene (TMB).

Table 1 lists the initial conditions of each smog chamber experiment. To approximate atmospheric conditions in the experiment, NO_x and ammonium sulfate particles were introduced into the chamber to coexist with the aromatic HCs. The initial concentration of these substances was adjusted to around the same concentration as the air in Japan.

Table 1 Initial Concentration Conditions of C7 to C9 Aromatic HC Smog Chamber Experiment

No.	Type	Component	Initial concentration		
			Applicable aromatic HC (ppbC)	NO _x (ppb)	Ammonium sulphate particles (μg/m ³)
1	C7	Toluene	749	38	5
2			1118	37	6
3	C8	<i>o</i> -xylene	569	43	3
4			689	37	7
5	C9	1,2,4-TMB	728	38	5
6			809	49	4

Fig. 3 shows an example of SOA generation and HC decrease due to photochemical reactions, which is one of the results of the smog chamber experiment described above. Data about the quantities of SOA generation and precursor decrease was obtained from these experimental results.

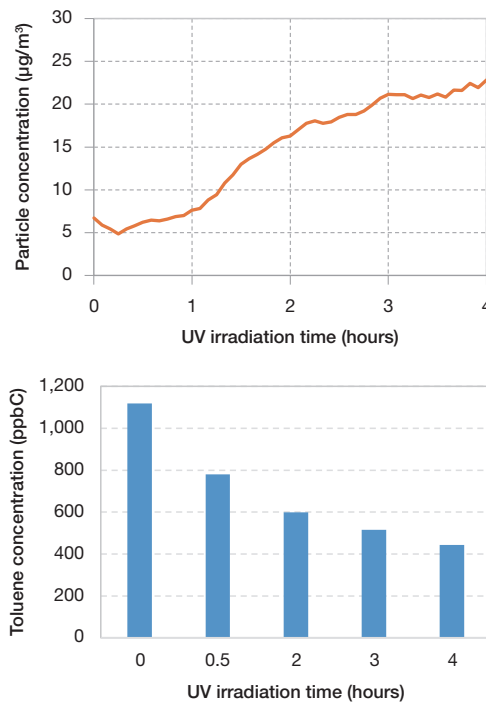


Fig. 3 SOA Generation and Precursor Decrease due to Photochemical Reactions in Smog Chamber Experiment No. 2

The two-product model is a theory that describes the relationship between SOA generation and precursor decrease. This theory attempts to quantitatively explain the generation of SOA, which occurs alongside a wide range of other products, by assuming that only two types of products with different volatility and yield are generated. Under this theory, the

relationship between SOA generation and precursor decrease under constant temperature conditions (25°C) can be expressed as follows by Equations 1 and 2.

$$Y_i = \frac{SOA_i}{\Delta HC_i} = M_0 \left(\frac{\alpha_{1,i} \kappa_{1,i}}{1 + \kappa_{1,i} M_0} + \frac{\alpha_{2,i} \kappa_{2,i}}{1 + \kappa_{2,i} M_0} \right) \quad (1)$$

$$M_0 = POA + \sum_i SOA_i \quad (2)$$

where,

- i : type of HC component
- SOA_i : SOA generated from i ($\mu\text{g}/\text{m}^3$)
- ΔHC_i : decrease of i ($\mu\text{g}/\text{m}^3$)
- Y_i : SOA yield of i
- M_0 : organic aerosols (OA) ($\mu\text{g}/\text{m}^3$)
- $\alpha_{1,i}, \alpha_{2,i}$: yield of semi volatile compounds generated from i
- $\kappa_{1,i}, \kappa_{2,i}$: distribution constant of semi volatile compound gas/particles generated from i at 25°C
- POA : coexisting OA under initial conditions ($\mu\text{g}/\text{m}^3$)

An equation that estimates the SOA generated from each aromatic HC listed in **Table 1** can be obtained by substituting the data for the quantity of SOA generation (SOA_i) and the decrease of each aromatic HC (ΔHC_i) from the smog chamber experiment into Equations 1 and 2, and identifying the parameters $\alpha_{1,i}, \alpha_{2,i}, \kappa_{1,i}$ and $\kappa_{2,i}$.

In addition, Equations 1 and 2 also show that the SOA yield changes in accordance with the coexistence of organic aerosols (OA). This indicates that the effects of the coexisting OA were considered in the evaluation of the SOA formation potential of gasoline vehicles.

2.3 Estimation of SOA formation potential of gasoline vehicle emissions

The maximum quantity of SOA that can be generated from the HC components present in gasoline vehicle exhaust gas during test cycle driving was predicted. The concentration of each HC component that is present in gasoline vehicle emissions and regarded as an SOA precursor (i.e., paraffin with a carbon number of C6 or higher, naphthene, and aromatic HCs⁽⁴⁾) were substituted into Equations 1 and 2 to calculate the SOA concentration.

The HC component concentrations of the gasoline vehicle emissions used in these calculations assumed that the exhaust gas generated in test cycle driving were diluted to the atmospheric NMHC concentration level in Japan (i.e., approximately 100 ppbC). In addition, the parameters $\alpha_{1,i}, \alpha_{2,i}, \kappa_{1,i}$ and $\kappa_{2,i}$ established by previous studies were used for the generation potential of HCs not evaluated in this study (i.e., paraffin with a carbon number of C6 or higher and naphthene,

and C6 aromatic HC). The SOA concentrations obtained in this way were substituted into Equation 3 to calculate the quantity of SOA generated during test cycle driving.

$$E_{SOA} = \frac{V_{mode} \sum_i SOA_i}{D_{mode}} * 1000 \quad (3)$$

where,

- E_{SOA} : quantity of SOA generated by vehicle (mg/km)
- V_{mode} : volume of exhaust gas during test cycle driving diluted to atmospheric NMHC concentration levels (m^3)
- D_{mode} : distance driven in test cycle (km)

3. Results

3.1 SOA formation potential if HC components

Each parameter of the two-product model expressed in Equation 1 was identified using the results of the C7 to C9 aromatic smog chamber experiment listed in **Table 1**, and compared with previous study.⁽⁵⁾ As illustrated in **Fig. 4**, the rise in the SOA yield as the OA concentration increased was the same in both cases. However, the SOA yield in this study was lower than in the previous study. This is thought to be due to the effect of the different light sources used in the smog chamber experiments.

Fig. 2 indicates that the light source used in this experiment approximates the actual UV spectrum of the sun more closely. As a result, it contains a large component of visible light with a wavelength of 420 nm or higher. In this case, since nitrate radicals absorb light with a wavelength of between 420 and 600 nm and decompose,⁽⁶⁾ nitrate radicals do not contribute to the reactions that generate SOA. The same conditions occur in the actual atmosphere during the day. In contrast, smog chamber experiments in previous studies used UV light with a spectrum containing a peak at a wavelength of around 350 nm. Light from a lamp like this contains virtually no light with a wavelength of 420 nm or higher. In this case, it is thought that the nitrate radicals contribute to the SOA generation reactions and increase the SOA yield.

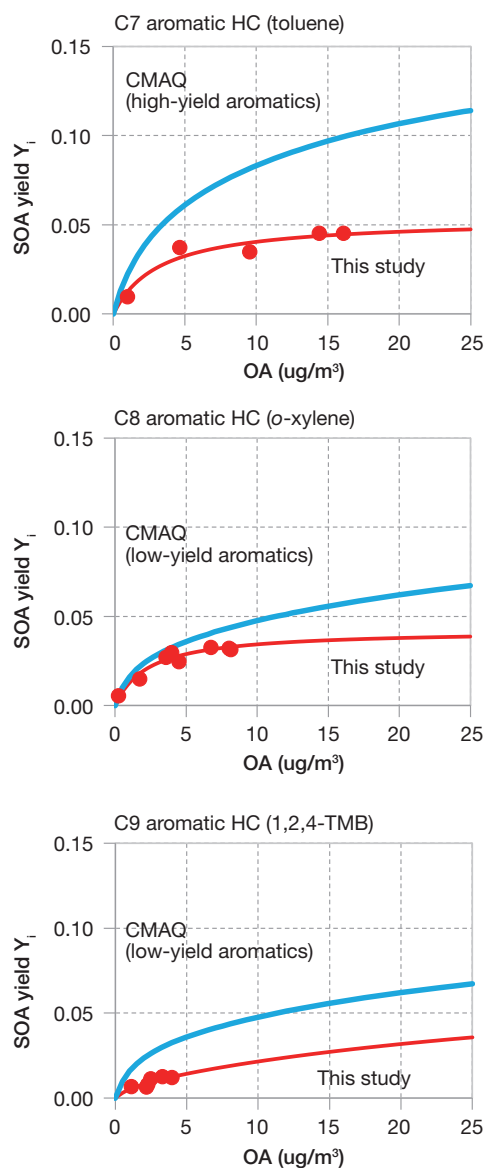


Fig. 4 Comparison of SOA Formation Potential of Aromatic HCs between this and Previous Studies (CMAQ 5.0 vs. Aero 6)

3.2 SOA formation potential of gasoline vehicle emissions

The SOA formation potential of the three gasoline vehicles listed in **Table 2** was estimated using the method described in Section 1.3. **Table 3** shows the Equation 1 parameters for the SOA precursors investigated in this study.

The HC component concentrations in the exhaust gas used in this estimation were obtained by diluting the exhaust gas emitted from a vehicle in the Worldwide-Harmonized Light Vehicles Test Cycle (WLTC, cold start conditions) using a dilution tunnel, and then performing quantitative analysis with the GC. However, since the NMHC concentration of the exhaust gas after dilution in the tunnel was higher by a factor of 1 or 2 than the atmospheric concentration, it was assumed that

the exhaust gas had been diluted further to around the same NMHC concentration as occurring in the actual atmosphere (100 ppbC). In addition, as described in Section 1.2, the estimation also factored in the effects of OA coexisting in the atmosphere.

Table 2 Test Vehicle Specifications

	A	B	C
Powertrain	2.5-liter V6 (DOHC)	Turbocharged 1.2-liter inline 4-cylinder (DOHC, IC*)	1.8-liter inline 4-cylinder (DOHC + 2 motors)
Fuel	Premium unleaded gasoline		Regular unleaded gasoline
Fuel injection system	Direct in-cylinder fuel injection		Electronically controlled fuel injection
Vehicle weight	1,660 kg	1,575 kg	1,730 kg
Model year	2005	2016	2017

* DOHC: dual overhead cam, IC: intercooler

Table 3 Two-Product Model Parameters for SOA Precursors

SOA precursor	$\alpha_{1,i}$	$\kappa_{1,i}$	$\alpha_{2,i}$	$\kappa_{2,i}$	Source
Paraffin (C6 or higher), naphthene	0.0718	50	0	0	CMAQ5.0 /aero6
C6 aromatics	0.0720	3.3113	0.888	0.0090	
C7 aromatics	0.0537	0.308	0	0	This study
C8 aromatics	0.0423	0.431	0	0	
C9 aromatics	0.0080	0.757	0.0755	0.0239	

Figs. 5 to 7 show the estimated results for the SOA formation potential of vehicles A to C. For each vehicle, the quantity of generated SOA rose in accordance with the increase in coexisting OA in the air. In addition, the contribution ratio of the C7 to C9 aromatic HCs, which were originally considered to be the main SOA precursors, was less than half. A large contribution in vehicles A and C was made by paraffin with carbon number of C6 or higher and naphthene. The relative contribution of other precursors probably increased because this study applied lower SOA formation potential parameters to the C7 to C9 aromatics than in previous studies.

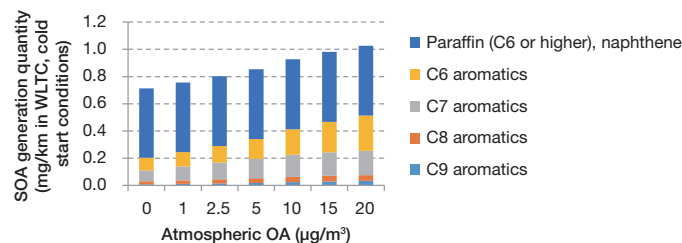


Fig. 5 SOA Formation Potential of Emissions of Vehicle A (Emissions Dilution Ratio: 355 Times, NMHC Concentration in Emissions after Dilution: 97 ppbC)

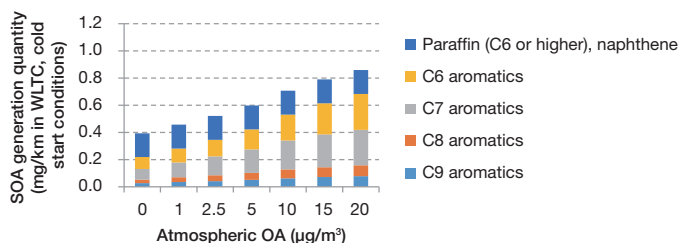


Fig. 6 SOA Formation Potential of Emissions of Vehicle B (Emissions Dilution Ratio: 407 Times, NMHC Concentration in Emissions after Dilution: 100 ppbC)

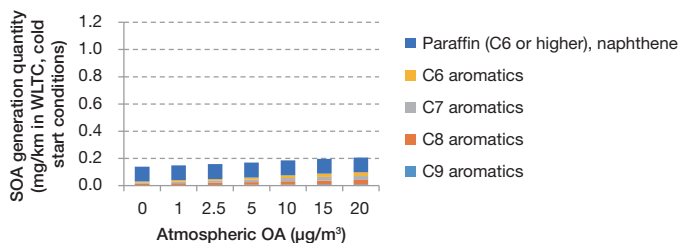


Fig. 7 SOA Formation Potential of Emissions of Vehicle C (Emissions Dilution Ratio: 243 Times, NMHC Concentration in Emissions after Dilution: 103 ppbC)

Next, **Fig. 8** shows the calculated results for the ratio between the PM emissions and the quantity of SOA formation of vehicles A to C in the WLTC (cold-start conditions). The ratio changes in accordance with the coexisting atmospheric OA concentration. In this study, the ratio between PM emissions and SOA generation was between 0.3 and 1.7.

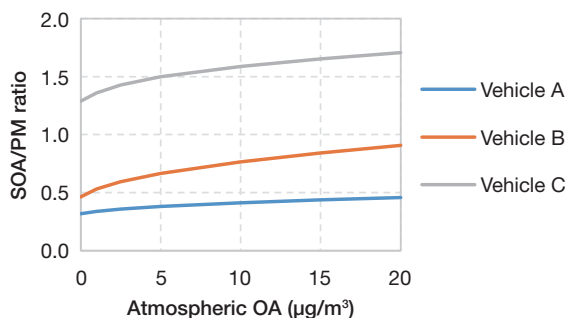


Fig. 8 SOA Generation/PM Emissions Ratio of Gasoline Vehicles (WLTC, Cold Start Conditions)

4. Conclusion

This study aimed to evaluate the SOA formation potential of gasoline vehicle emissions under as close as possible to actual atmospheric conditions. The results of smog chamber experiments using a light source with a spectrum approximating that of actual solar radiation found that the SOA formation potential of C7 to C9 aromatic HCs is lower than that identified in previous studies. This discrepancy is thought to be because nitrate radicals are photolyzed by visible light with a wavelength of 420 nm or higher and, therefore, do not contribute to SOA generation. Since the same state occurs in the atmosphere during daytime, this study probably successfully

simulated the actual conditions under which photochemical reactions occur in the atmosphere.

Obtaining a deeper understanding of the effects of experimental conditions (such as the wavelengths of light sources) on evaluations in experimental studies of SOA will be a major issue for promoting analysis of the actual behavior of SOA in the future.

References

- (1) Countermeasures to Suppress Emissions of Fine Particulate Matter in Japan (Interim Report) (Draft) (in Japanese). 6th Report Distributed by the Technical Committee on Fine Particulate Matter. Ministry of the Environment (2015).
- (2) S. Platt et al. "Secondary Organic Aerosol Formation from Gasoline Vehicle Emissions in a New Mobile Environmental Reaction Chamber." *Atmospheric Chemistry and Physics* Vol. 13 (2013) pp. 9141-9158.
- (3) T. Gordon et al. "Secondary Organic Aerosol Formation Exceeds Primary Particulate Matter Emissions for Light-Duty Gasoline Vehicles." *Atmospheric Chemistry and Physics* Vol. 14 (2014) pp. 4661-4678.
- (4) *Community Modeling and Analysis System*. https://www.airqualitymodeling.org/index.php/CMAQv5.1_SOA_Update
- (5) *Community Modeling and Analysis System: CMAQ Version 5.0/Aero 6* (particle concentration prediction model).
- (6) H. Stark et al. "Atmospheric In-Situ Measurement of Nitrate Radical (NO₃) and Other Photolysis Rates Using Spectroradiometry and Filter Radiometry." *Journal of Geophysical Research* Vol. 112 Issue D10 (2007).

Authors



D. HAYASHI



T. YAMASHITA

Optimization of Motion Controls of Highly Realistic Dynamic Driving Simulator in Urban Driving Scenarios

Quy Hung Nguyen Van*¹
 Shogo Konishi*¹
 Shoji Ito*¹

Abstract

The Toyota Dynamic Driving Simulator (TDDS), a highly realistic dynamic driving simulator, has been used to perform sophisticated simulations of driving support and automated driving systems, primarily in highway scenarios, since 2008. However, motion sickness has caused a number of test subjects to end participation in driving simulations of urban driving scenarios, which involves repeated deceleration, stopping, and restarting. Therefore, to help reduce motion sickness, this development focused on the control algorithms of the TDDS motion mechanism (the device that generates the acceleration and deceleration G of the vehicle) and the effectiveness of restricting the tilt angle and angular velocity of the dome (the spherical chamber that holds the actual vehicle set up). To compensate for the consequent reduction in simulated acceleration and deceleration G while reducing the tilt angle and angular velocity of the dome, the amount of translational movement was increased. Moreover, the gain of the simulated G with respect to the actual vehicle was lowered. In addition, to ensure that any reduction in perceived G would not result in a less realistic driving experience, a Z-axis vibration control was introduced to complement the simulated driving, acceleration, and deceleration sensations. As a result, the number of test subjects abandoning simulated driving experiments due to motion sickness was reduced to zero.

Keywords: *driving simulator, motion sickness evaluation, motion sickness suppression, acceleration and deceleration simulation, driving feel simulation, optimization control*

1. Outline of the Toyota Dynamic Driving Simulator

The Toyota Dynamic Driving Simulator (TDDS) consists of a vehicle motion system (dome) that generates actual physical sensations of acceleration and a visual system that simulates the traffic environment (**Fig. 1**). The most significant feature of the TDDS is its large-scale translational (XY) motion system for moving the dome, which is capable of traveling 35 meters in the longitudinal (X) direction and 20 meters in the lateral (Y) direction. In addition, to simulate the sensation of rotation at an intersection, the dome is also equipped with a turntable that has a rotational angle of $\pm 330^\circ$. Furthermore, the sensation of low-speed driving on city streets can be faithfully simulated via the four vibration application (shaker) systems that support the cockpit system on the turntable and that enable simulations of ride comfort.

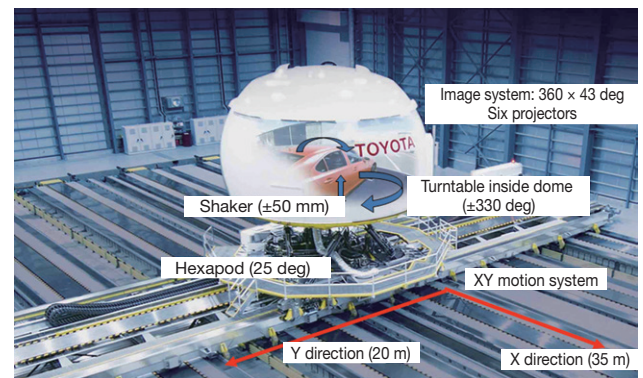


Fig. 1 Outline of TDDS

The visual system is capable of projecting simulated images of the driving environment onto a spherical screen (height: 4.5 meters, inner diameter: 7.0 meters), which is laid out on the inside surface of the dome. These images are created by twenty-four image generators using six 4K projectors fixed to the ceiling that generate a 360° full-circle lateral field of view (upward angle: 23° , downward angle: 20°).

*¹ Automated Driving & Advanced Safety System Development Div., Advanced R&D and Engineering Company

2. Analysis of Motion Sickness in Simulated Urban Driving Scenarios

An evaluation course that simulates driving in urban scenarios was created to analyze motion sickness generated by the TDDS.

2.1 Evaluation course and driving method

The evaluation course was a two-lane road (one lane in each direction) with thirteen stop-and-go intersections (**Fig. 2**) and a driving time of approximately 20 minutes at 40 km/h.

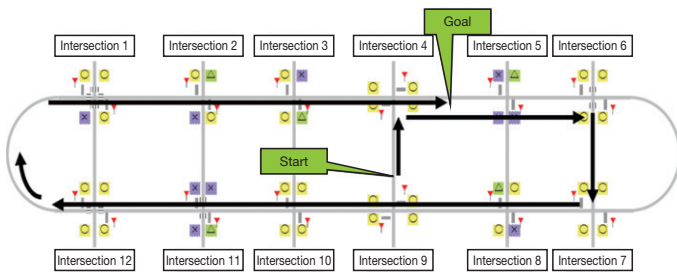


Fig. 2 Motion Sickness Evaluation Course

2.2 Motion sickness evaluation method

The evaluation was carried out in real-time during driving. The Simulated Simulator Sickness Questionnaire (SSSQ)⁽¹⁾ was also applied as an evaluation index immediately after driving.

2.3 Motion sickness evaluation results

Fig. 3 shows the SSSQ evaluation results (test subjects: 5). In addition, for comparison, **Fig. 3** also shows the SSSQ scores from past simulations of automated driving on highways.

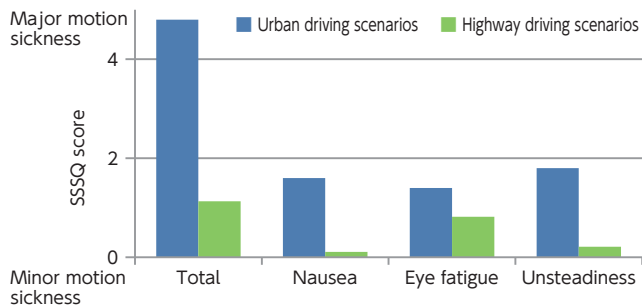


Fig. 3 SSSQ Scores from Urban and Highway Driving Scenarios (Average Total Score and Average of Each Questionnaire Item)

Fig. 3 indicates that the urban driving scenarios generated a much higher level of motion sickness than the highway driving scenarios. Large differences also occurred in the evaluation

scores for the nausea and unsteadiness evaluation items.

Two potential sources of driving simulator (DS) motion sickness are already known: motion sickness caused by the visual system and motion sickness caused by the motion of the dome that generates the actual physical sensations of acceleration. This development focused on the motion of the dome.

3. Analysis of Motion Control Factors Causing Motion Sickness

3.1 Outline of motion control

The TDDS simulates vehicle acceleration and deceleration (G force) using vehicle dynamics calculation software and a motion system called a Stewart platform.⁽²⁾ This system generates a realistic sensation of G that simulates the vehicle behavior and can be experienced by the driver (**Fig. 4**). The sensation of G experienced by the driver can be expressed by Equation 1.

$$G \text{ sensation} = \text{gain} \times (\text{XY direction } G + \text{tilting } G) \quad (1)$$

where,

XY direction G: simulated G component generated by the XY-direction motion of the dome

tilting G: simulated G component generated by the tilting motion of the dome. If the tilt angle of the dome is defined as θ , then tilting $G = g \times \sin(\theta)$ (g: gravitational acceleration)

Gain applied to actual G of vehicle: 0 to 1

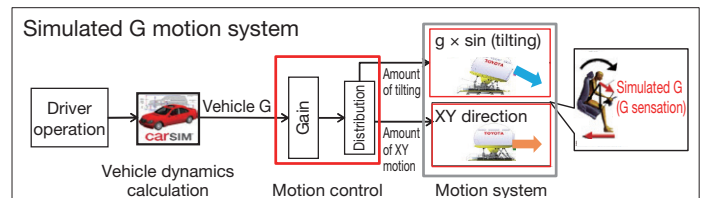


Fig. 4 Configuration of TDDS Motion Control

3.2 Comparison of motion controls in simulated urban and highway driving scenarios

Fig. 5 compares the motion controls (i.e., the dome tilt angle and tilt angle velocity) applied in simulated urban and highway driving scenarios. In the simulated urban driving scenarios, the proportion of high tilt angles (i.e., tilt angles of 6 degrees or higher) was greater than 5%. In contrast, the proportion of high tilt angles in the highway driving scenarios was less than 1%. In addition, the proportion of tilt angle velocities reaching 2 deg/s or higher was greater than 10% in the simulated urban driving scenarios but less than 1% in the highway driving scenarios. These results indicate that the dome generated a higher and faster degree of tilt in the urban driving scenarios than the highway driving scenarios.

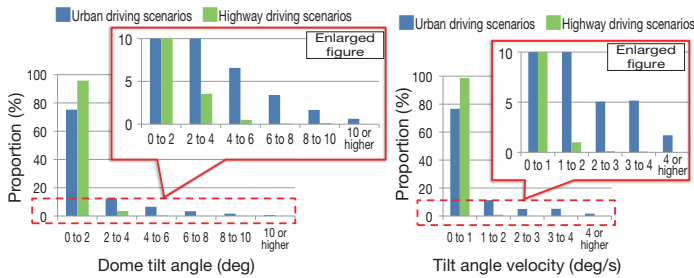


Fig. 5 Motion Comparison in Urban and Highway Scenarios (Left: Dome Tilt Angle, Right: Dome Tilt Angle Velocity)

3.3 Correlation of dome tilt angle and angular velocity with motion sickness evaluation

This section discusses the correlation between the real-time evaluation results for motion sickness during simulated urban driving and the motion of the dome (i.e., the tilt angle and the tilt angle velocity). It was found that the scenarios with the highest evaluation scores (4 points) for motion sickness (circled in red in **Fig. 6**) occurred during the simulation of vehicle acceleration and deceleration G during stops and starts near intersections (**Fig. 7**). In addition, these scenarios coincided with a dome tilt angle of higher than 10 deg and the maximum tilt angle velocity setting of 4 deg/s (**Fig. 8**).

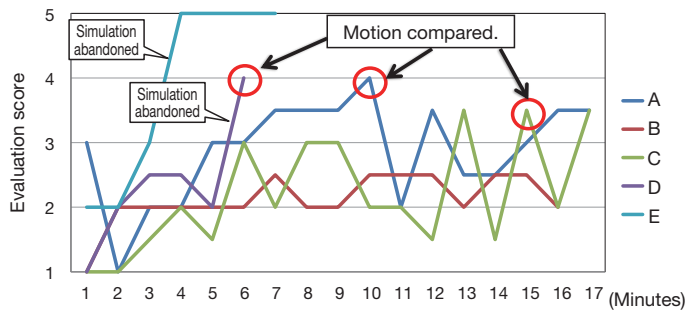


Fig. 6 Real-Time Motion Sickness Evaluation Scores



Fig. 7 Dome Motion Simulating Stop and Start G at Intersection

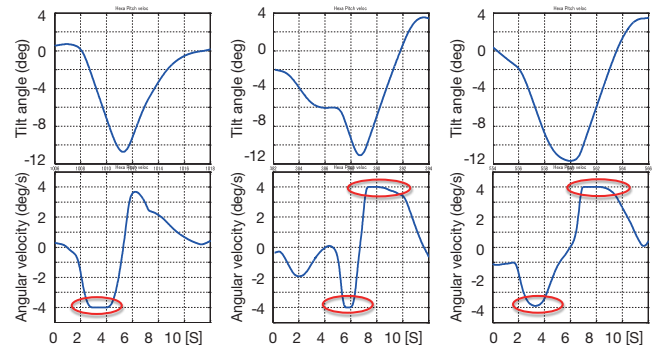


Fig. 8 Characteristics of Dome Motion when Driver Experiences Motion Sickness

3.4 Mechanism of motion sickness generation due to dome tilting

One motion sickness mechanism occurs when the driver feels a sense of incongruity between previous experiences and the combination of visual, vestibular, and somatic sensations generated by the simulator. The resulting sensory conflict or sensory contradiction are effective means of explaining motion sickness.⁽³⁾ The motion sickness generation mechanism of the TDDS was examined based on these ideas.

(1) Conflict between previous memories and current motion sensation

It is generally known that the semicircular canal of the inner ear detects angular acceleration of rotational motion when the tilt angle velocity reaches approximately 3 deg/s or higher.⁽³⁾ From the results described in Section 3.3 above, the dome was rotating at 4 deg/s when the test subjects experienced motion sickness. This type of rotation in the TDDS probably created a sense of incongruity since this degree of rotation is not actually generated in a vehicle during acceleration or deceleration.

(2) Sensory contradiction created by current motion sensation

A distinguishing feature of the motion system is a special control called dome washback. Washback refers to the control adopted by the motion system to prepare for the next simulated acceleration or deceleration action when the vehicle stops or is being driven at a constant speed. The dome moves automatically to the home position (XY motion coordinates X and Y = 0 and tilt angle = 0) so that the total G sensation experienced by the driver due to XY direction motion and tilting is zero (**Fig. 9**). While the images in the dome are stationary during washback control, the fact that the dome is moving generates sensory contradiction. In addition, the duration of washback control to return the dome to the home position increases in accordance with the size of the dome tilt angle used to simulate the G. A longer washback duration probably facilitates this sensory contradiction and aggravates motion sickness. In addition, fast Fourier transform (FFT) analysis of the dome tilt angle when the vehicle stops and starts

near an intersection found that the frequencies of these operations were within the frequency domain most likely to generate motion sickness (0.025 to 0.4 Hz: a frequency domain found to induce sensory contradiction⁽³⁾) (**Fig. 10**).

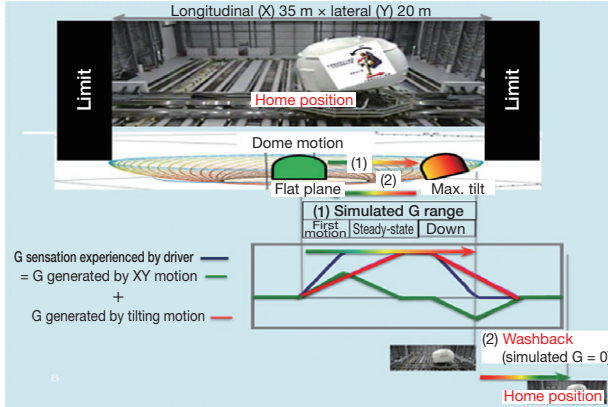


Fig. 9 Washback Motion

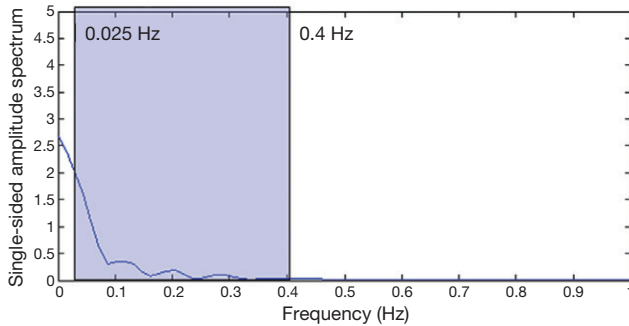


Fig. 10 Frequency Analysis of Dome Tilting

4. Design of New Control Algorithm

To suppress the motion sickness factors identified in the previous section, the tilt angle and angular velocity required to simulate acceleration and deceleration G must be restricted.

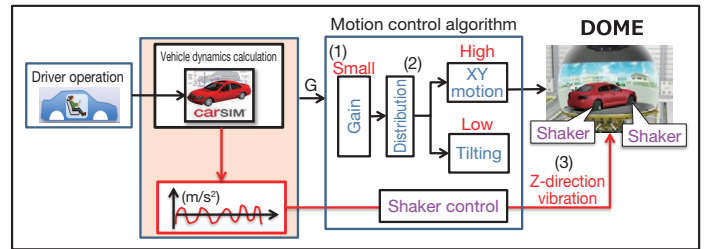
As shown in item (1) in **Table 1**, a new motion control algorithm was designed to simulate acceleration and deceleration G by increasing the amount of XY motion and prioritizing its role in G simulation. This approach was adopted to restrict the tilt angle and angular velocity of the dome and to compensate for the resulting reduction in simulated acceleration and deceleration G. In addition, as shown in item (2), the gain of the simulated G was reduced with respect to actual vehicle G to keep the dome within the range of the XY motion system. Then, as shown in item (3), Z-direction (vertical) vibration control was introduced to prevent a loss in driving feel after the reduction in gain compared to an actual vehicle. This approach was adopted to complement the simulated driving feel and sensations of acceleration and deceleration.

Table 1 Design of New Control Algorithm

Control portion	Previous design	New design	Aims of new design
(1) Distribution portion	High proportion of tilting	Low proportion of tilting	To restrict dome tilt angle and angular velocity
	Low proportion of XY motion	High proportion of XY motion	To maximize the G simulated by XY motion and to compensate for the restriction of G simulated by tilting
(2) Gain applied to actual vehicle G	Large	Small	- To keep the dome within the range of the XY motion system - To minimize the dome washback motion
(3) Z-direction vibration	None	New control	To complement the simulated driving feel and sensations of acceleration and deceleration using Z-direction vibration control (*) as a result of the reduction in gain compared to an actual vehicle

(*) The motion least likely to result in DS motion sickness⁽³⁾

Fig. 11 shows the configuration of the new motion control.



(1) G (small), (2) low proportion of tilting/high proportion of XY motion, (3) Z-direction vibration (new control)

Fig. 11 Configuration of New Motion Control

4.1 Development of motion control algorithm prioritizing XY motion

(1) Motion control parameter setting method

The TDDS controls the distribution of dome XY and tilting motions by applying frequency filters (Equations 2 and 3) to the simulated G, which was calculated by multiplying the actual vehicle G with the gain.

- Tilting distribution control filter

$$\frac{2\zeta_{LP}\omega_{LP}s + \omega_{LP}^2}{s^2 + 2\zeta_{LP}\omega_{LP}s + \omega_{LP}^2} \frac{\omega_{LPb}}{s + \omega_{LPb}} \quad (2)$$

where,

$\omega_{LPb}, \omega_{LP}$: cut-off frequency values
 ζ_{LP} : damping constant

- XY motion distribution control filter

W_1, W_2, W_3 : weightings estimated from real-time motion sickness evaluation score

$$\frac{s^2}{s^2 + 2\zeta_{HP}\omega_{HP}s + \omega_{HP}^2} \frac{s}{s + \omega_{HPb}} \quad (3)$$

where,

$\omega_{HPb}, \omega_{HP}$: cut-off frequency values
 ζ_{HP} : damping constant

The motion control uses these frequency filters to assign acceleration frequency components to each motion actuator (i.e., the tilting and XY motion systems).⁽²⁾

A range of different levels were applied to the frequency filter control parameters (the cut-off frequency values, damping values, and so on) for the simulated acceleration and deceleration G generated when stopping and starting at an intersection. The actual motion of the DS was then confirmed through simulations, enabling the method for setting effective parameters to prioritize XY motion (Table 2).

Table 2 Setting of Motion Control Parameters

Control parameter	Setting method	Effect
ω_{LPb}	Low value	Restricts dome tilting.
ζ_{LP}	High value	Restricts repeated tilting motions during washback.
ω_{HP}	Low value	- Maintains the simulated G from XY motion as long as possible. - Restricts the reduction in XY direction G during washback.
ζ_{HP}	High value	Restricts doubling-back XY motion around the home position during washback.

Since the minimum values that can be set for ω_{LPb} (cut-off frequency value for tilting) and ω_{HP} (cut-off frequency value for XY motion) are limited by the scale of the XY motion system, these values are also dependent on the size of the simulated G.

(2) Optimization of motion control parameters

An evaluation function (E) was defined to express the relationship between driver motion sickness and the dome tilting and XY motion amounts (Equation 4).

$$E(i, j) = W_1 \times f_1 (\text{max. tilt angle}_{ij}) + W_2 \times f_2 (\text{max. tilt angle}_{ij}) + W_3 \times f_3 (\text{tilt angle over-shoot}_{ij})$$

$$\min. \{E(i, j)\}$$

where,

$E(i, j)$: estimated TDDS motion sickness score

i: driver

j: evaluation scenario

f_1, f_2, f_3 : functions estimated from real-time motion sickness evaluation score

Constraints:

Max|XY motion range| < 12 m: range of TDDS XY motion

Max|XY speed| < 5 m/s: maximum possible speed of TDDS XY motion (4)

Using the real-time motion sickness evaluation results of five drivers, the parameters $f_1, f_2, f_3, W_1, W_2,$ and W_3 were identified so that the motion sickness scores estimated from the dome motion by evaluation function E approximated the real-time motion sickness evaluation scores (Fig. 12).

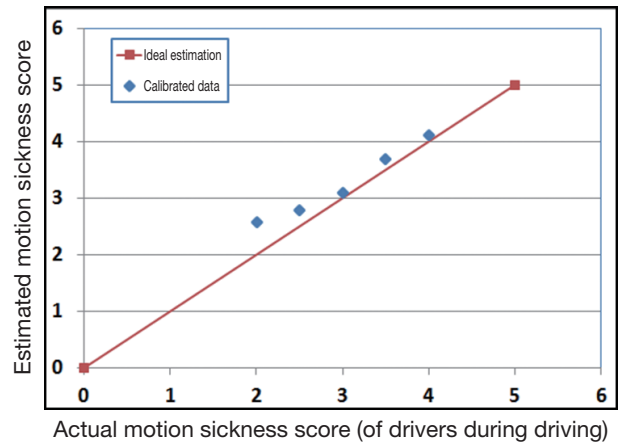


Fig. 12 Motion Sickness Scores Estimated Using Evaluation Function

Then, using the evaluation function E, the motion control parameters that result in the lowest estimated motion sickness score were calculated from past TDDS urban driving data (data from 28 drivers, including stopping and starting acceleration and deceleration near intersections, acceleration and deceleration during driving, acceleration and deceleration in scenarios such as turning left and right, and so on) (Table 3).

Table 3 Optimization Results for Motion Control Parameters

		(2) Gain applied to actual vehicle G			
		Large	Optimum range	Small	
(1) Tilting cut-off frequency (rad/s)	1.0	> 3.6 points (current)	3.6 points	3.1 points	Sense of incongruity caused by weak G sensation (sensory conflict between motion and images)
	0.6	Outside XY motion range	2.6 points	2.3 points	
	0.4	Outside range	Outside range	1.9 points	
	0.32	Outside range	Outside range	<1.9 points	
	0.24	Outside range	Outside range		
	0.16	Outside range	Outside range	Outside range	

As shown in **Table 3**, the estimated motion sickness score can be reduced by changing the cut-off frequency of the tilting frequency filter. These results also confirmed that optimizing the gain applied to actual vehicle G kept the dome within the range of the XY motion system.

Finally, the motion of the dome was compared between the new motion control parameters determined as shown in **Table 3** and the pre-optimization motion control parameters. The results confirmed that the dome tilt angle and angular velocity were reduced (**Fig. 13**) and that the frequency component likely to cause motion sickness due to tilting was restricted (**Fig. 14**).

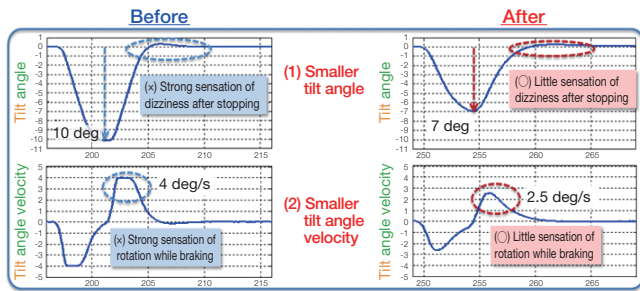


Fig. 13 Comparison of Dome Motion

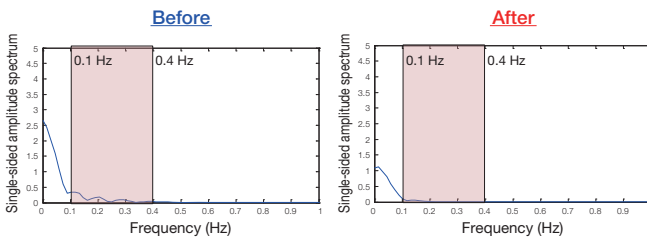


Fig. 14 Comparison of Dome Tilting Frequency

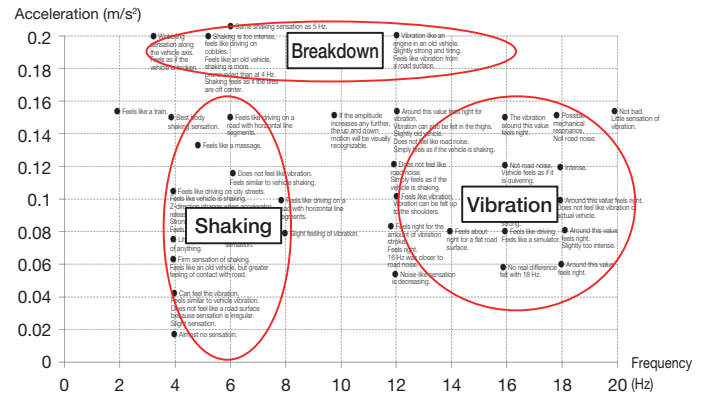
4.2 Complementing the simulated driving feel and sensations of acceleration and deceleration using vertical direction vibration controllers

One concern of the countermeasures to suppress motion sickness is a reduction in the G sensation experienced by the driver, resulting in poorer sensations of driving feel, acceleration, and deceleration. For this reason, it was decided to complement the sensations of driving feel, acceleration, and deceleration using Z-direction vibration, which has been found to have little impact on motion sickness.⁽³⁾

4.2.1 Design of Z-direction vibration

To help design the Z-direction vibration parameters (acceleration and frequency), a subjective evaluation was carried out to assess the Z-direction vibration generated by the shaker units of the DS. The results of this subjective evaluation (**Fig. 15**) showed that a frequency range of between 4 and 8 Hz generated the sensation that the dome was shaking. In contrast, a frequency of 12 Hz or higher generated no such sensation. In

addition, an acceleration of 0.16 m/s² or higher generated the sensation that the vehicle was about to topple over, which is connected to fatigue.



Frequency range of 4 to 8 Hz: whole vehicle shakes.
 Frequency of 12 Hz or higher: feels like vibration, not shaking.
 Acceleration of 0.16 m/s² or higher: feels like the vehicle is about to break, tiring to drive.

Fig. 15 Results of Subjective Evaluation of Z-Direction Vibration Parameters (Acceleration and Frequency)

Next, the Z-direction vibration in accordance with vehicle speed was studied to enable the application of constant vehicle vibration. The main Z-direction vibration frequencies of an actual vehicle during steady-state driving are 4, 12, and 18 Hz.⁽⁴⁾ Based on this actual vehicle Z-direction vibration data and the results of the subjective DS vibration experiments using the shaker units described in above in **Fig. 11**, it was decided to use two frequencies. At low vehicle speeds, low frequencies close to the 4 to 8 Hz range, which create a sensation as if the whole vehicle is shaking, were applied. At high vehicle speeds, high frequencies close to the 18 to 20 Hz range, which feel like vibration, were applied. In addition, the acceleration (intensity) of each vibration frequency was determined from a subjective driving evaluation. **Fig. 16** shows the designed vibration trend in accordance with vehicle speed.

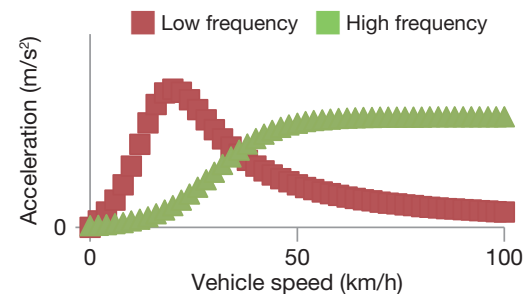


Fig. 16 Z-Direction Vibration in Accordance with Vehicle Speed

In addition, Z-direction vibration was also defined in accordance with vehicle acceleration as a response to driving operations. The vibration characteristics of the body were analyzed to ensure that the vibration would only be applied to

the hands and feet in contact with the vehicle control systems. Body parts are sensitive to a wide range of frequencies. For example, the torso and arms are sensitive to comparatively low frequencies (4 to 10 Hz), the hands to high frequencies (30 to 50 Hz), and the feet to frequencies of 2 Hz and higher.⁽⁴⁾ As a result, the frequency range between 4 and 10 Hz must be avoided to restrict the vibration application to just the hands and feet. In addition, to distinguish this vibration from the vibration applied in accordance with vehicle speed, it was decided to use vibration with a frequency of 20 Hz or higher. Finally, a subjective driving evaluation was carried out to verify the Z-direction vibration parameters (frequency and acceleration) used to simulate vehicle acceleration and deceleration. The system was designed to provide feedback to the driver in the form of engine response to accelerator operation when speeding up and changes in deceleration when slowing down (**Fig. 17**).

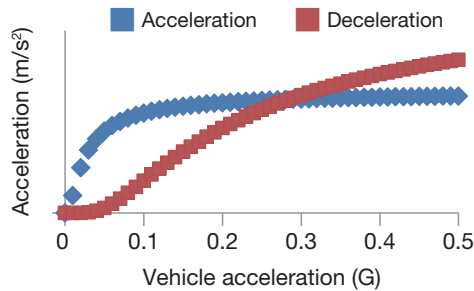


Fig. 17 Z-Direction Vibration in Accordance with Acceleration

5. Evaluation of Motion Sickness Suppression by New Motion Design

The SSSQ-based motion sickness evaluation was carried out again using the new motion controls incorporating the countermeasures described above. The evaluation results were as follows.

Current motion control (before):

SSSQ score = 4.8

New motion control (after):

SSSQ score = 1.0 (rate of simulation abandonment: 0%)

These results confirmed that the new motion control suppressed motion sickness (**Fig. 18**).

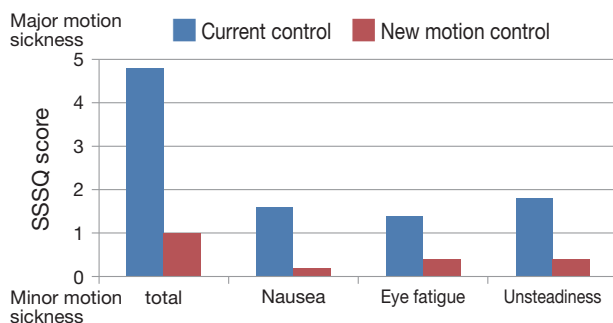


Fig. 18 SSSQ Scores Before and After Improvement

6. Conclusions

A new control algorithm was developed to counteract the motion sickness experienced in simulated urban driving scenarios by restricting the tilt angle and angular velocity of the motion system. This control was complemented by Z-direction vibration to offset the lower sensations of driving feel, acceleration, and deceleration caused by the trade-off reduction in vehicle acceleration and deceleration G. As a result, the motion sickness experienced in simulated urban driving scenarios was suppressed while maintaining realistic sensations of driving feel, acceleration, and deceleration.

A future goal is to realize even more realistic actual driving simulations by developing and verifying a control algorithm capable of adopting the optimum parameters in real-time in response to different driving scenarios (such as stopping and starting at an intersection, turning left and right, making evasive maneuvers, and so on).

References

- (1) M. Okuwa. "Driving Simulator Motion Sickness Evaluation Index (SSSQ)" (in Japanese). Project Report, Toyota Central R&D Labs., Inc. (2007).
- (2) T. Yokekawa. "Driving Simulator Motion: Drive Algorithm" (in Japanese). Internal Technical Report, Toyota Motor Corporation (2013).
- (3) N. Isu. "Motion Sensations and Motion Sickness when Driving" (in Japanese). *Simple Vehicle Modeling and Controls Event*, Japan Society of Mechanical Engineers (2016).
- (4) J. Plouzeau et al. "Vibrations in Dynamic Driving Simulator: Study and Implementation." *Science Arts & Métiers* (2013).

Authors



N.V.Q. HUNG



S. KONISHI



S. ITO

2018 Energy Conservation Grand Prize (Minister Prize of Economic, Trade and Industry) Energy-Saving by Rapid Heating of Thermoplastic CFRP Using Superheated Steam

Isao Yoshihara*¹

Yusuke Matsumoto*¹

Takashi Sakui*¹

1. Introduction

This initiative was carried out on a production line at Toyota’s Motomachi Plant, which is the body assembly plant for models such as the hydrogen-powered Mirai fuel cell vehicle (FCV), Crown, and various vehicles in the Lexus lineup. The Toyota Environmental Challenge 2050 contains the Plant Zero CO₂ Emissions Challenge, under which a wide range of initiatives are being carried out to help the environment by upgrading production lines, switching to different energy sources, and so on.

2. Energy Management Structure

The initiative described in this article is a joint development being carried out by three companies in different fields: vehicle manufacturing, energy, and facility manufacturing. Highly efficient development has been achieved by allocating specific roles based on each company’s strengths and ensuring close communication to share issues that arise (Fig. 1).

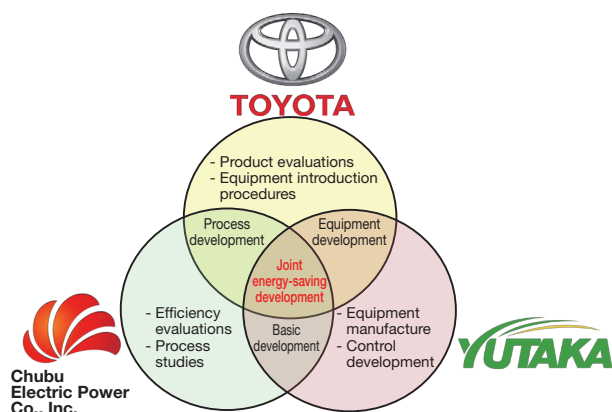


Fig. 1 Structure of Joint Development

3. Background and History

3.1 Carbon fiber reinforced plastic (CFRP)

CFRP possesses an excellent balance of strength and lightness, and its use is increasing in the aviation, automotive, and other industries. In the automotive industry, the use of

CFRP is being promoted as a weight-reduction measure to help lower the environmental impact of cars.

3.2 Conventional CFRP part production processes

Initially used for aviation parts in the 1990s, CFRP started to be used on cars in the 2010s in response to growing calls for higher fuel economy and lower weight. However, because vehicle production requires high productivity, the lengthy autoclave processes of the aviation industry could not be adopted directly. Therefore, in addition to the thermosetting resin used in aircraft, CFRP that uses thermoplastic resin for the matrix has also been developed. Carbon fiber reinforced thermoplastic (thermoplastic CFRP) has higher productivity than thermosetting CFRP because it requires only a few minutes to harden after being heated in the production process. However, this is still a new material and its production processes are still under development by manufacturers around the world. Fig. 2 shows the conventional thermoplastic CFRP production process. It is a pressure molding process that involves the heating of the CFRP matrix by far-infrared radiation. The heating time is 390 seconds per part, which is substantially longer than the required per-vehicle production time of 60 seconds. This is due to the low heating efficiency of CFRP, which derives from its characteristically low thermal conductivity. Therefore, as part of the Toyota Environmental Challenge 2050, an initiative was launched to increase the efficiency of the heating process, while at the same time raising the productivity of CFRP manufacturing.

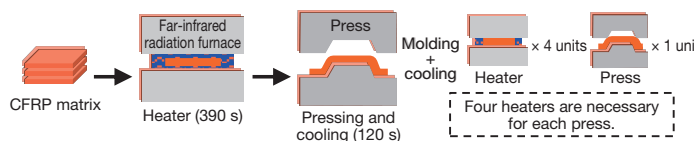


Fig. 2 Issues of Thermoplastic CFRP Production Process

4. Energy-Saving Concept and Details

4.1 Target setting

As illustrated in Fig. 2, the conventional heating process contains a fundamental imbalance, with four heating steps required for each molding step. A large number of heating steps increases capital investment, while also generating waste heat and heat dissipation. Therefore, this development aimed to

*¹ Production Technology Development Div., Production Engineering Development Center

achieve a balanced process with one heating step and one molding step, which would minimize the number of steps and eliminate waste, and thereby shorten the heating time. The specific numerical targets listed in **Table 1** were set.

Table 1 Numerical Targets

Item	Conventional	Target	
Heating time	390 s	120 s	-70%
Energy	24.2 kL/year	12.2 kL/year	-50%
CO ₂ emissions	72.9 tons/year	36.5 tons/year	-50%

4.2 Identification of issues

First, this development observed the thermoplastic CFRP sheets in cross-section during heating. Before heating, the resin and carbon fiber are pressed together. When heat is applied, the resin melts, the constraining force is released, and the sheet expands in the thickness direction. As a result, air layers form inside the sheet, which inhibit thermal conduction (**Fig. 3**). Since the thermal conductivity of air is very low, it is commonly used as a heat insulator. When infrared was used to shorten the heating duration by applying heat quickly, it was found that the surface tended to burn before the internal sheet temperature rose.

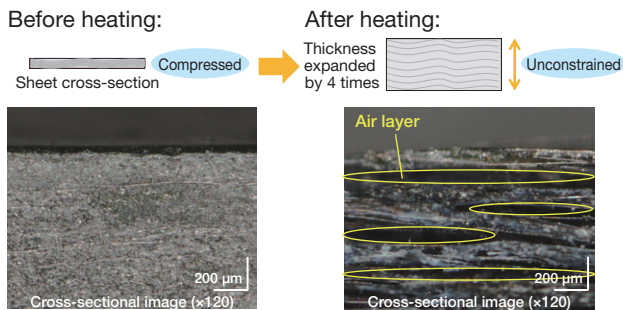


Fig. 3 Behavior during Heating of Thermoplastic CFRP Sheet

Therefore, this project faced the challenge of developing a machine capable of resolving the following two issues simultaneously.

Issue (1): Air layers that are generated during heating inhibit thermal conduction. To raise thermal efficiency, the heating method must factor in these air layers.

Issue (2): Rapid heating causes a temperature difference between the internal and surface sheet temperature. Heat must be applied simultaneously and evenly to the internal and surface areas of the sheet.

4.3 Application of superheated steam

To simultaneously resolve the two issues described above, the heat source must be capable of quickly penetrating the air layers inside the sheet. The development team focused on superheated steam ovens, an everyday heating appliance that has attracted attention in recent years. In these ovens, superheated steam penetrates into the food, enabling rapid and uniform heating. Superheated steam is name given to high-temperature steam created by further heating saturated water vapor generated by boiling water. Since this steam retains the latent heat of condensation, it contains a high heat amount and has excellent heat transfer efficiency (**Fig. 4**).

In addition, since high-temperature superheated steam is saturated with water molecules, it has a low oxygen content and therefore does not cause oxidation degradation, which is a major advantage. However, the adoption of superheated steam was restricted to the food industry, and had only recently started to attract attention as a heat application technology. Since superheated steam had never been used to heat CFRP, Toyota asked Chubu Electric Power Co., Inc. and Yutaka Electronics Industry Co., Ltd. to participate in a joint project to develop a heater for thermoplastic CFRP based on the heater for metal products that the two companies had previously developed.

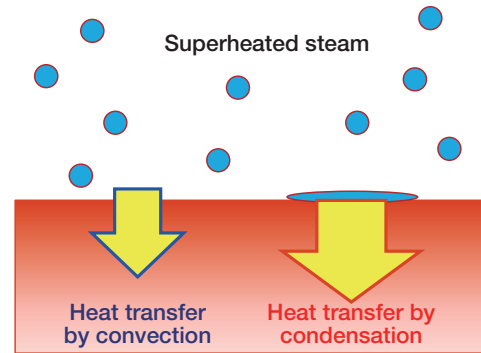


Fig. 4 Characteristics of Superheated Steam

4.4 Heater development

The temperature of steam, which had been heated to 150°C in a boiler, was increased to 400°C in a superheated steam generator. This 400°C superheated steam was then sprayed onto a sheet from a nozzle. Preliminary heating experiments that adopted this method confirmed that both the surface and internal areas of the sheet were heated at the same time. However, the insulating effect of expansion (called “adiabatic expansion”) reduced the temperature of the superheated steam from 400 to 300°C, and the heating time target was not satisfied (**Fig. 5**).

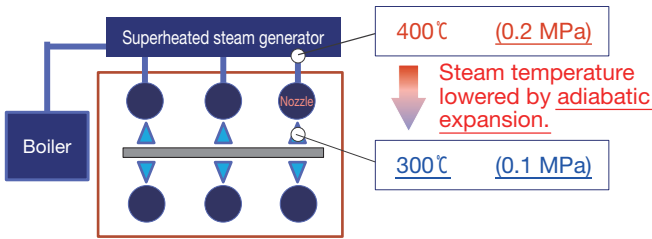


Fig. 5 Schematic of Heating Experiment

Therefore, as a countermeasure for the reduction in temperature caused by adiabatic expansion, electrical heaters were located directly under the nozzle to create a hybrid heat source. The steam is sprayed from the nozzle between the heaters to raise the temperature from 300 to 400°C (Fig. 6).

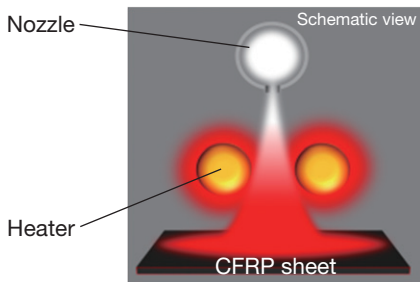


Fig. 6 Supplemental Heating Using Hybrid Heat Source

The velocity of the superheated steam was also optimized. Increasing the steam velocity raises the applied heat amount and can shorten the heating time. However, as the steam generator and electrical heaters are very bulky pieces of equipment, this can have the effect of increasing equipment costs by the power of two. This was the first development in the world to identify the velocity design parameters associated with equipment dimensions. By reflecting and optimizing these in the equipment design, the target heating time was satisfied and energy consumption was minimized. This also helped to minimize equipment costs (Fig. 7).

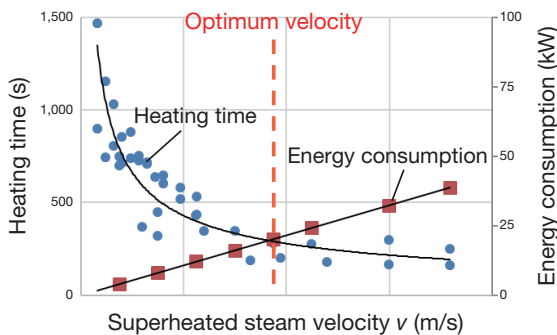


Fig. 7 Optimization of Superheated Steam Velocity

Based on these conditions, the optimum nozzle layout was examined based on computer aided engineering (CAE) analysis of fluid flows inside the equipment. The initial design sprayed the steam from a nozzle located perpendicular to the sheet. However, this caused temperature variations in the planar direction across the sheet. Fluid flow CAE of the nozzle shape, angle, and position was used to calculate an optimum pattern of flows that run in opposite directions up and down the sheet (Fig. 8).

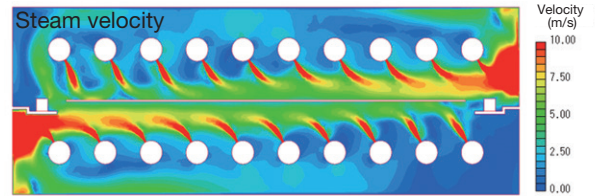


Fig. 8 Optimization of Superheated Steam Flow Pattern

Fig. 9 shows an image and a schematic of the heater incorporating these countermeasures. The header that receives the superheated steam is located inside the heater as a further energy-saving measure since the heat dissipated from the header can be used to warm the inside of the heater. This configuration is also less susceptible to oxidation (rust) since the inside of the heater is oxygen-free at high temperatures. For this reason, the internal structural parts of the heater can be manufactured from steel rather than stainless steel, which lowers the equipment manufacturing costs.

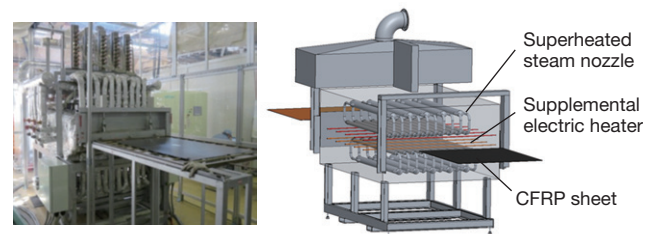


Fig. 9 Flow-Controlled CFRP Heater

4.5 Construction of production system using steam

The production process for thermoplastic CFRP requires the molds to be heated during the pressure molding. Since the developed equipment also requires an external boiler to generate the steam, a steam-based production system was constructed that consolidates these two processes (Fig. 10). Using the same steam for different purposes in two processes simplifies and streamlines the production line.

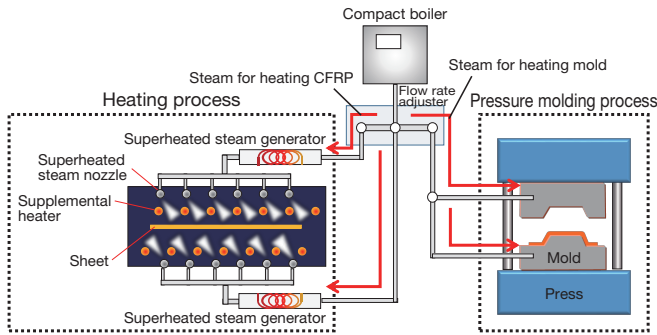


Fig. 10 Thermoplastic CFRP Production System Using Steam

5. Results

The initial targets for improved productivity and substantial energy saving were achieved (**Table 2**).

Table 2 Summary of Results

Item	Conventional	Target		Result		Evaluation
Heating time	390 s	120 s	-70%	120 s	-70%	Target achieved.
Energy (crude oil conversion)	24.2 kL/year	12.2 kL/year	-50%	5.2 kL/year	-77%	Target exceeded.
CO ₂ emissions	72.9 tons/year	36.5 tons/year	-50%	21.9 tons/year	-70%	Target exceeded

6. Summary

Weight reduction technologies will only gain in importance as the electrification of vehicles continues in the future. For this reason, it is highly possible that CFRP will replace steel or aluminum as a material for parts in both the body frame and interior. Toyota, the Toyota group, and part suppliers are all planning to adopt this technology. Specific development initiatives are already under way in the fields of CFRP recycling, the rapid heating of various materials, and the removal of oil and other contaminants.

This is a highly versatile technology with the potential to enter wider use both inside and outside the automotive industry.

Development of Technology for Collision Avoidance Assistance Using Active Steering Control

Motoki Nishimura*¹Kotaro Saiki*²Takahiko Murano*¹Tsunekazu Yasoshima*¹Naohide Uchida*¹

1. Outline

Over the last few years, active safety technologies such as collision damage mitigation brake systems have rapidly entered widespread use. Although reports have begun to confirm that these systems have a certain positive effect on safety, progress toward zero traffic accident casualties depends on further enhancing and expanding the performance of such widely adopted systems, and on practically adopting new advanced technologies. There are particularly high expectations for pre-collision systems (PCS), which seem to hold the key for collision avoidance and damage mitigation. **Fig. 1** illustrates how the developed PCS operates. When the system determines that a collision is possible, it provides a warning that urges the driver to take action. If the collision risk increases, the system controls the brakes to help avoid the collision or to mitigate collision damage if the collision cannot be avoided. However, from the standpoint of interfering with driver operation of the vehicle, there are limitations on how far collisions can be avoided by braking control alone. In response to this issue, a PCS with active steering assist was developed that helps to avoid a collision or mitigates collision damage by combining the conventional warning and pre-collision braking controls with steering control. This system activates when it determines that a collision may be avoidable by steering control and that avoidance may not be feasible using braking control only, as in the case with a conventional PCS.

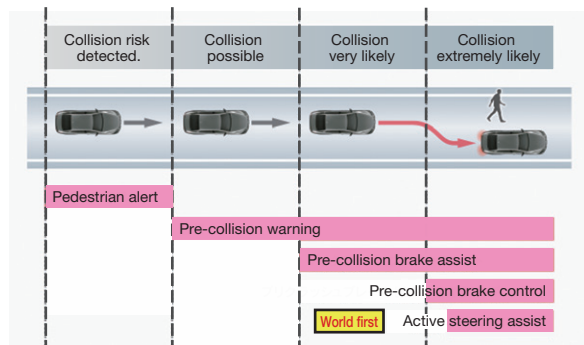


Fig. 1 Outline of Operation of PCS with Active Steering Assist

2. Details of Technology

One precondition for system operation is the existence of a route to avoid a collision with the target object.

In addition, to prevent the vehicle from colliding with a different object after steering around the original target, the system detects the road surface in front of the vehicle rather than just the target object, and steers the vehicle within the area where no objects exist.

2.1 Road surface detection using stereo camera

A newly designed stereo image sensor was adopted that uses a three-dimensional (3D) image processing technology called dense stereo matching to estimate the likely road surface area from 3D stereo image data.

2.2 Generation of collision avoidance path

Fig. 2 uses a potential collision with a pedestrian to illustrate the generation of an avoidance path. The avoidance path is generated by combining two types of steering: steering to help avoid the collision with the pedestrian and steering to help prevent lane departure. Steering control based on this avoidance path is applied in combination with braking control.

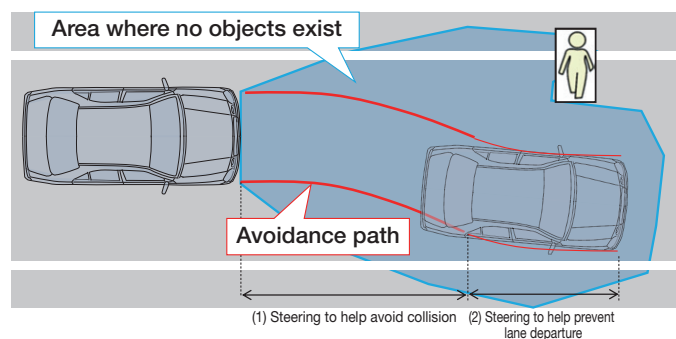


Fig. 2 Generation of Collision Avoidance Path

3. Conclusion

This article has outlined the development of a collision-avoidance assistance system that combines conventional braking control with steering control. This is the world's first commercially available system that judges collision risk and applies steering control to help avoid a collision. Development is continuing to further popularize and expand this system.

*¹ Automated Driving & Advanced Safety System Development Div., Advanced R&D and Engineering Company

*² Toyota Motor Technical Research and Service (Shanghai) Co., Ltd.

Reduction of Exterior Mirror Aerodynamic Noise Using New Airflow Concept

Yuta Ito*¹

Jiro Takamitsu*¹

Vinh Long Phan*²

Hiroshi Tanaka*²

1. Background and Purpose

It is known that aerodynamic noise can be reduced by lowering the velocity and vorticity of airflows. Vehicle exterior mirror designers aim to achieve this objective through mirror geometry that creates an airflow path at the inner surface of the mirror, which expands from the front to the rear of the vehicle without causing airflow separation (in other words, a mirror shape that opens out toward the rear of the vehicle). However, this approach makes it difficult to reduce weight and drag by adopting a smaller mirror while also further enhancing the visibility of the vehicle occupants.

Therefore, this development focused on Bernoulli's principle to establish a new airflow concept capable of reducing aerodynamic noise while also reducing size and enhancing visibility. (This concept was originally presented at the 2017 annual Autumn Congress of the Society of Automotive Engineers of Japan (JSAE).)

2. Description of Technology

2.1 Sources of aerodynamic noise around exterior mirrors

According to Powell (Equation 1), aerodynamic noise occurs at locations with large vorticity and velocity values (Fig. 1).

$$\frac{\partial^2 \rho}{\partial t^2} - c^2 \nabla^2 \rho = \rho_0 \nabla \cdot (\omega \times v) \quad (1)$$

where,

- ρ : air density
- ω : vorticity vector
- v : velocity vector

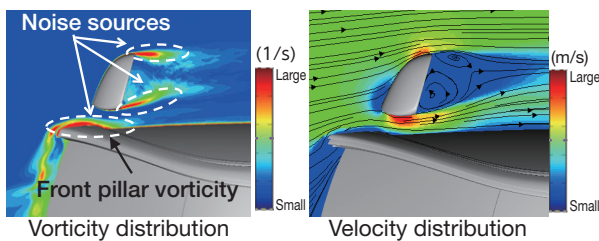


Fig. 1 Aerodynamic Noise Sources around Exterior Mirrors

2.2 New airflow concept

Fig. 1 shows that noise is generated when the airflow velocity increases at the inner surface of the mirror (V-shaped grooves). Bernoulli's principle suggests that this velocity, and therefore aerodynamic noise, can be reduced by increasing the pressure at the inner surface (Figs. 2 and 3).

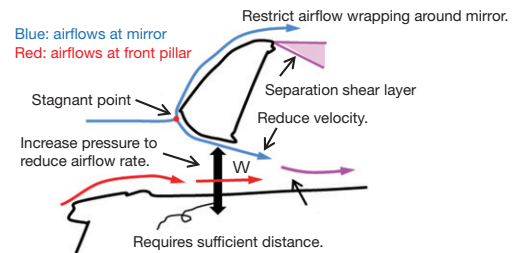


Fig. 2 New Airflow Concept

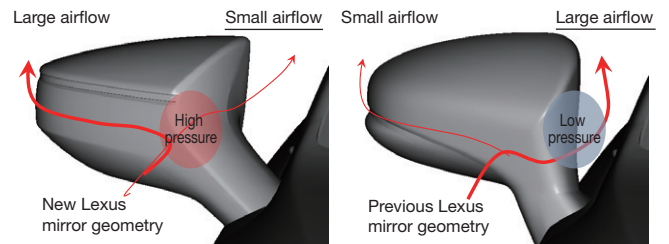


Fig. 3 Measures to Increase Pressure by Changing Mirror Geometry

One issue was to prevent air flowing around the mirror and directly striking the side window. After studying this issue, it was found that a distance of at least 65 mm was required between the side window and the mirror (parameter W in Fig. 2).

3. Conclusion

Fig. 4 compares the measured interior noise results of the previous Lexus mirror with the results of the new Lexus mirror developed based on the new airflow concept. The new concept substantially reduced noise.

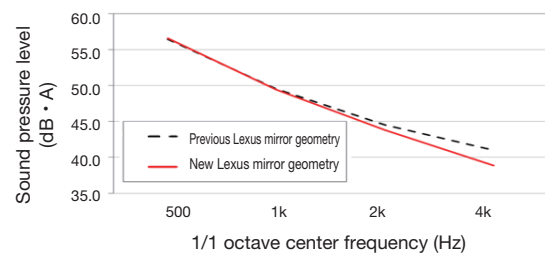


Fig. 4 Comparison of Interior Noise with Both Mirrors

*¹ Lexus Vehicle Evaluation and Engineering Div., Lexus International Company

*² Mobility Evaluation and Engineering Div., Advanced R&D and Engineering Company

Study of Occupant Head Injuries Using Human FE Models in Side Collisions

Shota Hashimoto*¹

Yasuo Yamamae*¹

Yuichi Kitagawa*¹

Tsuyoshi Yasuki*¹

1. Introduction

In traffic collisions that occur in the U.S., side collisions are responsible for the next highest number of fatalities after frontal collisions. For this reason, devices such as curtain shield airbags have been developed to help protect the heads of rear side occupants in a side collision, and the safety of vehicles in a side collision is also addressed by regulations and safety assessments. There is also growing interest in the safety of far side occupants, as demonstrated by studies and the like into adding new assessment items in Europe.

This research simulated vehicle vs. vehicle side collisions under various conditions using human finite element (FE) models to identify the relationship between occupant behavior, head injuries, and collision conditions.

2. Calculation Models and Conditions

A mid-size sedan was used for the struck vehicle, an SUV was used for the striking vehicle, and the Total Human Model for Safety (THUMS) Version 4 AF05 human FE model, developed jointly between Toyota and Toyota Central R&D Labs., Inc., was used for the occupant models. Four occupant models were positioned in the struck vehicle, in the front and rear seats on the near and far sides of the collision.

The striking vehicle speed, struck vehicle speed, impact angle, and impact position were defined as parameters, and the striking vehicle was collided with the left side of the struck vehicle. The striking vehicle speed was set to 50, 60, and 70 km/h, and the struck vehicle speed was set to 0 km/h, half the speed of the striking vehicle, and the same speed as the striking vehicle. The impact angle was set to 60, 90, and 120 degrees, and the impact position was set to 800, 1,500, and 2,000 mm from the center of the front tires. A total of 81 cases were calculated.

3. Results and Discussion

The calculation results showed that an impact between the heads of occupants tends to result in a serious head injury. The conditions for an impact between heads were considered. To help identify the boundary between collisions that resulted in an impact between heads and collisions that did not, **Figs. 1** and **2** illustrate the relationship between collision conditions. When the struck vehicle speed was low (less than 40 km/h), an

impact tended to occur between the heads of front-seat occupants at an impact angle of 90 degrees. Similarly, when the struck vehicle speed was low, an impact tended to occur between the heads of rear-seat occupants at an impact position of 2,000 mm.

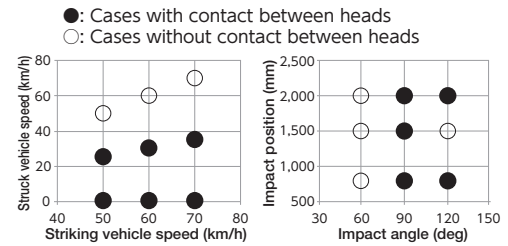


Fig. 1 Collision Conditions Resulting in Contact between Heads of Front-Seat Occupants

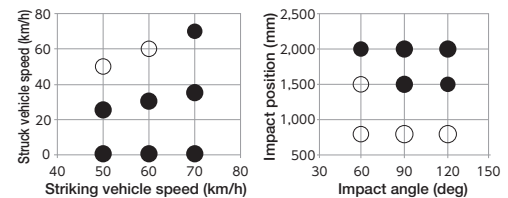


Fig. 2 Collision Conditions Resulting in Contact between Heads of Rear-Seat Occupants

4. Conclusion

The collision conditions with a high tendency to result in an impact between the heads of vehicle occupants were identified. Under the scope investigated by this research, impacts between heads tended to occur when the struck vehicle speed was low and when the near side occupants were located close to the impact position of the striking vehicle. Occupant behavior in vehicle vs. vehicle side collisions was simulated in detail factoring in vehicle deformation and the occupant protection system. As a result, detailed knowledge was obtained about the mechanism that results in impacts between heads inside a vehicle, which is a major cause of occupant fatalities in side collisions. Conditions that might result in an impact between the heads of near side and far side occupants were identified based on a wide range of collision conditions, and the validity of the European assessment test method was demonstrated theoretically. This research was carried out as a part of a project conducted by the Japan Automobile Manufacturers Association (JAMA) and the results were partially obtained using the “K” supercomputer located at the Riken Advanced Institute for Computational Science (project number: hp150176).

*¹ Mobility Evaluation and Engineering Div., Advanced R&D and Engineering Company

Modeling of Spark Channel Shortening under High Velocity Flow Conditions

Yasushi Noguchi*¹
Takayuki Fuyuto*²

Ryo Masuda*²
Yoshiyuki Mandokoro*²

Shogo Sayama*²
Akimitsu Sugiura*³

1. Introduction

The application of large amounts of exhaust gas recirculation (EGR) and lean-burn are important combustion technologies for increasing efficiency and decreasing emissions in spark injection (SI) engines. Lean-burn technologies reduce the temperature of the combustion gas, and can help to improve knock tolerance and lower heat loss. However, combustion becomes unstable as the dilution ratio (i.e., the amount of air or EGR gas in the mixture) increases, exacerbating cycle-to-cycle variations in combustion and applying an upper limit to the achievable dilution ratio. These cycle-to-cycle variations in combustion are greatly affected by the characteristics of the early combustion phase, such as the initial shape, size, and location of the flame.

This research modeled individual short circuits and blow-outs of spark channels based on discharge theory, and incorporated these models into a three-dimensional (3D) spark ignition model used for computational analysis of combustion in a spark injection (SI) engine. The validity of the constructed model was verified by test results obtained from a spark measurement swirl chamber.

current, and secondary voltage of the discharge circuit), a spark channel model (incorporating the discharge elongation, as well as the short circuits, blow-outs, and restrikes of spark channels), and an initial flame kernel model (incorporating ignition, flame propagation, and extinction). In addition, the effects of the shape of the spark plug on the gas flow are directly considered by the fluid solver by incorporating the spark plug into the computational grid of the combustion chamber.

2. Experimental Apparatus

A spark measurement swirl chamber (**Fig. 1**) was used to evaluate the spark ignition model. Since this swirl chamber was installed on the head of a visualized engine, it was possible to analyze the discharge behavior under high-temperature and high-pressure conditions equivalent to those in an actual engine. In the tests, expanded shadowgraph images of the area close to the spark plug were obtained, and the current and voltage were measured at the secondary side of the ignition circuit. **Table 1** shows the test conditions. Ignition energy E was set to 200 mJ in all conditions, and measurements were obtained over 50 cycles under each condition.

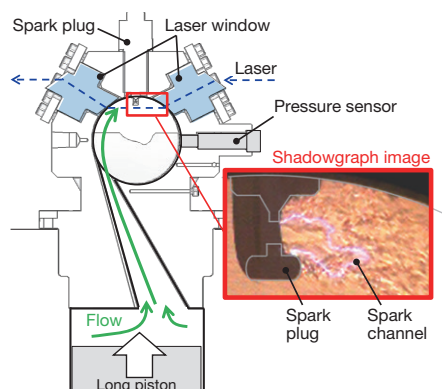


Fig. 1 Outline of Experimental Apparatus

Table 1 Experimental Conditions

Air/fuel ratio	Pressure p at ignition timing (bar)	Flow velocity U at plug gap (m/s)
20	10	65
24	10	65
30	10	65
25	10	52
26	10	78
26	15	78

3. Outline of Ignition Model

The 3D spark ignition model constructed in this research to analyze SI engine combustion consists of an electrical circuit model (incorporating the electrical resistance, secondary

4. Verification

4.1 Behavior from spark discharge to initial flame kernel

Fig. 2 compares the calculated results with visualized shadowgraph images of the spark and initial flame behavior (typical cycle close to the average behavior) at an EGR rate of 25%. The time elapsed from electrical breakdown is shown at

*¹ Measurement Instrumentation & Digital Development Innovation Div., Vehicle Development Center

*² Toyota Central R&D Labs., Inc.

*³ Denso Corporation

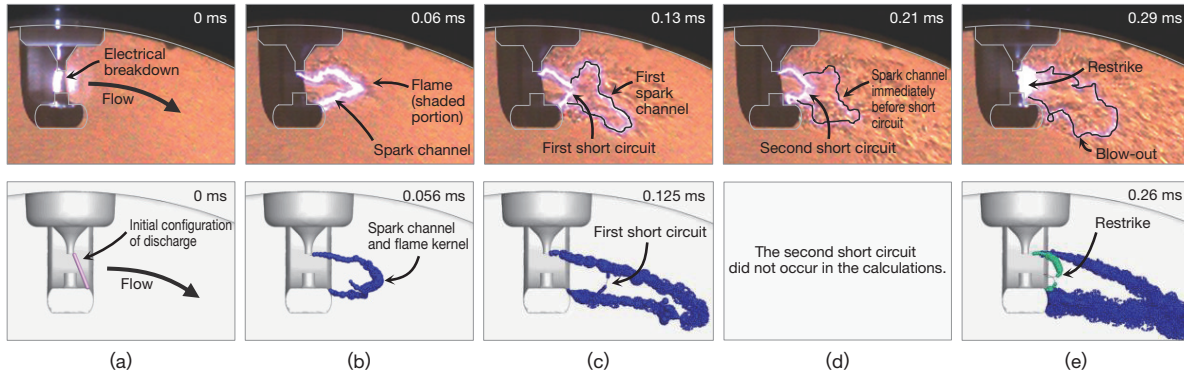


Fig. 2 Comparison of Experimental and Calculated Results for Spark Channel and Flame Kernel: (a) Electrical Breakdown, (b) Elongation and Ignition of Spark Channel, (c) First Short Circuit of Spark Channel, (d) Second Short Circuit of Spark Channel, (e) Blow-Outs and Restrike

the top-right of each figure. In the process from electrical breakdown to the elongation and short circuit, blow-out, or restrike of the spark channels, the measured behavior in which short circuits occurred in the first half of the discharge and blow-outs and restrikes occurred in the latter half was simulated closely by the calculation.

4.2 Misfire limit

Fig. 3 compares the calculated and measured results for the misfire limit EGR rate. This comparison uses the relationship between the EGR rate and the early combustion period (0 to 2% combustion duration) for the calculated results, and the misfire rate and early combustion period (calculated from the in-cylinder waveform measured using the pressure sensor installed on the side of the swirl chamber) in the 50 measured cycles at each EGR rate for the measured results. In the measurements, cycles that did not reach the 10% combustion point were regarded as misfires. Additionally, the images at the top of the graph show the calculated results for the flame surface immediately after the discharge ends at EGR rates of 25, 28, and 29%.

In the measured results, combustion occurred in all cycles with EGR rates of 25 and 28% and misfire cycles did not occur. In contrast, at an EGR rate of 31%, misfires occurred in approximately 90% of the cycles. In this case, since flame extinction occurred before 2% combustion was achieved in 20% of the misfire cycles, the early combustion period could not be plotted. In these conditions, it may be estimated that the EGR rate at which complete misfire occurs in all cycles is over 31%.

In the calculated results, the flame became increasingly thinner immediately after discharge ended as the EGR rate rose, and the early combustion period increased. In addition, the trends for the early combustion period and its relationship with the EGR rate closely matched the measured data. Finally, at an EGR rate of 29%, the flame immediately after discharge ended was not capable of propagation under its own energy and was extinguished. In this case, since flame extinction occurred

before 2% combustion was achieved, the early combustion period could not be plotted. Since this provides visual confirmation that the early combustion period increased in accordance with the rising EGR rate (i.e., the flame speed decreased), leading to misfire, an “x” is plotted at the top of the graph for expedience (EGR rate = 29%). When the misfire limit EGR rate is compared, misfire occurred in the measured results at an EGR rate of 31% and in the calculated results at 29%. Consequently, the misfire limit EGR rate error when calculated under these conditions may be estimated to be approximately 2 percentage points.

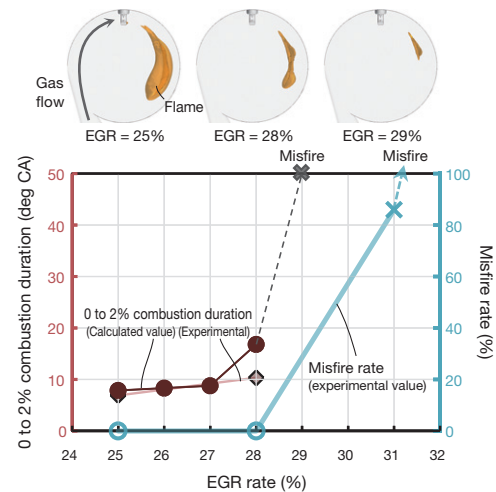


Fig. 3 Comparison of Misfire Rates in Accordance with Increase in EGR Rate

5. Conclusion

This article described the construction of models for short circuits and for blow-outs and restrikes of spark channels in SI. By combining these models with a spark channel model (particle series model) and an electrical circuit model, it was possible to predict the discharge to ignition processes, coupled

with the elongation, short circuit, blow-out, restrike, and discharge waveform (time history of current and voltage) behavior of spark channels. The discharge behavior of the developed model under high velocity flow and high lean-burn conditions was verified using an ignition measurement swirl chamber. In the process from electrical breakdown to the elongation and short circuit, blow-out, or restrike of the spark channels, the measured behavior in which short circuits occurred in the first half of the discharge and blow-outs and restrikes occurred in the latter half was simulated closely by the calculation. In addition, in the lean burn design limit prediction, the misfire limit EGR rate error estimated under the conditions described in this article was approximately 2 percentage points.

This technology allows discharge behavior to be identified and optimized, and should be useful when designing ignition systems with stable ignition characteristics during the development of high-efficiency engines.

The JSAE Technological Development Prize (69th JSAE Awards)
Development of Vehicle Dynamics Integrated Management (VDIM) System for Driver Comfort during Cornering

Yoshitaka Fujita*¹
 Tetsuya Morino*³

Mitsuo Fukuda*²
 Yoshiaki Tsuchiya*⁴

Toru Takashima*³

1. Introduction

Demand is growing for technology capable of enhancing safety and dynamic performance, while also ensuring the comfort of the driver and vehicle occupants during driving. With the aim of further enhancing driver comfort and confidence in both the linear and non-linear driving ranges, a vehicle dynamics control system was developed that integrates yaw, lateral, and roll motions.

2. System Configuration

An integrated vehicle dynamics control system with six degrees of freedom was constructed that uses the four-wheel steering system to control yaw and lateral motions, the active stabilizers that control roll moment, and the variable damping control shock absorbers and electronic stability control (ESC) (Fig. 1).

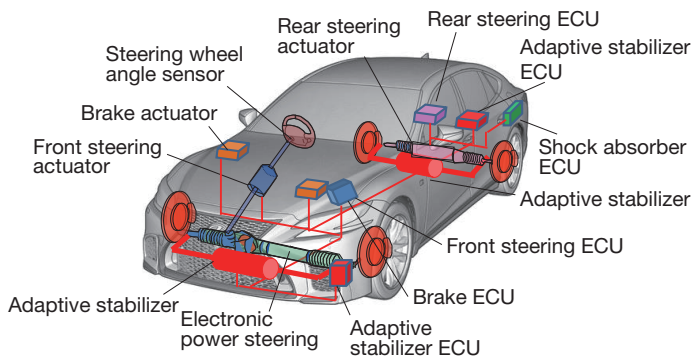


Fig. 1 System Configuration

3. Enhancement of Comfort during Cornering

In the case of lateral motion, appropriate ranges are known to exist for the steering angle and yaw rate phase, and for the yaw rate and lateral acceleration phase. In addition, research results have indicated that the steering angle and roll angle phase affects errors in trajectory after entering a curve, and that this also has an appropriate range. This development focused on and studied the lateral acceleration and roll angle phase. Fig. 2

shows the time from lateral acceleration to the roll angle, alongside the results of a subjective driver evaluation. The horizontal axis of Fig. 2 indicates the time difference between the yaw rate and lateral acceleration, which acts as an index for the rear grip feeling generated by the vehicle. In a vehicle that emphasizes stability (i.e., a vehicle with a small time difference between the yaw rate and lateral acceleration), a natural time difference from lateral acceleration to the yaw rate to generate a rear grip feeling is between 20 and 80 ms. In contrast, in a vehicle that emphasizes cornering performance (i.e., a vehicle that prioritizes the yaw rate), the optimum range is lower (between 30 and 70 ms). Values further outside the optimum range were expressed as uncomfortable by drivers in the subjective evaluation. Therefore, this demonstrates that an optimum time difference between lateral acceleration and the roll angle exists for drivers.

Additionally, research also covered occupants reading, writing, or sleeping in the rear seats. Based on analysis results that highlighted the major impact of lateral jerk, planar and roll motions capable of suppressing lateral jerk in response to steering were studied. As a result, a reduction in actual lateral acceleration gain was confirmed, demonstrating that rear seat comfort during cornering was enhanced.

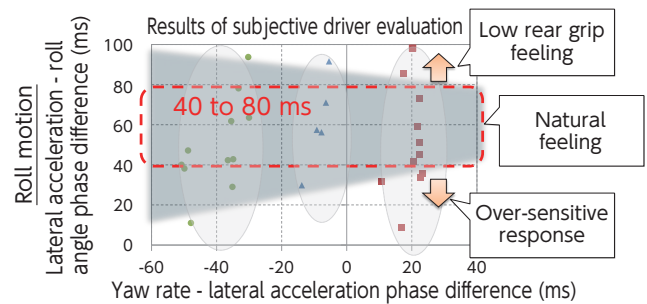


Fig. 2 Time Difference between Lateral Acceleration and Roll Angle

4. Conclusion

This system, which carries out integrated control of lateral and roll motions, enhances driver comfort and vehicle dynamics, while also enabling vehicle behavior that enhances rear seat comfort. This system should be useful in helping to ensure occupant comfort in the automated vehicles of the future.

*¹ Chassis Development Div., Vehicle Development Center
 *² TNGA Management Div., Vehicle Development Center
 *³ Advanced Chassis Development Div., Advanced R&D and Engineering Company
 *⁴ Aisin Seiki Co., Ltd.

The JSAE Technological Development Prize (69th JSAE Awards)
Advanced Active Safety Technology with Steering Function for Collision Avoidance and Emergency Stop Assistance

Keitaro Niki*¹

Tsunekazu Yasoshima*¹

Kazuhiro Morimoto*¹

Masaki Takano*³

Kotaro Saiki*²

1. Background

Although automatic braking and other active safety systems have become more widespread in recent years, efforts are ongoing to help further reduce accident casualties by enhancing and expanding the performance of such widely adopted systems and to develop new advanced technologies.

This article describes further advances in the safety system packages that have been adopted on a wide range of Toyota's lineup inside and outside Japan, starting with the development of the new active safety technologies described in Sections 2 and 3.

2. Pre-Collision System with Active Steering Assist

Fig. 1 shows an outline of this system. When the system determines that a collision is possible, it provides a warning that urges the driver to take action. If the collision risk increases, the system starts to provide assistance by controlling the brakes. However, from the standpoint of interfering with driver operation of the vehicle, there are limitations on how far collisions can be avoided by braking control alone. Therefore, in response to this issue, the world's first pre-collision system (PCS) with active steering assist was developed that combines pre-collision braking control with steering control. This system activates when it determines that collision avoidance may not be feasible by brake control only and that a collision may be avoidable by steering control.

One precondition for system operation is the existence of a route to avoid a collision with, for example, a pedestrian in front of the vehicle. In this case, the vehicle must avoid colliding with a different object after steering around the pedestrian. Therefore, the system detects the road surface in front of the vehicle rather than just the pedestrian, and steers the vehicle within the area where no objects exist.

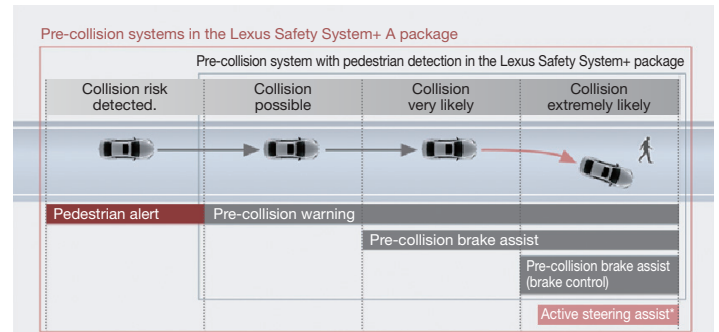


Fig. 1 Outline of Pre-Collision System with Active Steering Assist

2.1 Road surface detection using stereo camera

A stereo camera located at the top of the windshield uses a three-dimensional (3D) image processing technology called dense stereo matching to estimate the likely road surface area from the disparity distribution obtained from the stereo images.

2.2 Generation of collision avoidance path

As shown in **Fig. 2**, to avoid the pedestrian while remaining within the area where no objects exist, an avoidance path is generated by combining two types of steering: steering to help avoid the collision and steering to help prevent lane departure. The system carries out steering control based on this avoidance path while applying braking control.

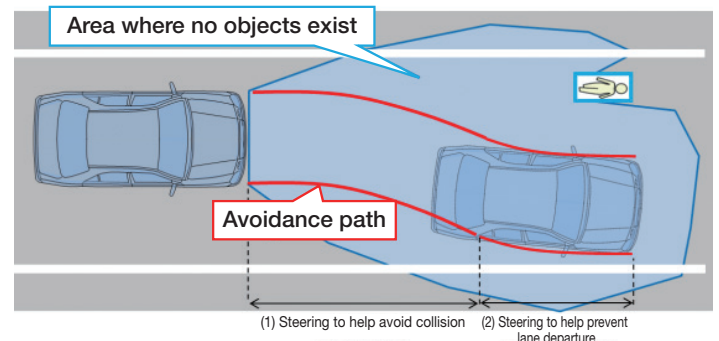


Fig. 2 Generation of Collision Avoidance Path

*¹ Automated Driving & Advanced Safety System Development Div., Advanced R&D and Engineering Company

*² Toyota Motor Technical Research and Service (Shanghai) Co., Ltd.

*³ Toyota Research Institute - Advanced Development, Inc.

3. Driver Emergency Stop Assist

With accidents caused by driver illness becoming an increasingly pressing social issue, the Japanese Ministry of Land, Infrastructure, Transport and Tourism has issued the world's first guidelines for emergency driving stop systems (i.e., systems that slow and stop the vehicle in the event of an emergency), which automatically stop the vehicle within the driving lane if the driver is affected by a sudden medical issue and finds it difficult to continue driving. These guidelines are designed to encourage the early introduction and promote the widespread adoption of such systems. Toyota shares the ultimate aim of reducing the number of traffic accident casualties to zero and has prioritized the adoption of measures against these types of accidents. As a result, it has developed the Driver Emergency Stop Assist system, which is the first system to comply with these Japanese guidelines.

Fig. 3 shows an outline of the developed system. To ensure that the vehicle stops inside the driving lane, the lane-keeping assistance function must be in operation as a precondition for system activation. If this condition is satisfied, the system operates in three phases.

3.2 Slow down/stop assist

In addition to flashing the hazard lamps, the system automatically sounds the horn to warn people in the surrounding area. At the same time, the vehicle is gradually slowed to a stop within the driving lane. In addition, the system also disables accelerator pedal operation since the medical emergency may cause the driver to inadvertently press the accelerator pedal and send the vehicle out of control. If the driver has not suffered a medical emergency, the driver can cancel system operation in this phase simply by gripping the steering wheel or performing another driving action.

3.3 Assistance request

After the vehicle has stopped, the system automatically locks the parking brake and contacts an emergency call center to facilitate rapid emergency treatment and traffic restrictions. The system also automatically unlocks the vehicle doors to speed up the assistance.

4. Conclusion

This article described the Pre-Collision System with Active Steering Assist and the Driver Emergency Stop Assist system, which are two key technologies in Toyota's latest active safety packages.

In Japan, accidents between vehicles and pedestrians are responsible for the largest proportion of traffic accident fatalities. As braking control is effective in only 60% of these cases, the Pre-Collision System with Active Steering Assist combines braking control with steering control and may help to reduce these accidents by a further approximately 16% (figures calculated by Toyota).

In addition, the Driver Emergency Stop Assist system has been developed and launched as a first step toward the widespread adoption of such systems. It is hoped that this will help to raise awareness of these systems, help to gauge the degree of system acceptance, and encourage society and other automakers to increase system adoption. As a result, it is also hoped that these systems will help to reduce the number of traffic accidents caused by sudden medical issues. It is planned to adopt both systems in more models in the future by using the developed technologies as a basis for more widely applicable systems.

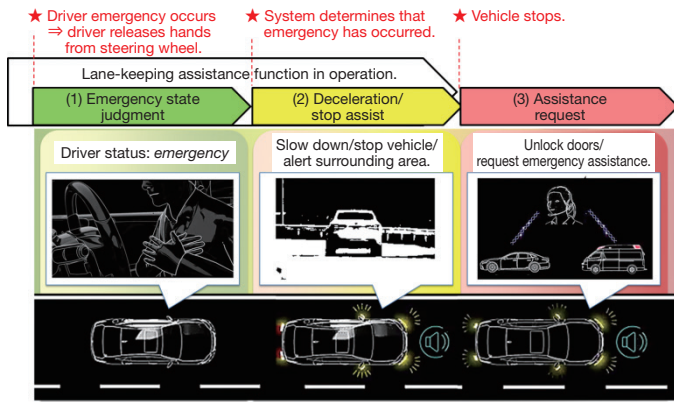


Fig. 3 Outline of Driver Emergency Stop Assist

3.1 Driver emergency state judgment

If the driver makes no attempt to take control of the vehicle after a two-stage warning process, the system judges whether a driver emergency has occurred. The first stage involves an indication and an audible alarm that prompts the driver to grip the steering wheel, or to press the accelerator or brake pedal. In the second stage, the warnings in stage 1 are supplemented by control that restricts the vehicle speed to prompt the driver to press the accelerator pedal. To help prevent a rear-end collision, the speed restriction is applied gradually and the hazard lamps are flashed.

Best Poster Paper Presentation Award at 2018 Annual Congress of Society of Automotive Engineers of Japan, Inc.

Development of Corrosion-Resistant and Adhesion-Resistant Hard Facing Material for Engine Valves

Yuki Kamo*¹

Kimihiko Ando*¹

Takayuki Yamada*²

Akihiko Kawata*³

1. Introduction

Laser-clad valve seats were adopted on engines developed under the Toyota New Global Architecture (TNGA) design philosophy to help enhance thermal efficiency and specific power by optimizing the shape of the intake ports. However, one issue inhibiting the global roll out of these engines has been the adoption of this technology with blended ethanol fuels. Therefore, a corrosion- and adhesion-resistant hard facing material for engine valves has been developed, which restricts valve and valve seat wear even under severely corrosive and adhesive environments created by highly concentrated ethanol fuels in regions that use 85% (E85) or 100% (E100) ethanol blends.

2. Outline of Hard Valve Facing

When a valve closes, the impact force as the valve contacts the seat and the explosive pressure drives the valve into the seat. This may result in sliding between the valve and valve seat, as well as wear.

Under high-temperature, corrosive, and adhesive environments, valve and valve seat wear can be reduced by welding heat-, corrosion-, and adhesion-resistant alloys to the valve face by cladding. This is called a hard facing (Fig. 1).

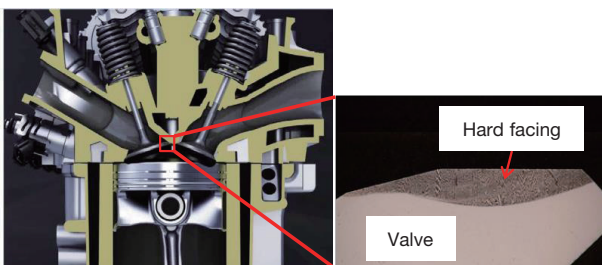


Fig. 1 Cross-Section of Hard Valve Facing

3. Issues of Highly Concentrated Ethanol Fuels

Highly concentrated ethanol fuels have reductive properties and contain a high proportion of formic acid, a strongly corrosive non-oxidizing acid. These fuels break down the oxide layer on the surface of hard valve facings, which causes corrosion pitting and exposes the metal surface of the valve, thereby increasing valve seat wear when materials contact and adhere to the valve seat. These conditions are particularly severe in TNGA engines, which have high thermal efficiency and specific power.

4. Development of New Hard Facing Material

A corrosion- and adhesion-resistant Co-Cr-Mo-Ni-W-C alloy was developed that is capable of constantly maintaining the oxide layer under severely corrosive and adhesive environments in which the oxide layer is constantly exposed to formic acid and sliding. This is accomplished by the formation of a thin and strong chromium (Cr) oxide film on the hard valve facing surface. The regenerative capability of the Cr oxide film is strengthened by the molybdenum (Mo) in the alloy.

5. Confirmation of Effectiveness

Immersion tests using a formic acid solution and adhesive wear tests were carried out. The results found that the developed alloy has superior corrosion and adhesion resistance to the conventional Stellite 6 alloy (Co-Cr-Ni-W-C) material (Figs. 2 and 3). Actual engine durability tests also confirmed the effectiveness of the developed alloy in reducing valve seat wear (Fig. 4).

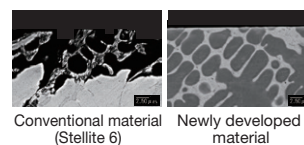


Fig. 2 Immersion Test Results

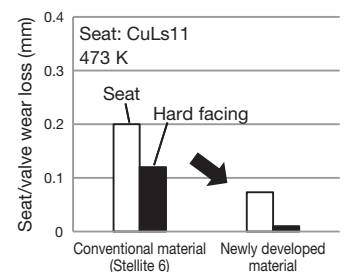


Fig. 3 Adhesive Wear Tests

*¹ Material Engineering Div. No. 1, Advanced R&D and Engineering Company

*² Vehicle Center & Companies Human Resources Dept., Advanced R&D and Engineering Company

*³ Powertrain Function Development Div., Advanced R&D and Engineering Company

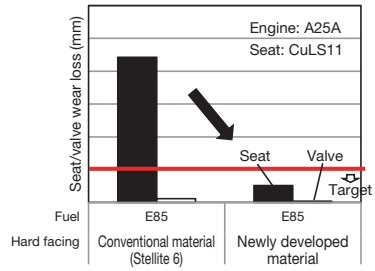


Fig. 4 Difference in Actual Engine Durability Test Results

6. Summary

This material has been adopted on TNGA engines installed in flexible fuel vehicles (FFVs) compatible with E85 and E100 fuels. The development and adoption of this material helped to resolve some of the issues preventing the global adoption of TNGA engines.

Best Poster Paper Presentation Award at 2018 Annual Congress of Society of Automotive Engineers of Japan, Inc.
Development of New CVT with Low-Speed Gear for 2.0-Liter Class Vehicles

Daisuke Tomomatsu*¹
 Shinya Kuwabara*¹

Masanori Shimizu*²
 Mitsuhiro Fukao*³

Kenichi Yamaguchi*¹

1. Introduction

A new steel belt continuously variable transmission (CVT) was developed for 2.0-liter engine vehicles to help enhance fuel efficiency and dynamic performance, and efforts were made to improve transmission efficiency and achieve a wider gear range. This was accomplished by adopting a power transmission mechanism with launch gears (a world first for a steel belt CVT) and arranging the belt closer to more efficient high gear ratios (Figs 1 and 2).

between the pulleys and the gears, and deformation of these elements may affect the orientation of C2. In this case, computer aided engineering (CAE) and verification experiments (measurements using deflection meters) found that deformation of the gear and gear supports was having a major impact on C2 (Fig. 5).

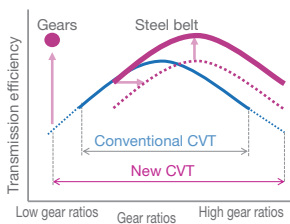


Fig. 1 Concept

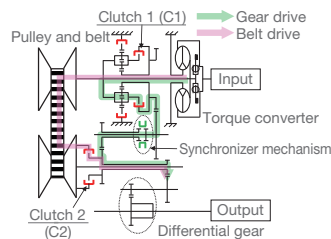


Fig. 2 Cross-Sectional View

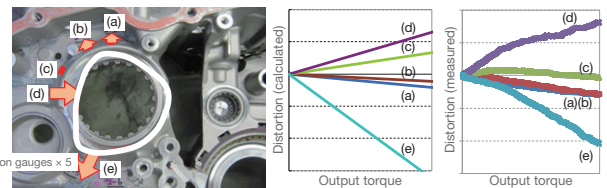


Fig. 5 Analysis of Gear Support Distortion (Comparison between Calculations and Measurements)

2. Issues of New Structure

This CVT shifts from gear drive to belt drive by switching the clutch engagement (called “C-to-C” below). The timing at which gear drive clutch C1 should be released and belt drive clutch C2 should be engaged was an issue due to the resulting driveshaft torque vibration and variations in vehicle longitudinal acceleration (Fig. 3). After analyzing the factors behind these issues, it was found that the μ -V characteristics of C2, which had a positive gradient in stand-alone tests, had a negative gradient after installation in the CVT assembly (Fig. 4).

The stiffness of the gears and case was identified as a major contributing factor. Addressing this issue (Fig. 6) improved the μ -V characteristics of the CVT assembly and resolved the torque vibration (Figs. 7 and 8).

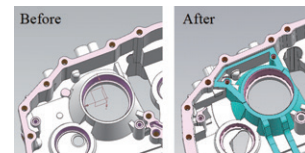


Fig. 6 Stiffer Gear Supports

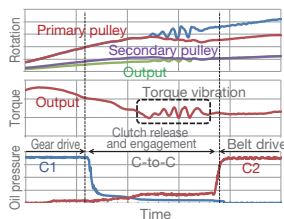


Fig. 3 Vibration

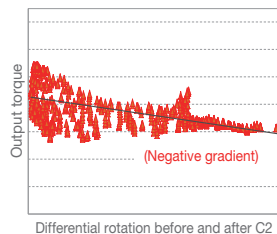


Fig. 4 μ -V Characteristics (CVT)

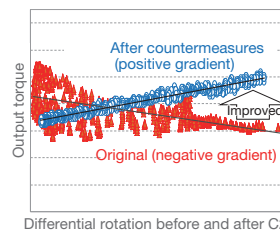


Fig. 7 μ -V Characteristics (Comparison)

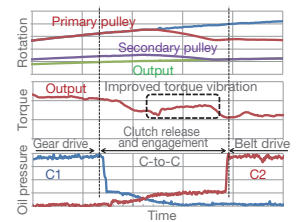


Fig. 8 C-to-C Waveform (after Countermeasures)

3. Conclusion

The factors causing torque vibration were identified through CAE analysis and experimental verification, helping to develop a CVT with excellent fuel efficiency and dynamic performance.

The knowledge obtained through this verification will be applied to the development of CVTs mated with engines with different displacements. It is also planned to promote model-based development for other phenomena by confirming the consistency of CAE analysis results through verification experiments.

*¹ Powertrain Development Div. No. 1, Powertrain Company
 *² Powertrain Function Development Div., Powertrain Company
 *³ Electric Powertrain Performance Development Div., Vehicle Development Center

Development of Heat-Resistant Cast Steel for Turbine Housing with High Exhaust Temperature

Yuzo Ishikawa*¹

Takumi Hijii*¹

Go Kuramoto*¹

Takashi Maeshima*²

1. Introduction

A recent trend is to use turbochargers to improve fuel efficiency by boosting vehicle power while reducing engine size. In addition, with exhaust gas at temperatures of 1,273 K or higher used to boost turbocharging performance, highly heat-resistant materials are needed for turbocharger turbine housings. Conventionally, this part has used austenitic heat-resistant cast steel. Although this material has extremely good heat resistance, it contains a high proportion of high-cost elements (such as nickel (Ni) and chromium (Cr)) and rising part costs caused by the addition of alloying elements and poor machinability have been a long-standing issue.

Conventional alloy development involves optimizing the alloy composition while repeatedly manufacturing (casting) candidate component materials and evaluating the material characteristics. This research used thermodynamic simulation software (Thermo-Calc) to select the alloy composition by calculating the thermodynamics of multiple systems and predicting the microstructure of candidate alloys. This approach reduced the number of conventional manufacturing and evaluation cycles for the candidate component materials, thereby shortening the development process.

The development process mentioned above helped to identify the optimum microstructure for reducing cost while ensuring equivalent heat resistance to the existing austenitic heat-resistant cast steel in the applicable temperature range (1,273 K). In addition, it also enabled the development of a heat-resistant cast steel for turbine housings with excellent machinability by controlling the dispersion of hard particles and soft inclusions in the microstructure.

2. Composition Design Concept for Alloy Development

Fig. 1 shows the composition design approach for the developed material. Since turbine housings are exposed to thermal cycles between room temperature and 1,273 K, the thermal fatigue properties of the material are important. Therefore, the alloy composition design aimed to ensure the same thermal fatigue properties as the conventional material, while lowering the Ni and Cr content. Specifically, the Ni and Cr content were determined within the range that restricts brittle σ -phase precipitation, which acts as a potential origin

point for cracks. Then, niobium (Nb) was added to improve the high temperature strength of the matrix structure and to suppress crack propagation. It should be noted that, although the conventional material contains σ -phase, its high Ni and Cr content ensured good thermal fatigue properties.

Machinability is an issue with the conventional material due to hard particles in the microstructure that accelerate the wear of mechanical cutting tools. This development improved machinability by controlling the dispersion of hard particles (carbides) that form into networks and clump together, and by generating soft inclusions.

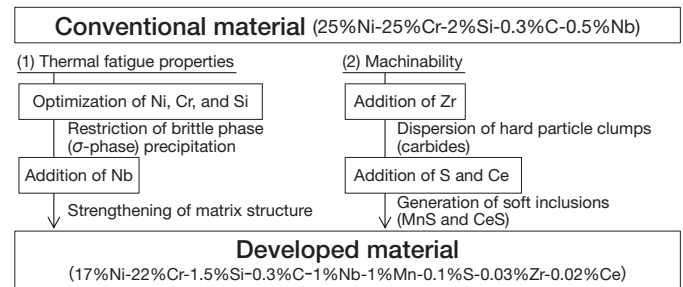


Fig. 1 Alloy Design Approach

3. Composition Design of Developed Material

3.1 Relationship between main components and σ -phase identified utilizing thermodynamic simulation

Fig. 2 shows the relationship between the Cr and Ni content and the amount of σ -phase precipitation, as obtained by thermodynamic simulation. The map indicates the range in which σ -phase precipitation does not occur. These results identified a range in which the Ni and Cr content of the conventional material (25%Ni-25%Cr) could be reduced without σ -phase precipitation. The map also shows the composition range in which the material cost target cannot be achieved and the composition range in which, based on past knowledge, the thermal fatigue property requirements are unlikely to be satisfied. Excluding these ranges, thermal fatigue was evaluated using two compositions in which σ -phase precipitation does not occur: A) 16%Ni-21%Cr and B) 17%Ni-22%Cr.

*¹ Material Engineering Div. No. 1, Advanced R&D and Engineering Company

*² Toyota Central R&D Labs., Inc.

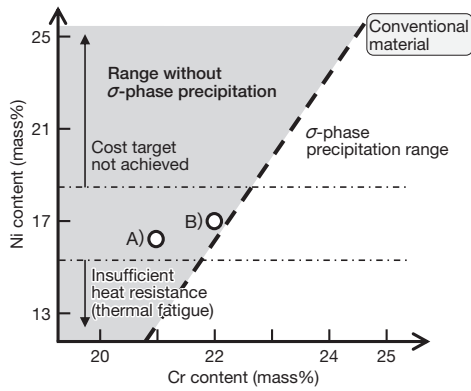


Fig. 2 Ranges without σ -Phase Precipitation (Cr-Ni Map)

3.2 Improvement of thermal fatigue properties

Fig. 3 shows the thermal fatigue test results. The thermal fatigue life of composition A) was much shorter than the conventional material. In contrast, since the thermal fatigue life of composition B) was only 5% shorter than the conventional material, the development studied how to further enhance the material properties by strengthening the base metal (particularly high temperature strength) based on composition B).

One effective way of improving high temperature strength is precipitation strengthening using carbides. In general, Nb, tungsten (W), and molybdenum (Mo) are used as additional elements to precipitate carbides. Nb was chosen for the strengthening element in this study because of its cost and its effect at high temperature. After evaluations of different amounts of Nb in the system, it was decided to add 1% of Nb to composition B). This approach raised the high temperature strength above that of the conventional material, while also improving thermal fatigue life. Therefore, composition C) 17%Ni-22%Cr-1%Nb was selected as the base composition of the developed material.

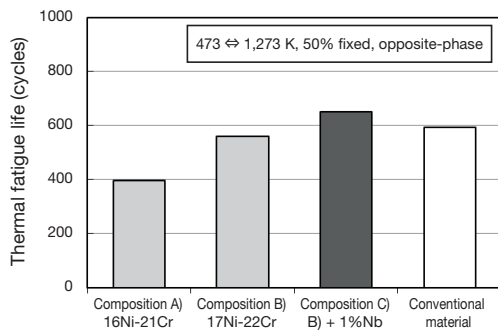


Fig. 3 Comparison of Material Thermal Fatigue Life

3.3 Improvement of machinability

Fig. 4 (1) shows the microstructure of composition C), which was selected as described in Section 3.2. Network clumps of the carbide $M_{23}C_6$ were observed in the microstructure. These

carbide clumps are thought to increase cutting resistance and worsen machinability. Therefore, the following two approaches were considered with the aim of lowering cutting resistance: dispersing the formation of carbide clumps, and generating soft inclusions to enhance machinability.

The evaluation results of various additives identified zirconium (Zr) as an effective component for dispersing carbides. In addition to Zr for dispersing carbides, sulfur (S) and cerium (Ce) were added to form soft inclusions (manganese sulfide (MnS) and cerium sulfide (CeS)), resulting in the reformed microstructure shown in Fig. 4 (2). As a result, machinability was improved substantially, as illustrated in Fig. 5.

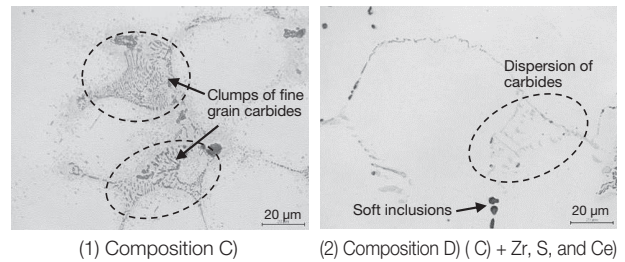


Fig. 4 Microstructure Comparison (Magnification: 400 Times)

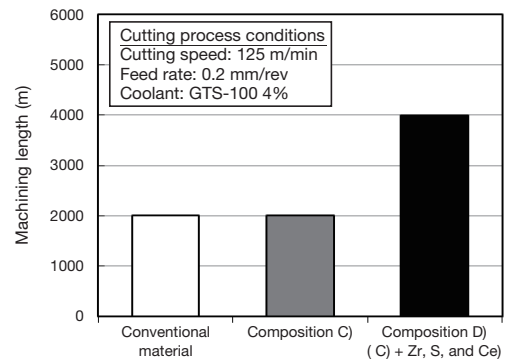


Fig. 5 Results of Machinability Evaluation

4. Conclusions

The development of an austenitic heat-resistant cast steel was able to control the σ -phase while ensuring thermal resistance. As a result, the Ni content of the conventional material was reduced from 25 to 17% and the Cr content from 25 to 22%, achieving material cost savings of 16%. In addition, machinability was improved by controlling the formation of carbides and generating soft inclusions, thereby reducing machining costs by 11%.

This material was adopted for the turbine housing of the 3.5-liter V6 V35A-FTS engine installed in the Lexus LS500 that was launched in December 2017. In the future, this material is expected to find widespread application as an exhaust system material capable of being used at high temperatures around 1,273 K.

1. Introduction

A wide range of research has been carried out into control methods for improving vehicle ride comfort, including a newly proposed method called triple skyhook control (tSH). tSH has a damping effect over a wider frequency range than typical skyhook damper control methods, while also enabling simple feedback-based control of the acceleration, velocity, and displacement of the sprung mass. However, although tSH can be applied without modification to heave and pitch motions that can be expressed in characteristic polynomial expressions of second order lag systems, it cannot be applied in the same way to roll motion since this is a complex form of motion coupled with planar motion through the tire side force.

2. Outline of Technology

When the tSH control command value shown in Equation 1 was applied to roll motion while disregarding the coupling with planar motion, the target characteristics were not obtained, and a diminished control effect occurred in the range around 2 to 4 Hz, in which vehicle occupants tend to feel discomfort.

$$M_{xc} = -\alpha D(s)(I_x s^2 + C_x s + K_x')\phi_2 \quad (1)$$

Therefore, this research used a cross-sectional unicycle model that factors in the coupling between roll and planar motion (**Fig. 1**) to analyze and formularize the coupling motion. As a result, as shown in Equation 2, the effects of the coupling motion could be considered by expressing the roll moment of inertia as first order lag.

$$M_{xc} = -\alpha D(s) \left(\left(I_x + \frac{mh_s^2}{1 + \frac{V}{Cg}s} \right) s^2 + C_x s + K_x' \right) \phi_2 \quad (2)$$

To verify this effect, the proposed control was implemented on an actual vehicle equipped with a four-wheel active suspension system. **Fig. 2** shows the power spectral density (PSD) of roll angular acceleration when the vehicle was driven on an uneven road surface at 100 km/h. At a frequency around 2 to 4 Hz, at which the conventional control was insufficiently effective, the proposed control achieved the targeted vibration damping action, thereby confirming the effectiveness of the developed method.

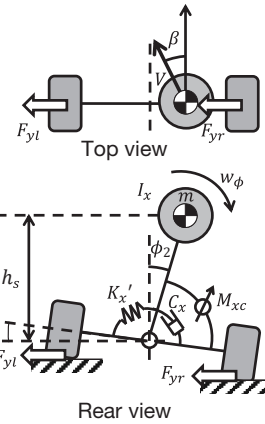


Fig. 1 Cross-Sectional Unicycle Model

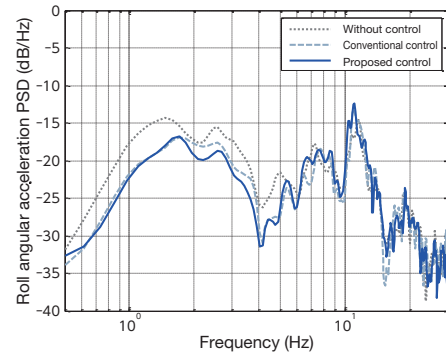


Fig. 2 Effect of Proposed Control (Actual Vehicle, 100 km/h)

3. Conclusion

This research identified the theoretical characteristics of the complex roll motion mechanism and created a simple formula by an appropriate method of approximation. As a result, this research was able to successfully design a control that achieved the targeted effect.

*¹ Chassis Development Div., Vehicle Development Center

*² Vehicle Engineering Development Div., Vehicle Development Center

Back Number Index



Vol. 57 No. 1 (2010)
Special Feature: Prius



Vol. 57 No. 2 (2011)
Special Feature:
Next-Generation Electric Storage
and its Applications



Vol. 58 No. 1 (2012)
Special Feature:
Japanese Originality



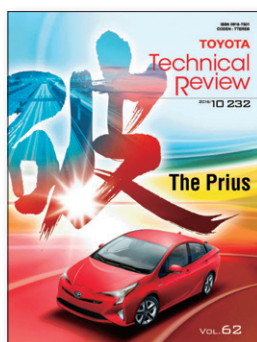
Vol. 59 (2013)
Special Feature:
Production Engineering



Vol. 60 (2014)
Special Feature: Powertrain



Vol. 61 (2015)
Special Feature 1: The Mirai FCV
Special Feature 2: ITS and
Advanced Driving Support Systems



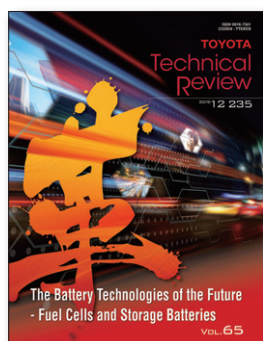
Vol. 62 (2016)
Special Feature: The Prius



Vol. 63 (2017)
Challenging and Innovative
Technological Development



Vol. 64 (2018)
Special Feature:
TNGA Powertrains



Vol. 65 (2019)
Special Feature:
The Battery Technologies of the Future
- Fuel Cells and Storage Batteries

Distributor: Ohmsha, Ltd.

Tel: 81-3-3233-0641

https://www.ohmsha.co.jp/magazine/partners_magazine.htm

¥2,800 (excluding tax)

Thank you for reading the *Toyota Technical Review* (TTR).

It is my pleasure to present Volume 66, which is the 236th edition of the TTR since its publication began.

Due to the outbreak of the novel coronavirus COVID-19, we have all been facing an incredibly difficult period. Our lives have been so deeply affected that expressions such as “the new normal” have become part of our everyday vocabulary.

This pandemic has also wreaked havoc with global production and sales throughout the automotive industry. The outcome of the once-in-a-century transformation that we are facing is becoming even more unpredictable.

Under these trying conditions, Toyota is striving to remake itself for a new age by building strong new alliances and accelerating its reinvention into a mobility company.

This special edition of the TTR combines two special features: the redesigned Mirai and the GR Yaris.

Toyota is also reinventing its vehicle development for the new age. As part of these efforts, the redesigned Mirai was developed to achieve the highest level of both driveability and environmental performance, while the GR Yaris was developed to demonstrate how technologies honed under the harshest race conditions can be applied to the building of ever-better cars.

Although developed under widely different approaches, both cars feature elements that will be indispensable for the future of vehicle development at Toyota. The articles in this edition of the TTR cover topics such as vehicle planning, which highlights Toyota’s future approach to vehicle development, and basic technologies. Among other information, I hope that these articles will provide fresh and interesting insights about the different emphases applied throughout vehicle development.

Finally, I’d like to extend my sincere gratitude to all the writers and editorial team members who used their valuable time to guide this edition of the TTR to publication during the incredibly busy period of the coronavirus pandemic.

I hope to continue creating a useful, informative, and interesting publication for your reading pleasure.

(Publisher: Yonemura)

TOYOTA Technical Review Vol. 66

©2021 TOYOTA MOTOR CORPORATION, Printed in Japan
(All rights reserved)

Publisher’s Office	R&D and Engineering Management Div. TOYOTA MOTOR CORPORATION 1 Toyota-cho, Toyota, Aichi, 471-8572 Japan 81-565-28-2121 (Operator)
Publisher	Koichi Yonemura
Planning	Jun Toyama
Editor	Ayako Hirano Technical Administration Dept., Toyota Office TOYOTA ENTERPRISE INC.
Printer	Shintec Hozumi Co., Ltd. 5-3-1 Neuramachi, Miyoshi, Aichi, 470-0217 Japan
Distributor	Ohmsha, Ltd. 81-3-3233-0641 (Operator) http://www.ohmsha.co.jp/index_e.htm
Published	March 22, 2021

Printed on recycled paper.



TOYOTA Technical Review

2021 / **3**
VOL.66 236

発売元 株式会社 オーム社
定価 2,800円(本体3,080円)
Distributor: Ohmsha, Ltd.
¥2,800 (excluding tax: ¥3,080)